ENHANCING THE PERFORMANCE OF CRUMB RUBBER MODIFIED ASPHALTS THROUGH CONTROLLING THE INTERNAL NETWORK STRUCTURE DEVELOPED

A Dissertation
Submitted to the Graduate Faculty
of the
North Dakota State University
of Agriculture and Applied Science

By

Mohyeldin Safwat Ahmed Ragab

In Partial Fulfillment of the Requirements
for the Degree of
DOCTOR OF PHILOSOPHY

Department:
Civil and Environmental Engineering

April 2016

Fargo, North Dakota

North Dakota State University

Graduate School

Title

ENHANCING THE PERFORMANCE OF CRUMB RUBBER MODIFIED ASPHALTS THROUGH CONTROLLING THE INTERNAL NETWORK STRUCTURE DEVELOPED

By

Mohyeldin Safwat Ahmed Ragab

The Supervisory Committee certifies that this ***disquisition*** complies with North Dakota State University's regulations and meets the accepted standards for the degree of

DOCTOR OF PHILOSOPHY

SUPERVISORY COMMITTEE:

Dr. Magdy Abdelrahman
Chair

Dr. Dinesh Katti

Dr. Kalpana Katti

Dr. Erik Hobbie

Dr. Xinnan Wang

Approved:

04/29/2016
Date

Dr. Dinesh Katti
Department Chair

ABSTRACT

Sustainability presents a pathway for future generations to have a better life. Cradle to cradle methodology is the essence of sustainability. In cradle to cradle approach, we aim to reutilize a given waste instead of disposing or landfilling it. Each year, millions of waste tires are disposed of in landfills. This poses a major challenge environmentally and economically. Environmentally, those tires become prone to fire hazards as well as being a place for rodents and mosquitos to reside at. Economically, on the other hand, each tire has an average of about 50% valuable polymers as well as oily components. One of the methods to utilize the valuable raw materials in waste tires is to recycle it in the form of ground tire rubber also known as crumb rubber modifier (CRM). Although CRM has been widely used as an asphalt modifier, however, due to the complexity of asphalt as well as the waste nature of CRM, the full understanding of the CRM modification mechanism with asphalt has not been fully understood. Understanding of the modification mechanisms involved in the CRM interaction with asphalt would enable us to produce a crumb rubber modified asphalt (CRMA) with enhanced properties. In the current research work, an attempt is made to better understand the mechanism of interaction between CRM and asphalt and the nature of components from asphalt and CRM that take part in the interaction between them. In addition, we investigate the effectiveness of CRM as a modifier for asphalt on the macro and microscale aspects.

Another part of the current research work deals with a second waste material; used motor oil. Used motor oil (UMO) presents yet another challenge to environment. With the ever increasing motor vehicles produced with advanced technologies and increased advanced motor oil demand. This presents a burden on the environment, with the continuous production of UMO. In the current research work, we investigated the feasibility of utilizing UMO as a modifier for as-

phalt and CRMA. We also investigated the effect of UMO on the micro and macroscale aspects of asphalt.

ACKNOWLEDGEMENTS

First, I wish to thank my main advisor Dr. Magdy Abdelrahman for his guidance and academic support during my research here in North Dakota State University (NDSU). Also, I would like to thank my committee members: Dr. Dinesh Katti, Dr. Kalpana Katti from Civil and Environmental Engineering department, Dr. Erik Hobbie from Materials and Nanotechnology department and Dr. Xinnan Wang from the Mechanical Engineering department for their help and patience during my study.

I would like to thank the Civil and Environmental Engineering Department at NDSU, and National Science Foundation (NSF) for financial support during this research. Additional thanks to Polymers and Coating department for using their advanced characterization equipment. Special thanks to Dr. Chunju Gu in the Polymers and Coating lab department for helping in this issue.

Finally, thanks for my family and especially my parents and my wife for their patience. I would like to express my thanks and gratitude to Mrs Jan Lofberg for all her help and support. Special thanks for all the team research members in CEE materials lab: Dr. Ehab Noureldin and Mr. Anthony Waldenmaier, who helped the author during his work to complete this research. Special thanks to my close friends: Dr. Bakr Mourad, Dr. Ahmed El Fatih, Amr Salem and Ahmed El Ghazaly, who supported me here in my life in the US.

DEDICATION

In the beginning, I thank God for his support and blessings during my whole life and studying here in US, without which I would have never achieved any of my goals. I dedicate this work to my father, mother, brother, and sisters for their help and support during my whole personal and career life.

Special dedication to my lovely wife who never stopped helping and supporting me and was always there for me. I dedicate this work to my dear children who are the jewels of my life.

TABLE OF CONTENTS

LIST OF TABLES

LIST OF FIGURES

LIST OF ABBREVIATIONS

CRM.....Crumb Rubber Modifier

CRMA.....Crumb Rubber Modified Asphalt

3D.....Three Dimensional

TGA .....Thermo Gravimetric Analysis

FTIR.....Fourier Transform Infrared Spectroscopy

GPC.....Gel Permeation Chromatography

AFM.....Atomic Force Microscopy

RTFO .....Rolling Thin Film Oven

BBR.....Bending Beam Rheometer

DSR.....Dynamic Shear Rheometer

PAV.....Pressure Aging Vessel

LIST OF SYMBOLS

G*……. Complex modulus

δ……. Phase angle

S(60)…….. Creep stiffness

m-Value……. Rate of the change in creep stiffness by time

CHAPTER ONE. INTRODUCTION

In service conditions, the rheological and performance behavior of asphalt are mainly influenced by its chemical and molecular characteristics. Correlation between the chemical and molecular characteristics of asphalt and how they affect its internal network buildup structure leading to changes on its serviceability can be a way to approach the optimum goal of controlling the properties of asphalt in service conditions. To accommodate for the ever increasing traffic loadings in varying climatic environments and to have asphalt being able to resist failures such as permanent deformation, cracking and water damage, major emphasis was placed on improving the level of performance and service life of roads. For improving the asphalt characteristics and overcoming potential deficiencies, specific performance enhancers were investigated. These include crumb rubber modifier (CRM), polymer modifier (PM) and chemical reaction modification. A better understanding of the asphalt behavior and its interaction with modifiers such as CRM and how they alter the internal network structure of the modified asphalt would enable for a more controlled service behavior and would allow for choosing the optimum asphalt-CRM mix that withstands the anticipated lifetime serviceability without any premature failure.

Problem Statement

The investigation of the macro scale rheological behavior of CRMA has been extensively carried out. However up to this point, no clear correlation between the changes that occurred in the modified asphalt, in terms of property enhancement or deterioration, and the development of the internal network structure within the modified asphalt as a result of interaction of asphalt with CRM has been established. In addition, although the effect of development of internal network structure within the polymer modified asphalt has been found to be profoundly enhancing the asphalt's rheological properties. However, up to this point no study has been dedicated to in-

vestigate the development of internal network structure within the CRMA and how such internal network structure affects the modified asphalt properties. The nature of the constituents that migrate from/into CRM into/from the asphalt and how they affect the modified asphalt internal network structure buildup needs to be further investigated. Although, changes occurring the modified asphalt can be foreseen from the enhancement or deterioration obtained in rheological, performance, and storage stability test results, however the factors controlling the nature of enhancement or deterioration has not been fully characterized. The establishment of a correlation between the types of components exchanged between asphalt, CRM, and the development of the internal network structure in modified asphalt needs to be further elaborated. Although the rheological approach provides evidence for the occurrence of modification in the modified asphalt internal network structure; however the nature and factors responsible for such modifications can't be explained by the utilization of rheological approach alone. The need for employment of other techniques that are able to explain the internal network structure changes of modified asphalt during CRM interaction with asphalt thus arises. Techniques such as Fourier Transform Infrared (FTIR) Spectroscopy, Gel Permeation Chromatography (GPC) and Thermogravimetric Analysis (TGA) can provide a direct approach to better elucidate the nature of the interaction between CRM and asphalt and how they alter the modified asphalt internal network structure. This arises from the fact that the macro-scale (rheological) properties are in fact a demonstration of the micro, nano, and molecular scale interactions that lead to the occurrence of changes within the modified asphalt internal network structure during the interaction between asphalt and CRM. Investigation of the nature of changes within the modified asphalt internal network structure as a result of interaction of asphalt with CRM that are obtained from the aforementioned characteri-

zation techniques can provide a direct approach to synthesis a modified asphalt with enhanced in-service properties.

Objective

The aim of this study is to investigate the changes that occur to the modified asphalt internal network structure after interacting with modifiers such as CRM. The understanding of changes occurring in the internal network structure of modified asphalt and the mechanisms through which they are developed would provide a better route to establish a correlation between the types of components exchanged between asphalt, CRM and the performance related properties and storage stability of modified asphalts. This would lead to obtaining better in-service performance for the modified asphalts. The determination of the effect of variation of the asphalt-CRM interaction parameters (interaction time, speed, and temperature) and how they affect the development of the internal network structure of the modified asphalt would be the proper means to explore the tendency to improvement within the modified asphalt's serviceability characteristics. This would be achieved through studying the factors behind the changes occurring in the modified asphalt internal network structure as a result of interacting with modifiers such as CRM and how that relate to the measured physical properties.

Approach

To accomplish the objectives of the proposed work, asphalt-CRM interactions will be carried out under diverse conditions of interaction time, temperature and mixing speeds. The effect of the aforementioned interaction conditions on the development of the internal network structure within the modified asphalt would be investigated. Detection of the existence of the internal network structure in the modified asphalt would be carried out for the asphalts synthesized under different interaction conditions. Effect of raw materials variation in terms of asphalt types

and CRM types and concentrations on the internal network structure development in the modified asphalt would be studied. The characterization of the developed internal network structure would be investigated. The effect of the CRM dissolved amounts and components under the different interaction conditions on the modified asphalt internal network structure development would be carried out. Dynamic mechanical analysis would be carried out to detect the existence of the internal network structure in modified asphalt and also to investigate the physical changes occurring to the modified asphalt and liquid phase (asphalt after CRM extraction) as a result of the development of internal network structure. The changes on the molecular size distribution as a result of internal network structure development would be investigated. Storage stability tests would be carried out on the modified asphalt to determine the effectiveness of the developed internal network structure. The effect of internal network structure development on the changes in micromechanical properties of modified asphalt would be investigated.

CHAPTER TWO. LITERATURE REVIEW

Introduction

Approximately 300 Million scrap tires were generated within the US in 2005, of which 14% have been landfilled [2]. The disposal of scrap tires in landfills encompasses two major problems: wasting of valuable materials and environmental pollution hazards. Multiple approaches have been utilized in waste management systems to alleviate the aforementioned problems so as to create market for scrap tires [3]. Most of the scrap tires have been employed in markets like: tire derived fuels, civil engineering raw materials and ground rubbers. In 2005, the consumption of each of those markets was roughly 52%, 16% and 12% of generated scrap tires, respectively [2]. A very significant capacity to use scrap tires among all those approaches has been seen for tire derived fuel markets despite their very low value recovery process of waste rubbers and associated air pollution problems. This in turn strengthen the utilization of scrape tires in the other two markets, based on economical as well as environmental friendly justifications with significant potential for growth [4]. Natural rubber (NR), Polyisoperene, and synthetic rubber (SR), Styrene-Butadiene Rubber and/or Butadiene Rubber cross-linked with sulfur and reinforced with Carbon Black (CB) are the constituents that make up the complex engineered vulcanized compound known as tire rubber. To improve the workability and softness of tire rubber and to prevent aging and oxidization, other additives like aromatic hydrocarbons and antioxidants have been utilized in its synthesis [5]. In mid 1960s, the approach of utilizing ground tire, known as Crumb Rubber Modifier (CRM), for the surface treatment of asphalt pavements was initially introduced. Later in the 1970s, the utilization of CRM as an asphalt modifier expanded to hot mix asphalt industry [4]. The dry process and wet process are the two main methods of employment of CRM in asphalt modification. In the dry process, CRM is added to preheated ag-

gregate before introducing the asphalt into it. On the other hand, in the wet process the CRM is interacted with asphalt before adding asphalt to aggregate [4]. The wet process received most of the attention of researchers and industries because of its relatively lower production cost and associated enhanced final product performance [4, 6].

In 1990s, the Strategic Highway Research Program (SHRP) set definitions for the performance related properties of asphalt and modified asphalt [7]. Three major binder related distresses, with their mechanism of development on pavement, define Asphalt binder properties. Those are rutting, fatigue cracking, and thermal cracking. The dissipation of energy on pavement via permanent deformation and micro-cracks, are the two mechanisms with which rutting and fatigue cracking are developed, respectively. Rutting, which occurs at high service temperatures is initiated as a result of the dispersion of the applied energy through viscous deformation of material. The viscous deformation of materials leads to the permanent deformation of the pavement as a result of the dispersed energy creating distresses in the pavement. In rutting, the amount of the work dispersed correlates to $\frac{G*}{\mathrm{Sin}(\delta)}$, where G* is complex modulus that relates to stiffness and δ is the phase angle that relates to elasticity. Thus preventing rutting through improving the physical properties of the asphalt can be achieved by increasing its stiffness and/or increasing its elasticity. This means higher complex modulus (G*) and lower phase angle (δ). On the other hand, fatigue cracking, which occurs at intermediate service temperatures of the pavement, results from the dispersion of applied energy through creation of micro-cracks leading to the creation of cracks on pavement. In fatigue, the dispersed energy can be defined by G*. Sin(δ). Thus preventing fatigue cracking can be achieved by decreasing asphalt stiffness through lowering the G*, and/or increasing the elasticity by decreasing the phase angle (δ). The third main asphalt distress is thermal cracking. Thermal cracking takes place as a result of sudden decrease in temperature

leading to rapid contraction of the pavement layers. If the formed internal stresses exceed the stress relaxation ability of the binder as a result of the fast pavement contraction, this eventually leads to the creation of cracks in the pavement. To alleviate the thermal cracking problem in asphalt pavements, the stiffness of the asphalt binder should be decreased, while the rate of the stress relaxation, m-value, must be increased. On the other hand, as asphalt ages and hardens during its service life, the stiffness, elasticity and stress relaxation ability of the asphalt changes. This in turn affects the occurrence of the aforementioned distresses. In addition, each of the aforementioned asphalt distresses occurs at different periods of the lifetime of the pavement. At early ages of the pavement (2 to 3 years after construction), rutting can be observed because the asphalt's stiffness is at its minimum level. However, the opposite can be seen for thermal and fatigue cracking as both occur at the end of pavement life (after 7 to 10 years), as a result of the significant increase in the stiffness of the pavement because of asphalt binder aging. According to the SHRP grading system, before having the asphalt binders tested they undergo aging at two levels, short-term aging through Rolling Thin Film Oven (RTFO) and long term aging through Pressure Aging Vessel (PAV), to predict the binders' behavior at different ages.

The asphalts molecular attributes, microstructure, and composition strongly influence the binders' stiffness and elasticity. The nature and extent of the internal network structure in the asphalt matrix heavily affects the elasticity of asphalt. On the other hand, the average molecular weight and polarity of asphalt relates strongly to the stiffness of the asphalt [8]. Thus the characterization of the effect of a given modifier on the molecular behavior and composition of the asphalt and how the modifier affects asphalt's internal network structure represents a major importance. CRM changes the asphalt's properties in different manners. It alleviates the rutting problem [9-11] and fatigue cracking [12, 13] of the binder. On the other hand, there is conflicting

opinions about its role with low temperature cracking. This stems from the fact that CRM decreases the stiffness of asphalt at low service temperatures and thus leading to improvement in low temperature behavior of asphalt [10, 14-16], however, it decreases the rate of stress relaxation which negatively affects low service temperature performance of asphalt [6, 17]. Another major drawback of CRM is its severe deteriorating effect on the storage stability of asphalt as a result of separation of CRM particles from the liquid phase of asphalt during storage and handling of CRM Asphalt (CRMA) at high temperatures [11, 18]. Due to the complexity of the CRM, throughout the interaction with asphalt its composition and structure continues to change. This in turn alters the composition and molecular structure of asphalt matrix leading to the development of the asphalt's final physical properties. Swelling [19] and dissolution [14, 20] are the two main mechanisms with which CRM interacts with asphalt. Swelling is the governing mechanism at low interaction conditions when CRM particles absorb light molecular weight components of asphalt and increase in their size up to 5 times from their original size [19, 21, 22]. However, upon increasing the interaction temperature or interaction time or both, CRM particles start dissolving into the asphalt matrix and release their components into the asphalt matrix [21, 23].

The behavior of CRM during the interaction with asphalt is attributable to multiple factors [21, 24]. Generally, those factors can be categorized into two main aspects; interaction parameters and material parameters [24]. Interaction parameters are those dealing with temperature, mixing speed, and time. Material parameters, on the other hand, deal with both the CRM attributes and asphalt properties. CRM attributes such as CRM source, processing method, size, and concentration should be considered. Asphalt properties include; its grade, chemical composition or molecular weight distribution. The utilization of different interaction parameters leads to

different CRM particles behavior that results in modifying the asphalts' properties differently. Modification of the physical properties of asphalt occurs when the CRM particles swell as a result of the absorption of the asphalts' low molecular weight components and behave as elastic fillers in asphalt leading to an increase in the asphalts' viscosity and complex modulus [19, 25]. The change in the CRM composition, as a result of dissolution and partial release of CRM components in the asphalt matrix, and the utilization of the remaining swollen particles within the asphalt improves asphalt viscoelastic properties [10, 14]. Each CRM particles' component can individually interact with asphalt constituents and eventually change asphalt properties. Multiple research works have investigated the effect of each of these individual components on asphalt modification [15, 26-28]. Carbon black has affinity with the asphaltene portion of asphalt as a result of its high polarity [26]. Natural Rubber (NR), on the other hand, shows more compatibility with asphalt in comparison to Synthetic Rubbers (SR). In synthetic rubber such as the Styrene-Butadiene Rubber (SBS), the poly butadiene block of the SBS show higher compatibility with asphalt components than the styrene block that acts mostly as a crosslinking agent [29, 30]. Additionally, antioxidants present in CRM can prevent asphalt from oxidation [31]. Thus, it is important to investigate the effect of release of each of these components from CRM during interaction with asphalt and their possible contribution in asphalt internal network structure modification. In addition, it becomes of essential importance to investigate the effect of different parameters (interaction and material) on crumb rubber modified asphalt (CRMA) internal network structure behavior during the interaction with CRM.

Origin of Networks in Asphalt

Asphalt is a hydrocarbon material containing about 90-95%wt hydrogen and carbon atoms with the remaining 5-10 % of the atoms in the asphalt consisting of two types: a) Heteroatoms and b) Metals [1].

Heteroatoms

These are nitrogen, oxygen, and sulfur atoms. They are called so because they can replace carbon atoms in the asphalt molecular structure. They are responsible for the hydrogen bonding in asphalt which contributes for many of the asphalt's unique chemical and physical properties as a result of forming associations between molecules. The hydrogen bonding arises from the polarity of a given molecule as a result of heteroatoms presence. Heteroatoms type and amount are a function of both the crude oil(s) from which the asphalt was produced and the state of aging of the asphalt. The aging of asphalt is deeply affected by heteroatoms, especially sulfur, due to their increased chemical reactivity over hydrogen and carbon which leads to their vulnerability to oxidation over hydrocarbons. Although aging is not merely oxidation, as it incorporates other processes that occur when asphalt is exposed to the environment such as loss of volatiles through evaporation or other degradation, attack by water and light, yet oxidation is a governing factor in such processes [1].

Metals

Atoms such as vanadium, nickel, and iron that are present in very small quantities in the asphalt, usually less than 1%, represent the metals subcategory in asphalt chemical composition. Such metals may play an important role in the aging process [1].

Asphalt Molecular Groups

Various models have been adopted to explain the networks in asphalts. One of the most prominent models explain the network in asphalt in terms of the molecules that forms up the asphalt. Hydrocarbons, heteroatoms, and metals all combine in the asphalt in a wide range of different molecules that can be grouped into three major categories: a) aliphatics, b) cyclics and c) aromatics [1].

Aliphatics

The aliphatic molecule hexane contains six carbon atoms and fourteen hydrogen atoms. From this it can be understood that the term aliphatic (literally, "oily") can best be described as a linear or chain-like in which the carbon atoms are linked end to end [1].

Cyclics

In such molecules two hydrogen atoms are given up to form a cycle, or ring, where the molecule has six carbon atoms with two less hydrogen atoms than hexane [1].

Aromatics

They are named so for their strong odor, they are characterized by forming a "ring" of aromaticity, or shared electrons. The aromatic benzene ring has six-carbon and only six hydrogen atoms in its structure [1].

It should be elaborated that the most important effect that aromatics bring to asphalt is their flat shape, whereas cyclics and aliphatic molecules are three-dimensional and form shapes that keep the molecules apart, aromatics are flat and can closely stack on top of one another.

To understand how the chemical changes associated with each molecule affects the asphalt properties; a comparison between the boiling and freezing points of the three molecules illustrates that they show different boiling and freezing points. Hexane which is an aliphatic hy-

drocarbon has a boiling point of 69°C and a freezing point of -95°C. On the other hand, cyclohexane , a cyclic hydrocarbon, has a boiling point of 81°C and a freezing point of 6°C. Benzene, an aromatic, has a boiling point of 80°C and a freezing point of 5°C [1].

Effect of the Structure on the Physical Properties

In all the molecular configurations discussed earlier the interaction between atoms was through the formation of strong covalent bonds. Such molecules can then interact with one another through the formation of other much weaker types of bonding that are actually responsible for determining many of asphalt's physical properties. Three types of "weak" bonds that require relatively little energy to break and are susceptible to both heat and mechanical forces are mainly the governing bonds in asphalt aside covalent bonds, which are; a) pi-pi bonding, b) hydrogen (or polar) bonding and c) Van der Waals forces [1].

Pi-Pi bonding

In this bonding, stacks of molecules are formed by the aromatic molecules due to their flat shape resulting in the interaction of the electrons in the aromatic rings forming such bonds. Such interaction is only manifested in the aromatic molecules and results in the molecules ability to easily slide around on top of one another. pi-pi bonding depends on the amount and type of aromatic molecules present in a given asphalt [1].

Hydrogen (polar) bonding

The presence of heteroatoms within a molecule usually renders it polarity characteristics; this typically affects asphalt's physical properties by interacting with other molecules through the formation of hydrogen bonds. Such bonds are present as a result of the interaction of a heteroatom on one molecule with a hydrogen atom next to a heteroatom on a different molecule. The formation of hydrogen bonds involves the presence of two heteroatoms. Heteroatoms play a cru-

cial role in determining the physical properties of asphalt cements; this in turn makes hydrogen bonding probably the most important form of weak molecular interactions. Hydrogen bonding depends on the number of heteroatoms present in a given asphalt [1].

Van der Waals forces

This involves the interaction between long chains of aliphatic hydrocarbons to intertwine. This type of bonding is dependent on the amount and type of aliphatic molecules in a given asphalt [1].

Asphalt Chemical Makeup

According to Jones and based upon the research done by Strategic Highway Research Program (SHRP) researchers, the following can be attributed to asphalt chemical makeup:

- Asphalt consists of two functional families of molecules: a) Polar and b) Non-polar.
- Polar molecules are characterized according to their: a)Strength and number of polar group(s), b) Molecular weight and c) Degree of aromaticity
- Non-polar molecules are characterized according to their: a) Molecular weight, b) Degree of aromaticity
- The degree to which the polar and non-polar fractions can dissolve in each other, or their "compatibility", is controlled by the relative aromaticity of the two fractions [1].

Behavior of Asphalt Molecules

The behavior of asphalt molecules is governed by either one of two ways and their mutual interaction; a) Polar behavior and b) Non polar behavior. In the polar behavior and during service temperatures, the molecules participate in the formation of a "network" through hydrogen and pi-pi bonding that gives the asphalt its elastic properties. Whereas, the non-polar molecular behavior is manifested by matrix in which the network is formed, thus contributing to the viscous

properties of the asphalt. In such categorization, weakly polar molecules are considered non-polar [1].

Polar molecules behavior

As explained earlier, these molecules will participate in the formation of the network with a wide range of molecular types and sizes. This results in their contribution to the performance of the asphalt through the network. Owing to their direct effect on the network formation, the relative strength and number of polar sites per molecule are considered to be the most important attribute of the polar molecules. “Nonaqueous-acid-base titration” is the technique used to determine the amounts of polar materials present in asphalt. On the other hand, nuclear magnetic resonance (NMR) analysis technique is used to determine another important parameter affecting polar molecules, which is the degree of aromaticity. The molecular weight of the polar molecules is not as important as strength of polarity and aromaticity in controlling the performance of asphalt [1].

Non-polar molecules behavior

Unlike Polar molecules, the molecular weight of Non-polar molecules is a major factor affecting the performance of asphalt as it directly affects its low-temperature cracking properties. An abundance of high molecular weight non-polar molecules will lead to asphalts that stiffen and perform poorly at low service temperatures due to brittleness [1].

The degree of aromaticity of the non-polar materials controls the performance of asphalt at low temperature, non-polars that are waxy (a type of aliphatic molecule) in nature may precipitate or crystallize at low temperatures, resulting in poor performance. This behavior can be overcome if the non-polars are cyclic or aromatic in nature [1].

Compatibility between Polar and Non-Polar Molecules

The importance of non-polar molecules arises from that fact that they are the substance in which the polar molecules must interact, thus their compatibility with the polar molecules must be considered. Similar chemistry molecules will mix easily and be compatible, whereas different chemistry molecules will be incompatible leading to segregation in the solution [1].

The amphoterics

The term amphoterics means an asphalt molecule that has both an acid and basic group in the molecule, but not at the same site. An example of this would be a carboxylic acid (COOH).

Another example would be the sulfoxide (S=O) on the same asphalt molecule [1]. Amphoterics have been found to relate excessively to the viscoelastic behavior of asphalt as a result of their contribution to the formation of the previously mentioned asphalt network, owing to their acidic-basic site per molecule property. Thus during aging, the production of polar materials is not in itself sufficient to cause major changes in the physical properties of asphalt. It is the generation of amphoteric molecules in nature that causes significant physical property changes [1].

Polar-polar interactions, pi-pi interactions of aromatic rings and the Van der Waals interactions of the long-chain hydrocarbons are the predominant behavior of asphalt molecules in the tank, or unaged state. Because these bonds are weak and easily broken by heating, asphalt's Newtonian behavior prevails at elevated temperatures. Aging process results in the oxidation of potential sites such as benzylic hydrogen and aliphatic sulphur into carbonyls and sulfoxides, respectively. These add to polar-polar interactions, leading to increased viscosity at service temperatures. Such increase will be modest because these are still weak bonds and the asphalt will continue to behave as a Newtonian fluid at mix temperatures. However if the molecules within asphalt has two or more active sites per molecule , which are points where oxidation can take

place or a point of an oxidized atom, then many new sites for polar-polar interactions will allow for the formation of chains between numerous molecular associations, thus resulting in large increase in both viscosity and physical properties [1].

The effect of nonpolar molecules in asphalt

Nonpolar molecules in asphalt plays a major role in affecting the properties of both the asphalt and the pavement as they make critical contribution to the low-temperature properties of the pavement, where they align themselves, resulting in shrinkage of the asphalt volume. This shrinkage, if too sever, will cause thermal cracking, as it happens without crystallization. This is a function of their molecular weight and shape, which could prevent collapse and retard low-temperature cracking.

A second contribute-on of the nonpolar molecules is their role as a solvent for the polar materials, allowing for the formation of associations between the later. A balance between the amount of both the polar and non-polar molecules in the asphalt should be achieved to attain improved service conditions for pavement, otherwise pavement damage can occur [1].

The Proposed Relationship between Chemistry and Pavement Performance

The interaction between polar molecules in the asphalt results in the formation of associations within asphalt, associations provides the later with its physical properties. Such properties are also impacted by the nonpolar “solvent” fraction, around and through which the associations of polar molecules form [1].

Based on the aforementioned information it is clear that asphalt poses a complex chemical structure that leads to its complex physical and rheological behavior [32, 33]. This is due to the fact that asphalt is a byproduct of the distillation process of crude oil and thus is made up from various hydrocarbons including the extreme polar, extreme aromatic, and largest molecular

weight components of crude oils. Asphaltene and maltene are the two distinct groups of materials that make up asphalt [34]. Asphaltene is made up through the agglomeration of the most polar components of asphalt and thus it is considered the most complex part of asphalt. The viscosity development of the asphalt is mainly attributed to asphaltene as it has the highest tendency for association with other components. On the other hand, maltene is composed of resins, waxes, aliphatic, and aromatic compounds. Asphaltene molecules can be described as micelle components dispersed and stabilized in the maltene [35]. Asphaltene is the only asphalt fraction that is insoluble in aromatic solvents. Atomic Force Microscopy (AFM) and X-ray diffraction (XRD) were utilized by multiple researchers to investigate the physical structure of asphaltene [36-39].Based on some of those research work, it is hypothesized that asphaltene is made up of layered structures with interlayer distance of approximately 3.6 A°. “Gel-type” asphalts and “Sol-type” asphalts are two proposed categories for asphalt types [40]. Based on that categorization, “Gel-type” asphalts poses insufficient aromatic and maltene fractions to fully disperse (peptize) the asphaltene fraction; whereas, “Sol-type” asphalts on the other hand have enough aromatic components and resins to properly peptize the asphaltene particles and thus cannot form an extensive microstructure. This in turn yields the asphaltene in Gel-type asphalts to form large agglomerations which can, in extreme circumstances, form a continuous network structure throughout the asphalt [40]. The dispersion state of the asphaltene in asphalt matrix is the governing parameter for the determination of the asphalt type [40]. Based on such asphaltene dispersion state, the different physical properties of asphalts are affected. High temperature susceptibility, high ductility, and low rates of age hardening are mostly attributable to “Sol-type” asphalts. On the other hand, opposite physical behavior can be seen for the “Gel-type” asphalts. Most asphalts’ behavior lie in between those two types of asphalts [40].

The viscoelastic behavior of asphalt is attributable to the complex chemical composition of asphalt and the internal association between its components. Being viscoelastic translates to having the asphalt's physical properties highly dependent on loading rate and temperature. At high temperatures or low loading rates, asphalt acts as a fluid, whereas, at low temperatures or high loading rates it becomes very brittle and stiff [33, 41]. This leads to having the traffic load in different climatic environments deterministic to the asphalt pavement in-service behavior. To resist rutting or permanent deformation distresses, the asphalt pavements should poses stiffness at high temperatures. On the other hand, to resist thermal cracking, the asphalt pavement should be flexible enough to disperse the energy through deformation rather than micro cracking at very low temperatures. To accommodate for the increasing traffic in different climatic environments, these pavement functionalities are required. The conventional asphalts physical performance doesn't accommodate the continuously increasing demand of today's roads that require increased traffic loads and volume. This in turn calls for the utilization for different types of modification to improve the pavement performance based on current needs [21].

Figure 2.1 illustrates the proposed network model and its building molecules in asphalts as envisioned from the literature review and based on the work of Jones [1].

Origin of Network in Crumb Rubber Modifier

A complex engineered vulcanized compound synthesized from Natural Rubber (NR), Polyisoperene, and Synthetic Rubber (SR), Styrene-Butadiene Rubber and/or Butadiene Rubber that are highly cross-linked with sulfur and reinforced with Carbon Black, makes up a car or a truck tire. Aromatic hydrocarbons and antioxidants are also added to improve the workability and softness of a tire as well as to eliminate its aging and oxidization, respectively [5].

Table 2.1 illustrates the average amount of such components in a tire. Originally, a tire is engineered to be durable and to withstand harsh weathering and loading conditions. Taking into consideration the synthesis procedures as well as components involved in the manufacturing of a tire make it almost impossible to recycle [3]. Crumb rubber is the waste tire rubber that is shredded into small particle sizes less than 6.3 mm. Ambient and cryogenic shredding are the two methods employed for the size reduction of waste tire rubber. The waste tire rubber particles are shredded into smaller sizes, with the steel and fiber components removed. The difference between ambient and cryogenic methods is mainly the processing temperatures. The tires areshredded into fine particles using ground mill at ambient temperature for the former, while they undergo size reduction to fine particles at freezing temperature for the later.

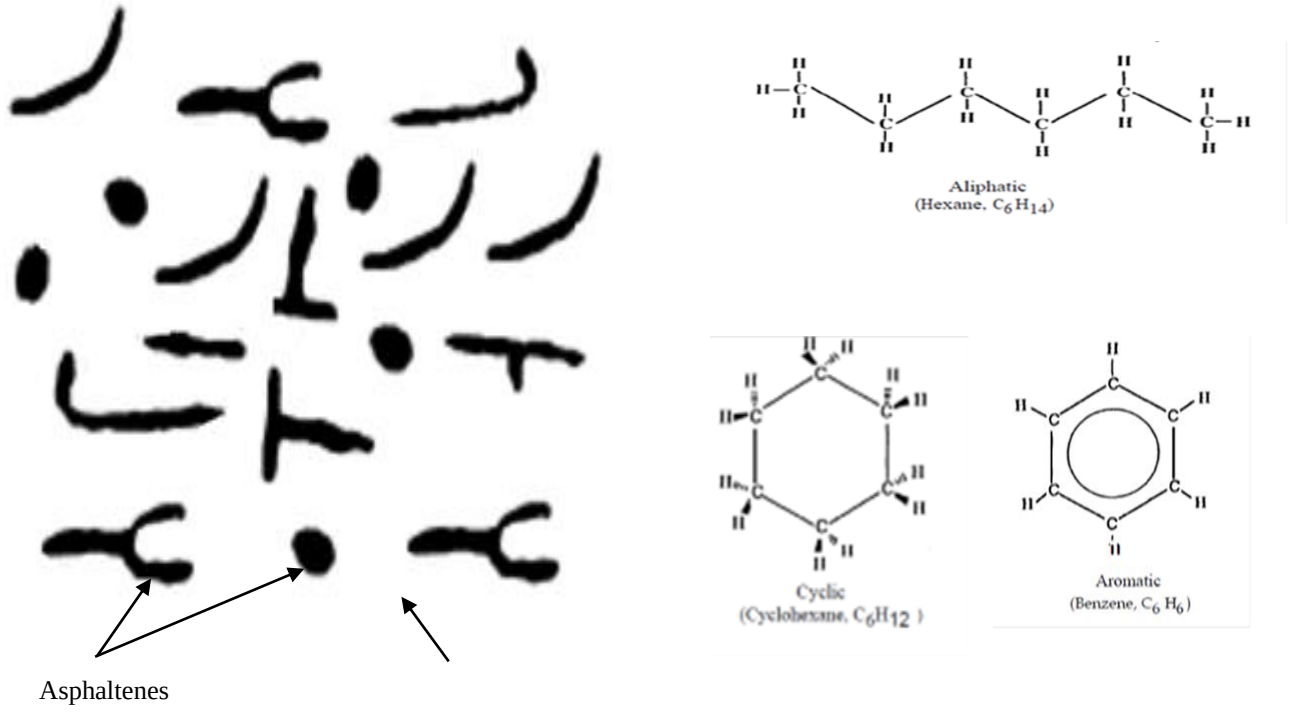

Figure 2.1. Suggested model for networks in asphalts [1].

The CRM particles morphology and surface characteristics are defined in terms of the processing methods of CRM [19, 42]. CRM processed through the cryogenic method poses very smooth and regular surface in contrast with the one produced by the ambient method. This leads to having the former of a lower interaction rate with asphalt [4].

Table 2.1.Typical composition of CRM

Component	Weight %
Natural rubber	19. 4
Synthetic rubber	37. 5
Carbon black	20. 8
Fabric, fillers, accelerators, antioxidants, etc.	22. 2

The gradation size of CRM particles also poses an important role in the determination of the rate of reaction between asphalt and CRM as it alters the CRM's average surface area of particles. The finer the CRM size the more reactive it is with asphalt as a result of the increase in the contact surface area [9].

The source of the CRM is also important as it affects the attributes of the CRM. The three main sources for CRM are passenger car tires, truck tires or a mix of both sources. Compared to passenger car tires, truck tires have more natural rubber in their composition. The compatibility of the CRM extracted from different tire sources with asphalt varies depending upon the source it was produced from due to the difference in chemical composition. This will be highlighted more hereafter.

How CRM Affect the Network Structure in Asphalt

The "Dry Process" and the "Wet Process" are the two main methods with which CRM is added to asphalt. Both methods were developed in the late 1960s [4]. In the Dry Process, the CRM substitute part of the fine aggregate in the asphalt mix as it is to the aggregates before in-

troducing the hot asphalt binder. The Dry Process was introduced in Sweden under the trade name of Rubit and was later registered in US under the trade name of Plusride. One of the drawbacks of this method is that it substantially increases the amount of asphalt needed for the mix leading to the increase of the construction costs. In the "Wet Process" the CRM is added to the asphalt binder before being mixed with aggregate [6]. In such method, the interaction between asphalt and CRM occurs at high temperatures for certain amount of time. CRM swells and modify the properties of the asphalt as a result of the utilization of high interaction temperatures along the interaction time. Both of the aforementioned techniques requires that the extracted rubber from waste tires is ground into small particle sizes ranging from 25 micron to 425 micron sieve. This mandates the preprocessing of the rubber extracted from waste tires [4]. Among these two processes, wet process got the attention of researchers and industries due to its better performance and relatively lower production cost along with more application for its final products [4, 6].

Different interaction conditions can be utilized for the addition of CRM to the asphalt. In the early stages of the wet process in 1960s, CRM was interacted with asphalt at 170°C for 45 min [19]. However, different interaction temperatures and mixing speeds were utilized by other researchers to interact the CRM with asphalt. This was done in an aim to understand the effect of interaction parameters on the property development of modified asphalt as related to the interaction mechanism between CRM and asphalt.

Effective Parameters

Multiple parameters are utilized for the interaction between asphalt and CRM. Several researchers have investigated the effect of each those parameters.

Two major categories can be utilized to address the effective parameters involved in the interaction between CRM and asphalt; interaction parameters and material parameters.

Interaction parameters are those dealing with interaction aspects between asphalt and CRM. These parameters involve the following; Interaction temperature, interaction mixing speed, and interaction time. For the interaction temperature, a typical number would be around 170˚C, whereas for the interaction mixing speed, 10Hz is mainly the used number in industry. An interaction time ranging from 45 min to 60 min is generally used in industry. Although those interaction parameters are typically used in the industry, they have been found to be not optimum production condition [14]. According to the results of Abdelrahman et al., the physical properties of the crumb rubber modified asphalts (CRMA) are improved after prolonged time at very low interaction temperatures (i.e. 160˚C and 10Hz) whereas, at higher interaction conditions (i.e. 190˚C and 30Hz) the properties are improved in the early stages of the interaction and later on the interaction time they start to degrade. On the other hand when utilizing high interaction conditions (i.e. 220˚C and 50Hz), the physical properties of the asphalt rubber deteriorate just after the beginning of the interaction [21, 24, 25].

The other category of parameters is the material parameters that include the properties of asphalt and CRM that contribute into the CRMA final properties. The asphalt properties can be summarized as; asphalt source, and asphalt grade. On the other hand, the CRM properties are; CRM source, CRM processing technique, CRM concentration, and CRM size.

Bahia et al. stated that the asphalt properties have more influence on the final properties of the CRMA than the CRM attributes [9]. In their work, the authors employed low interaction temperature and speed only, thus their conclusions can’t be generalized to other interaction conditions [9]. The utilization of ambient processed CRM with small sieve size particles leads to

higher rate of interaction with asphalt as a result of the increased CRM specific surface area exposed during the interaction. This leads to the acceleration of the interaction process. In addition, the swelling rate of CRMA is influenced by the source of tires that alters the composition and cross linking in the CRM particles [43]. Heitzman et al. related the high natural rubber content in CRM from truck tires to their higher compatibility with asphalt over CRM from passenger car tires [5, 44]. On the other hand, based on the solubility parameter of the CRM components and asphalt components, the synthetic polymer components should have had better compatibility with the aromatics fractions of asphalt over the natural rubber ones [22].

How the Network Structure Affect the Elasticity of Asphalt as a Result of Addition of CRM

Researchers have concluded that the interaction between asphalt and CRM is not chemical in nature [9, 45]. The light molecular components of asphalt are absorbed by the CRM at low interaction conditions leading to their swelling up to 3 to 5 times from their original size [4]. The utilization of higher temperature, mixing speeds and time leads to the degradation and dissolution of the CRM particles into the asphalt matrix [14, 21, 24].

As explained earlier, Abdelrahman et al. showed that the utilization of low interaction conditions leads to the continuous swelling of CRM throughout the interaction time and subsequently improves the high temperature physical properties of CRMA [21, 24, 25]. Other researchers showed the same observations [19]. On the other hand, the utilization of higher interaction conditions leads to the swelling CRM particles at the early stages of interaction time and employing more time into the interaction leads to the degradation of the CRM particles. Utilizing extreme interaction conditions (i.e. 220˚C and 50Hz) leads to the instant degradation of the CRM particles and consequently the continuous deterioration of the high temperature physical properties of the asphalts along the interaction time until they finally level [21, 24].

To properly address the behavior of CRM in the presence of asphalt, we discuss the analogy of polymers in solvents. Generally, the diffusion of small molecules of solvent into the structure of polymers leads to their swelling. The behavior of polymers in solvents varies based on their molecules arrangement. Amorphous polymers will swell as a result of diffusion of small molecules of solvent. This results in the change of the polymer into a gel state, later on, the polymers molecules start diffusing into the solvent. On the other hand, the mechanism of swelling is different for cross-linked polymers. At the early stages of crosslinked-solvent interaction, the polymer would swell as amorphous polymers and change into gel. However, unlike amorphous polymers, the swelling process in cross-linked polymers equilibrates resulting in having no diffusion of polymer chains into the solvent.

For CRM particles, being highly cross-linked means that they follow the behavior of those of cross-linked polymers. However, the swelling process of CRM particles occurs in a much longer path as a result of the relatively high molecular weight of asphalt. In addition, a different behavior for the dissolution of CRM in asphalt can be observed in comparison with the diffusion of amorphous polymeric components in the solvent. The swelling mechanism of CRM in asphalt has been thoroughly addressed in the literature [19]. Devulcanization and partial depolymerization of CRM have been observed along with their dissolution. The absorption of light molecular components of asphalt by CRM particles has been previously recorded [43]. The rate of swelling of CRM was found to be dependent on the viscosity of the asphalt. Faster swelling rate of CRM particles is attributable to the lower viscosity of asphalt. In addition, the asphaltene fraction of the asphalt was found to have minimal effect on the swelling process of the CRM particles as the asphaltene content of the residual binder increases significantly after interaction with CRM [43]. On another work investigating the component exchange between the CRM and as-

phalt during interaction, it was shown that the linear chain structures aliphatic components of the asphalt penetrate to the CRM particles leading to the release of fatty acids from CRM particles into the asphalt matrix [22].

Based on the CRM activities during its interaction with asphalt explained earlier, Figure 2.2 illustrates the suggested model for CRMA network system. An explanation for the asphalt physical properties as affected by such network development will be explained hereafter.

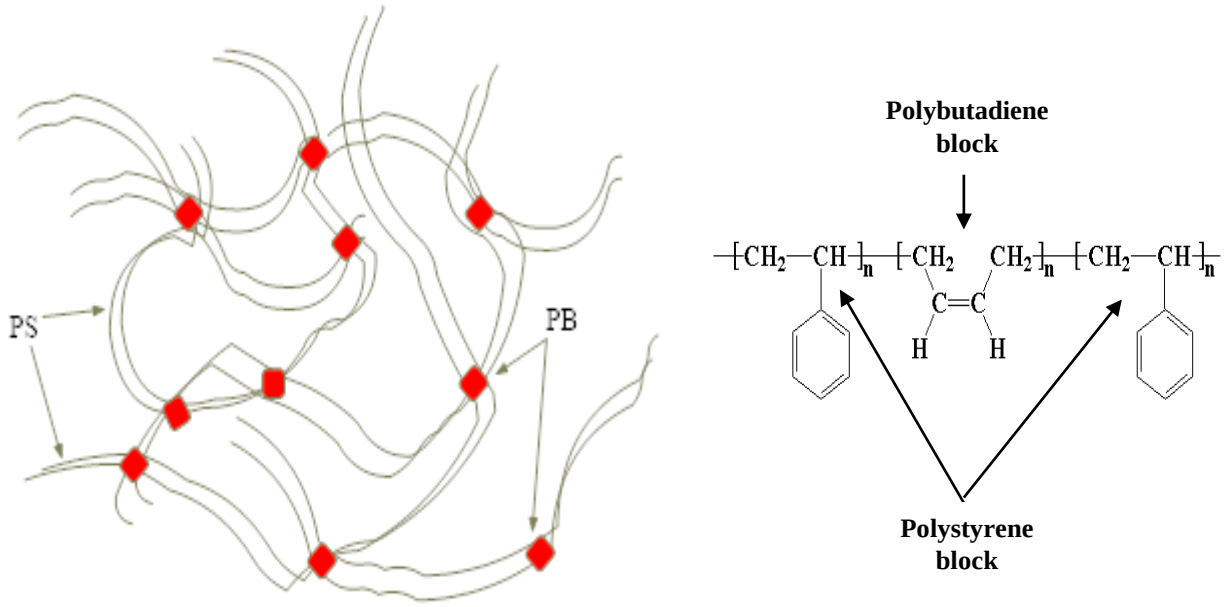

Figure 2.2. CRMA suggested network model.

The asphalt physical properties development is negatively affected by the presence of the CRM particles in swollen condition [10, 23]. According to the disintegration and devulcanization-depolymerization behavior of CRM under different interaction conditions; as the temperature and time of interaction of asphalt and CRM increase the disintegration of CRM particle is initiated leading to the release of its components into the asphalt in the form of polymeric chains. Increasing the mixing speed of the interaction leads to the acceleration of the CRM disintegration that can result in depolymerization of released polymeric chains [10, 23]. In addition, the ex-

treme increase in the interaction temperature (i.e. above 240˚C) leads to the complete disintegration of CRM components released to the asphalt matrix, Whereas cleavage of the polymeric chains will occur as a result of the increase of the interaction time. This was evident by the decrease in the average molecular weight of asphalt [14, 20]. The devulcanization-depolymerization of CRM particles in asphalt is heavily affected by the chemical composition of asphalt. Asphalts with higher amounts of aromatics dissolve CRM more readily [23]. This is attributable to the higher rate of diffusion of aromatics in CRM particles. In addition, asphalts with higher asphaltene and polar components content depolymerize the released polymeric components of the CRM faster [14].

To better understand the network formation mechanism resulting from the CRM component release in asphalt, we would resort in the next sections to discuss the types of internal networks in non-asphaltic and asphaltic materials.

Types of Internal Networks in Non Asphaltic and Asphaltic Materials

Interpenetrating Polymer Networks

(IPNs) are defined as a combination of two or more polymers in network form that are synthesized in juxtaposition. Most IPNs do not interpenetrate on a molecular scale; they may, however, form finely divided phases of only tens of nanometers in size. Many IPNs exhibit dual phase continuity, which means that two or more polymers in the system form phases that are continuous on a macroscopic scale [46].

Kinds of IPNs

IPNs can be made in many different ways. Brief definitions of some of the more important IPN materials are as follows:

• **Sequential IPN.** Polymer network I is made. Monomer II plus cross-linker and activator are swollen into network I and polymerized in situ. The sequential IPNs include many possible materials where the synthesis of one network follows the other.

• **Simultaneous interpenetrating network (SIN).** The monomers or prepolymers plus cross-linkers and activators of both networks are mixed. The reactions are carried out simultaneously, but by noninterfering reactions.

• **Latex IPN.** The IPNs are made in the form of latexes, frequently with a core and shell structure. A variation is to mix two different latexes and then form a film, which cross-links both polymers. This variation is sometimes called an interpenetrating elastomer network (IEN).

• **Gradient IPN.** Gradient IPNs are materials in which the overall composition or cross-link density of the material varies from location to location on the macroscopic level. For example, a film can be made with network I predominantly on one surface, network II on the other surface and a gradient in composition throughout the interior.

• **Thermoplastic IPN.** Thermoplastic IPN materials are hybrids between polymer blends and IPNs that involve physical crosslinks rather than chemical cross-links. Thus, these materials flow at elevated temperatures, similar to the thermoplastic elastomers, and at use temperature, they are cross-linked and behave like IPNs. Types of cross-links include block copolymer morphologies, ionic groups, and semicrystallinity.

• **Semi-IPN.** Compositions in which one or more polymers are cross-linked and one or more polymers are linear or branched are semi-IPN (SIPN) [46].

Many IPNs exhibit a microheterogeneous morphology. When the domains are on the order of 10-20 nm, the whole system is substantially all interphase material. Subsequently, the glass-transition temperature, T , tends to be very broad and stretches the range between the two

polymers. Although other multicomponent materials can be made to do the same thing, it seems especially easy with IPNs. Using the time-temperature superposition principle, a broad temperature transition also means a broad active frequency range of damping. Such materials are excellent for outdoor applications, aircraft, and variable temperature machinery [46].

Characterization of Network in Non Asphalt Systems

Usage of Interrupted Shear Flow Test for Time Dependency of Polymeric Structures

In the work by Santangelo and Roland, low molecular weight polystyrene melts were subjected to shearing flow which was periodically halted. Weak maxima in both the viscosity and normal stress were observed upon startup of the flow. The strain associated with the viscosity maxima was independent of shear rate, and consistent with the overshoot strains for entangled polymers. The stress overshoots disappeared or were of weaker intensity when the flow was resumed after a brief interruption. For sufficiently long rest periods between flow, the original behavior was reproduced. If the shearing is interrupted for a short time, the peak is absent or of reduced magnitude upon resumption of the flow. The strain associated with the overshoot appears to be independent of shear history. The stress overshoot disappears when the interrupted flow is resumed immediately. The magnitude of the peak is completely recovered for sufficiently long rest intervals ; 100 s [47].

In the work done by Tang et al.,A series of polyurethane (PU) and vinyl ester resin (VER) simultaneous and gradient interpenetrating polymer networks (represented as s-IPN and g-IPN, resp.) curing at room temperature were prepared by changing the component ratios of PU or VER in s-IPN, time intervals, and component ratio sequences of s-IPN in g-IPN. Their results indicated that multicomponent system can broaden the effective *Tg* range and move the range

toward higher regions corresponding to higher VER content. All the s-IPNs show one expended *Tg* peaks with maximum tan δ value higher than 0.4 in near 50◦C temperature ranges [48].

Characterization of the Network Structures in Asphalt and Modified Asphalts

Rheological Methods

According to Liao et.al., when the asphalt is modified by the SBS copolymer, the complex modulus increases as a function of the amount of SBS copolymer. This enhancement forms in two stages. At 3% SBS concentrations, local SBS networks begin to form. This localized networking can reinforce the asphalt binder. At 5% SBS concentration, the local networks begin to interact forming a critical network that leads to a sharp increase in the complex modulus. The complex modulus increases by a factor of 6 with just a 5% weight addition of the SBS. It is important that the critical content for network formation be exceeded; otherwise, the SBS does not show significant improvement over unmodified binders. However, once the critical networks begin to form, increases in polymer content are accompanied by less significant property increases. This critical content may be dependent on asphalt and polymer source [49].

In the work done by Wekumbura et. al, asphalt modified by SBS and EVA copolymers concentrations from 2 to 8% by weight was investigated in interrupted shear flow tests. The destruction and reformation of the internal network structure of polymer-modified asphalts was demonstrated in this test. For neat asphalt, at the start-up of each shearing phase, no prominent stress overshoots were seen. This indicates that the shear stress reaches steady state value immediately and once the steady shearing is stopped, stress relaxes quickly [50]. When the shearing is resumed after 30 s, the stress followed the same pattern as at the beginning of the test. The reason for showing this type of behavior was due to the weak associations, e.g., bipolar attractions, hydrogen bonding etc., which are easily destroyed by stressing or temperature variations [50].

On the other hand, each modified asphalt exhibited stress overshoots at the inception of shearing and the magnitudes of these overshoots were a function of polymer concentration and polymer type [50].

TEM Methods

According to Liao et.al., when the asphalt is modified by the SBS copolymer, blends of SBS polymers and asphalt exhibit a multiphase morphology. SBS is dispersed as small particles in the asphalt. When the miscibility of SBS is restricted, the polymer that appears in small proportion usually segregates into small regions. Secured in the continuous matrix formed by the asphalt, these small regions are called the discrete phase [49].

The combination of these two constituent materials yields a PMA in which SBS and asphalt are combined to result in a material that has properties different from those of either constituent. In this way, it is possible to improve substantially the properties of asphalt and to obtain a novel material with engineering properties superior to those of the constituents. Different types of SBS showed distinctively different morphologies. Because of differences in molecular weight, polarity, and structure, there exists the chemical dissimilarity between asphalt and SBS [49].

A phase inversion results from the SBS copolymer swollen by the oils and the asphalt enriched in asphaltenes containing virtually no polymer. The SBS copolymers represent a triblock structure in which polystrene is the thermoplastic end block, and polysbutadiene is the rubbery midblock. Within the polymer-rich phase, there are two microphases—swollen polybutadiene and essentially pure polystyrene domains, which act as physical crosslink sites to form a network. When the polymer-rich phase forms the continuum, the SBS-modified asphalt displays rubber-like elasticity [49].

SEM Methods

In the work by shin et al, The effects of polymer modification on microstructure, morphology, and failure modes of asphalt binders were carried out. One of the most striking results is that a highly entangled fibrillar network structure has been observed from both straight and polymer-modified asphalt binders after an electron beam etching. This network structure was observed in both straight asphalts (AC-5 and AC-10) and polymer-modified asphalt binders [51].

Therefore, the structure was not from the polymer phase but from the asphalt. It is envisioned that the beam volatilizes the low molecular weight oils in the asphalt by localized heating, thereby revealing the network of the high molecular weight asphaltene and resin from a suggested two-phase asphalt model. It was also observed that the network structure disappeared upon annealing at 50°C, and after cooling down to room temperature, the similar structure recurred with an additional beam exposure on the same spot. Furthermore, the network structures once formed lasted a long time and were stable under continuous beam exposure for more than hours. These results indicate that the network structure appeared because of the evaporation of low molecular weight oil phase under the localized beam exposure. Similarly, the disappearance of the structure upon annealing might be due to the oils diffusing back into the entanglement structure. The deformation behavior of the network structure was also investigated using tensile stage in ESEM. Surprisingly enough, the entangled chains were elongated considerably without losing their network structure, integrity, or three-dimensional entities [51].

Thermal Methods

In thermal analysis, the change materials' properties are measured against temperature [52]. This characterization method poses three main advantages in comparison to other methods; the first one is its superior accuracy and sensitivity to the change in materials properties, whereas

the second advantage is the very small samples amount leading to significant reduction in the cost and effort of sample preparation, finally, its relatively short time [53]. On the other hand, thermal analysis provided information about the physical and chemical changes in the material and can't account for the mechanical properties of materials. Thermal analysis most common method is thermo-gravimetric analysis (TGA).

Thermo-Gravimetric Analysis (TGA)

In TGA the weight change of a sample of pre-known weight is measured accurately against temperature. Through this method, fingerprinting of each component within a materials is carried out through the determination of the decomposition temperature of such component. TGA has been utilized by various researchers to determine the composition of multi-component samples [54-59]. The composition of a multi-component material can be determined through different methods of TGA analysis depending on the complexity of material. The ramp method is the most used and conventional method of TGA analysis. In such method, the sample is heated up to a predetermined temperature utilizing a constant heating rate while measuring the mass loss of the sample as a function of temperature [60]. Although commonly used, this method cannot identify the components with close decomposition temperatures. To overcome this drawback, a more advanced and sophisticated TGA method is utilized, known as the Stepwise Isothermal Thermo-Gravimetric (SITG) analysis. In such method, the sample is subjected to a programmed heating method to ensure the separation of the decomposition processes of different components having close decomposition temperatures [60-62].

The utilization of TGA analysis in asphalt and rubber industry has been carried out extensively. Dong et al. used TGA to analyze the decomposition of the asphaltene fraction of asphalt [63]. Based on their work, the asphaltene decomposes in a very narrow temperature (350°C to

450°C). The offset of oxidation of the asphalt and modified asphalt has been investigated by TGA [64]. It was found that the polymers shifts the oxidation and decomposition offsets of asphalt to the right (higher temperatures). The mass loss of asphalt during the curing blend of polymer modifier and asphalt was investigated by TGA. It was found that at 200°C and for 90 min, the mass loss during the curing blend of asphalt and polymer modifier is negligible [27]. TGA method is also utilized to characterize the composition of multi-component samples of CRM in the rubber industry. Although TGA can be a very powerful method to determine the proportion of natural rubber and synthetic rubber in binary blend of polymers, however, this method can't distinguish between the different types of synthetic polymers like styrene-butadiene rubber (SBR) and butadiene rubber (BR) [55]. The pyrolysis of waste tire rubbers was also investigated by TGA [54, 57-59, 65]. It was found that CRM can be divided into oily components, natural rubber, synthetic rubber, and finally the fillers like carbon black, those materials decompose at below 200°C, between 300°C and 350°C, between 350°C and 400°C, and at temperatures above 400°C, respectively.

FTIR Methods

FTIR method is an established method to investigate asphalt binders. Table 2.1 lists the asphalt's IR characteristic bands of asphalt.

Several researchers have investigated the effect of addition of CRM to asphalt through FTIR. In the work by Zhigang et al., the authors investigated the effect of addition of desulfurized crumb rubber (DCR) to asphalt in the presence of reactive additives.

Table 2.2. IR characteristic bands of asphalt.

Band Position (cm^{-1})	Band Assignment	References
1032	S=O stretching	Masson et al., Zhang et al., and Abbas et al. [27, 66, 67]
1376	C-H symmetric bending of CH_3	Zhang et al., Fang et al., and Yao et al. [27, 68, 69]
1419	C-H bending of -$(CH_2)_n$-	Socrates [70]
1437	C-H asymmetric bending of -$(CH_2)_n$-	Yao et al. [69]
1448	C-H asymmetric bending of -$(CH_2)_n$-	Socrates [70]
1458	C-H asymmetric bending of -$(CH_2)_n$-	Zhang et al. and Yao et al. [35, 69]
1603	C=C stretching (aromatic)	Zhang et al., Fang et al., and Yao et al. [27, 68, 69]
1730	C=O Carbonyl	Zhang et al. and Yao et al. [35, 69]
2853	C-H symmetric stretching (aliphatic)	Zhang et al. and Yao et al. [35, 69]
2870	C-H symmetric stretching (aliphatic)	Socrates [70]
2924	C-H symmetric stretching (aliphatic)	Yao et al. [69]
2954	C-H symmetric stretching (aliphatic)	Socrates [70]

The effect of the kinds and content of the reactive additive on properties of DCR modified bitumen (DCRMB) was investigated. The changes of the chemical structure of DCRMB without and with the addition of the reactive additive were analyzed by FTIR. The authors found that the bands at 1660 and 1030cm^{-1} were assigned to C=C double bonds and sulfoxides, respectively. The group of peaks at 747, 813 and 873cm^{-1} were attributed to substituted aromatic ring structures, and the peak at 1376cm^{-1} was attributed to the flexural vibrations of C-H bond of methyl. For DCRMB without the addition of the reactive additive, the peak at 1660cm^{-1} was strong, but the corresponding peak weakened apparently with the addition of reactive additives, the peak nearly disappeared. Because these two kinds of reactive additives, sulfur and disopropylbebzene

peroxide, can initiate the cross linking reaction of C=C double bonds, and both bitumen and DCR have some C=C double bonds, the change of the peak at 1660cm $^{-1}$ verified that the chemical reaction between C=C double bonds in bitumen and DCR has happened with the addition of reactive additives [71].

In the work by Daly et al, the authors utilized FTIR to detect what functional groups are not passing the PTFE filters used for GPC analysis (percentage insoluble in THF). The authors found that an original Styrene Butadiene Styrene (SBS) or styrene ethylene butadiene styrene (SEBS) polymer (or aged polymer will have distinct peaks in FTIR spectra at wavelengths 1600cm^{-1} and 966-969cm^{-1}). However, the authors found none of these peaks on filter papers for the samples examined in their project. These indicated that the percent of insoluble polymeric species is insignificant compared to the percent of asphaltenes insoluble in THF and thus they applied composition corrections based upon weights of insolubles accordingly [72].

In another work by Ali et al., the change in composition of RTFOT and PAV oxidized asphalts was identified from infrared FTIR spectroscopy. Both RTFO and PAV oxidized asphalts showed an increase in the carbonyl absorption band from 1650 to 1820 cm^{-1} as aging severity increases. The C–O single bond stretching (910–1300 cm^{-1}) and sulfoxide (950–1050cm^{-1}) showed increase with oxidation severity. The authors showed that there exists a correlation between the increase in infrared absorption of oxygen-containing groups and the oxygen content of aged materials.

Based on the authors' findings, the FTIR method could also be used in order to recognize and quantify the polymeric material in polymer modified asphalts. The authors listed the following characteristic absorption bands in the FTIR spectra for some polymer modified asphalts as follows; 966 and 698 cm^{-1} for styrene-butadiene-styrene (SBS), 724 cm^{-1} for polyethylene

(LDPE), 974 cm^{-1} for polypropylene (PP) [73]. Table 2.3 illustrates the characteristic bands for CRM collected form several research works.

Table 2.3. IR characteristic bands for CRM.

Band Position (cm^{-1})	Band Assignment	References
550–400	S-S bonds	[74]
967.8	bending vibration of trans 1,4-2 alkenes in poly butadiene	[75]
1060–1120	iterative butadiene units	[76]
1383	bending (wagging) motion of a S-CHn for Butadiene	[77, 78]
1520	[C═C] stretching in Carbon Black	[79]
1705	lactone ring [C═O] in Carbon Black	[80]
2350	═CN group in the nitrile component of CRM	[76]
3601	phenolic group [OH] stretching in Carbon Black	[81]

Chromatography Methods

Information about the molecular structure of the material such as; weight average molecular weight, number average molecular weight, polydispersity, and molecular size distribution are obtained through Chromatography methods. It has become a useful method in characterization of petroleum materials due to its capacity, simplicity and rapidness.

Ion Exchange Chromatography (IEC) and Gel Permeation Chromatography (GPC) were utilized in the literature to separate the neat asphalt into meaningful chemically fractions and also to investigate the effect of such fractions on the asphalt mechanical and physical behavior [33]. It is believed that the average molecular weight of the asphalt is increased by aging, this leads to having asphalts with lower molecular weight more prone to aging [82, 83]. On the other hand, researchers have stated that the swelling and dissolution of CRM and polymeric modifiers is faster in asphalts with lower molecular weight [22].

Chromatography methods have been utilized also to investigate the effect of addition of the CRM into the asphalt on the molecular weight distribution of final CRMA [20, 23, 84]. Based on such research, the increase in the rate of mass transfer from rubber to asphalt is directly related to either the increase in CRM concentration or decrease of CRM particle sizes.

The utilization of the chromatography methods in asphalt has been mainly carried out in comparative bases due to chemical complexity and wide range of molecular weight of asphalt components. The division of the asphalt's chromatogram into different sections while utilizing the amount of each of these sections to investigate the changes occurring in asphalt is the most commonly used approach for asphalt chromatography investigation. This is mainly carried out by dividing the asphalt chromatogram into 3 semi-equal sections based on their elution time: Large Molecular Size (LMS), Medium Molecular Size (MMS) and Small Molecular Size (SMS) [85, 86]. The correlation between the amounts of each of these sections to the final performance of the asphalt has been carried out by several researchers [83, 84, 86, 87]. Based on various research works, the LMS fractions of asphalt is strongly correlated to the final physical properties of the asphalt [88].

CHAPTER THREE. MATERIALS, EXPERIMENTAL DESIGN, AND CHARACTERIZATION

Introduction

In this chapter, the raw materials used in this research work are highlighted. In addition, the reason behind the utilization of such raw materials is explained. Later on, the mixing (interaction) parameters utilized in this work are discussed. The reason for employing such interaction parameters is also discussed. Following that, the characterization techniques employed for the investigation of the as received raw materials as well as the interacted samples are discussed. The reasons for the choice of each characterization technique are explained and highlighted.

The core of this research work is to investigate the enhancement of the asphalt after modification with CRM and/or UMO. The measure of this enhancement is based upon the characterization of the physical properties that indicates the expected in-service properties. In addition, the understanding of the reason behind the enhancements in the modified asphalt properties is carried out through the utilization of advanced chemical, molecular, and thermal characterization techniques.

As explained in the literature various techniques have been employed to investigate the network structures in asphaltic and non-asphaltic materials. Those techniques span from physical to chemical as well as thermal and morphological approaches. The basic and straight forward physical approach is the rheological investigation of the materials in question. This involves the investigation of the G* and δ values and determining how the change in the network buildup affects their values. Another approach in the physical investigation is the determination of shear stress profile as a result of applying a constant shear rate. This provides an insight about the presence and extent of network development within the material. The chemical approaches in-

volve column chromatography of the asphalt and modified asphalt. This is done utilizing adsorption-desorption chemistry to separate the asphalt into four component; asphaltenes, saturates, naphthene aromatics, and polar aromatics. Thermal approaches such as Thermogravimetric analysis (TGA) can be employed on the whole and fractionated asphalt to determine the change in the thermal behavior as a result of network formation. Morphological approaches such a atomic force microscopy (AFM), on the other hand, detects the change in morphology of the investigated asphalt as a result of network formation.

Processing

Raw Materials

In the current work, three asphalt binders were investigated in combination with three type of crumb rubbers. The reason for utilizing multiples raw materials is to obtain a wide span idea about the concept of enhancement in the modified asphalt by investigating different PG grade asphalts and CRM sources. For asphalts, PG 52-34 (named HU-52), PG 58-28 (named NF-58), and PG 64-22 (named HU-64) based on the Superpave grading system were tested. The PG 52-34 is the softest asphalt, followed by PG 58-28, and finally PG 64-22. This allowed for investigating which asphalt type and nature better interact with the CRM. Most of the interaction in this work were carried out utilizing a cryogenic processed crumb rubber type obtained from a mixed source of scrap tires (named CRM). The second type of crumb rubber was an ambient processed type obtained from truck tires (named TR). The third type was also an ambient processed crumb rubber obtained from passenger tires (named WTG). Thus, the CRM sources was varied to reflect the effect of materials source (mixed sources of scrap tires, truck tires, and passenger tires). In addition, it was also varied to reflect the processing (ambient or cryogenic). As most of the crumb rubber modifier used is the one from the mixed source (CRM), utilizing such

type were generally categorized by (CRM) unless other types were used (TR or WTG). In most of the interactions utilized in this research work, the crumb rubber modifier particle size was smaller than mesh #30 and larger than mesh #40 according to the US standard system. Some interactions utilized CRM with a sieve size smaller than mesh #20 and larger than mesh #30 or with a sieve size smaller than mesh #40 and larger than mesh #60 according to the US standard system. Most of the interactions employed a CRM percentage of 10%, while some interactions utilized a CRM of either 15 or 20% of the initial asphalt binder weight in selected interactions.

Used motor oil (UMO) was utilized as a rejuvenator for asphalt modification with or without utilizing CRM. In the interactions utilizing UMO, the percentages of UMO of the initial asphalt binder or CRMA weight varied to either 3 or 9% with CRM, if present, being of 10 or 20%, respectively.

Asphalt-CRM Interactions

Abdelrahman et al. and other researchers showed that the utilization of low interaction conditions (i.e. 160˚C and 10Hz) leads to the continuous swelling of CRM throughout the interaction time and subsequently improves the high temperature physical properties of CRMA [21, 24, 25]. On the other hand, the utilization of higher interaction conditions (i.e. 190˚C and 30Hz) leads to the swelling CRM particles at the early stages of interaction time and employing more time into the interaction leads to the degradation of the CRM particles. Utilizing extreme interaction conditions (i.e. 220˚C and 50Hz) leads to the instant degradation of the CRM particles and consequently the continuous deterioration of the high temperature physical properties of the asphalts along the interaction time until they finally level [21, 24]. Thus to properly address such variation in CRMA based on the different interactions conditions employed, we opted in this research work to conduct interactions for prolonged time (480 minutes) under three different tem-

peratures (160, 190 and 220°C) and three mixing speeds (10, 30 and 50Hz). The reason for the selection of such mixing speeds and temperatures is the need to determine the effect of high, moderate, and low interaction speed and/or temperature on the final product. As explained in the literature, elevated mixing speeds or temperatures tend to break the CRM particles swiftly, and thus release of its components into the asphalt. However, extremely high temperature of mixing speeds lead to loss of the modification effect to interacted samples.

The interactions were conducted in 1 gallon cans, and a heating mantle connected to a bench type controller with a long temperature probe (12”) was used to heat the material. A high shear mixer was used to mix the binder, CRM, and UMO. Samples were taken at 15, 60, 120, 240, and 480 minutes of interaction time and kept at -12°C to avoid any unwanted reactions. All interactions in this research were carried out under a blanket of nitrogen gas to minimize binder oxidation. A specific coding for the samples was adopted in the current work, starting with the asphalt type, followed by the interaction temperature, interaction speed, interaction time, and lastly CRM percentage.

Characterization

As explained earlier, the characterization approach aimed at investigating the properties relating to the in-service properties of asphalt such as physical properties, in addition advanced chemical, molecular, and thermal analysis were employed to understand the reason behind a given enhancement or deterioration of the modified asphalt physical properties.

Physical Characterization Approaches

Dynamic mechanical analysis

Dynamic Shear Rheometer from Bohlin Instruments CVO, (Worcestershire, UK) was used for viscoelastic analysis of neat and modified asphalt samples. Single point test and temper-

ature sweep test were performed on the samples to investigate the high temperature behavior of modified asphalt. The single point test was performed on asphalt samples at the high temperature grading of the asphalt investigated; 52, 58, and 64°C with 10 radian/sec using 25 mm diameter parallel plates. The temperature sweep test was performed on the liquid phase and whole matrix modified asphalt at a temperature range of 10°C to 70°C with 6°C increments to understand the behavior of asphalt at the different in-service conditions. 25mm diameter plates were used for tests that conducted above 45°C, and 8mm diameter plates were used for tests that were conducted below 45°C. The gap between plates for CRMA samples was selected to be 2 mm, which is the minimum gap size that does not affect the results due the presence of CRM particle. For samples without CRM the gap was selected to be 1 mm. For all tests that were conducted at temperatures below 45°C using the 8 mm diameter plates, the 2 mm gap size was selected, regardless of the type of the sample.

Interrupted shear tests

Dynamic Shear Rheometer from Bohlin Instruments CVO, (Worcestershire, UK) was used for the interrupted shear flow tests analysis of neat and modified asphalt samples. The aim of the interrupted shear flow test is to investigate the materials ability to self-heal by imposing a predefined shear rate and then measuring the resulting shear stress. Normally for materials that have network structures and entanglement of such network structures, the materials response to the sudden shearing would be an instantaneous resistance to shearing that is manifested as a shear stress overshoot that fades with time. Allowing the material to rest would eventually result in the regaining of the network structures and entanglements and this leads to increase of the shear stress overshoot with the increase of the rest period. In this work we utilized a series of successive tests to investigate the shear stress profile of the samples. In all tests, the shear rate

was controlled to be 2 s^{-1}. However, to control the rest periods, we imposed a thermal equilibrium period as that of the required rest period. Following that, all the samples with the required imposed rest period were ran successively and the measured shear stress profiles were collected. In that case we use rest periods (thermal equilibrium periods) of 30, 900, 1200, 1800, and 2400s. Three testing temperatures were utilized for the testing of the modified asphalt binders based on the high temperature criteria of the PG grading of each asphalt type. Thus PG-52-34 asphalt was tested at 52°C, PG 58-28 asphalt was tested at 58°C, and PG-64-22 asphalt was tested at 64°C.

Microindentation investigation

In order to understand how the CRM affects the micromechanical properties of asphalt, microindentation testing was carried out on the liquid phase of asphalt. This represents a major importance as the asphalt thickness on aggregate during mixing of hot mix asphalt ranges around 6-10 μm. Thus utilizing microindentation would allow us to anticipate and investigate the behavior of asphalt thin layers, similar to that on the aggregate during mixing, by calculating the hardness and elastic modulus of the liquid phase of asphalt. The procedure of asphalt sample preparation for indentation testing was illustrated in the literature [89, 90]. The preparation of the CRMA liquid phase thin film involves the utilization of a glass slide surface that is covered with a high temperature resistant tape. A rectangular window of size 1.5x0.5″ (38,1x12.7mm) is made inside the high temperature resistant tape. Following that, CRMA is heated to 160°C and poured into the square window in the high temperature resistant tape. In order to have a smooth CRMA surface, the glass substrate coated with CRMA is placed in the oven at 160°C for 5 min. After that, the glass substrate is removed out of the oven and cooled down to room temperature. The CRMA film's thickness ranges between 550–600 μm to ensure that the measured values for hardness and elastic modulus are not influenced by the glass substrate.

In this research work, a FISCHERSCOPE HM2000S indenter was utilized in the indentation tests. Indentation tests were carried out utilizing a tungsten carbide metal spherical tip of diameter 2mm that conforms with ISO 14577-3. All indentation tests were carried out under load control mode. The indentation load configuration was to start with a constant loading rate followed by a holding period at maximum load and finalizing with a unloading rate similar to the loading one. The maximum load was 5mN. The loading and unloading times were 20s. The dwell time at maximum load was 60s to minimize the viscous effect on the unloading portion of the material [89-91]. All tests were carried out at ambient temperature. For each sample a minimum of 5 indentations were carried out to determine the hardness and elastic modulus. A minimum distance of 12mm between two indentations was utilized to avoid the pile up and sink-in effect for successive indentations and also to conform to the ASTM guidelines of having the required distance of at least 6 indent radii away from the previous indentation point. In this work the utilization of Oliver and Pharr method for the analysis of the indentation test data is carried out [92]. Oliver and Pharr method not only accounts for the curvature in the unloading data but also provides a physically justifiable approach for determining the indentation depth to be used in conjunction with the indenter shape function to establish the contact area at peak load [92]. The analysis starts by defining a reduced modulus Er that accounts for the effects of nonrigid indenter on the load-indentation behavior as follows [93]:

$$\frac{1}{E_r} = \frac{1-v_s^2}{E_s} - \frac{1-v_i^2}{E_i} \qquad \text{(Eq.1)}$$

where Es=Young's modulus of the sample; υs=Poisson's ratio of the sample; Ei=Young's modulus of indenter, υi =Poisson's ratio of indenter; and Er=reduced modulus.

The unloading portion of the indentation curve relates to the reduced modulus as follows [92, 94]:

$$E_r = \frac{\sqrt{\pi}}{2}\frac{S}{\sqrt{A}} \quad \text{(Eq.2)}$$

where S=dP/dh=initial unloading stiffness and A=contact area.

To determine the initial unloading stiffness, Oliver and Pharr utilized curve fitting of the indentation depth versus loading/unloading data using the following power-law function [92]:

$$P = \alpha(h - h_f)^m \quad \text{(Eq.3)}$$

where h=any depth of penetration; hf =unrecoverable or plastic depth; and α and m=constants.

In this regard, m is a power-law exponent that is related to the geometry of the indenter [95]. The initial unloading slope, S, is determined by differentiating Eq. 3 and evaluating the derivative at the peak load and displacement [89].

Based on Oliver and Pharr approach, the total displacement h is given as [92]:

$$h = h_c + h_s \quad \text{(Eq.4)}$$

where hc is the vertical distance along which contact is made (contact depth) and hs is the displacement of the surface at the perimeter of the contact [92]. The contact depth hc can be determined from the experimental data by extrapolating the tangent line to the unloading curve at the maximum loading point down to zero load. hs can be estimated from the intercept value for depth hi that relates to the contact depth hc associated with the maximum loading point as follows [92]:

$$h_c = h_{max} - \varepsilon \frac{P_{max}}{S} \quad \text{(Eq.5)}$$

where Ɛ=geometric constant and Pmax is the maximum indentation load.

The hardness can be obtained as follows [92]:

$$H = \frac{P_{max}}{A} \quad \text{(Eq. 6)}$$

where A=projected area of contact at the peak load.

Molecular Investigation by Gel Permeation Chromatography

To understand the molecular behavior change of the modified asphalt, GPC analysis was utilized. The GPC can be used to measure the molecular size distribution (MSD) for a given material, thus it part of our testing was directed to measure change in the MSD for the asphalt after modification. This in turn gave an idea about interaction mechanism between asphalt and CRM/UMO and how the MSD is changed based on the utilization of different raw materials and /or interaction conditions. Another important use for GPC analysis is to investigate the change in the weight average molecular weight as well as the polydispersity to better understand molecular attributes of components that migrated from asphalt to CRM and vuce versa, thus another testing was carried out utilizing such approach. For the aforementioned reasons, the GPC testing was carried out utilizing two apparatus and settings in this research work. The first apparatus was utilized for the testing the changes in the LMS of the liquid phase of the asphalt, whereas the second apparatus was used to measure the weight average molecular weight as well as the polydispersity for the asphalt and its fractions.

The first equipment is a Waters Corporation, Model: 515 HPLC pump, and 2410 Refractive Index Detector (RID) machine with computerized software. A series of two columns was used for separating constituents of asphalt binder by molecular size. Samples were dissolved into THF and then filtered through a 0.2µm PTFE syringe filter prior to injection into the injection module. A sample volume of 50µl was injected into GPC injector for each test.The asphalt binder constituents are generally classified into several groups [96-99].

In this apparatus, the elution started at 12min and finalized at 21min. The GPC chromatogram was thus divided into three equal parts, large molecular size (LMS), medium molecular size (MMS) and small molecular size (SMS), corresponding to 12-15min , 15-18min , and 18-21min, respectively. The LMS value in the quantitative data of the chromatogram was used to characterize the binder properties. The LMS were only plotted and utilized to characterize the modified binder fractions' change in properties. Research has shown that the LMS components of binder had better correlations with asphalt binder properties than other components [100-102]

The second equipment is a Tosoh Bioscience, model: HLC-8320-GPC. Samples were dissolved into THF and then filtered through a 0.2µm PTFE syringe filter prior to injection into the injection module. The area under the curve for a GPC chromatogram represents 100% of the samples molecules injected into the GPC system [103]. The asphalt binder constituents are generally classified into several groups [96-99]. In this apparatus, the elution started at 0 minutes and finalized at 50 minutes, however molecular changes were recorded from 0 to 20 minutes. The changes in the molecular size distribution (MSD) for this range were utilized to characterize the modified binder fractions' change in properties.

Chemical Investigation by Column Chromatography Analysis

To understand how the different asphalt fractions, interact with CRM and/or UMO, separation of asphalt into four fractions; asphaltenes, saturates, naphthene aromatics, and polar aromatics was done. Testing was carried out following the Corbett method utilizing ASTM D4124 "Standard Test Methods for Separation of Asphalt into Four Fractions". Recovery of the asphalt fractions was carried out utilizing an RV 10 basic rotary evaporator obtained from IKA.

Chemical Interaction Investigation by FTIR Analysis

A Thermo Scientific Nicolet 8700 FTIR machine was utilized for the analysis of the samples in order to determine whether a chemical reaction or change has happened to the asphalt after modification with CRM. In addition, FTIR was carried out to investigate the existence of CRM components released in the liquid phase of asphalt. The CRMA liquid phase was diluted in toluene with a concentration of 50 mg per each mL of toluene. Various researchers have utilized such concentrations in their FTIR investigation [12, 104-106]. Samples were laid on the KBr disks and left for a period of 15 minutes to ensure that the solvent has completely evaporated. Transmission spectroscopy was carried out using a two face polished KBr disk. The number of scans employed was 32. The resolution was 4 with wavenumbers ranging from 4000 or 2000 cm^{-1} to 600 cm^{-1}. Baseline correction was carried out utilizing the rubberband baseline correction method. In rubberband correction method the spectra are divided in n ranges (n being the number of baseline points) which are of equal size. The minima are determined within these n ranges. The baseline points are connected by straight lines. From the bottom up a rubberband is stretched over this curve. Each baseline point which is not exactly on the rubberband is omitted. The rubberband serves as baseline.

The spectra normalization was carried out to ensure proper bands comparability. Vector normalization was carried out for spectra normalization of compared samples. Vector normalization method calculates the average y-value of the spectrum. The average value is subtracted from the spectrum decreasing the mid-spectrum to y = 0. The sum of the squares of all y-values is calculated and the spectrum is divided by the square root of this sum.

To ensure that the chosen concentration of samples is proper, trial samples for the neat as well as the CRMA were investigated utilizing concentrations of 12.5, 25, 50, 75, and 100mg/mL.

The results of the FTIR spectra for those samples are illustrated hereafter.As can be seen for the results illustrated in Figure 3.1 for the HU 52 neat saturates samples, Figure 3.2 for the HU-52-190-50-8hr saturates samples, and Figure 3.3 for HU-52-190-50-8hr PA samples, it is clear that utilizing a concentration of 50mg/1mL provided the least saturation. This can be explained in term of the higher sample thickness for the higher concentration samples above 50mg/1mL that resulted in starvation of the detector and signal saturation. On the other hand, for lower concentration below 50mg/1mL the saturation was caused by overwhelming data reception on the detector as a result of the very low concentration of sample. Another for the low concentration saturation could be the evaporation of some of the components of the sample due to the very low concentration resulting in such behavior as a result of lack of some sample components.

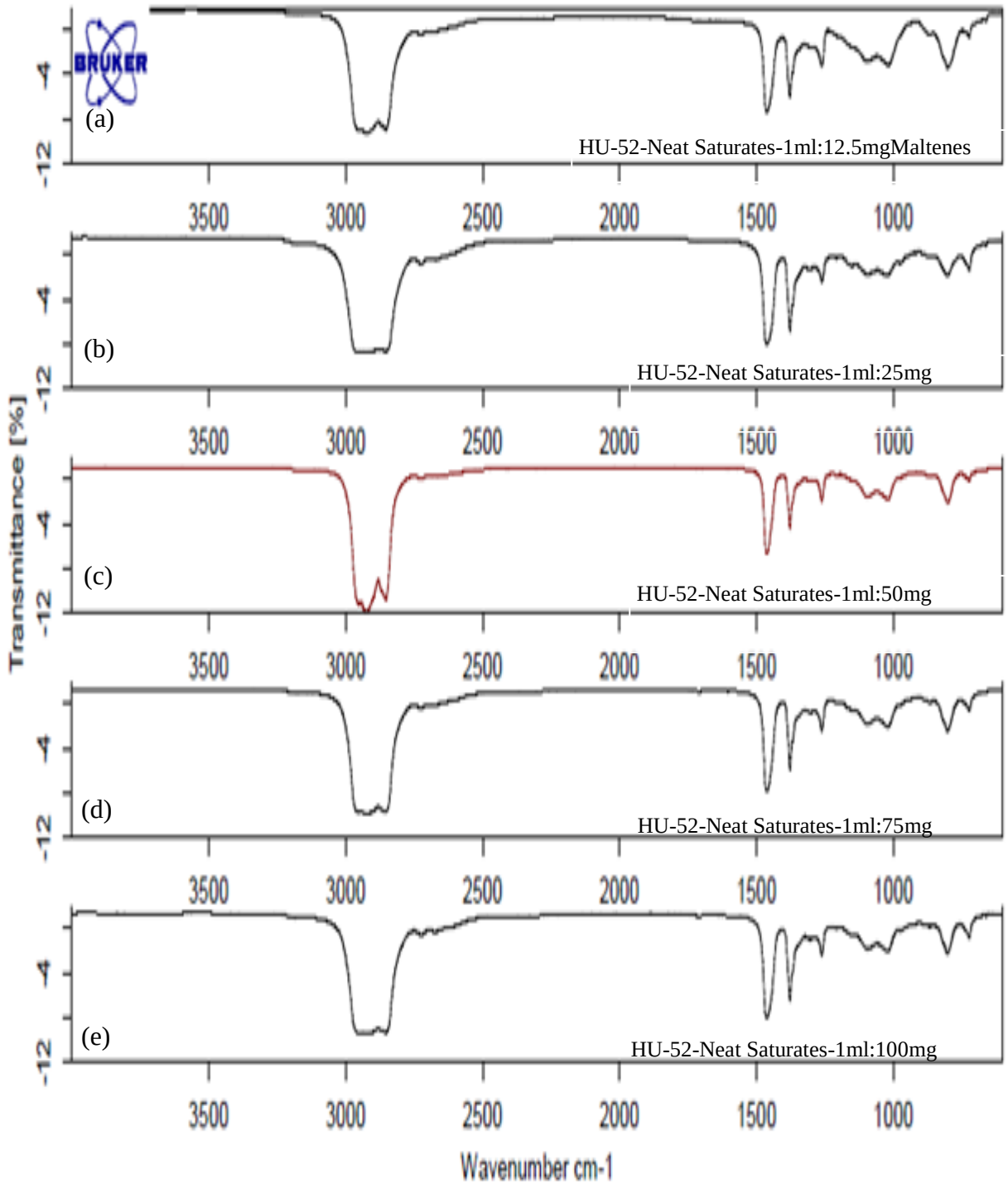

Figure 3.1. Effect of solvent concentration on the FTIR spectra for the HU-52-Neat saturates samples; a)1ml:12.5mg, b) 1ml:25mg, c) 1ml:50mg, d) 1ml:75mg, and e) 1ml:100mg.

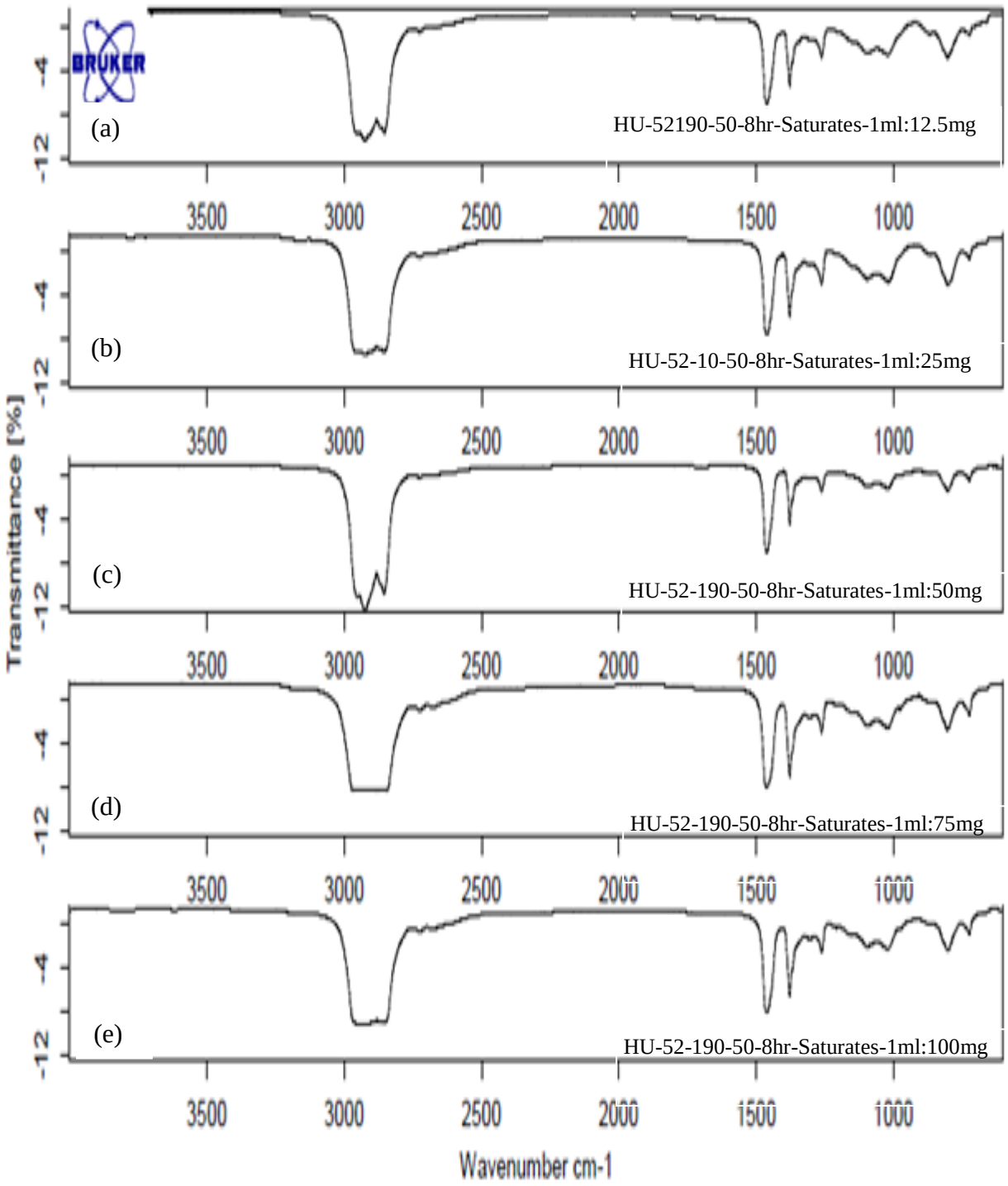

Figure 3.2. Effect of solvent concentration on FTIR spectra for the HU-52-190-50-8hr saturates samples; a)1ml:12.5mg, b) 1ml:25mg, c) 1ml:50mg, d) 1ml:75mg, and e) 1ml:100mg.

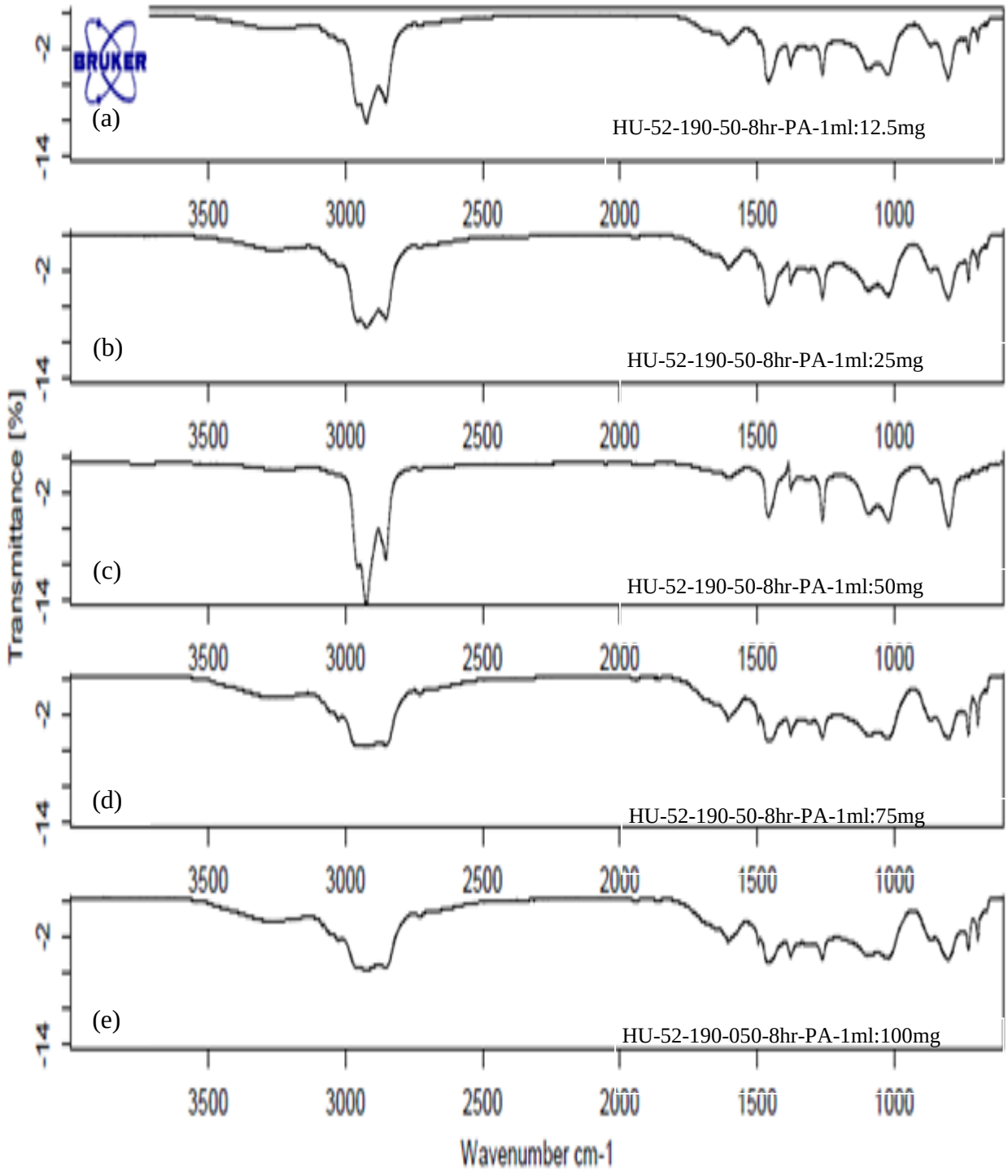

Figure 3.3. Effect of solvent concentration on the FTIR spectra for the HU-52-190-50-8hr PA samples; a)1ml:12.5mg, b) 1ml:25mg, c) 1ml:50mg, d) 1ml:75mg, and e) 1ml:100mg.

Thus, as can be seen from Figure 3.1, 3.2, and 3.3 the best spectra were attributable to the samples with 1mL:50mg sample concentration. This is evident from the fact that such concentration showed minimal saturation effects as compared to all samples concentrations.

To further illustrate the effect of concentration of sample on the FTIR spectra, utilization of different asphalt as well as CRM type will discussed hereafter.

Figure 3.4 illustrates the effect of solvent concentration on FTIR spectra for the NF-neat-saturates samples at a)1ml:12.5mg, b) 1ml:25mg, c) 1ml:50mg, d) 1ml:75mg, and e) 1ml:100mg, respectively. As can be seen from Figure 3.4(f), samples with 1ml:100mg showed increased saturation effects by obvious flattening of bands at wavenumber ranges 3000-2800 cm^{-1}. The bands are more pronounced with the decrease of sample concentration illustrated in Figures 3.4 (a, b, c, and d).

Figure 3.5 illustrates the effect of solvent concentration on FTIR spectra for the NF-neat-asphaltenes samples at a)1ml:12.5mg, b) 1ml:25mg, c) 1ml:50mg, d) 1ml:75mg, and e) 1ml:100mg, respectively. As can be seen from Figures 3.5(d and e), the bands at wavenumber ranges 3000-2800 cm^{-1} were showing flattening indicating saturation. This indicates that samples with concentration of 1ml:75mg, and 1ml:100mg were not appropriate.

The same trend, but with major extent, can be seen in Figure 3.6 that illustrates the effect of solvent concentration on the FTIR spectra for the NF-58-190-50-4hr-Asphaltene-samples; a)1ml:12.5mg, b) 1ml:25mg, c) 1ml:50mg, d) 1ml:75mg, and e) 1ml:100mg. Where samples with concentrations of 1ml:75mg, and 1ml:100mg, illustrated in Figures 3.6 (d and e), respectively, had major distortion in their bands as a result of increase concentration of sample.

Figure 3.7 illustrates the effect of solvent concentration on the FTIR spectra for the NF-58-190-50-8hr PA samples; a)1ml:12.5mg, b) 1ml:25mg, c) 1ml:50mg, d) 1ml:75mg, and e)

1ml:100mg. In those samples, the band saturation can be seen in wavenumber ranges of 3000-2800cm^{-1}for samples with concentration of 1ml:75mg, and 1ml:100mg, illustrated in Figures 3.7(d and e) indicating that such sample concentrations were not appropriate.

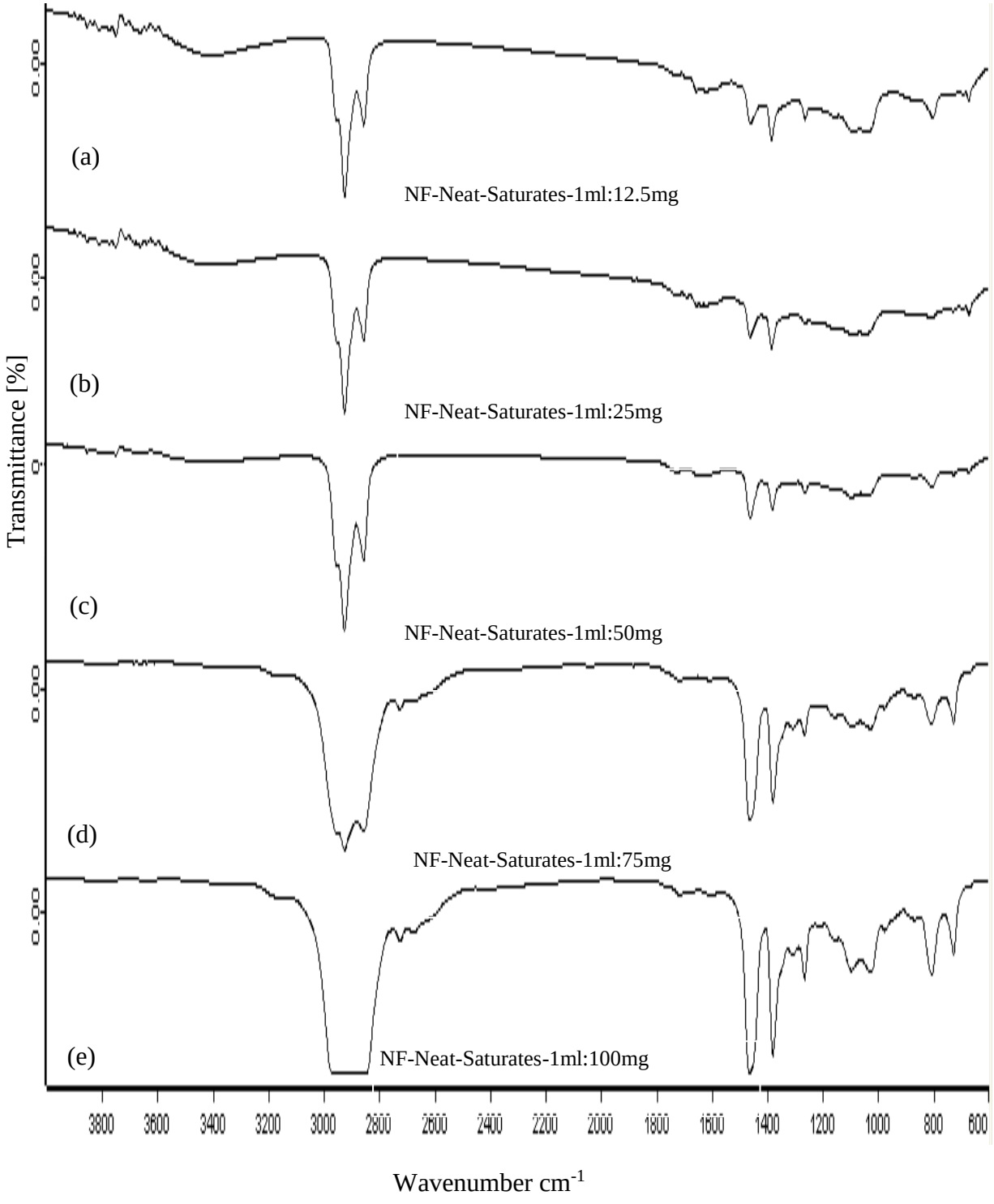

Figure 3.4. Effect of solvent concentration on FTIR spectra for the NF-neat-saturates samples; a)1ml:12.5mg, b) 1ml:25mg, c) 1ml:50mg, d) 1ml:75mg, and e) 1ml:100mg.

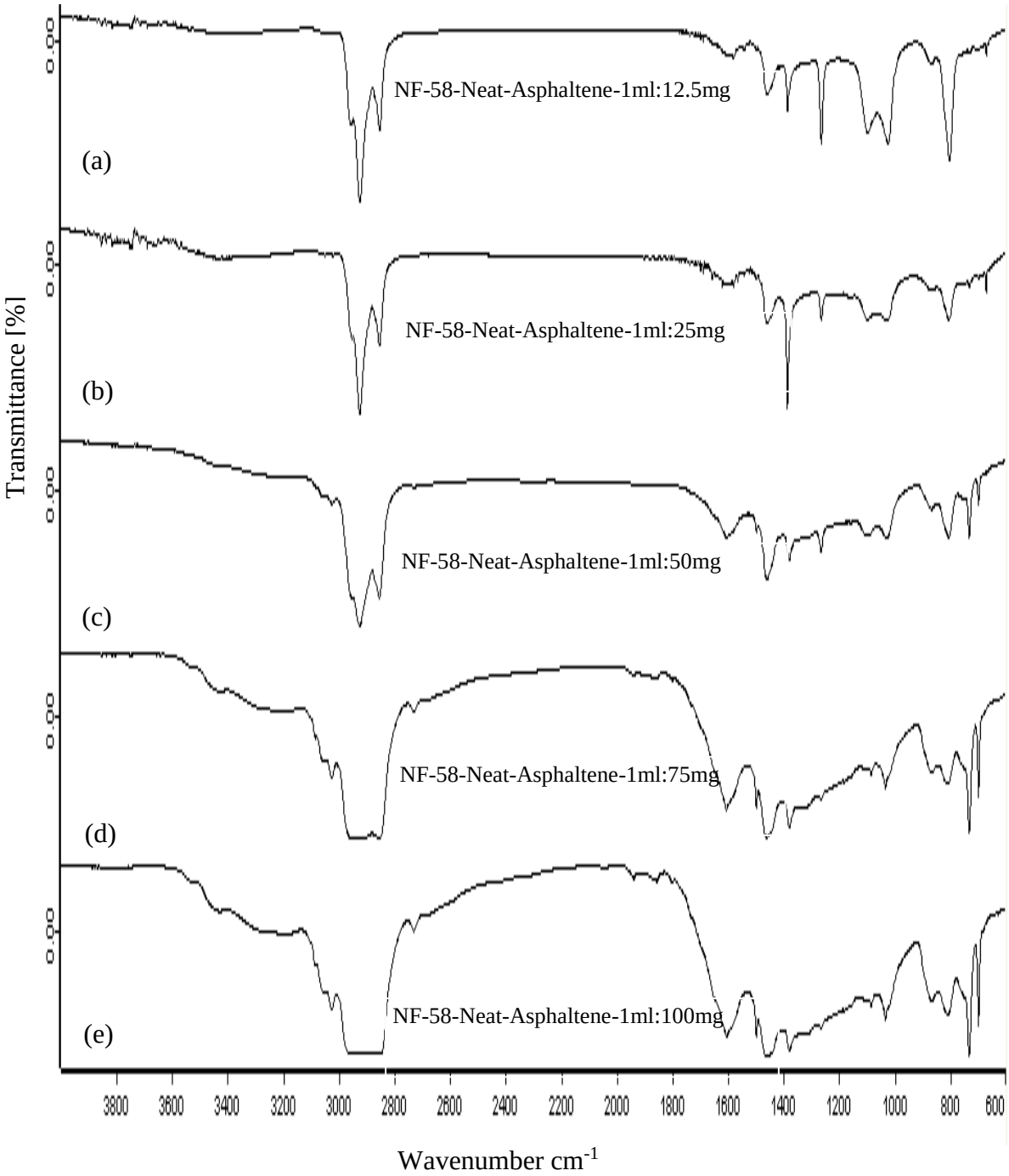

Figure 3.5. Effect of solvent concentration on the FTIR spectra for the NF-58-neat-Asphaltene-samples; a)1ml:12.5mg, b) 1ml:25mg, c) 1ml:50mg, d) 1ml:75mg, and e) 1ml:100mg.

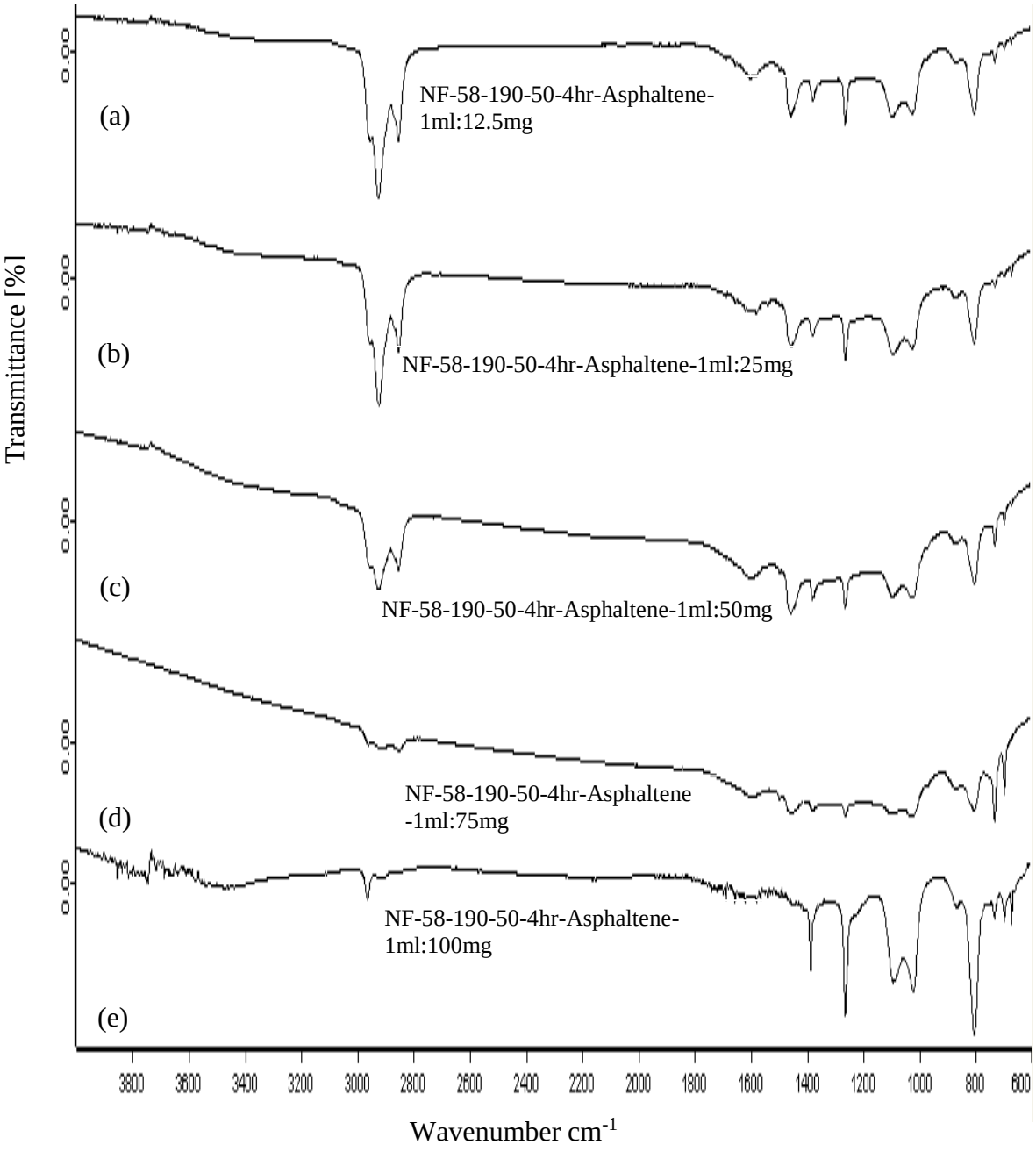

Figure 3.6. Effect of solvent concentration on the FTIR spectra for the NF-58-190-50-4hr-Asphaltene-samples; a)1ml:12.5mg, b) 1ml:25mg, c) 1ml:50mg, d) 1ml:75mg, and e) 1ml:100mg.

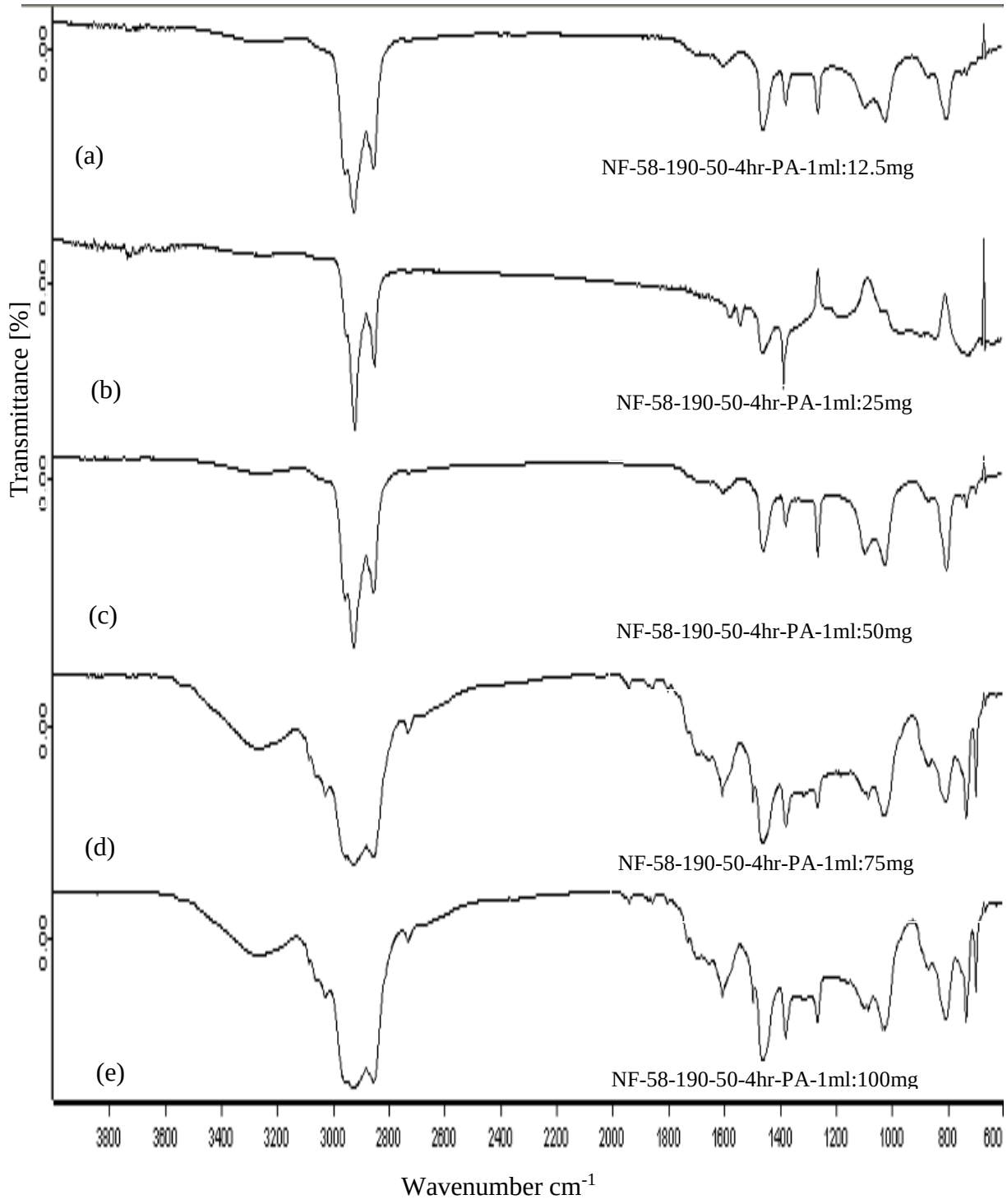

Figure 3.7. Effect of solvent concentration on the FTIR spectra for the NF-58-190-50-8hr PA samples; a)1ml:12.5mg, b) 1ml:25mg, c) 1ml:50mg, d) 1ml:75mg, and e) 1ml:100mg.

Thermal Analysis

TGA analysis

A TA instruments Q-500 TGA was utilized for Thermogravimetric analysis in this research work. Two testing approaches were employed, Ramp and Step-wise Isothermal. The Ramp method has been utilized by several researchers to investigate the composition of multi-component polymeric materials including CRM [55, 57-59]. To investigate the changes in composition of CRM samples during interaction with asphalt, the decomposition temperature range of each component in CRM samples is obtained using their mass loss rate in the related derivative of thermograph (DTG) and also temperatures reported in other studies [54, 107]. To distinguish between the different components in a multi-component sample like CRM, the sample is heated to high temperatures while monitoring the mass loss due to decomposition as a function of temperature and simultaneously graphing that in a thermograph (TG) [108]. For the TGA testing carried out in this research work, ASTM E-1131 standard was followed with minor modifications to conduct composition analysis on the CRM prior and after interaction with asphalt. The as received and extracted CRM samples were heated to 600°C by utilizing a heating rate of 20°C/min. Based on the decomposition temperature ranges for each component in the CRM sample, the related TGA curve is divided into four different regions [109]. The first region (25–300°C) is related to the oily components in the CRM, the second region (300°C to the minimum (mid) point between the two peaks in the DTG curve) is corresponded to natural rubber portion of the CRM and the third region (second region to 500°C) is corresponded to synthetic rubber portion of the CRM and finally the residue at 500°C is corresponded to filler components, like carbon black, in the CRM [109].

Stepwise Isothermal TGA (SITGA) was utilized to determine the exact decomposition temperatures for the different components present in the asphalt fractions. a TA Instruments' Q500 TGA was utilized. SITGA prevents overlapping between decomposition temperatures of different components in the sample. This is carried out utilizing a programmed heating process that enables the obtaining of higher accuracy results in comparison with the conventional ramp method that utilizes a constant heating rate to heat the sample. In the SITGA method, 20 to 25 mg of sample was heated at a constant rate (20°C/min) until the mass loss rate of the sample, measured automatically with the instrument, reached above a predefined constant (>1%/min). At this point the temperature of the sample was kept constant until the mass loss rate of the sample reached below a predefined constant (<0.5%/min). The sample was heated again, at the predefined rate, to the new temperature where the mass loss criteria, mentioned above, was satisfied again. This process was repeated until the temperature of the sample reached a predefined temperature (600°C). The type and concentration of each component in the sample was defined based on its specific decomposition temperature and the amount of decomposing mass at that temperature, respectively [61].

Dissolution Test

To investigate the effect of CRM dissolution on the CRMA properties, dissolution tests were conducted on all CRMA samples through extraction of CRM from CRMA samples, using a mesh#200. In this method 5±2 g of CRMA was diluted in toluene and drained through a mesh#200. The retained particles were washed with extra toluene, until the filtrate became colorless, and dried in the oven at 60˚C to assure removal of all solvent residues. Dissolved CRM amounts represent the difference between the expected weights of CRM to the actual weight of CRM after extraction from a known weight CRMA sample.

Extraction of Liquid Phase

In order to make physical, chemical, molecular, and thermal analysis on the liquid phase (CRMA after removal of CRM particles) of CRMA, the liquid phase of CRMA was extracted by removing the non-dissolved CRM particles from CRMA matrix. To this end, the required amount of CRMA sample was heated to 165˚C and drained through mesh# 200 (75µm) for 25 min. The extracted liquid phase was stored at -12˚C immediately to prevent any unwanted reactions.

Short Term Aging

In order to simulate the aging occurring during the mixing and compaction of HMA, short term aging was carried out following ASTM D2872 “Standard Test Method for Effect of Heat and Air on a Moving Film of Asphalt (Rolling Thin-Film Oven Test)”. Testing was done using a Coopers RTFO obtained from Cooper Technology, UK.

Long Term Aging

In order to simulate the aging of asphalt after being in the field from 6-10years, long Term aging was carried out following ASTM D 652 ”Standard Practice for Accelerated Aging of Asphalt Binder Using a Pressurized Aging Vessel (PAV)”. Testing was done using a PAV 9300 machine obtained from Prentex Alloy Fabrication, Inc.

Low Temperature Properties

The low temperature behavior of asphalt is extremely important as it determines whether the asphalt would fail during low temperature cycles or not. Thus we can investigate the effect of CRM on the low temperature performance of asphalt. Determination of the low temperature properties of asphalt and modified asphalt was carried out following ASTM D6648 “Standard Test Method for Determining the Flexural Creep Stiffness of Asphalt Binder Using the Bending

Beam Rheometer (BBR)". Testing was carried out using a bending beam rheometer machine obtained from Applied Test Systems (ATS).

Atomic Force Microscopy (AFM)

In the current work phase detection atomic force microscopy (PDM) was utilized for the investigation of the morphology of CRMA liquid phase after interaction with CRM. Being an intermittent contact AFM method [110], PDM thus alleviates problems associated with tip pollution by soft and adhesive bitumen, which leads to the dragging of material on its surface [111]. Image is thus produced by recording the difference between the oscillation signal sent to the instrument cantilever and its actual oscillation as it is affected by tip sample interactions [112]. PDM can thus effectively map domains with various rheological properties [113, 114]. A Veeco DI-3100 AFM was utilized for the investigation of the change in the surface morphology of the asphalt sample as a result of occurrence of the 3D network structures. Phase detection mode (PDM) was employed to determine the change in the morphological profile of the asphalt samples. This is carried out by measuring the phase shift of the oscillating cantilever relative to the driving signal. This phase shift can thus be correlated to the specific material properties that effect the tip/sample interaction. Friction, adhesion, and viscoelasticity can be differentiated by the phase shift recorded during PDM. A Cantilever with stiffness of 7.5 N/m and resonance frequency of 150kHz was utilized in the testing.

The preparation of the CRMA liquid phase thin film involves the utilization of a glass slide surface that is covered with a high temperature resistant tape. A rectangular window of size 1.5x0.5″ (38,1x12.7mm) is made inside the high temperature resistant tape. Following that, CRMA is heated to 160°C and poured into the square window in the high temperature resistant tape. In order to have a smooth CRMA surface, the glass substrate coated with CRMA is placed

in the oven at 160°C for 5 min. After that, the glass substrate is removed out of the oven and cooled down to room temperature. The CRMA film's thickness ranges between 550–600 µm.

Experimental Design

In order to fulfill the objectives of this research work, the following experiments were designed using the experimental and characterization methods highlighted previously in this Chapter. Three main sections summarize the experimental design; experimental design for interactions, experimental design for sample treatment, and experimental design for analytical tests. Each of these experimental designs is explained in the form of flowchart as follows:

Interactions

The interactions in this research were conducted based on the flowchart in Figure 3-1. There are two variables investigated; materials parameters and interaction parameters. In the interaction parameters the temperature, time and mixing speed were variated. In the materials parameters the asphalt PG grade was changes (PG52-34, PG 58-28, PG 64-22) and the CRM processing (cryogenic and ambient) as well as the CRM source, concentration, and size.

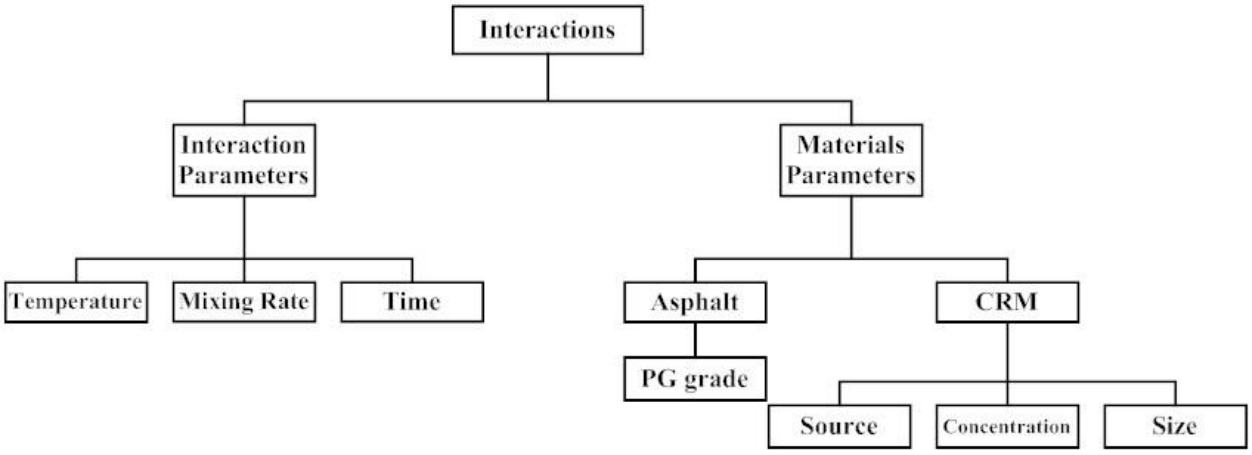

Figure 3.8. Experimental Design for Interactions.

Sample Treatments

The obtained samples from interactions will be treated based on the chart in Figure 3-2. The sample treatment involved the investigation of the whole matrix samples as well as the liquid phase ones. The whole matrix samples testing were carried out to simulate the short and long term aging behavior represented by the RTFO and PAV tests, respectively. The liquid phase was further separated using the column chromatography to investigate the change in the asphalt fractions as a result of formation of the 3D-network structure.

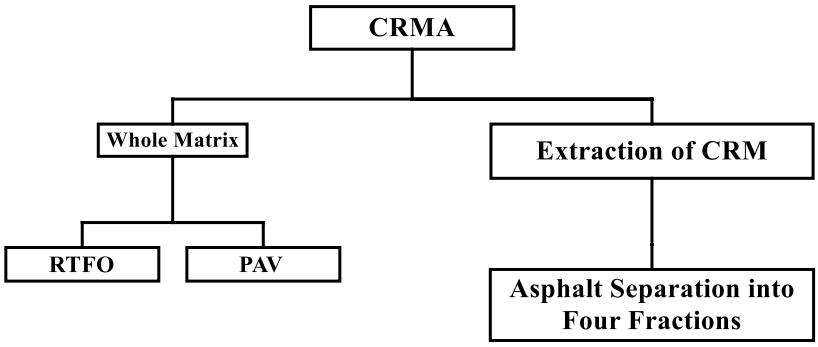

Figure 3.9. Experimental Design for Sample treatments.

Analytical Tests

The analytical tests were conducted based on chart in Figure3-3. The analytical tests involved tests carried out on the extracted CRM and asphalt (whole matrix and liquid phase). The CRM was investigated using TGA and dissolution tests. Whereas the whole matrix was investigated utilizing BBR and DSR tests. The liquid phase tests involved the analysis of the four fraction utilizing TGA, FTIR, and GPC. On the other hand the whole matrix (unfractioned) was investigated utilizing microindentation, DSR, GPC, FTIR, and AFM.

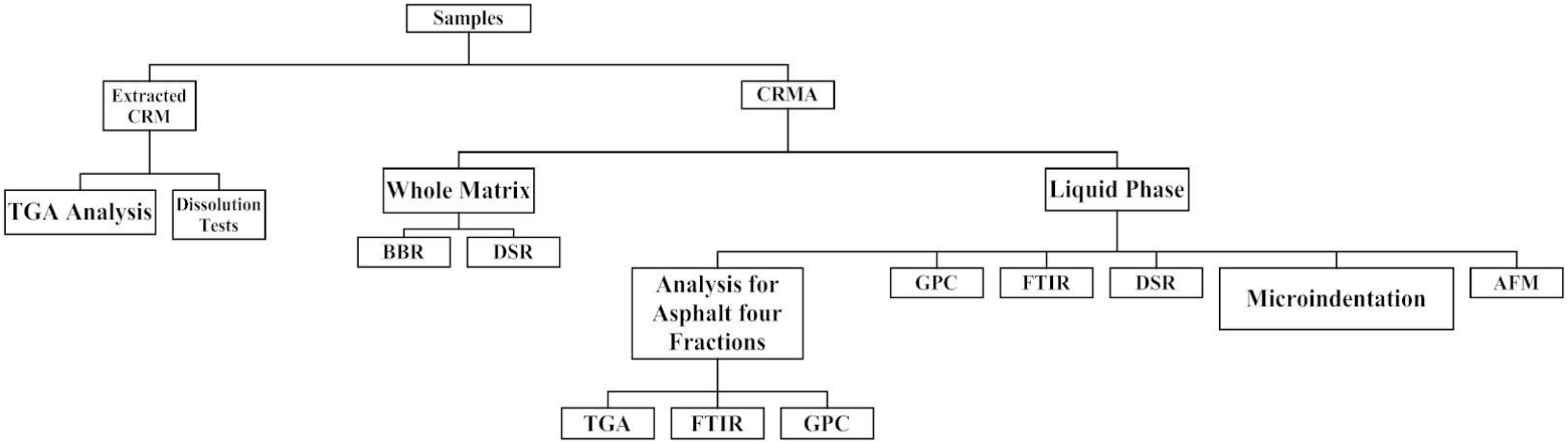

Figure 3.10. Experimental Design for Analytical Tests.

CHAPTER FOUR. INTERNAL NETWORKS IN ASPHALTS AND RUBBER MODIFIED ASPHALTS

Introduction

In this chapter, the investigation of the methods to detect the presence of network structures in asphalt is carried out. The various characterization techniques employed for achieving this purpose are utilized. This includes physical, molecular, chemical, and thermal approaches. To discuss the networks in asphalt, one should investigate the effect of CRM in asphalt. Various studies have been made to investigate the effect of CRM addition on the rheology of asphalt. Abdelrahman et al. investigated the effect of interaction parameters (interaction temperature, time and mixing speed) between asphalt, CRM and virgin polymer (VP) on the rheological properties of the modified binder [115-117]. They found that the development of the high temperature properties; complex modulus (G*) and phase angel (δ), doesn't occur by the same process. The CRM particle swelling was found to be responsible for the increase in G*. Whereas the occurrence of decrease in δ values continues even during the early stages of CRM depolymerization, suggests that the swelling is not the sole factor affecting the development of δ. They stated that the material exchange between asphalt, CRM and VP is responsible for the rate of change of both G* and δ. In addition, the development of a three dimensional (3D) network structure within the binder structure can be anticipated from the value of both G* and δ. Such observation was also made by Saylak et al., who indicated the occurrence of a direct relation between the values of the elastic component and the degree of cross-linking of the material that gives the material its elastic characteristics [118]. Changes in the cross-linking of a binder will result in a change in the magnitude of the elastic component. Wekumbura et al. investigated the effect of addition of either Styrene Butadiene Styrene (SPS) or Ethylene-Vinyl-Acetate (EVA) polymers, on the de-

struction and recovery of internal network structure of polymer modified asphalt (PMA) [50]. The authors proved through interrupted shear flow tests that there exist three dimensional (3D) entangled polymer network structures within the PMA. Such internal networks once destroyed/disturbed by shear flow, can reform with time and impart the ability of self-healing to the PMA. They also suggested the usage of interrupted shear testing for investigating the effectiveness of a given asphalt polymer modifier. In this chapter we utilize the temperature sweep rheological approach to provide evidence for the occurrence of changes in the modified asphalt internal network and we also investigate the effect of the internal network structure formation on the molecular materials properties of asphalt.

Detection of Internal Networks in Asphalt by Physical Testing

In this section temperature sweep viscoelastic testing as well as interrupted shear flow tests are carried out to investigate the presence of 3D network in asphalt.

Temperature Sweep Viscoelastic Test on Whole Matrix of Asphalt

Figure 4.1 illustrates the temperature sweep viscoelastic properties; (a) G* and (b) δ, for the HU-52 CRMA synthesized at different mixing speed and temperatures after 8hr of interaction time. As can be seen form Figure 4.1(a), the G* values for the samples interacted at 190°C and 50Hz were the highest amongst the other samples. In addition, G* values showed slight variation for the samples interacted at 160°C and 50Hz, 190°C and 10Hz , and 220°C and 50Hz. On the other hand, an interesting behavior for the δ values for all samples can be seen in Figure 4.1(b). This can be explained in terms of the occurrence of a distinct plateau region that appears on the phase angle graph. The appearance of the plateau region indicates the creation of 3D entangled internal network structure in asphalt [119, 120]. The plateau region was much expressed for the samples interacted at 190°C and 50Hz, however it was also evident for the rest of samples

interacted at the other interaction conditions. This indicates that, for the whole matrix of HU-52 CRMA, a 3D network structure is present for the samples interacted at either low (160°C), moderate (190°C), or high (220°C) interaction temperatures when utilizing interaction speeds within the range of 10 to 50Hz, after 8hr of interaction time.

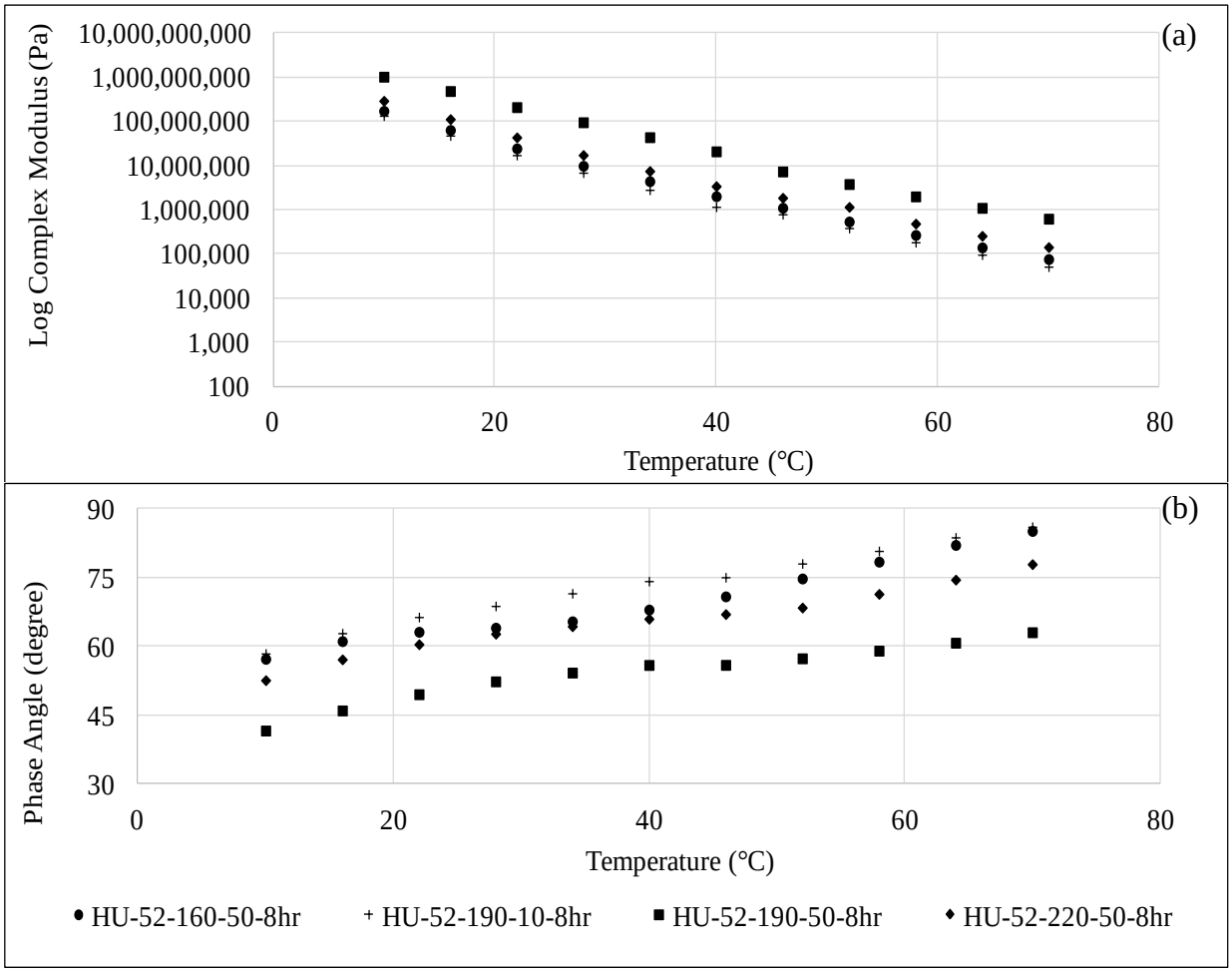

Figure 4.1. Temperature sweep viscoelastic properties for the whole matrix of HU-52 asphalt interacted at different conditions; a) G* and b) δ.

Figure 4.2 illustrates the temperature sweep viscoelastic properties; (a) G* and (b) δ, for the NF-58 CRMA synthesized at different mixing speed and temperatures after 8hr of interaction time. As can be seen form Figure 4.2(a), a similar behavior to that for the HU-52 asphalt, illus-

trated in Figure 4.1(a), can be seen for the G* values for the samples interacted at 190°C and 50Hz as they were the highest amongst the other samples. Similarly, G* values showed slight variation for the samples interacted at 160°C and 50Hz, 190°C and 10Hz , and 220°C and 50Hz.

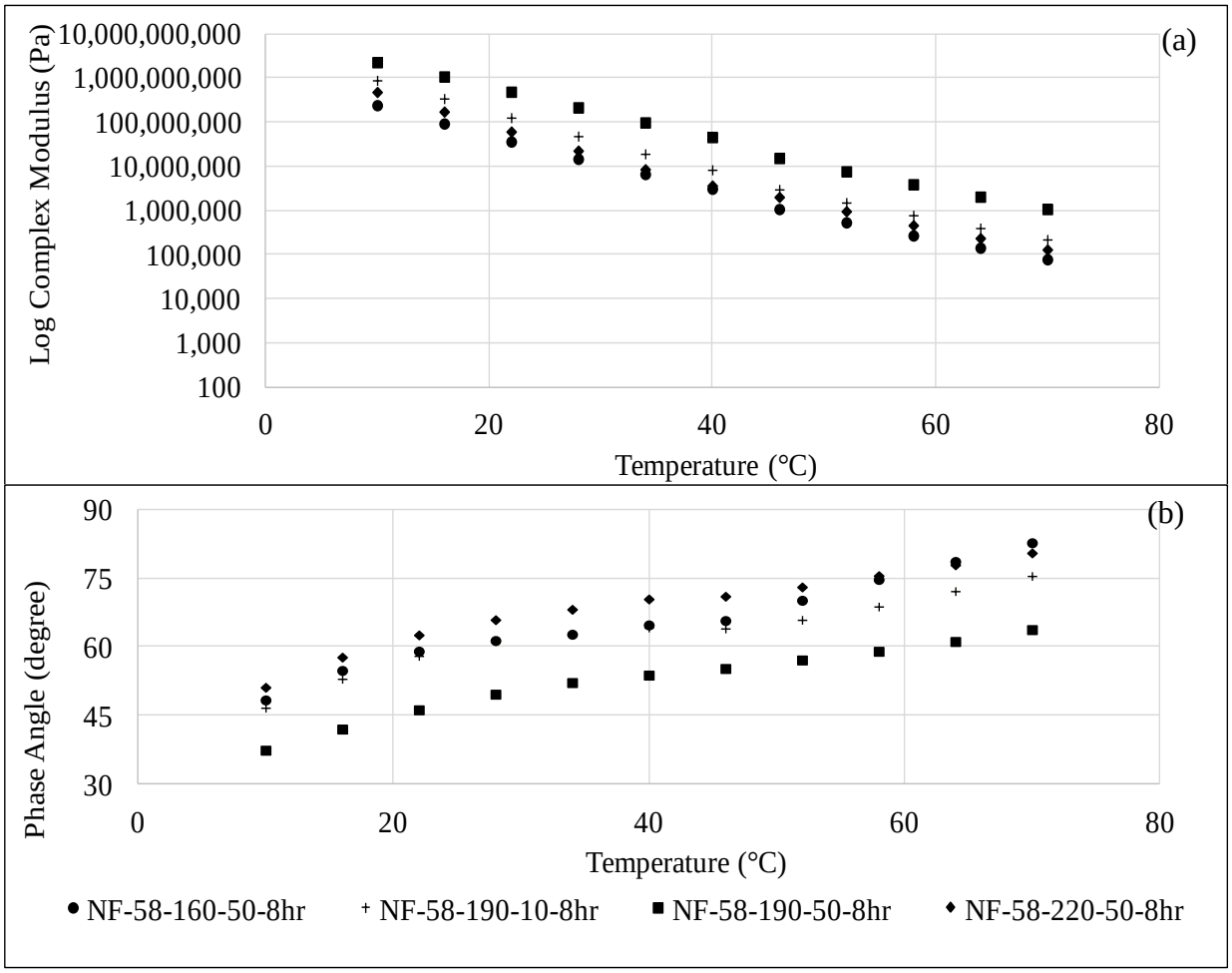

Figure 4.2. Temperature sweep viscoelastic properties for the whole matrix of NF-58 asphalt interacted at different conditions; a) G* and b) δ.

In addition, the same distinctive behavior for the δ values for all samples can be seen in Figure 4.2(b), where a distinct plateau region appears on the phase angle graph. As explained earlier, the appearance of the plateau region indicates the creation of 3D entangled internal network structure in asphalt [119, 120]. Similar to HU-52, the plateau region was much expressed for the samples interacted at 190°C and 50Hz, however it was also evident for the rest of samples

interacted at the other interaction conditions. This indicates that, for the whole matrix of NF-58 CRMA, a 3D network structure is present for the samples interacted at either low (160°C), moderate (190°C), or high (220°C) interaction temperatures when utilizing interaction speeds within the range of 10 to 50Hz, after 8hr of interaction time.

Figure 4.3 illustrates the temperature sweep viscoelastic properties; (a) G* and (b) δ, for the HU-64 CRMA synthesized at different mixing speed and temperatures after 8hr of interaction time.

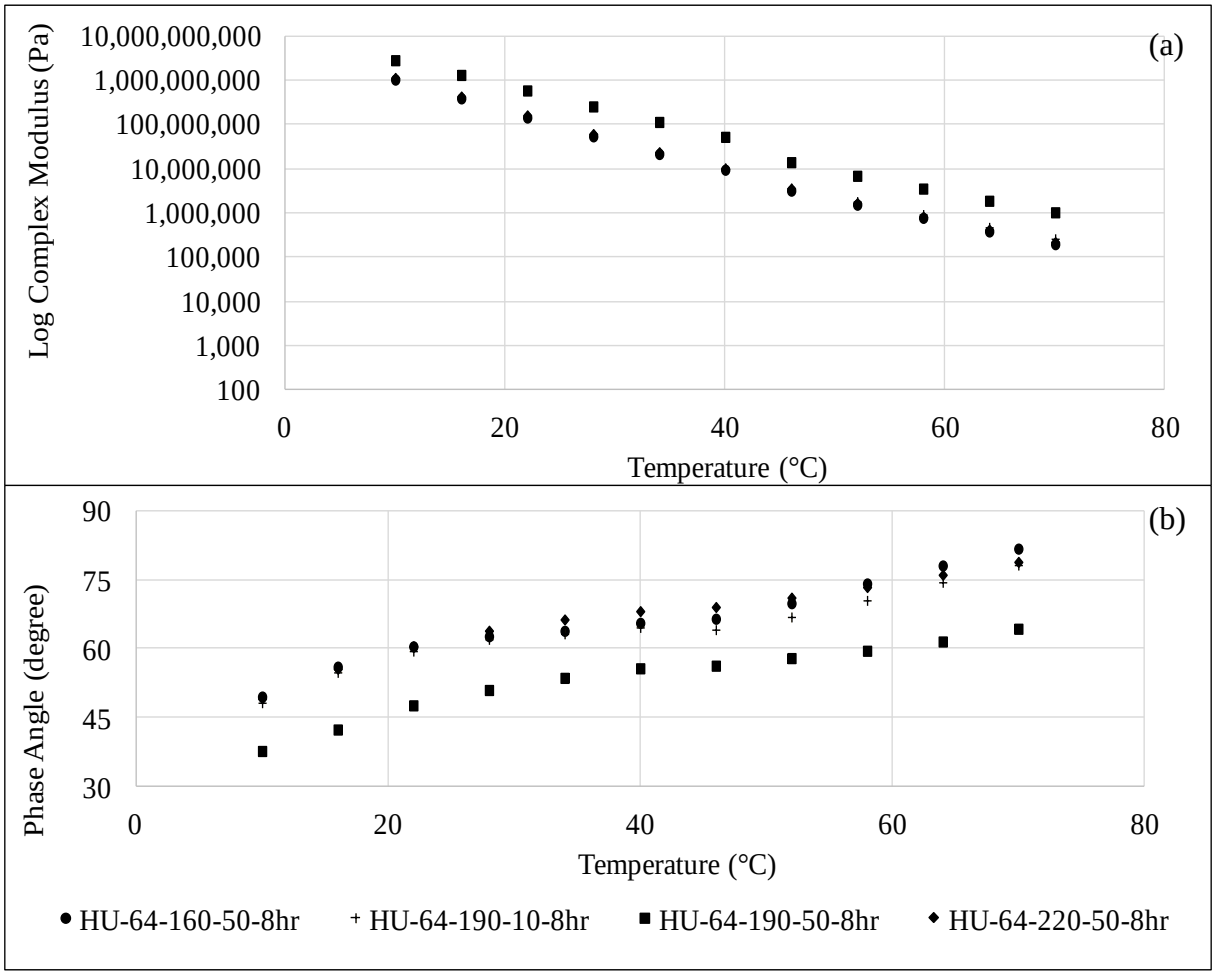

Figure 4.3. Temperature sweep viscoelastic properties for the whole matrix of NF-58 asphalt interacted at different conditions; a) G* and b) δ.

As can be seen form Figure 4.3(a), a similar behavior to that for the HU-52 and NF-58 asphalts, illustrated in Figures 4.1(a) and 4.2(a), can be seen for the G* values for the samples interacted at 190°C and 50Hz as they were the highest amongst the other samples. In addition, G* values showed slight variation for the samples interacted at 160°C and 50Hz, 190°C and 10Hz , and 220°C and 50Hz. It can be seen also that the same distinctive behavior for the δ values for all samples can be seen in Figure 4.3(b), where a distinct plateau region appears on the phase angle graph. As explained earlier for HU-52 and NF-58 samples, the appearance of the plateau region indicates the creation of 3D entangled internal network structure in asphalt [119, 120]. Similar to HU-52 and NF-58 samples, the plateau region was much expressed for the samples interacted at 190°C and 50Hz, however it was also evident for the rest of samples interacted at the other interaction conditions. This indicates that, for the whole matrix of HU-64 CRMA, a 3D network structure is present for the samples interacted at either low (160°C), moderate (190°C), or high (220°C) interaction temperatures when utilizing interaction speeds within the range of 10 to 50Hz, after 8hr of interaction time.

Interrupted Shear Flow Test on Liquid Phase of Asphalt

In this section, interrupted shear flow test is employed to detect the presence of 3D networks in asphalt. In This test the sample is subjected to a constant shear rate while measure the response shear stress of the sample. Presence of a shear stress overshoot indicates the presence of 3D network.

Utilization of low interaction temperature and high interaction speed for the 3D network structure development

Figure 4.4(I, II, and III) illustrates the results obtained from the interrupted shear flow test for CRMA interacted at 160°C with 50Hz after 8hr for (I)HU-52, (II)NF-58, and (III)HU-64

with (a)30, (b)900, (c)1200, (d)1800, and (e)2400s of rest periods, respectively. As can be seen from Figure 4.4 (a, b, c, d, and e), lack of occurrence of a stress overshoot can be seen and the shear stress reaches steady state value immediately, indicating the absence of a 3D network structure within its liquid phase. This can be explained in terms of the insufficient CRM released components to form the 3D network structure in the liquid phase as a result of the low interaction temperatures, although high interaction speed was utilized [121].

Utilization of medium interaction temperature and low interaction speed for the 3D network structure development

Figure 4.5(I, II, and III) illustrates the results obtained from the interrupted shear flow test for CRMA interacted at 190°C with 10Hz after 8hr for (I)HU-52, (II)NF-58, and (III)HU-64 with (a)30, (b)900, (c)1200, (d)1800, and (e)2400s of rest periods, respectively. Figure 4.5(a, b, c, d and e) shows the lack of occurrence of a stress overshoot where the shear stress reaches steady state value immediately, indicating the absence of a 3D network structure within its liquid phase. This is due to the insufficient CRM components release that was not able to form the 3D network structure in the liquid phase as a result of the combination of medium interaction temperature and low interaction speed [121].

Utilization of medium interaction temperature and high interaction speed for the 3D network structure development

Figure 4.6(I, II, and III) illustrates the results obtained from the interrupted shear flow test for CRMA interacted at 190°C with 50Hz after 8hr for (I)HU-52, (II)NF-58, and (III)HU-64 with (a)30, (b)900, (c)1200, and (d)1800, and (e)2400s of rest periods, respectively. As can be seen from Figure 4.6(I) for the HU-52 asphalt, the existence of the 3D network structure is evident from the occurrence of a peak stress overshoot at the beginning of the loading time that is

almost equal to double the steady state stress value. It can also be noticed that with increasing rest periods, the CRMA achieves its original stress overshoot. As reported in the literature, such behavior for the shear stresses indicates the existence of 3D internal network structure [50, 122]. Based on the results obtained from this work and after comparison with the literature, as entangled polymeric systems are known to show the same behavior of stress overshoots and recovery of peak magnitudes of stress overshoots with time, it can be deduced that there exists a 3D network structure within the liquid phase of the HU-52 CRMA [50].

On the other hand, Figure 4.6(II) illustrates the same trend of a peak stress overshoot at the beginning of the loading time, however with less strength. This can be explained in terms of the abundance of asphalt fractions responsible for the swelling and component release of CRM that were more in case of HU-52, as will be explained later in the asphalt fractions section.

Figure 4.6(III) illustrates the same trend of a peak stress overshoot at the beginning of the loading time, however with the least strength. This is attributable to the lack of the abundance of asphalt fractions responsible for the swelling and component release of CRM that were more in case of HU-52 and NF-58, as will be explained later in the asphalt fractions section.

Utilization of high interaction temperature and high interaction speed for the 3D network structure development

Figure 4.7(I, II, and III) illustrates the results obtained from the interrupted shear flow test for CRMA interacted at 220°C with 50Hz after 8hr for (I)HU-52, (II)NF-58, and (III)HU-64 with (a)30, (b)900, (c)1200, and (d)1800, and (e)2400s of rest periods, respectively. As can be seen from Figure 4.7(a, b, c, and d), lack of occurrence of a stress overshoot is evident and the shear stress reaches steady state value immediately, indicating the absence of a 3D network structure within its liquid phase. This can be explained in terms of the occurrence of excessive

devulcanization and depolymerization activities for the CRM at such interaction conditions that lead to the annihilation of the effects of CRM released components leading to absence of the 3D network structure as a result of the high interaction temperatures [116, 121, 122].

Effect of CRM percentage on the 3D network structure development

Figure 4.8(I, II, and III) illustrates the results obtained from the interrupted shear flow test for HU-52 CRMA interacted at 190°C with 50Hz after 8hr for (I)10%CRM, (II)15%CRM, and (III)20%CRM with (a)30, (b)900, (c)1200, (d)1800, and (e)2400s of rest periods, respectively. As can be seen from Figure 4.8(a, b, c, d and e), the highest occurrence of a stress overshoot is attributable to the samples with 10%CRM, whereas stress overshoot is also seen for the samples with 15%CRM. On the other hand, lack of a stress overshoot is seen for samples with 20%CRM and the shear stress reaches steady state value immediately, indicating the absence of a 3D network structure within its liquid phase.

This can be explained in terms of the insufficient asphalt fractions required for the swelling and release of CRM as the CRM percentage increase. Based on the current results, a 10%CR is providing the best results in terms of 3D network formation.

Effect of CRM type on the 3D network structure development

Figure 4.9(I, II, and III) illustrates the results obtained from the interrupted shear flow test for HU-52 CRMA interacted at 190°C with 50Hz after 8hr for (I)10%CRM, (II)10%WTG, and (III)10%TR with (a)30, (b)900, (c)1200, (d)1800, and (e)2400s of rest periods, respectively. As seen from Figure 4.9(I), the occurrence of the stress overshoot is attributable to the samples with 10%CRM (cryogenic processed mixed source CRM). On the other hand, Figures 4.9(II) and 4.9(III) show lack of occurrence of a stress overshoot where the shear stress reaches steady state value immediately, indicating the absence of a 3D network structure within its matrix.

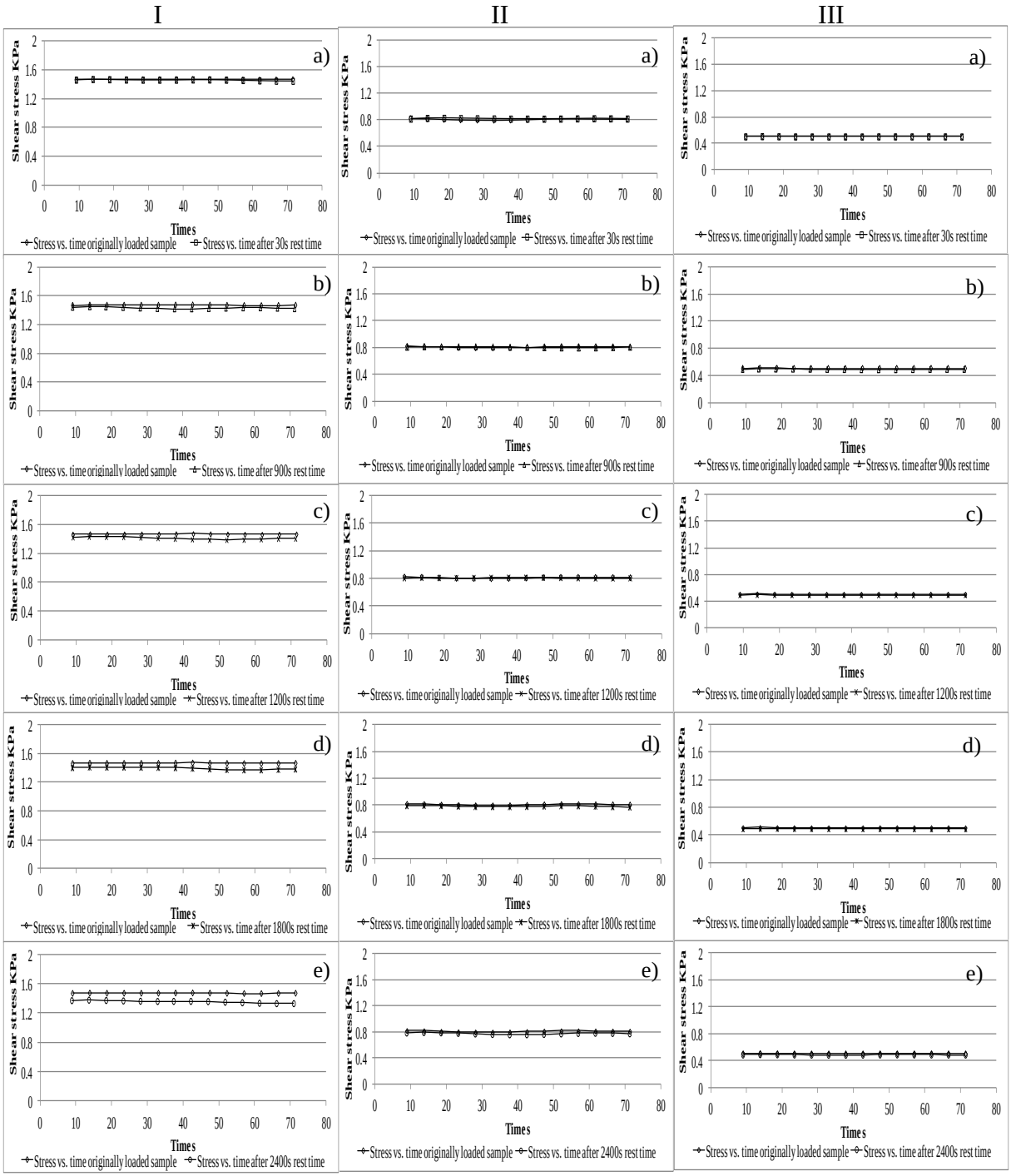

Figure 4.4. Shear stress vs. time of CRMA interacted at 160°C and 50Hz after 480minutes I)HU-52, II)NF-58, and III)HU-64 subject to shear rate of $2s^{-1}$ at a)30s, b) 900s, c)1200, d)1800s, and e) 2400s rest interval.

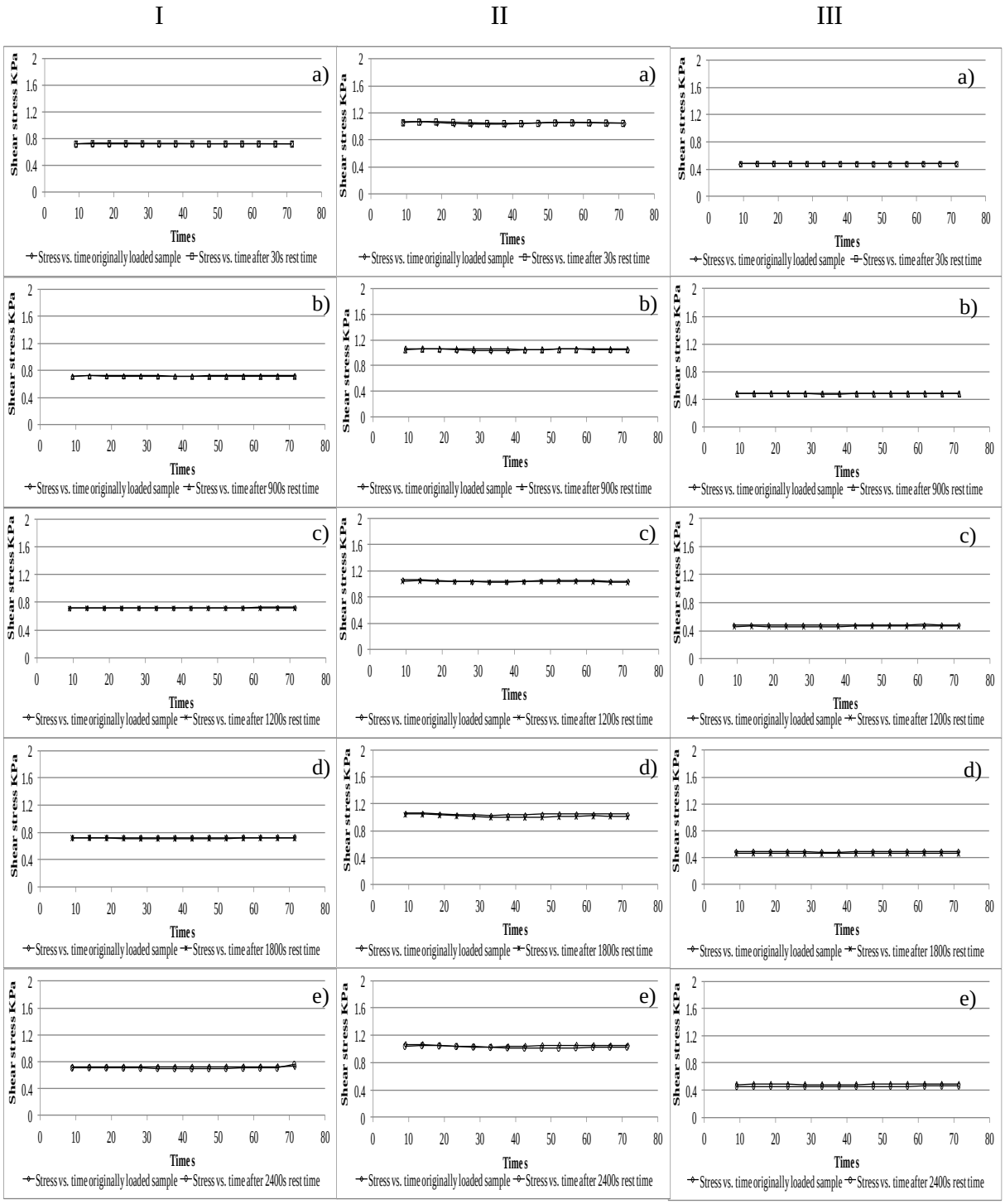

Figure 4.5. Shear stress vs. time of CRMA interacted at 190°C and 10Hz after 480minutes I)HU-52, II)NF-58, and III)HU-64 subject to shear rate of 2s-1 at a)30s, b) 900s, c)1200, d)1800s, and e) 2400s rest interval.

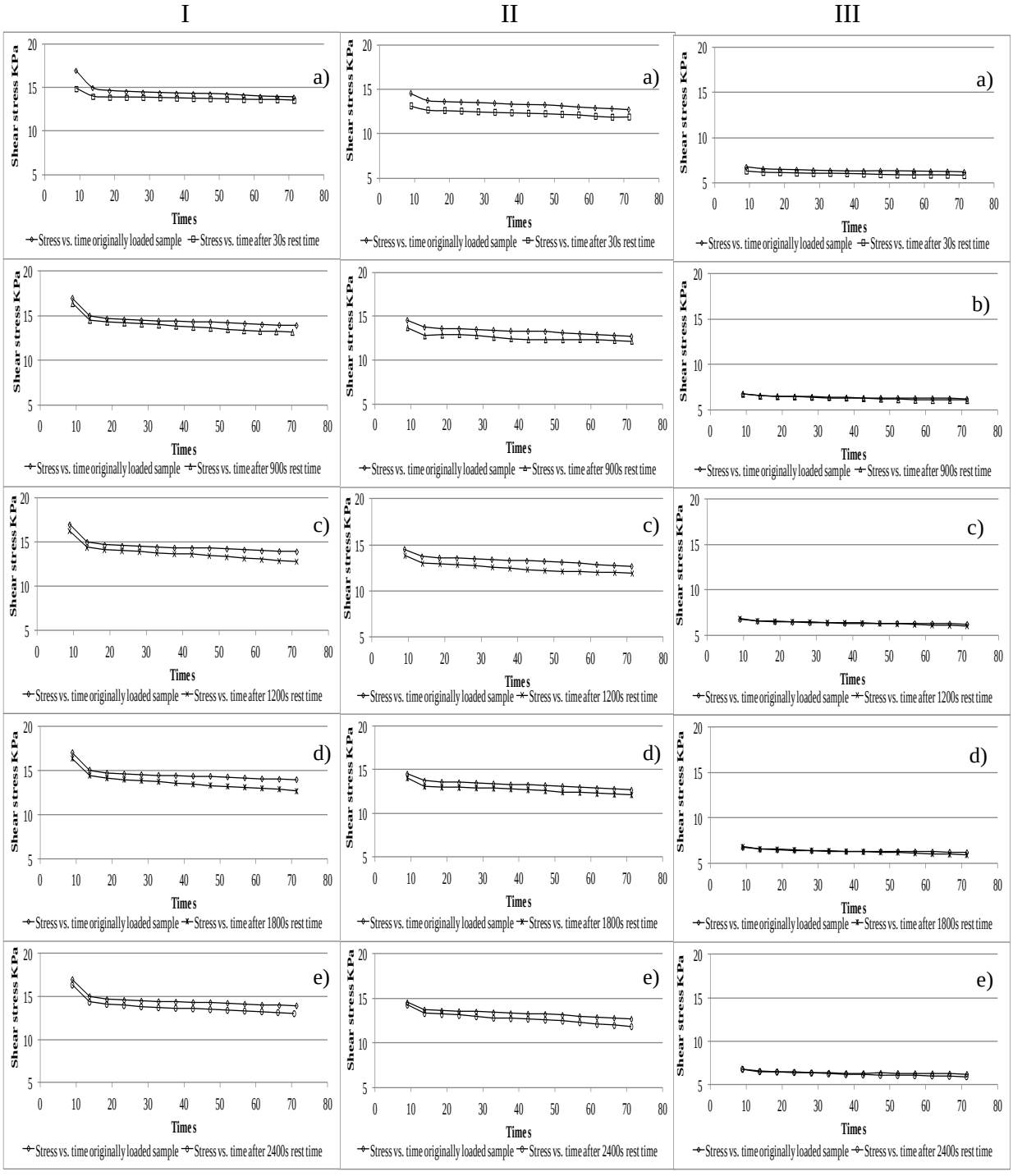

Figure 4.6. Shear stress vs. time of CRMA interacted at 190°C and 50Hz after 480minutes I)HU-52, II)NF-58, and III)HU-64 subject to shear rate of 2s-1 at a)30s, b) 900s, c)1200, d)1800s, and e) 2400s rest interval.

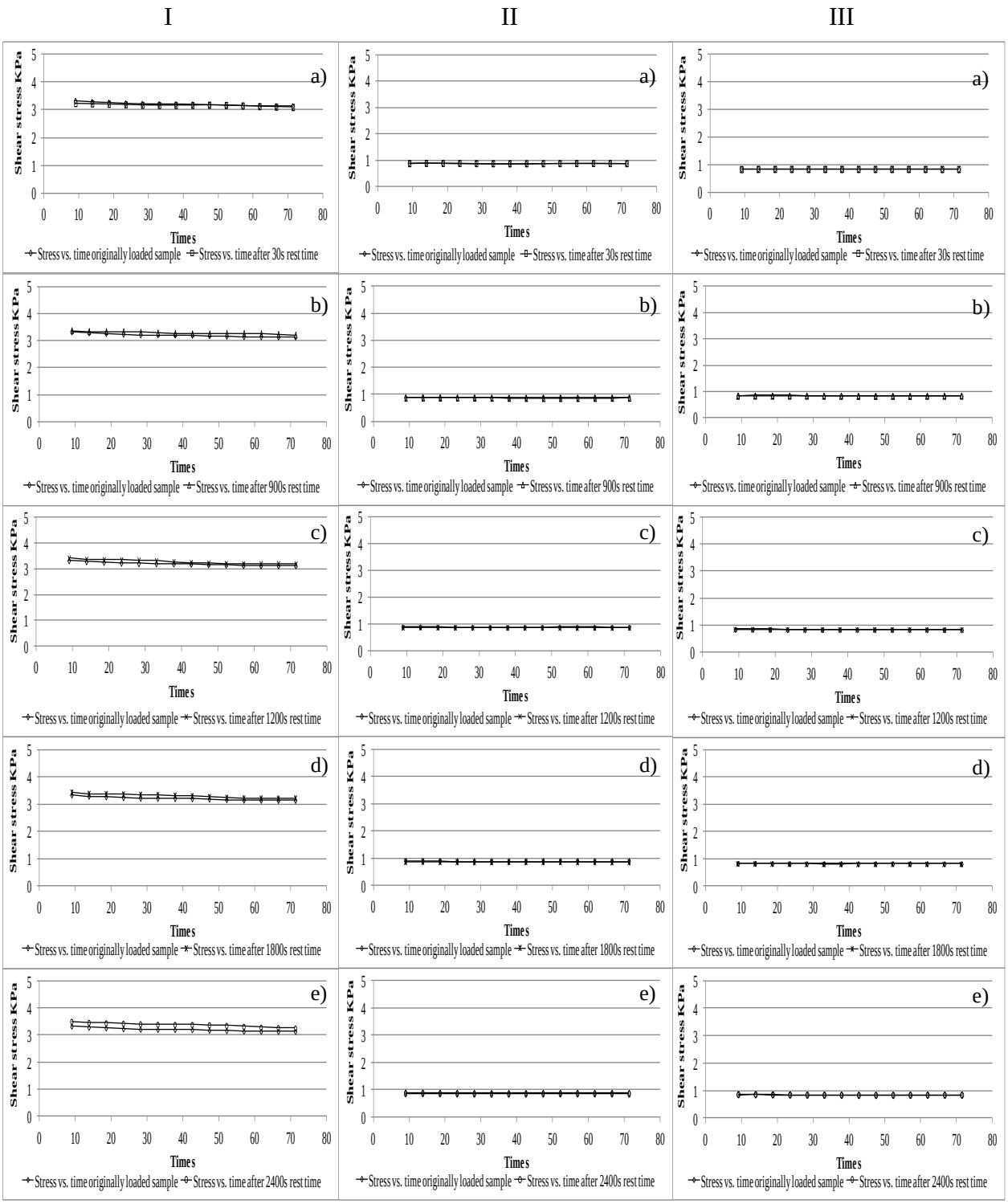

Figure 4.7. Shear stress vs. time of CRMA interacted at 220°C and 50Hz after 480minutes I)HU-52, II)NF-58, and III)HU-64 subject to shear rate of 2s-1 at a)30s, b) 900s, c)1200, d)1800s, and e) 2400s rest interval.

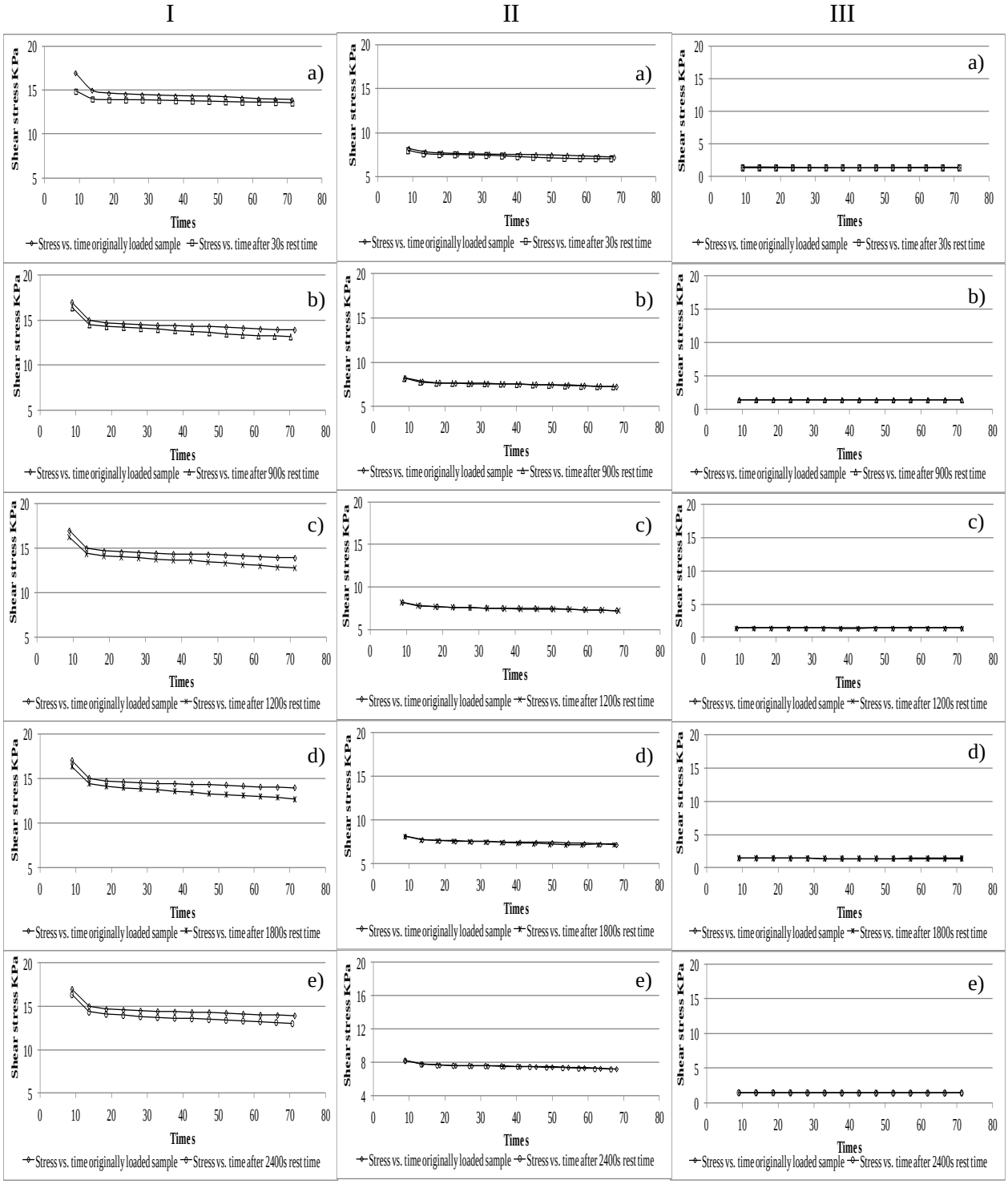

Figure 4.8. Shear stress vs. time of CRMA interacted at 190°C and 50Hz after 480minutes for HU-52 asphalt modified with I)10%CRM, II)15%CRM, and III)20%CRM subject to shear rate of 2s-1 at a)30s, b) 900s, c)1200, d)1800s, and e) 2400s rest interval.

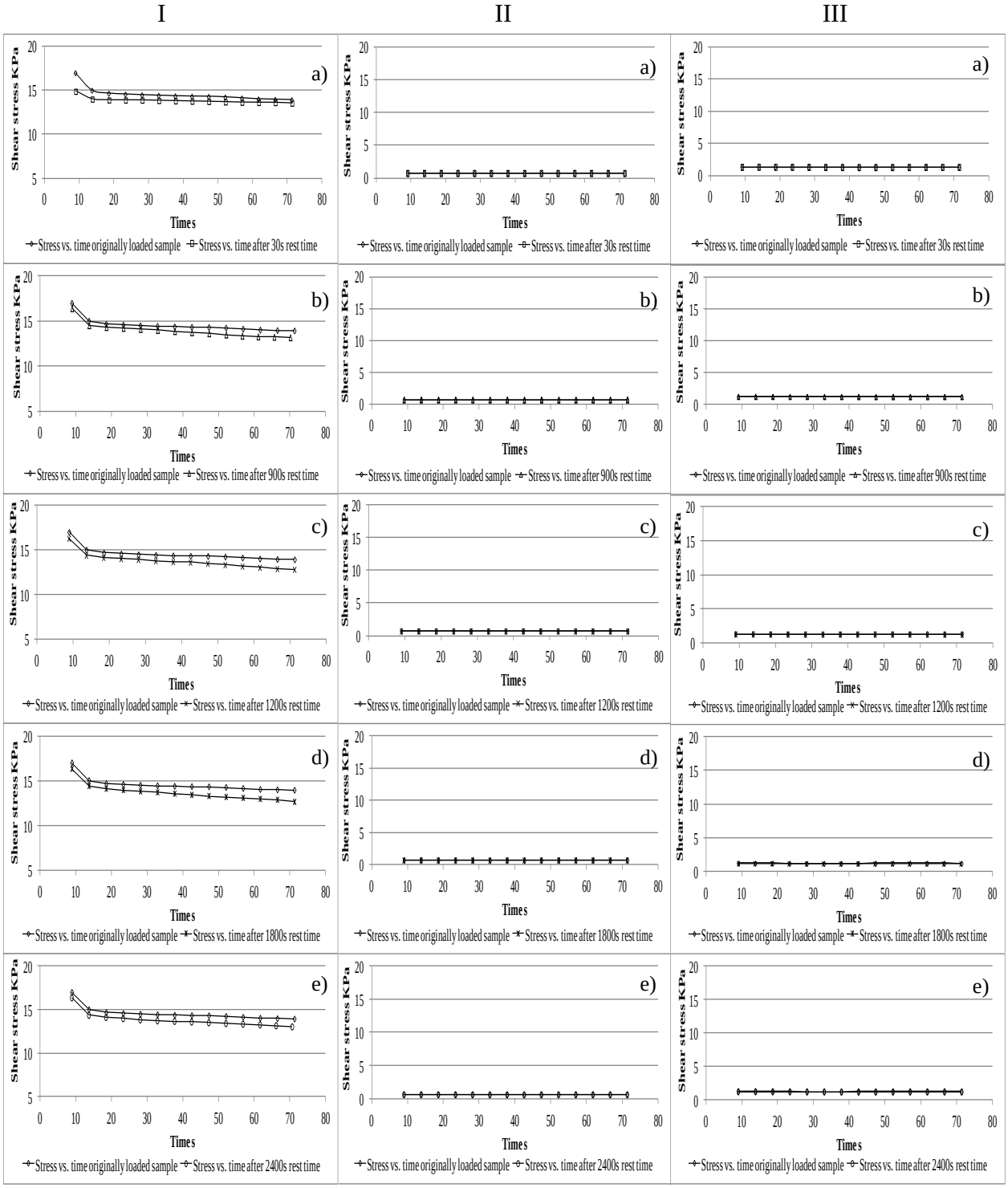

Figure 4.9. Shear stress vs. time of CRMA interacted at 190°C and 50Hz after 480minutes for HU-52 asphalt modified with I)10%CRM, II)10%WTG, and III)10%TR subject to shear rate of 2s-1 at a)30s, b) 900s, c)1200, d)1800s, and e) 2400s rest interval.

This indicates that the utilization of the ambient processed WTG or TR, either form a truck or passenger car sources didn't release the sufficient components to associate in the formation of 3D network structures.

Detection of the Networks in Asphalt by Molecular Testing

GPC was utilized to investigate the triggering effects for the 3D network structure formation in the samples that showed the existence of such networks and for the others that didn't have it.

Gel Permeation Chromatography

Figure 4.10(I and II) illustrates GPC analysis for neat and the CRMA samples as (I) Chromatograms and (II) %LMS, at interaction speeds a)10Hz, b)30Hz, and c)50Hz, respectively. Figure 4.10(I-a) illustrates the GPC chromatograms for the neat asphalt and the 10% CRMA interacted at interaction temperature of 190°C and mixing speed of 10Hz, while Figure 4.10(II-a) illustrates the LMS% increase for the CRMA interacted at interaction temperature of 190°C and mixing speed of 10Hz. As illustrated from Figure 4.10(I-a), a slight shift of the chromatograms' profile towards the left is associated with the increase in interaction time. Figure 4.10(II-a) shows a gradual increase in the LMS fractions for the CRMA that starts from almost 1.2% at 15min interaction time and maximizes to 3.5 % at 8 hrs of interaction time. Similar observations were recorded by other researchers [123]. The increase of LMS is related to the rubber absorbance of low molecular weight aromatics leading to the increase of asphaltenes proportion on the modified asphalt liquid phase [123].

Figure 4.10(I-b) illustrates the GPC chromatograms for the neat asphalt and the CRMA interacted at interaction temperature of 190°C and mixing speed of 30Hz. Figure 4.10(II-b) illustrates the corresponding LMS% increase. As illustrated in Figure 4.10(I-b), a larger shift, com-

pared to the chromatograms of the samples related to the interactions at 10Hz, of the chromatograms' profile towards the left is associated with the increase in interaction time.

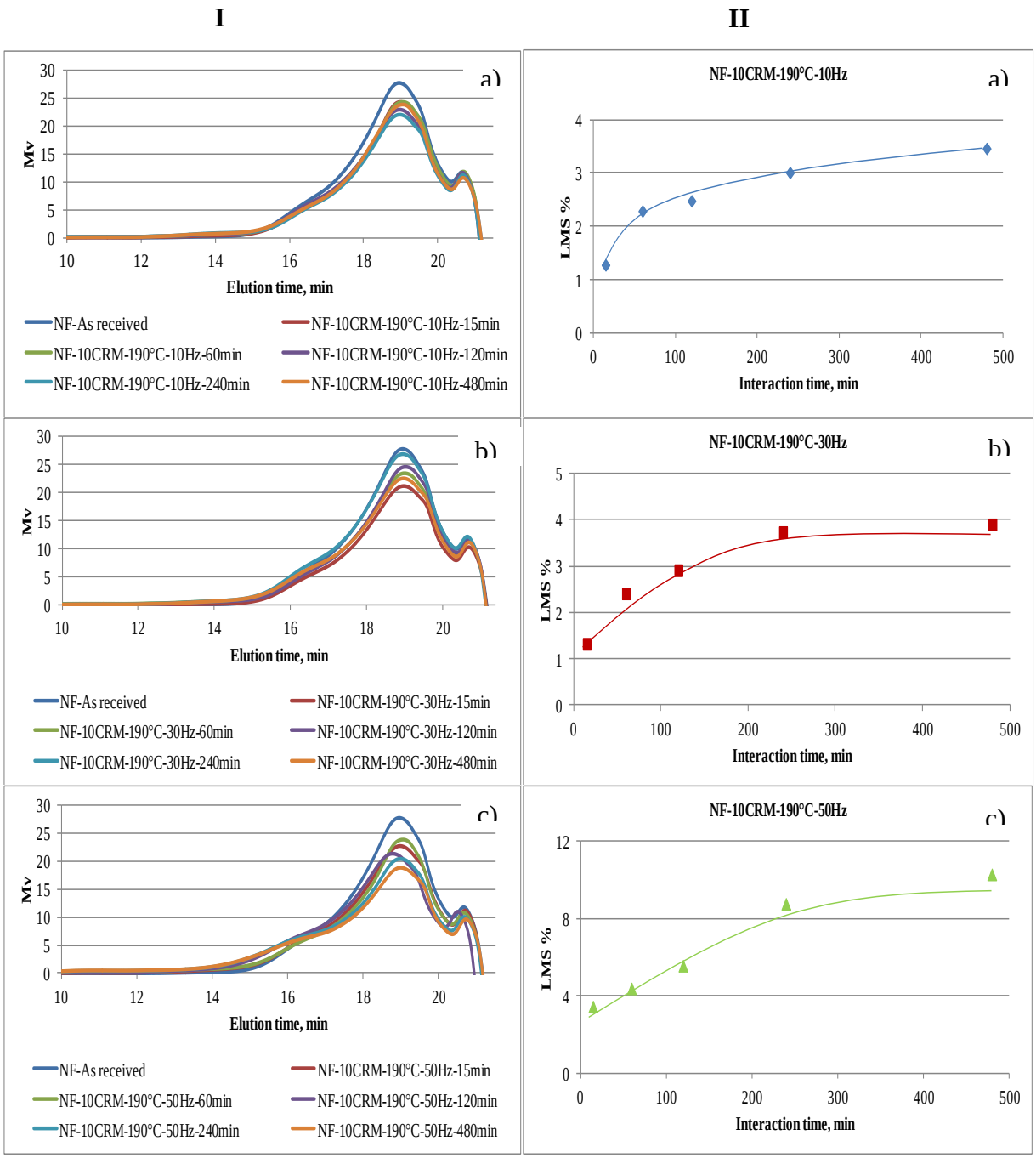

Figure 4.10. GPC analysis for neat and the CRMA samples I) Chromatograms, II) LMS, % at interaction speeds a)10Hz, b)30Hz, and c)50Hz

Figure 4.10(II-b) shows a gradual increase in the LMS fractions for the CRMA that starts from almost 1.3% at 15min of interaction time and maximizes to 4% at 8 hrs of interaction time. This indicates that the rate of increase in the LMS value relates not only to the CRM presence and interaction time, but also to the increase in the interaction speed. As the interaction speed is increased, the rate of rubber absorbance of low molecular weight aromatics also increases leading to the increase of asphaltenes proportion on the modified asphalt liquid phase [123].

Figure 4.10(I-c) illustrates the GPC chromatograms for the neat asphalt and the CRMA interacted at interaction temperature of 190°C and mixing speed of 50Hz. Figure 4.10(II-c) illustrates the corresponding LMS% increase. As illustrated in Figure 4.10(I-c), the largest shift of the chromatograms' profile towards the left can be related to 50Hz interaction speed as compared to the 10Hz and 30Hz chromatograms at the utilized interaction times. Figure 4.10(II-c) shows a consistent increase in the LMS fractions for the CRMA that starts from almost 3.5% at 15min interaction time and maximizes to 10.5% at 8 hrs of interaction time. For both the 10Hz and 30Hz interaction speeds, the increase in LMS% can be attributed to the rubber absorbance of low molecular weight aromatics leading to increased proportion of asphaltenes in liquid phase of asphalt. However, the extent of increase of the LMS in the case of the high speed of the 50Hz cannot be explained in terms of CRM absorbance of low molecular weight fractions of asphalt only because of the occurrence of other mechanisms at such a high speed, namely depolymerization and devulcanization of CRM [23, 122]. It is expected that for the high interaction speed samples, CRM particles are partially devulcanised and depolymerized in the asphalt resulting in the release of CRM components into the liquid phase of asphalt. It is suggested that the increase in the LMS for this specific interaction condition is due to the association of such released components with the liquid phase of asphalt resulting in the formation of the detected 3D network structure.

These results provide evidence for the ability of the GPC technique to be utilized in the detection of the formation of 3D network structure in the liquid phase of CRMA.

Figure 4.11 illustrates the comparison between the % increase in the LMS concentration for the different interaction speeds. Interestingly, a unique resemblance between the G* behavior and the LMS% can be found, as will be illustrated in chapter 5. This provides evidence that the LMS portion of the asphalt chromatogram shows good relation to the rheological behavior (G*) of the binder.

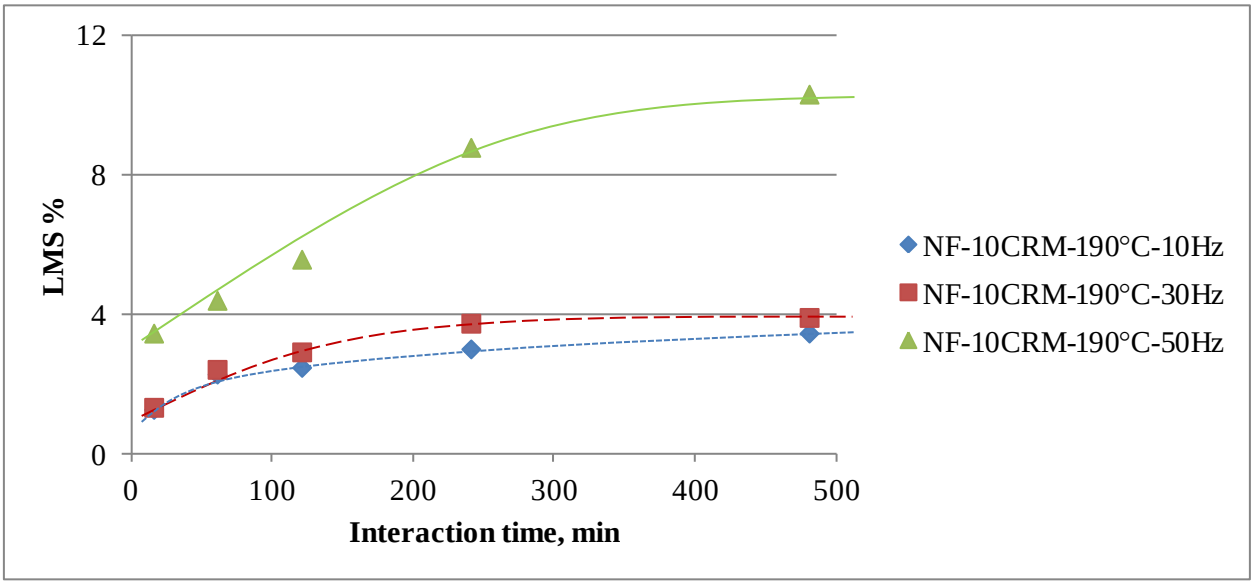

Figure 4.11. Comparison of LMS% increase for the different interaction speeds.

The ability of the GPC to detect the existence of a 3D network structure can be seen from the apparent difference in the LMS% increase between the samples that developed the 3D network structure and the ones that lacked it. Based on the resemblance between the G* behavior and LMS% increase for the samples having a 3D network structure in their liquid phase, the utilization of both techniques can be employed to verify the existence of such network structure. As the existence of the 3D network structure in the liquid phase of the CRMA provides superior enhancements in the CRMA performance; this indicates that GPC can be considered an efficient

technique directly relating the CRMA property enhancement (G* development) to its internal structure.

Detection of the Network by FTIR Analysis of the Liquid Phase of Asphalt

FTIR analysis was utilized to determine the state of existence of the released CRM components within the liquid phase of CRMA under the effect of the different interaction parameters utilized. Figure 4.12(a, b, c) illustrates the FTIR spectroscopy of samples: NF-190-10, NF-190-30, and NF-190-50, respectively. As can be seen from Figure 4.12(a), after 8 hours of interaction time, peaks for the out-of-plane C-H bends of the aromatic ring that are supposed to be intense at 698 and 756 cm^{-1} for the Polystyrene are not present. In addition, peaks at 966 cm^{-1} for the trans component in Polybutadiene are not present also. This indicates that at lower interaction speeds, the main mechanism involved in CRM interaction with asphalt is the rubber absorbance of low molecular weight maltenes [22]. Figure 4.12(b) illustrates the FTIR spectroscopy of samples NF-190-30 interacted at different times. As can be seen from Figure 4.12(b), after 8 hours of interaction time, the same observation of absence of distinctive peaks of either Polystyrene and Polybutadiene can be seen indicating that at such combination of interaction conditions, most of the CRM activities are related to CRM particle swelling. Figure 4.12(c) illustrates the FTIR spectroscopy of samples NF-190-50 interacted at different times. As can be seen from Figure 4.12(c), peaks for the out-of-plane C-H bends of the aromatic ring can be clearly seen at 698 and 756 cm^{-1} for the Polystyrene. In addition, peaks at 966 cm^{-1} for the trans component in Polybutadiene are present also. This indicates that at combination of high interaction speed (50Hz) and moderate interaction temperature (190°C), two mechanisms are involved in CRM interaction with asphalt; the first is the rubber absorbance of low molecular weight maltenes, whereas the most intense

mechanism is occurrence of devalcunization leading to the partial dissolution of CRM in the liquid phase of asphalt.

Figure 4.13 illustrates the FTIR spectra comparison of as received asphalts and samples interacted for 480min at: (a) 160°C and 50Hz, (b) 190°C and 50Hz, and (c) 220°C and 50Hz, for (I) HU-52 and (II) HU-64. As shown in Figures 4.13(I-a) and (II-a), even after 8 hours of interaction time, peaks for the out-of-plane C-H bends of the aromatic ring that are supposed to be intense at 698 cm^{-1} for the Polystyrene are not present. In addition, peaks at 966 cm^{-1} for the trans component in Polybutadiene are not present also. This indicates that at lower interaction conditions (160°C and 50Hz), the CRM components release is minimal and the main CRM interaction with asphalt is the CRM absorbance of low molecular weight maltenes [22].

Figures 4.13(I-b) and (II-b), illustrate the existence of peaks for the out-of-plane C-H bends of the aromatic ring at 698 for the Polystyrene (Arrow for PS in Figure 4.13(I-b) and (II-b)). In addition, peaks at 966 cm^{-1} for the trans component in Polybutadiene can be seen (Arrow for PB in Figure 4.13(I-b) and (II-b)). This indicates that at combination of high interaction speed (50Hz) and moderate interaction temperature (190°C), two mechanisms are involved in CRM interaction with asphalt; the first is the CRM absorbance of low molecular weight maltenes, whereas the most intense mechanism is occurrence of devalcunization leading to the partial dissolution of CRM in the liquid phase of asphalt.

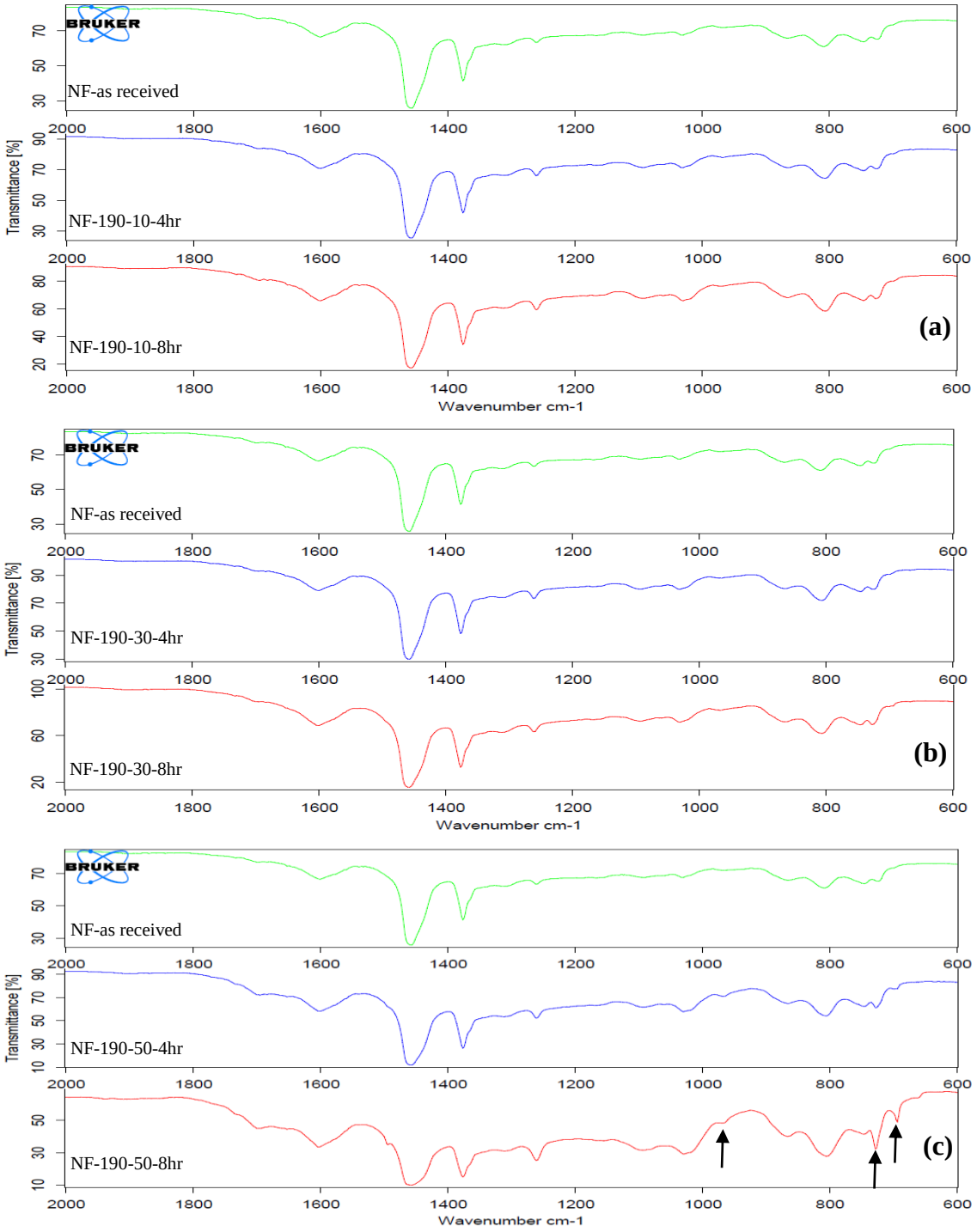

Figure 4.12. FTIR spectra comparison of as received asphalt and samples interacted at: (a) 190°C and 10Hz, (b) 190°C and 30Hz, and (c) 190°C and 50Hz, for the different interaction times.

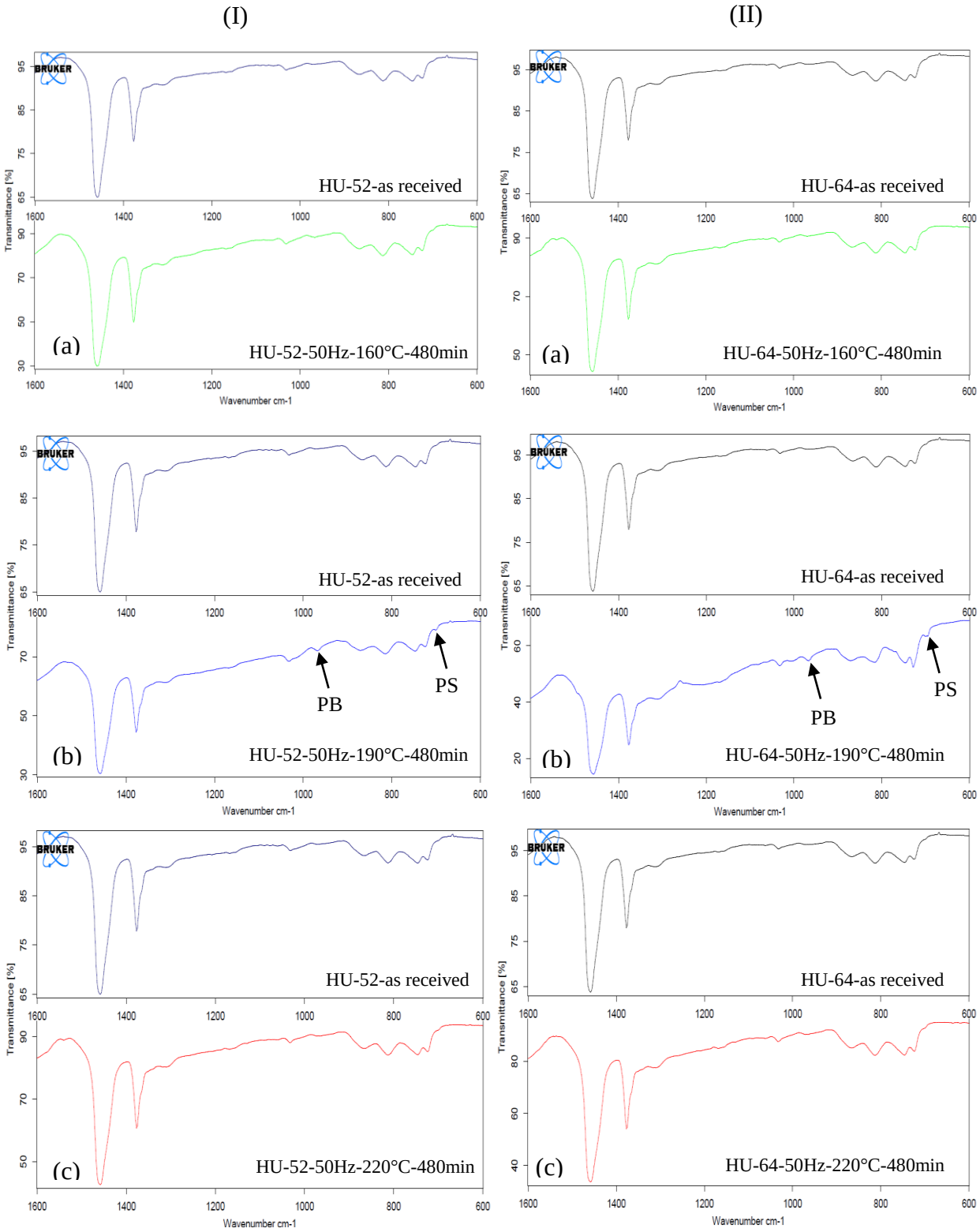

Figure 4.13. FTIR spectra comparison of as received asphalts and samples interacted for 8 hrs at: (a) 160°C and 50Hz, (b) 190°C and 50Hz, and (c) 220°C and 50Hz, for (I) HU-52 and (II) HU-64

As shown in Figure 4.13(I-c) and (II-c), the same observation of absence of distinctive peaks of either Polystyrene and Polybutadiene can be seen indicating that at such combination of interaction conditions (220°C and 50Hz), the devulcanization and deploymerization effects are dominating leading to the annihilation of CRM released components.

Detection of the Network by Investigating the Released Components of CRM in Liquid Phase of Asphalt

In this section, dissolution tests and TGA investigation were utilized to determine the amounts and nature of components released from CRM to as-phalt that resulted in the formation of the network structures in asphalt liquid phase.

Dissolution Behavior and Thermo-Gravimetric Analysis (TGA) of Crumb Rubber Modifier

Figure 4.14 illustrates the change in compositional analysis of extracted CRM for the samples interacted at temperature of 160°C and mixing speed of 10, 30 and 50Hz for an interaction time of 8 hours.

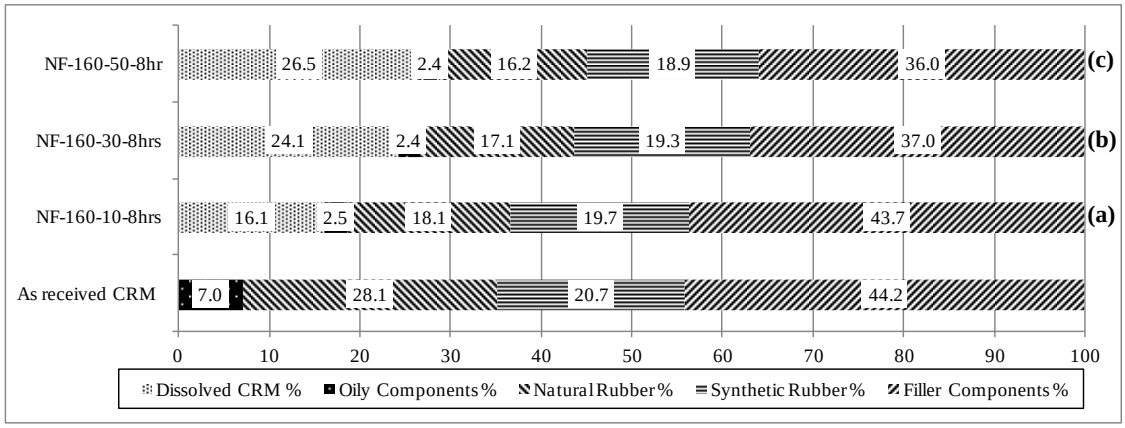

Figure 4.14. Components concentration in extracted CRM samples in comparison with original CRM for the samples interacted at 160°C and mixing speed: (a) 10Hz, (b) 30Hz, and (c) 50Hz.

As can be seen in Figure 4.14(a, b, c) after 8 hours of interaction time; 16.1, 24.1, and 26.5% partial dissolutions in CRM were calculated for the mixing speeds of 10, 30, and 50Hz, respectively.

As can be seen from the released components values, the major components released were expressed in terms of oily components and natural rubber. For the samples interacted at 160°C and 10Hz illustrated in Figure 4.14(a), the resultant CRM compositions were 2.5% oily components, 18.1% natural rubber, 19.7% synthetic rubber, and 43.7% filler components from original values of 7, 28.1, 20.7, and 44.2%, respectively. This indicates that the utilization of an interaction speed of 10Hz with interaction temperature 160°C was not sufficient to release most of the CRM components into asphalt. At this combination of low mixing speed and temperature, the only governing effect is the particle effect of swollen CRM within asphalt as a result of the absorption of light molecular aromatics [22]. Whereas for the samples interacted at 160°C and 30Hz shown in Figure 4.14(b), the composition analysis of interacted CRM after 8hrs of interaction time was 2.4% oily components, 17.1% natural rubber, 19.3% synthetic rubber, and 37% filler components. The highest release of CRM components was associated with the samples interacted at 160°C and 50Hz (Figure 4.14(c)) with values of 2.4% oily components, 16.2% natural rubber, 18.9% synthetic rubber, and 36% filler components. Relating the released CRM components to the fact that such CRMA had weak enhancement in the rheological properties G* and δ (as will be illustrated later in chapter 5), can be explained in terms of the minor release of CRM components that were not sufficient to initiate or sustain a 3D network structure, that would have enhanced the G* and δ significantly. Under such low interaction temperature (160°C) and with the utilization of various mixing speeds (10, 30, and 50Hz) the main CRM activities controlling the CRMA performance is mainly the swelling of CRM [22].

Figure 4.15(a, b, c) shows the variation in compositional analysis of extracted CRM after 8 hrs of interaction time for the samples interacted at temperature of 190°C and mixing speed of 10, 30, and 50Hz, respectively.

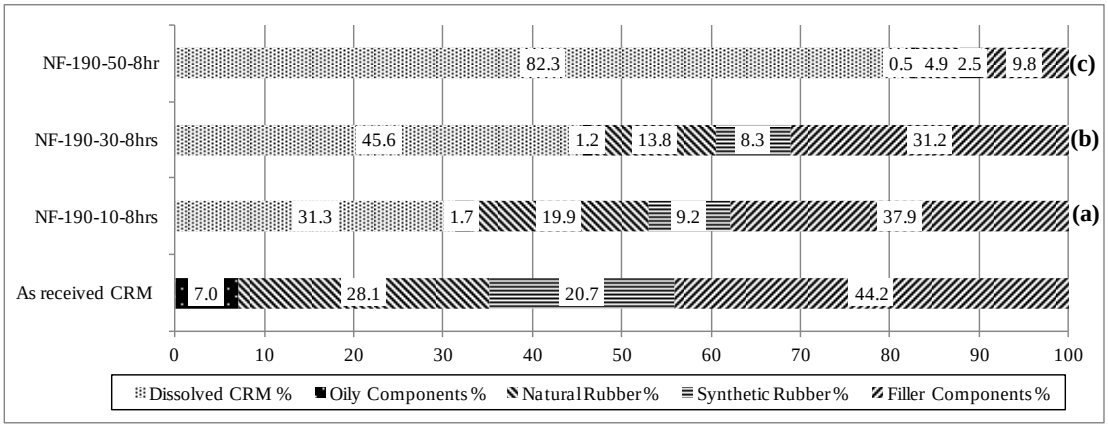

Figure 4.15. Components concentration in extracted CRM samples in comparison with original CRM for the samples interacted at 190°C and mixing speed: (a) 10Hz, (b) 30Hz, and (c) 50Hz.

Figure 4.15(a, b, c) illustrates a general increase in CRM dissolution rate for CRM samples extracted from CRMA as compared to the dissolution rates for the CRM extracted under interaction temperature of 160°C, illustrated in Figure 4.14(a, b, c). This indicates that the effect of interaction temperature is prevalent over the effect of interaction speed in controlling the dissolution rate of CRM and thus property enhancement of CRMA. For the CRM extracted from CRMA interacted with 190°C and 10Hz, after 8hrs of interaction time shown in Figure 4.15(a), the oily components reached 1.7% and the natural rubber reached 19.9% from an original value of 7% and 28%, respectively. Whereas, the synthetic rubber decreased from 21% to 9.2%. On the other hand, the filler components decreased from 44% to 37.9%. Such release of CRM components had similar effect as that of the samples interacted at 160°C and 10Hz in terms of the insufficiency of CRM released components required to initiate or sustain a 3D network structure, that would have enhanced the G* and δ significantly, as will be illustrated in chapter 5.

Figure 4.15(b) shows the variation in compositional analysis of extracted CRM at 8hrs of interaction time for the samples interacted at temperature of 190°C and mixing speed of 30Hz. As can be seen in Figure 4.15(b), for the extracted CRM from CRMA, utilization of interaction time of 8hrs resulted in 45.6% dissolution in CRM. The oily components reached 1.2% and the natural rubber reached 13.8% from an original value of 7% and 28%, respectively. Whereas, the synthetic rubber decreased from 21% to 8.3% and the filler components reached 31.2% from an original value of 44.2%. Relating that to the weak enhancements in G* and δ values for the samples interacted at 190°C and 30Hz, illustrated in chapter 5, it is evident that the lack of abundance of CRM released components at such interaction conditions resulted in minimized property enhancements.

Figure 4.15(c) illustrates the change in compositional analysis of extracted CRM at 8hrs of interaction time for the samples interacted at temperature of 190°C and mixing speed of 50Hz. A different behavior for the dissolution as well as the discharge of CRM components can be seen at such combination of moderate interaction temperature (190°C) and high mixing speed (50Hz). As can be seen in Figure 4.15(c), 82.3% partial dissolution in CRM was calculated. For such interaction conditions, major CRM components release was calculated, where the oily components became 0.5%, the natural rubber reached 4.9%, the synthetic rubber decreased to 2.5%, and the filler components reached 9.8%, from original values of 7, 28.1, 20.7, and 44.2%, respectively. Relating the aforementioned extracted CRM compositional analysis to the superior rheological values for both G* and δ of the same samples (as will be illustrated later in chapter 5) and the shear stress overshoot behavior (illustrated in Figure 4.6), indicates that at such combination of high mixing speed (50Hz) and moderate interaction temperature (190°C), the release of CRM is not only limited to the oily components and the natural rubber but rather involves all CRM com-

ponents including the remaining synthetic rubber as well as the filler components. Such release of CRM components helps initiating and sustaining the formation of 3D network structure that significantly enhances the CRMA rheological properties (G* and δ). This can be explained in terms of occurrence of devulcanization effects that lead to the release of rubber components into the liquid phase of asphalt. However, at such combination of interaction conditions (190°C and 50Hz), depolymerization effects are not major, thus the released rubber components are not readily destroyed (by depolymerization) and thus can undergo other processes involving the association within the CRMA liquid phase resulting in the produced 3D network structure, was seen in the FTIR section.

Figure 4.16(a, b, c) illustrates the change in compositional analysis of extracted CRM at 8hrs of interaction time for the samples interacted at temperature of 220°C and mixing speed of 10, 30, and 50Hz, respectively.

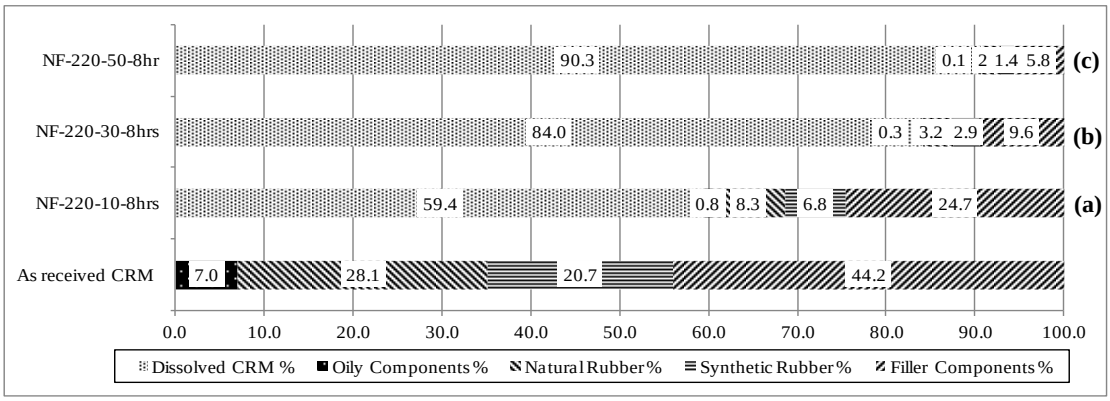

Figure 4.16. Components concentration in extracted CRM samples in comparison with original CRM for the samples interacted at 220°C and mixing speed: (a) 10Hz, (b) 30Hz, and (c) 50Hz.

As can be seen from Figure 4.16(a), for the CRM extracted from CRMA interacted with 220°C and 10Hz, after 8hrs of interaction time, CRM dissolution was 59.4% with the oily components being 0.8% and the natural rubber having a value of 8.3%. Whereas, the synthetic rubber

decreased to 6.8%, and the filler components reached 24.7%. Relating that to the rheological properties measured for these samples, that will be illustrated later in chapter 5, it can be deduced that although, more than half the CRM particles had dissolved in the CRMA liquid phase, however as a result of the increased interaction temperature (220°C) and regardless of the reduced interaction speed (10Hz), the excessive devulcanization and depolymerization effects were strong enough to annihilate the effect of the CRM released components in the liquid phase of CRMA.

Figure 4.16(b) shows the variation in compositional analysis of extracted CRM with the increase of interaction time for the CRMA samples interacted at temperature of 220°C and mixing speed of 30Hz . As can be seen from Figure 4.16(b), utilization of interaction time of 8hrs resulted in a 84% partial dissolution in CRM with major CRM components release manifested in the oily components reaching 0.3%, the natural rubber being 3.2%, the synthetic rubber becoming 2.9%, and the filler components reaching 9.6%, from original values of 7, 28.1, 20.7, and 44.2%, respectively. The same trend can be seen for the CRM extracted from CRMA samples interacted at 220°C and 50Hz, illustrated in Figure 4.16(c). After 8hrs of interaction time, the CRM dissolution was 90.3%, with oily components reaching 0.1% and the natural rubber of about 2% from an original value of 7% and 28.1%, respectively. Whereas, the synthetic rubber decreased from 20.7% to 1.4% and the filler components decreased from 44.2% to 5.8%. Although the similarity can be seen for the amount of released CRM components between the samples interacted at 190°C with 50Hz at 8hrs of interaction time and the samples interacted at 220°C with 50Hz after 8hrs of interaction time. However, it will be illustrated later in chapter 5 that sever deterioration in both G* and δ is associated with the samples interacted at 220°C and 50Hz, whereas superior enhancements in both G* and δ can be seen for the samples interacted at

190°C and 50Hz [124]. This indicates that with nearly similar CRM dissolved/released components, the effect of interaction temperature can dramatically enhance or deteriorate the properties of CRMA. The high interaction temperature (220°C) annihilated the modification effects of the released CRM components, even at almost 90.3% dissolution percent for the samples interacted at 220°C and 50Hz. The case was different for the interaction temperature of 190°C with interaction speed of 50Hz, where at almost similar CRM dissolution; the released CRM into the CRMA liquid phase had the effect of formation of 3D network structure that significantly enhanced the CRMA rheological properties.

Figure 4.17(a, b) illustrates the change in compositional analysis of extracted CRM for the samples interacted at a temperature of 160°C and mixing speed of 50Hz for Hu-52 and HU-64 asphalts. As shown in Figure 4.17(a) for the extracted CRM from HU-52, utilization of interaction time of 15min resulted in a 13% partial dissolution in CRM with the major components released expressed in terms of oily components and natural rubber. The dissolution of CRM increases to 16, 21, 22 and 26.7% for the 60, 120, 240, and 480min interaction times, respectively. Such increase in dissolution of CRM is associated with a major release of most of the oily components, as well as natural rubber, whereas minor release of both the synthetic rubber and the filler components can be seen, even after 480min of interaction time.

The same trend can be seen for the compositional analysis of extracted CRM from HU-64 CRMA illustrated in Figure 4.17(b). Almost the same dissolved amounts can be found for the CRM extracted from HU-52 and HU-64 CRMA samples. Relating the released CRM components to the rheological behavior of CRMA ,that will be illustrated later, implies that the weak enhancement in the CRMA rheological properties, G* and δ, can be explained in terms of the minor release of CRM components that were not sufficient to initiate or sustain a 3D entangled

network structure. Under such low interaction temperature (160°C) and even with the utilization of a high mixing speed (50Hz), the main CRM activities controlling the CRMA performance are the swelling of CRM [22].

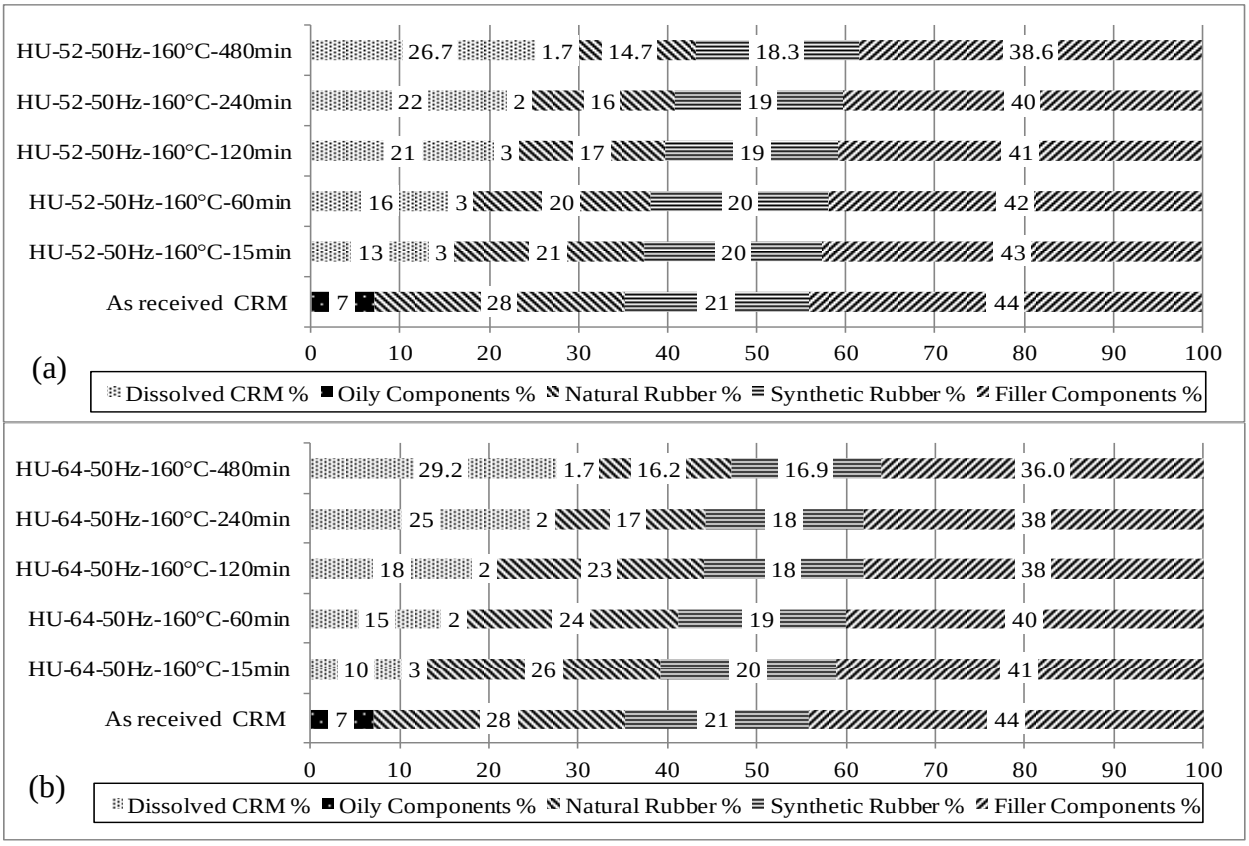

Figure 4.17. Components concentration in extracted CRM samples in comparison with original CRM: (a)HU-52-50Hz-160°C and (b)HU-64-50Hz-160°C

Figures 4.18(a, b, c, d) show the variation in compositional analysis of extracted CRM with the increase of interaction time for the samples: (a)HU-52-10Hz-190°C ,(b)HU-64-10Hz-190°C , (c)HU-52-30Hz-190°C and (d)HU-64-30Hz-190°C, respectively.

Figure 4.18(a, b, c, d) illustrates an increase in CRM dissolution rate for CRM samples extracted from both asphalt types investigated as compared to the dissolution rates for the CRM extracted under interaction conditions of 160°C and 50Hz, illustrated in Figure 4.17(a, b). This

indicates the effect of interaction temperature is prevalent over the effect of interaction speed in controlling the dissolution rate of CRM and thus property enhancement of CRMA. Figure 4.18(a, b) illustrates the minor release of both synthetic rubber and filler components from the CRM into the liquid phase of asphalt alongside the interaction time. On the other hand, release of both the oily components and the natural rubber is abundant with the increase of interaction time. Such minor release of CRM components had similar effect as that of the samples interacted at 160°C and 50Hz in terms of the insufficiency of CRM released components required to initiate or sustain a 3D entangled network structure, that would have enhanced the G* and δ significantly, as will be illustrated later in chapter 5. This can be seen from the rheological results, that will be illustrated later, where minor property enhancements can be seen for both G* and δ with the main cause being the CRM particle swelling in the presence of minor CRM released components.

As can be seen in Figure 4.18(c) for the extracted CRM from HU-52 CRMA interacted at 30Hz and 190°C, the same trend that was observed earlier for the samples interacted at 50Hz and 160°C manifested in the release of most of the oily components, as well as natural rubber with minor release of both the synthetic rubber and the filler components can be seen, even after 480min of interaction time. A similar trend can be seen for the compositional analysis of extracted CRM from HU-64 CRMA illustrated in Figure 4.18(d). After 480min of interaction time, the oily components reached 1.2% and the natural rubber reached 10.8% from an original value of 7% and 28%, respectively. Whereas, the synthetic rubber decreased from 21% to 14.3% and the filler components reached 36.2% from an original value of 44%. Relating that to the G* and δ values illustrated later in chapter 5, shows that the lack of abundance of CRM released components at such interaction conditions resulted in minimized property enhancements.

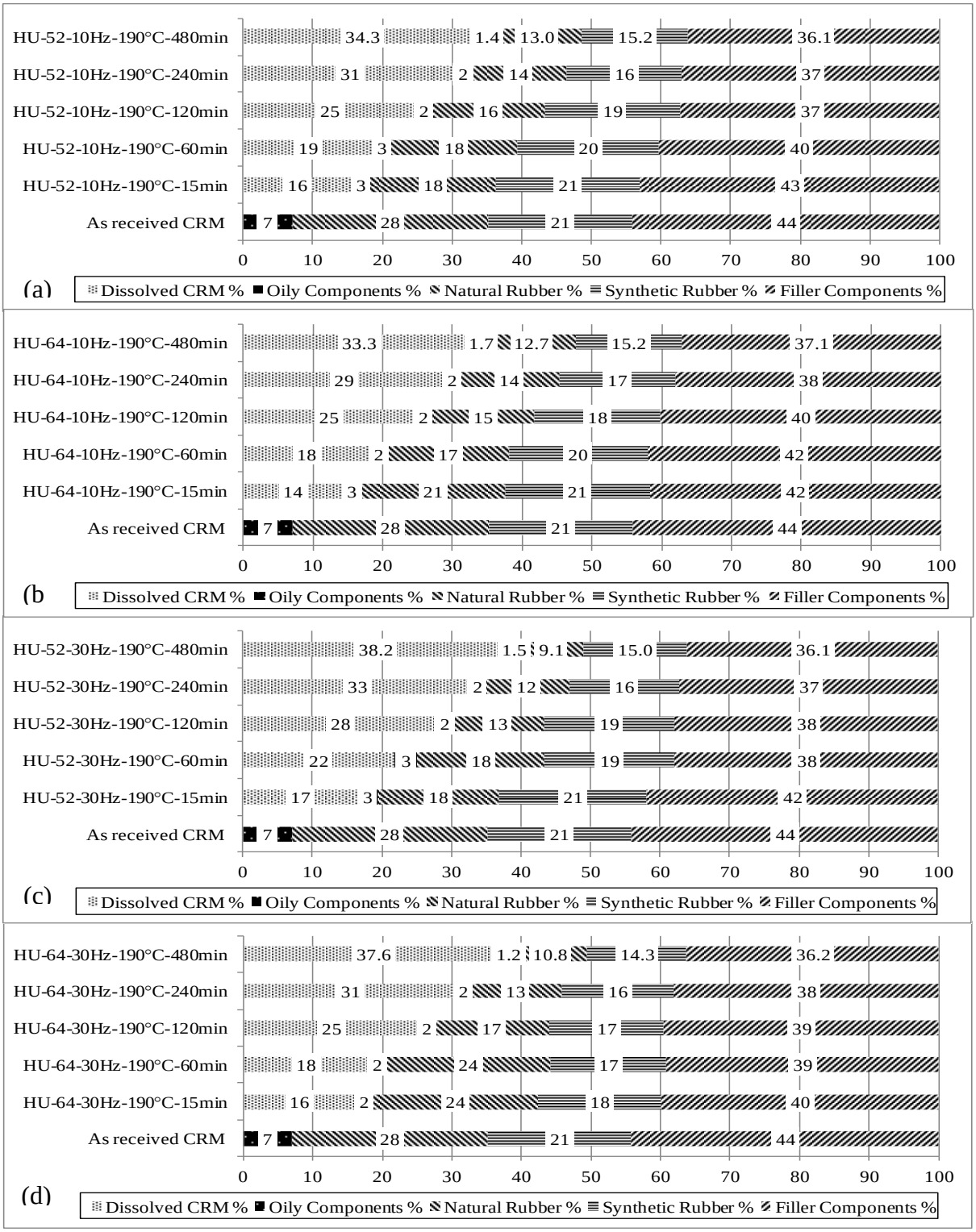

Figure 4.18. Components concentration in extracted CRM samples in comparison with original CRM: (a)HU-52-10Hz-190°C ,(b)HU-64-10Hz-190°C , (c)HU-52-30Hz-190°C and (d)HU-64-30Hz-190°C

Figure 4.19(a, b) illustrates the change in compositional analysis of extracted CRM with the increase of interaction time for the samples interacted at temperature of 190°C and mixing speed of 50Hz for HU-52 CRMA and HU-64 CRMA, respectively. A different behavior for the dissolution as well as the discharge of CRM components can be seen at such combination of moderate interaction speed (190°C) and high mixing speed (50Hz). As shown in Figure 4.19(a), utilization of interaction time of 15min resulted in a 25% partial dissolution in CRM with the major components released expressed in terms of oily components and natural rubber. However, extending the interaction time up to 480min resulted in a major CRM components release manifested in increase in CRM dissolution to 30, 62, 78 and 83% for the 60, 120, 240, and 480min interaction times, respectively. Such increase in dissolution of CRM is associated with a major release of most of CRM components after 480min of interaction time, where the oily components reached 0.5%, the natural rubber reached 4%, the synthetic rubber reached 3%, and the filler components reached 10%, from original values of 7, 28, 21, and 44%, respectively.

The same trend can be seen for the CRM extracted from the HU-64 CRMA samples interacted at 190°C and 50Hz, illustrated in Figure 4.19(b). After 480min of interaction time, the CRM dissolution was 85%, with oily components reaching 1% and the natural rubber of about 2% from an original value of 7% and 28%, respectively. Whereas, the synthetic rubber decreased from 21% to 3% and the filler components decreased from 44% to 9%. Relating the aforementioned extracted CRM compositional analysis to the rheological results of the same samples, illustrated section in the rheological analysis discussed later in chapter 5, indicates that at such combination of high mixing speed (50Hz) and moderate interaction temperature (190°C), the release of CRM is not only limited to the oily components and the natural rubber but rather involves all CRM components including the remaining synthetic rubber as well as the filler com-

ponents. Such release of CRM components coupled by the moderate interaction temperature (190°C) helps initiating and sustaining the formation of 3D entangled network structure that significantly enhances the CRMA rheological properties (G* and δ). This can be explained in terms of occurrence of devulcanization effects that lead to the release of CRM components into the liquid phase of asphalt, however at such moderate interaction conditions, depolymerization effects for the released CRM polymeric components are not major, thus the released CRM polymeric components are not readily destroyed (by deploymerization) and thus can undergo other processes involving the association within the CRMA liquid phase resulting in the produced 3D entangled network structure, as previously illustrated later in the FTIR section. The mechanism of formation of such 3D network structure in CRMA, will be further investigated in the asphalt fractionation section.

Figure 4.20(a, b, c, d) illustrates the change in compositional analysis of extracted CRM with the increase of interaction time for the samples : (a)HU-52-10Hz-220°C, (b)HU-64-10Hz-220°C (c)HU-52-50Hz-220°C and (d)HU-64-50Hz-220°C, respectively. As shown in Figure 4.20(a), for the CRM extracted from HU-52 CRMA, after 480min of interaction time, CRM dissolution was 63.3% with the oily components being 0.9% and the natural rubber having a value of 4.8%. Whereas, the synthetic rubber decreased to 8.5%, and the filler components reached 22.5%. On the other hand, for the compositional analysis of CRM extracted from HU-64 asphalt illustrated in Figure 4.20(b), after 480min of interaction time, the total dissolution of extracted CRM was 65.4% with oily components decreasing to 0.8%, natural rubber being 4.3%, synthetic rubber reaching 8.8% and filler components of 20.7%. Relating that to the rheological properties of the same samples, that will be illustrated in the rheological analysis section in chapter 5, it can be deduced that almost half the CRM particles had dissolved in the CRMA liquid phase;

however, as a result of the increased interaction temperature (220°C) and regardless of the reduced interaction speed (10Hz), the excessive devulcanization and depolymerization effects were strong enough to annihilate the effect of the CRM released components on the liquid phase of CRMA, a similar observation were recorded in the literature [116, 122].

As shown in Figure 4.20(c), for the extracted CRM from HU-52 CRMA interacted at 50Hz and 220°C, extending the interaction time up to 480min resulted in a major CRM components release manifested in CRM dissolution of 92% after 480min of interaction time. Such increase in dissolution of CRM is associated with a major release of most of CRM components.

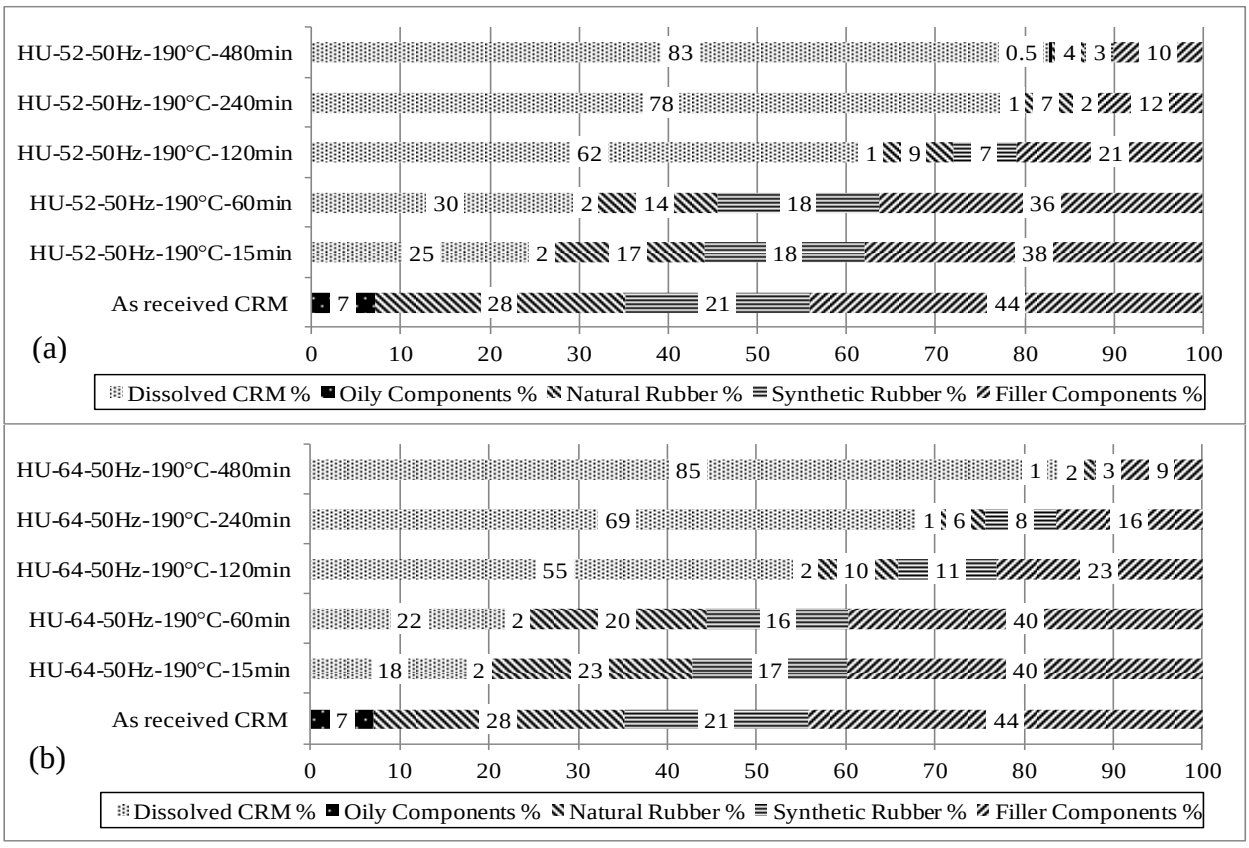

Figure 4.19. Components concentration in extracted CRM samples in comparison with original CRM: (a)HU-52-50Hz-190°C and (b)HU-64-50Hz-190°C

The same trend can be seen for the CRM extracted from the HU-64 CRMA samples interacted at 220°C and 50Hz, illustrated in Figure 4.20(d). After 480min of interaction time, the

CRM dissolution was 90%, with oily components reaching 0.1% and the natural rubber of about 2.3%. Whereas, the synthetic rubber decreased to 1.6% and the filler components decreased 5.8%. Although the similarity can be seen for the amount of released CRM components between the samples interacted at 190°C with 50Hz at 480min of interaction time and the samples interacted at 220°C with 50Hz at 480min of interaction time.

However, the comparison between the rheological parameters, G* and δ, illustrated in the rheological analysis section discussed in the next chapter, shows that with the nearly similar CRM dissolved/released components, the effect of interaction temperature can dramatically enhance or deteriorate the properties of CRMA.

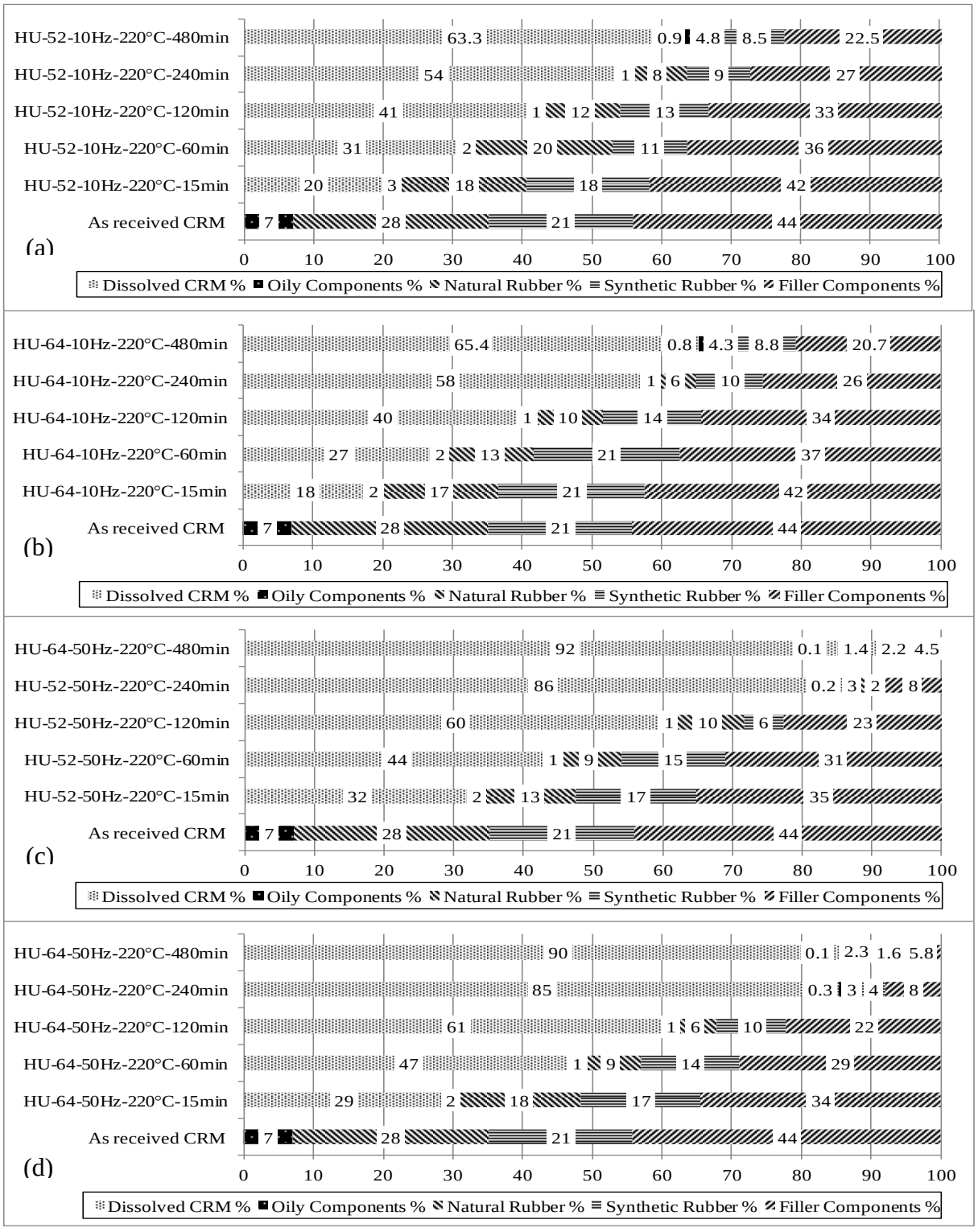

Figure 4.20. Components concentration in extracted CRM samples in comparison with original CRM: (a)HU-52-10Hz-220°C, (b)HU-64-10Hz-220°C (c)HU-52-50Hz-220°C and (d)HU-64-50Hz-220°C

CHAPTER FIVE. EFFECT OF THE INTERNAL NETWORK STRUCTURE ON THE MACRO AND MICRO MECHANICAL PROPERTIES OF ASPHALTS AND RUBBER MODIFIED ASPHALTS

Introduction

In the previous chapter we investigated the methods and approaches to detect the presence of network structures in asphalt. Those method ranged from physical, to chemical, as well as molecular and thermal approaches. In this chapter we delineate how the presence of the network enhances the in-service properties of asphalt. This is explained in terms of the macro and micro scale aspects. For the macro scale investigation aspect, it was decided to measure the G* and δ at the expected service temperature of the asphalt so as to determine how the asphalt, being an important part of the hot mix pavement (HMA), would behave in the presence of the network structure. As for the micro-scale investigation of the asphalt properties, this was carried out to simulate the expected behavior of the thin asphalt layer on aggregate which is in the thickness of few microns. Another important aspect covered in this chapter is the relation between the CRM dissolved amounts and released components on the network development on asphalt and how such network affects the micro-mechanical properties of asphalt. This gives us an insight about how the interaction parameters affects the dissolution and release of CRM which adversely have a major impact on the network development within asphalt that significantly alters the micromechanical properties of asphalt.

Rheological Analysis of the CRMA

In this section the rheological properties G* and δ are being investigated at the expected in-service pavement temperature for each asphalt type investigated.

Figure 5.1(I and II) illustrates, for asphalt NF-58, the progression of the rheological parameters, G*(I) and δ(II), for the different interaction speeds (10Hz, 30Hz and 50Hz) at interaction temperatures of a)160°C, b)190°C, and c)220°C, respectively. As can be seen from Figure 5.1(I-a), higher interaction speeds of 30Hz and 50Hz had the effect of improving the stiffness of the CRMA with comparable results over the interaction time at an interaction temperature of 160°C. On the other hand, the interaction speed of 10Hz produced lower values for the G*, indicating that energy input (temperature, speed and time) was not sufficient to initiate interaction between CRM and asphalt. At this combination of low mixing speed and temperature, the only governing effect is the particle effect of swollen CRM within asphalt as a result of the absorption of light molecular aromatics **[22]**.

Figure 5.1(II-a) shows the same trend for δ at the mixing speed of 10Hz, the lowest reduction in δ is assigned to that speed. Higher reduction in the value of δ can be seen for the higher speeds of 30 and 50Hz as the interaction time is increased. This indicates that at the lower interaction temperature of 160°C, higher interaction speeds are required to initiate the formation of cross linking within the CRMA matrix and thus improving its elasticity. As shown in Figure 5.1(I-b) and Figure 5.1(II-b), a different trend can be found for the progression of the rheological parameters G* and δ, for the different interaction speeds (10Hz, 30Hz and 50Hz) at a constant interaction temperature of 190°C, respectively.

Figure 5.1(I-b) shows a superior value for the G* for interaction speeds of 50Hz over the other two speeds (10Hz and 30Hz) during the interaction time. The combination of the moderate temperature of 190°C and high mixing speed of 50Hz had the effect of improving the stiffness of the CRMA over the other two interaction speeds along the interaction time.

Figure 5.1(II-b) shows the similar trend of superior improvement of δ for the same mixing speed (50Hz) over the other two speeds utilized. As shown from the behavior of both G* and δ over time, the improvement of the values of both rheological parameters is associated with higher interaction speed. This indicates that the combination of higher mixing speed with moderate interaction temperature provides sufficient energy input to sustain an interaction mechanism between CRM and asphalt. The amount of energy input for such combination enables the swelling of CRM by the light aromatic components of asphalt at the early stages of interaction and the release of some of the CRM components by depolymerization and devulcanization at later interaction stages; however, it doesn't extend the depolymerization and devulcanization processes to the degree of losing the CRM modification effects, as will be illustrated later for the 50Hz and 220°C combination. The interaction mechanism between CRM and asphalt affects the internal structure of the produced CRMA providing improved cross linking and thereby forming a 3D network structure within its matrix that increases both its stiffness and elasticity, as previously proven in the interrupted shear flow testing section.

The trend of the rheological parameters, G* and δ, for the three mixing speeds used (10Hz, 30Hz, and 50Hz) at the interaction temperature of 220°C is shown in Figure 5.1(I-c) and Figure 5.1(II-c), respectively.As can be seen from Figure 5.1(I-c), continuous deterioration of G* is associated with the highest interaction speed of 50Hz over the course of the interaction time. This can be explained in terms of the depolymerization and devulcanization effects that dominate the interaction between CRM and asphalt at such high interaction energy (temperature and speed) **[23, 122]**. On the other hand, a plateau behavior of the G* is prevalent for the mixing speeds of 10Hz and 30Hz up to 240 minutes of interaction time. Beyond 240 minutes of interaction time, the values of G* increases for both mixing speeds, with the 30Hz interaction speeds

sample showing superiority over the 10Hz interaction speed. This shows that for the high temperature interactions, moderate (30Hz) to low (10Hz) mixing speeds have the effect of minimizing the depolymerization and devulcanization effects that can lead to the property deterioration, associated with the high mixing speed (50Hz) at the same elevated temperature (220°C) **[23, 122]**. Figure 5.1(II-c) illustrates the behavior of δ; continuous property deterioration is dominant for the high mixing speed with the increase in interaction time. On the other hand, similar behavior for the δ is achieved for both the low (10Hz) and moderate (30Hz) mixing speeds. As the mixing time increases, the value of δ continues to decrease indicating improvement of the elasticity for the CRMA. The enhancements of both G* and δ for the low and moderate interactions speeds after 240 min of interaction can be explained as a result of the release of CRM components in the liquid phase of asphalt that initiate the formation of 3D network structure; however, such conditions were not as favorable as those for the 190ºC temperature and 50Hz speed interaction conditions that produced the well developed 3D network structure, as will be explained later.

Figure 5.2(a, b, and c) and 5.3 (a, b, and c) illustrate the development of rheological parameters, G*(I) and δ(II), for the two asphalt types investigated (HU-52 and HU-64) interacted at 50Hz and 160°C, 10Hz and 190°C, 30Hz and 190°C, 50Hz and 190°C, 10Hz and 220°C, and 50Hz and 220°C, respectively. As shown in Figure 5.2(I-a), a continuous increase for the G* values can be seen for the two CRMA types investigated, with the HU-64 CRMA samples having higher G* values over the other HU-52 samples. Under such a combination of low interaction temperature (160°C) and high mixing speed (50Hz), the only governing parameter for the enhancement in G* is the particle effect of swollen CRM within asphalt as a result of the absorption of light molecular aromatics **[22]**, as shown earlier in the thermal analysis section. On the

other hand, the higher values for G* for the HU-64 CRMA samples over the HU-52 ones can be attributed to the fact that the HU-64 asphalt is a stiffer binder, and thus it is expected that it would give higher G* values. Figure 5.2(II-a) shows the same trend for δ. A reduction in the value of δ can be seen for both CRMA types investigated, with the HU-64 CRMA samples showing better values over the HU-52 ones.However, for both CRMA types investigated, the enhancement in the G* and δ values are minor. This is due to the fact that at such a low interaction temperature (160°C) and even with the utilization of a higher mixing speed (50Hz), the release of CRM components is not sufficient to lead to the formation of a 3D network structure within the liquid phase of CRMA that would dramatically enhance its G* and δ values. This can be explained as a result of restriction of CRM particles activity on absorption of light molecular aromatics [22]. Sufficient release of CRM components under specific interaction conditions would have led to the formation of a 3D network structure within the liquid phase of CRMA providing enhancement in both G* and δ values, as was shown earlier in the thermal analysis section. Figure 5.2(I-b) shows superior values for the G* for the HU-64 CRMA samples over the HU-52 CRMA samples during the interaction time. However, the combination of the moderate temperature of 190°C and low speed of 10Hz with the associated minor release of CRM components into the liquid phase of CRMA was not sufficient to initiate and sustain the formation of the 3D network structure within the liquid phase of CRMA, as illustrated in the thermal analysis section.

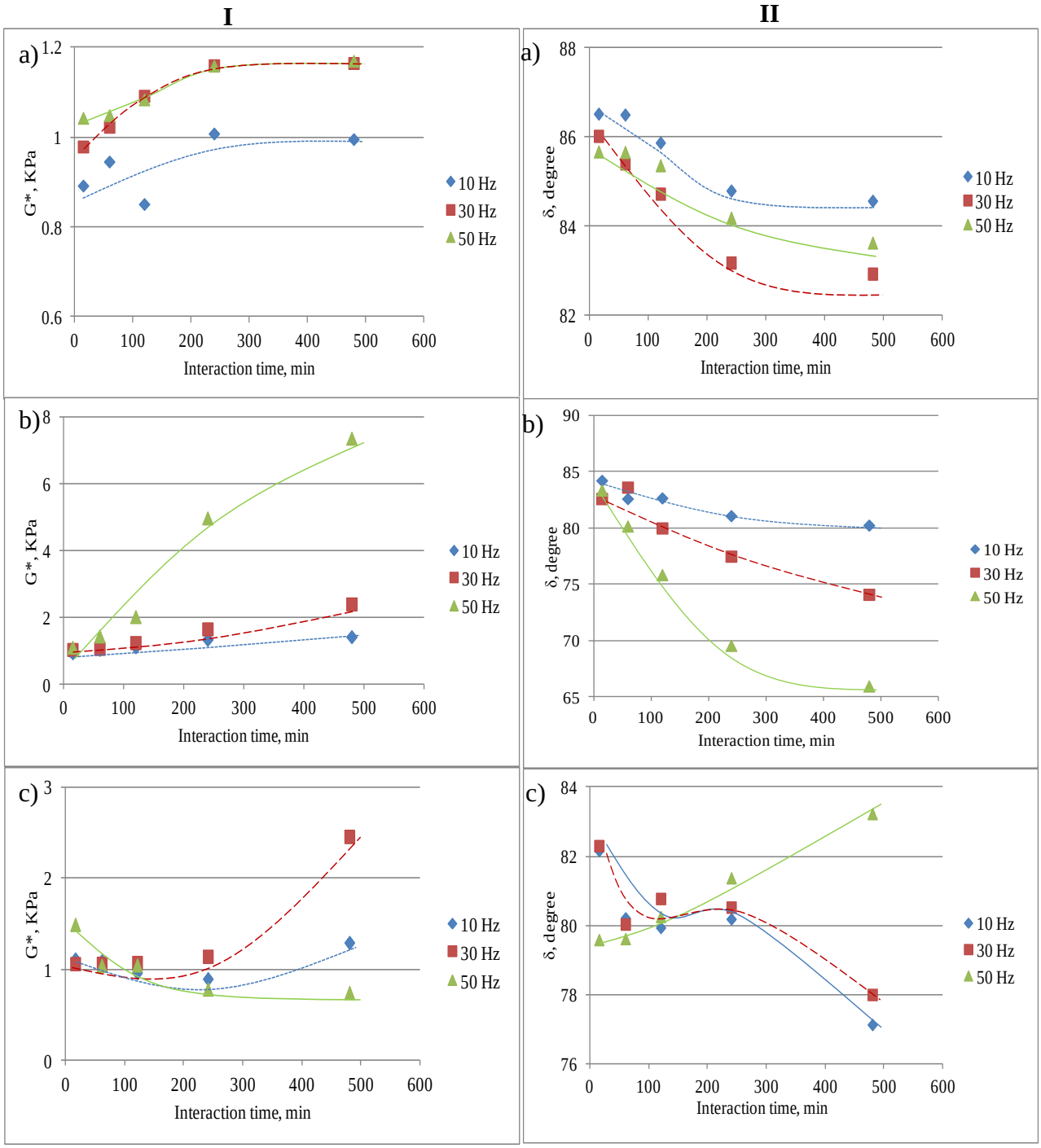

Figure 5.1. Development of rheological parameters of NF-58 CRM binder interacted under different interaction speed: I) G* and II) δ at temperatures a)160°C, b)190°C, and c)220°C

A Similar behavior can be seen in Figure 5.2(II-b) for the δ property progression with the interaction time, where the δ values continue their enhancement with the increase of interaction time with the HU-64 CRMA samples showing better enhancement over the HU-52 CRMA samples.

Figure 5.2(I-c) shows a weak plateau behavior for both asphalt types investigated, with the HU-64 samples of higher values than the HU-52 ones. Figure 2(II-c), illustrates the same trend for δ enhancement having the HU-64 samples exhibiting lower values than the HU-52, when measured for the same interaction time. As explained earlier, the enhancement in both the G* and δ values for these interaction conditions can be explained in terms of the swelling and minor depolymerization/devulcanization of CRM [22, 116, 122]. Such minor release of CRM components was not sufficient to initiate or sustain the development of a 3D network structure that would have produced major enhancement in both rheological parameters investigated, G* and δ, as proven in the thermal analysis section. However, it should be noticed that with the increase of interaction speed, temperature and time, property enhancement, in terms of G* increase and δ reduction, is achieved due to the increase of rate of dissolution of CRM and thus the addition of CRM components into the liquid phase of asphalt, as shown in the thermal analysis section discussed earlier. As shown in Figure 5.3(I-a), a major enhancement in the values of G* can be seen for the CRMA utilizing both the HU-52 and HU-64 asphalts, having the CRMA made with HU-52 of higher values than the HU-64 CRMA after 480min of interaction time. The same trend can be seen for the δ values shown in Figure 3(II-a). As explained earlier, similar observations were seen by utilizing another asphalt type NF-58. As explained earlier such behavior is attributable to the formation of 3D network structure within the liquid phase of CRMA . The reason of the formation of such 3D network structure can be explained in terms of the release of

CRM components into the liquid phase of CRMA, under such interaction parameters (interaction temperature 190°C, mixing speed 50Hz, and interaction time (480min) that was able to maintain and preserve the CRM components and associate them with the components of the liquid phase of asphalt as was shown in the thermal analysis section. In the previous chapter, through the utilization of the TGA and FTIR techniques, the analysis of the CRM extracted as well as the liquid phase from the three asphalt types showed that the utilization of interaction temperature 190°C, mixing speed 50Hz, and interaction time (480min) was favorable for the formation of the 3D network structure.

As shown in Figure 5.3(I-b), for both asphalt types investigated, the G* values suffer deterioration alongside the interaction time, after a brief increase within 60min of interaction time for the HU-64 and 120min of interaction time for the HU-52 samples. The same observation can be drawn for the δ values, as illustrated in Figure 5.3(II-b). Unlike what occurs for moderate (190°C) interaction temperature with the utilization of low (10Hz) interaction speed, the utilization of a high interaction temperature (220°C) leads to destruction of released CRM components by excessive depolymerization and devulcanization, as can be seen from the deteriorated G* and δ values [116, 122].

As shown in Figure 5.3(I-c), property deterioration is prevalent after 120min of interaction time for both asphalt types investigated (HU-64 and HU-52). A similar trend of property deterioration can be seen for the δ behavior illustrated in Figure 5.3(II-c), where the δ values show a consistent increase after 60min of HU-64 CRMA samples. As explained earlier, the main reason behind such property deterioration is the excessive depolymerization and devulcanization effects [116, 122] that were increasingly manifested at such a combination of high interaction temperature (220°C) and mixing speed (50Hz) that lead to the destruction and annihilation of the

CRM released components effects on the CRMA liquid phase, as shown in the TGA and FTIR sections discussed in chapter four.

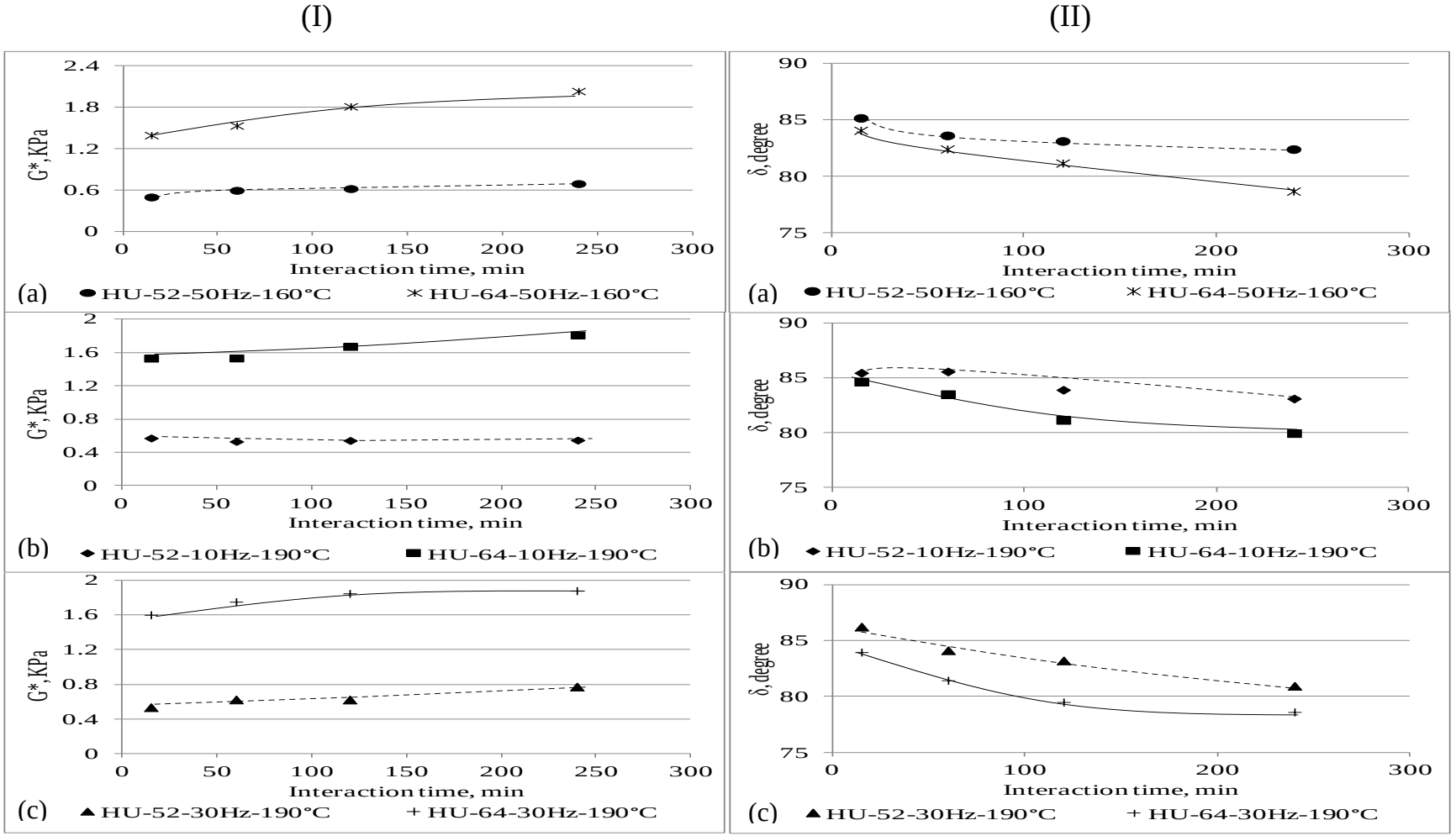

Figure 5.2. Development of rheological parameters of CRMA: (I)G* and (II)δ for samples interacted at (a) 50Hz and 160°C, (b) 10Hz and 190°C, and (c) 30Hz and 190°C

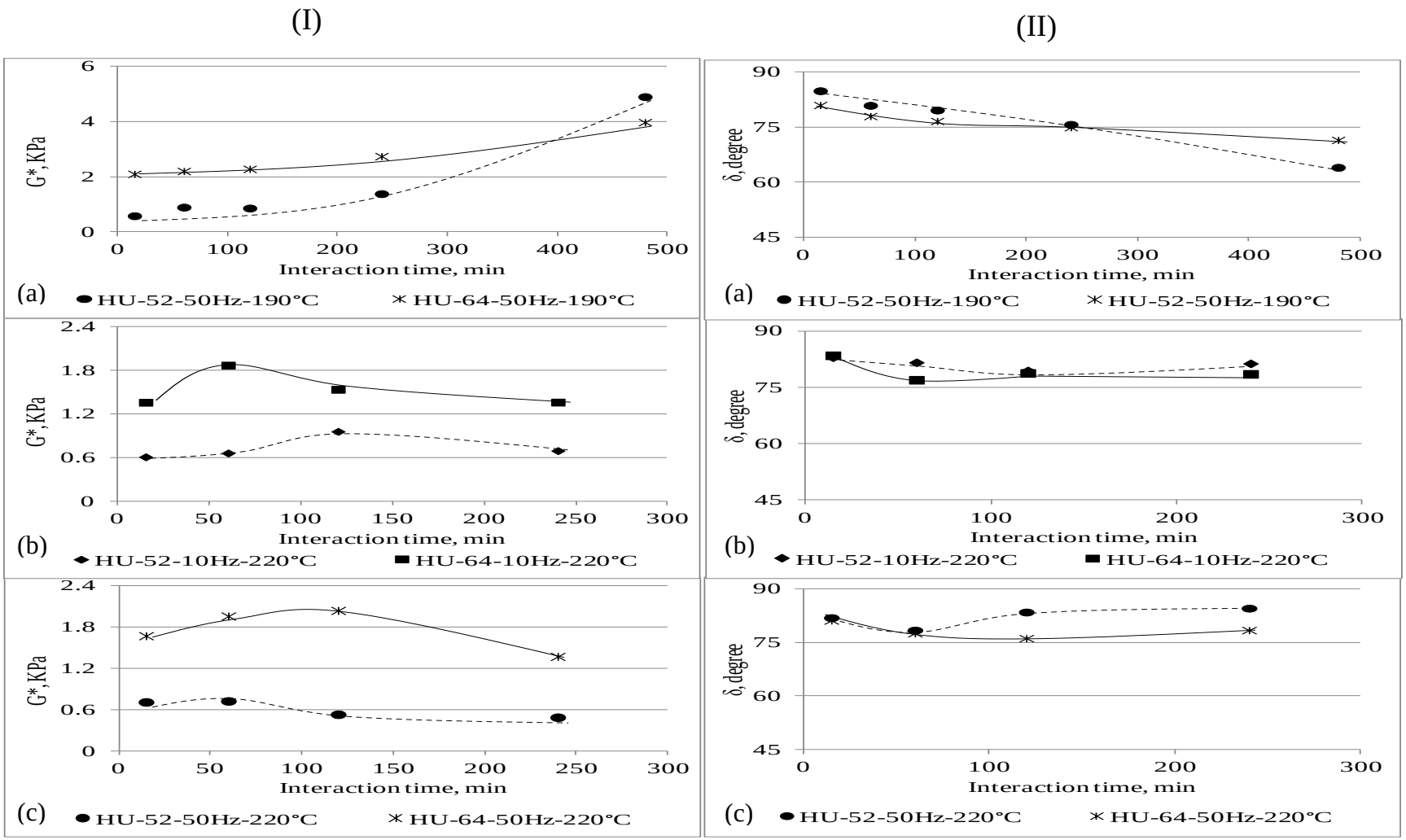

Figure 5.3. Development of rheological parameters of CRMA: (I)G* and (II)δ for samples interacted at (a) 50Hz and 190°C, (b) 10Hz and 220°C, and (c) 50Hz and 220°C

Microindentation Analysis

In this section, microindentation testing was utilized to investigate the effect of the network structures formation on the micro-mechanical behavior of thin asphalt layers similar to those laid on aggregate surfaces during mixing of asphalt with aggregate.

Figure 5.4 illustrates the force vs. indentation depth profiles for the NF-58 CRMA liquid phase samples interacted at 160°C with 30Hz after 1, 2, 4, and 8hrs of interaction time.

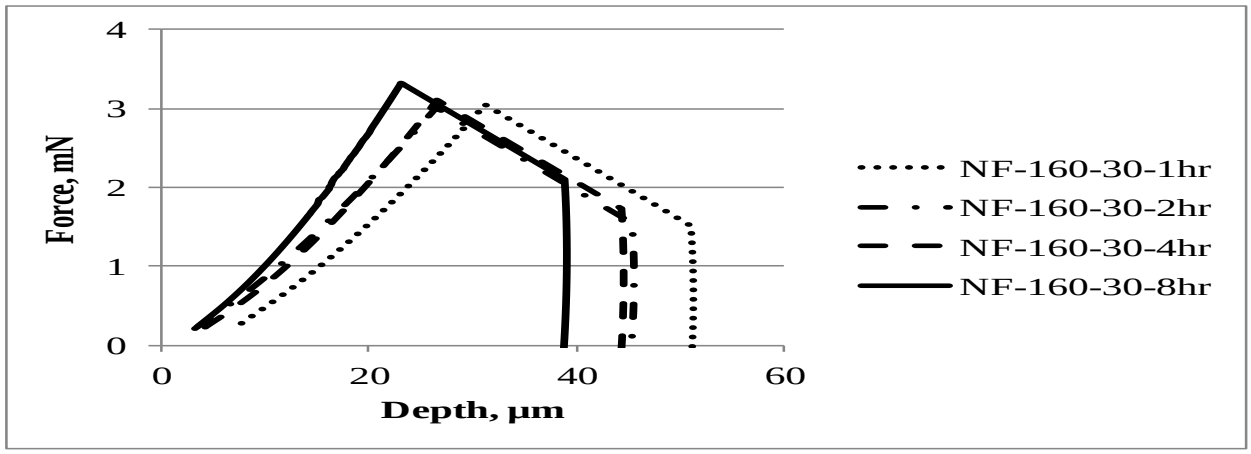

Figure 5.4. Force vs indentation depth profile for the samples interacted at 160°C and 30Hz.

As can be seen from Figure 5.4, the max load values shows a continuous decrease during the dwell time, similar observations were recorded in the literature for the indentation of asphalt [89]. This was explained in terms of the decrease in contact area due to delayed (viscous) flow of asphalt binders at the indentation location [89]. Another reason is the minute scale load carrying capacity of the asphalt binders and binder softening which results in being virtually impossible to keep the maximum applied load constant [89]. After 1hr of interaction time, the indentation depth was about 50µm. Increasing the interaction time to 2 and 4hrs gave almost similar values for the indentation depth of about 45µm. However, upon increasing the interaction time to 8hrs, further reduction in the indentation depth was recorded.

Figure 5.5 shows the hardness and elastic modulus values for the NF-58 CRMA liquid phase samples interacted at 160°C and 30Hz after 1, 2, 4, and 8hrs of interaction time. As shown in Figure 5.5, a continuous increase in both the hardness and elastic modulus can be seen with the increase of interaction time. The elastic modulus values of samples were 3.21, 3.58, 3.69, and 4.29Mpa, after 1, 2, 4, and 8hrs, respectively. On the other hand, the hardness values were 0.026, 0.032, 0.038, and 0.065MPa, after 1, 2, 4, and 8hrs of interaction time. This indicates that at such combination of interaction temperature (160°C) and interaction speed (30Hz) the increase in the elastic modulus values occurs gradually with interaction time up to 8hrs, whereas for the hardness, a major increase occurs from 4 to 8hrs (almost double the values). This could be as a result of the absorption of the low molecular weight aromatics from the CRMA liquid phase with increase of interaction time by the CRM that leads to stiffer binder [22].

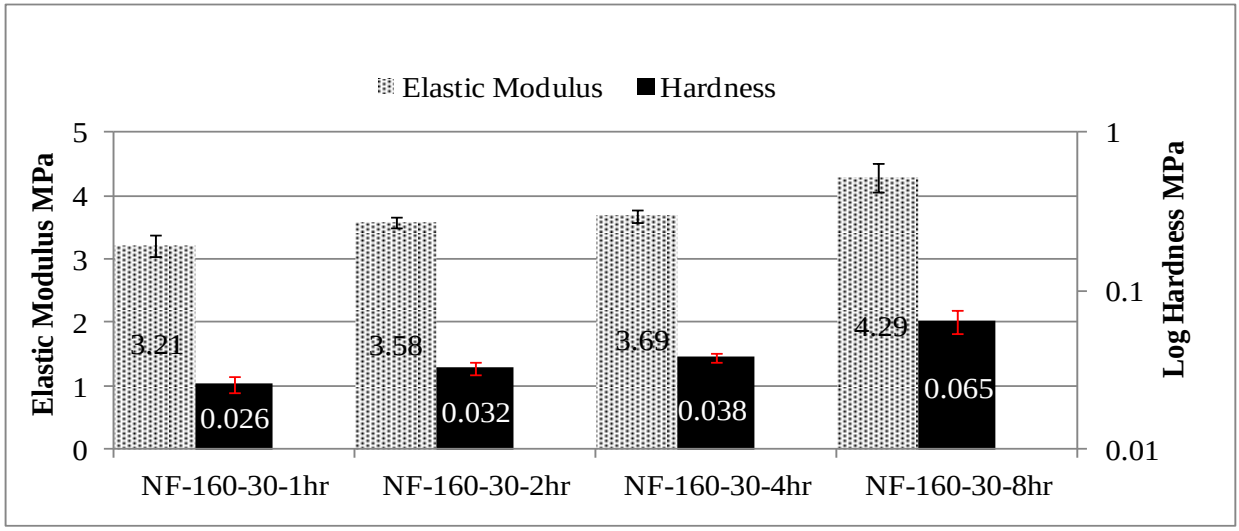

Figure 5.5. Comparison of hardness and elastic modulus for the samples interacted at 160°C and 30Hz.

Figure 5.6 illustrates the force vs. indentation depth profiles for the NF-58 CRMA liquid phase samples interacted at 160°C with 50Hz after 1, 2, 4, and 8hrs of interaction time. As can be seen from Figure 5.6, the behavior of the indentation depth shows a different trend than that il-

lustrated for the samples interacted at 160°C and 30Hz (shown in Figures 5.4 and 5.5). After 1 hr of interaction time, the indentation depth is about 50µm. However, upon increasing the interaction time to 2, 4, and 8hrs, we observe almost equal values for the indentation depth ranging around 40µm. This could be as a result of the increased interaction speed (50Hz) that resulted in accelerated absorption of the light molecular aromatics that was prevalent after 2hrs of interaction time, however, it is suggested that because of the low temperature utilized (160°C) an equilibrium status (saturation) is approached that leads to small variation in the indentation depth starting from 2hrs and up to 8hrs of interaction time [22].

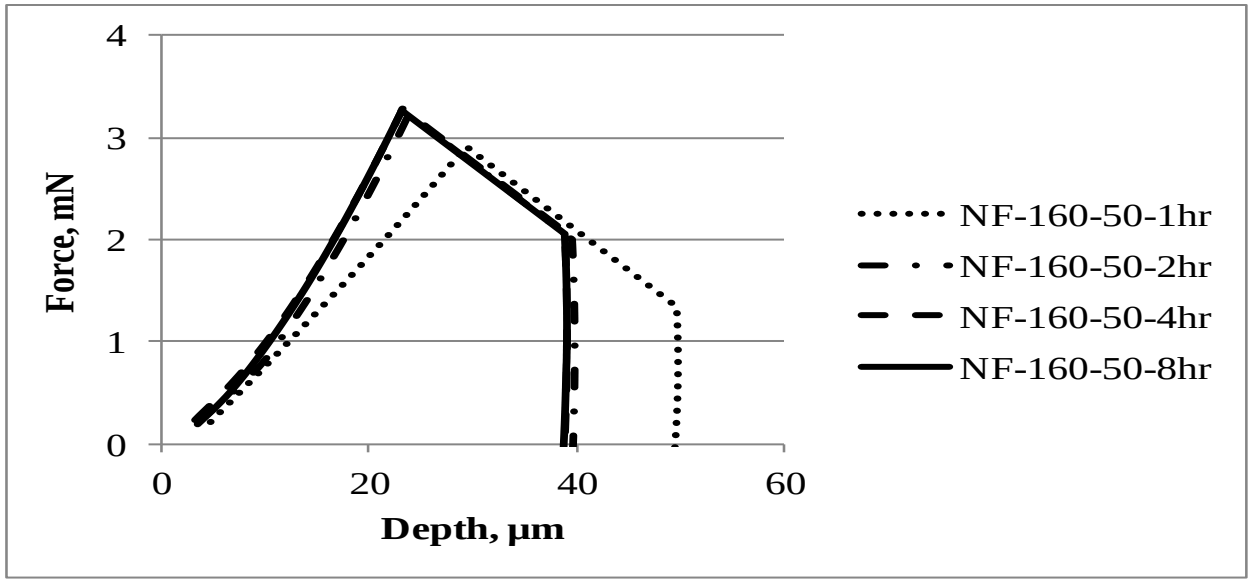

Figure 5.6. Force vs indentation depth profile for the samples interacted at 160°C and 50Hz.

The elastic modulus was 3.21MPa after 1hr of interaction time and increased to 4.16, 4.25, and 4.28MPa, after 2, 4, and 8hrs of interaction time. The same trend was seen for the hardness values that were 0.026, 0.057, 0.062, and 0.062MPa, after 1, 2, 4, and 8hrs of interaction times.

Figure 5.7 shows the hardness and elastic modulus values for the samples interacted at 160°C and 50Hz after 1, 2, 4, and 8hrs of interaction time. As illustrated in Figure 5.7, an increase in both the hardness and elastic modulus values is evident after 2hrs of interaction time. However, minimal increase can be seen for both the hardness and elastic modulus upon the increase from 2 to 4 and 8hrs.

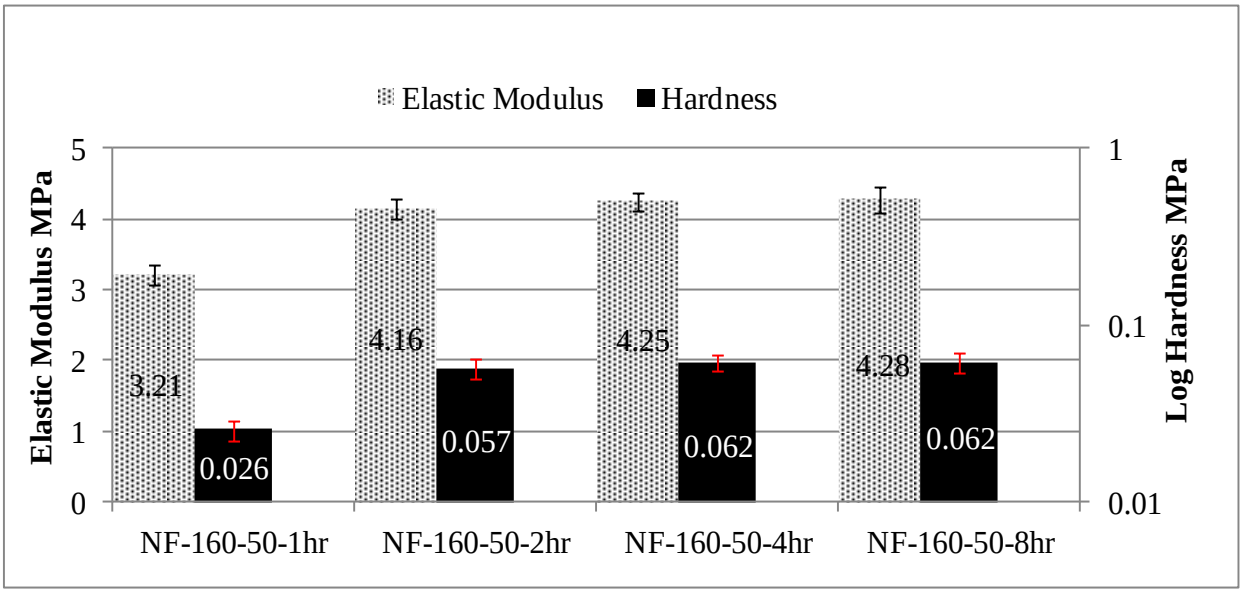

Figure 5.7. Hardness and elastic modulus for the samples interacted at 160°C and 50Hz.

Figure 5.8 shows the force vs. indentation depth profiles for the samples interacted at 190°C with 30Hz after after 1, 2, 4, and 8hrs of interaction time. As illustrated in Figure 5.8, a continuous decrease in the indentation depth can be seen with the increase in interaction time. The interaction depth was about 45µm after 1hr of interaction time and reached almost 30µm after 8hrs of interaction time. The indentation depth values for the samples interacted at 190°C and 30Hz show more reduction over the samples interacted at 160°C and 50Hz after 8hrs of interaction time. This shows that the behavior of the indentation depth shows higher dependency on the interaction temperature in comparison to the interaction speed.

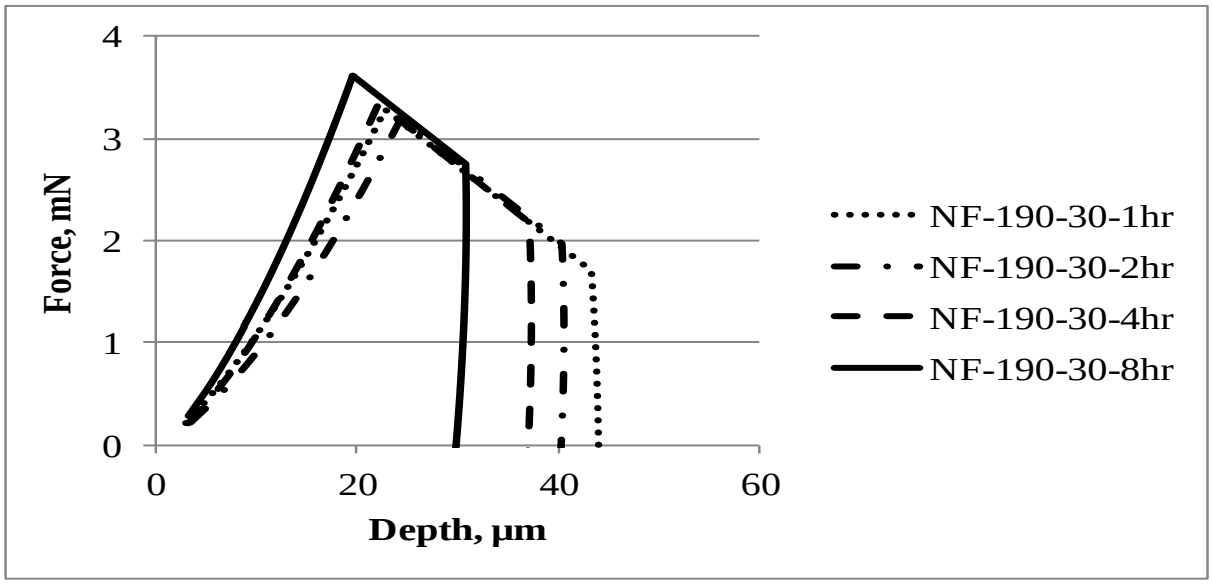

Figure 5.8. Force vs indentation depth profile for the samples interacted at 190°C and 30Hz.

Figure 5.9 illustrates the hardness and elastic modulus values for the samples interacted at 190°C and 30Hz after 1, 2, 4, and 8hrs of interaction time. The elastic modulus was 3.8, 4.1, 4.6, and 5.7MPa after 1, 2, 4, and 8hrs of interaction time, respectively. On the other hand, the behavior of the hardness followed a different trend. The hardness values were 0.05, 0.05, 0.08, and 0.15MPa, after 1, 2, 4, and 8hrs of interaction time. As can be seen from the hardness values, a gradual increase occurred in the first 4hrs of interaction time, whereas the hardness values were almost doubled upon the increase of interaction time from 4 to 8hrs.

As explained earlier, this could be as a result of the absorption of the low molecular weight aromatics from the CRMA liquid phase with increase of interaction time by the CRM that leads to stiffer binder. At such interaction conditions of moderate interaction temperature (190°C) and moderate interaction speed (30Hz), the depolymerization and devulcanization effects exerted on CRM are not major and thus the swelling of CRM plays the major role in property modification of CRMA [109, 116, 122].

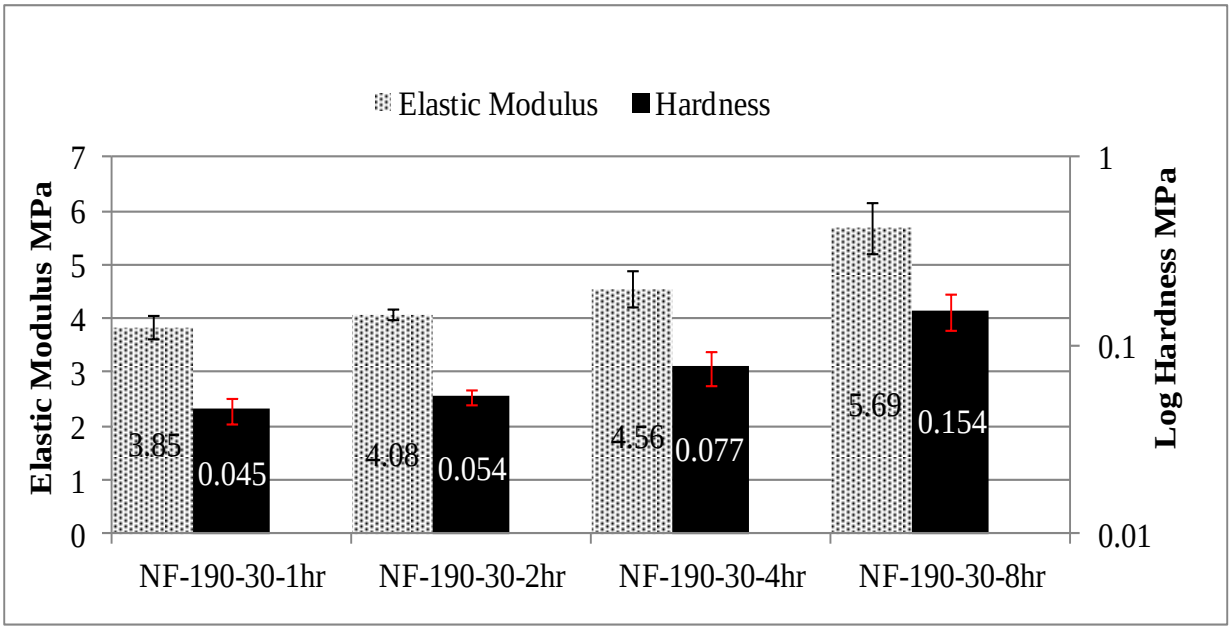

Figure 5.9. Hardness and elastic modulus for the samples interacted at 190°C and 30Hz.

Figure 5.10 illustrates the force vs. indentation depth profiles for the samples interacted at 190°C with 50Hz after 1, 2, 4, and 8 hours of interaction time. Figure 5.10 shows a different trend for the indentation depth than the previously illustrated samples interacted at either 160°C (with 30 or 50Hz) or 190°C with 30Hz. The indentation depth shows minimal decrease up to 2hrs of interaction time, however, a major decrease in the indentation depth occurs after 4 and 8hrs to decrease to almost half the value at interaction time of 8hrs as compared to 1hr of interaction time. This behavior is attributed to the increased devulcanization of CRM with minimal occurrence of depolymerization effects that resulted in the formation of 3D entangled network structures in the liquid phase of CRMA that lead to such major stiffening in the CRMA thus resulting in decreased indentation depth [50, 124].

Figure 5.11 illustrates the hardness and elastic modulus values for the samples interacted at 190°C and 50Hz after 1, 2, 4, and 8hrs of interaction time.

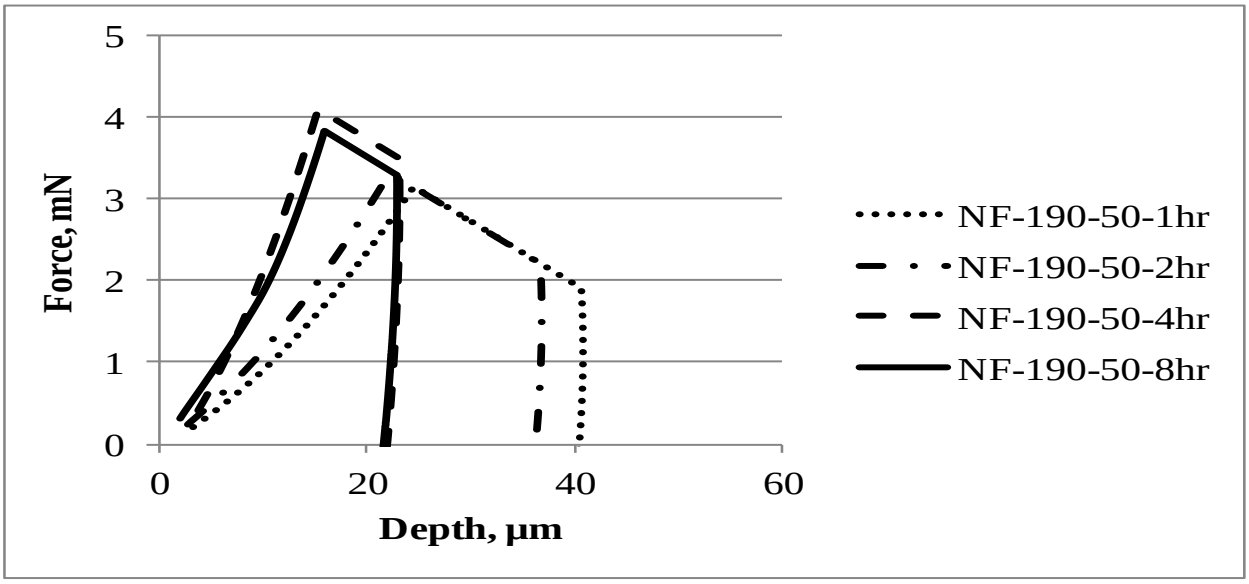

Figure 5.10. Force vs indentation depth profile for the samples interacted at 190°C and 50Hz.

As illustrated in Figure 5.11, the elastic modulus values shows a gradual increase from 1hr(4.3MPa) to 2hrs(4.7MPa) of interaction time. However, starting from 4hrs the elastic modulus values showed major enhancement (8.5MPa) and was almost double the values of the samples at 2hrs (4.7MPa). After 8hrs of interaction time, the elastic modulus was 10.6MPa. On the other hand, the hardness had a major increase of almost 5 times when the interaction time was increased from 2hrs(0.09MPa) to 4hrs(0.47MPa). The hardness values continue to increase at 8hrs to be 0.7MPa. As explained earlier, such distinctive increase in hardness and elastic modulus values after 4 and 8hrs of interaction time is explained in terms of the development of 3D entangled network structure in the CRMA liquid phase which is associated with such combination of moderate interaction temperature (190°C) and high interaction speed (50Hz) [50, 124].

Figure 5.12 illustrates the force vs. indentation depth profiles for the samples interacted at 220°C with 30Hz after 1, 2, 4, and 8 hours of interaction time. As shown in the figure, a different

behavior is observed for the indentation depth with the increase of interaction time. Up to 4hrs of interaction time, the indentation depth shows a continuous decrease.

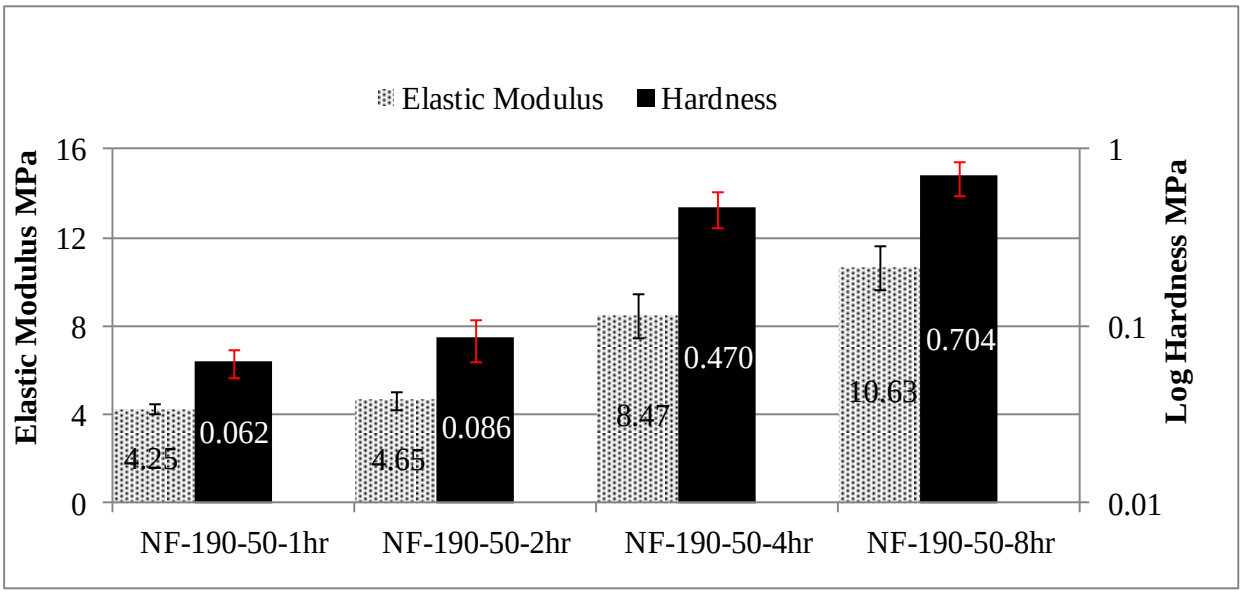

Figure 5.11. Hardness and elastic modulus for the samples interacted at 190°C and 50Hz.

However, after 8hrs of interaction time, an increase in indentation depth is recorded, indicating that the CRMA is showing less resistance to indentation load. Such behavior can be explained in terms of the increased depolymerization and devulcanization effects occurring for the released CRM components in the CRMA liquid phase that are associated with such interaction temperature (220°C) and even with moderate interaction speed (30Hz) [116, 122, 124].

Figure 5.13 illustrates the hardness and elastic modulus values for the samples interacted at 220°C and 30Hz after 1, 2, 4, and 8hrs of interaction time. As illustrated in Figure 5.13, the elastic modulus values shows a minimal increase from 1hrs (3.4MPa) to 2hrs (3.5MPa) of interaction time.

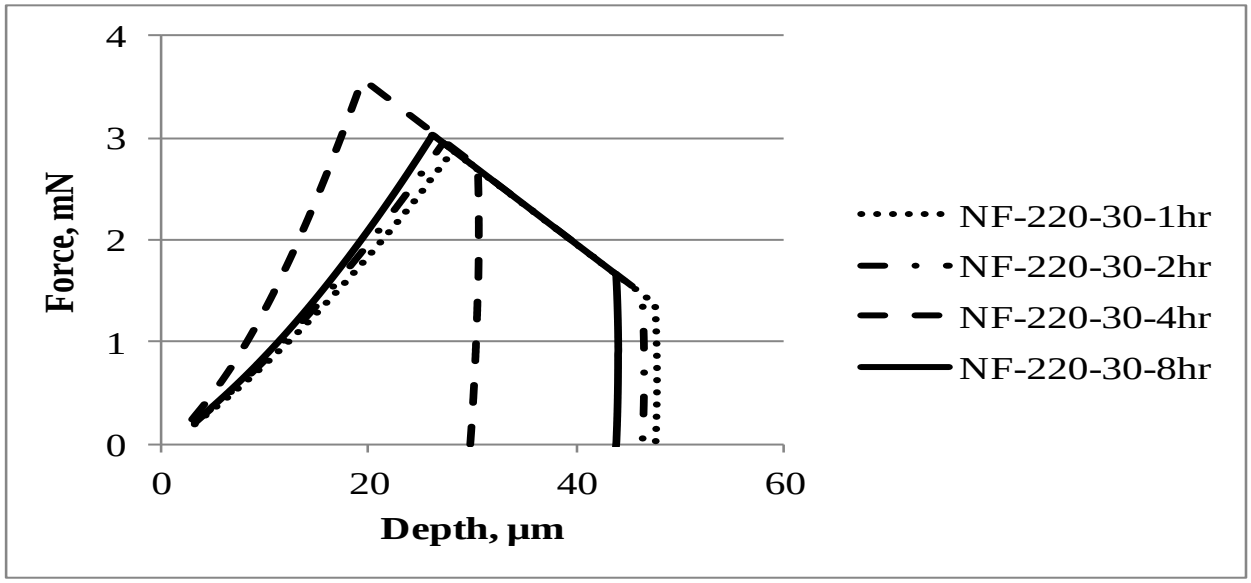

Figure 5.12. Force vs indentation depth profile for the samples interacted at 220°C and 30Hz.

The enhancement continues up to 4hrs (5.6MPa). However, at 8hrs of interaction time the elastic modulus values showed reduction (4MPa). The same behavior was observed for the hardness values. This is explained in terms of the increased deploymerization and devulcanization of CRM released components into the CRMA liquid phase, as explained earlier [116, 122, 124].

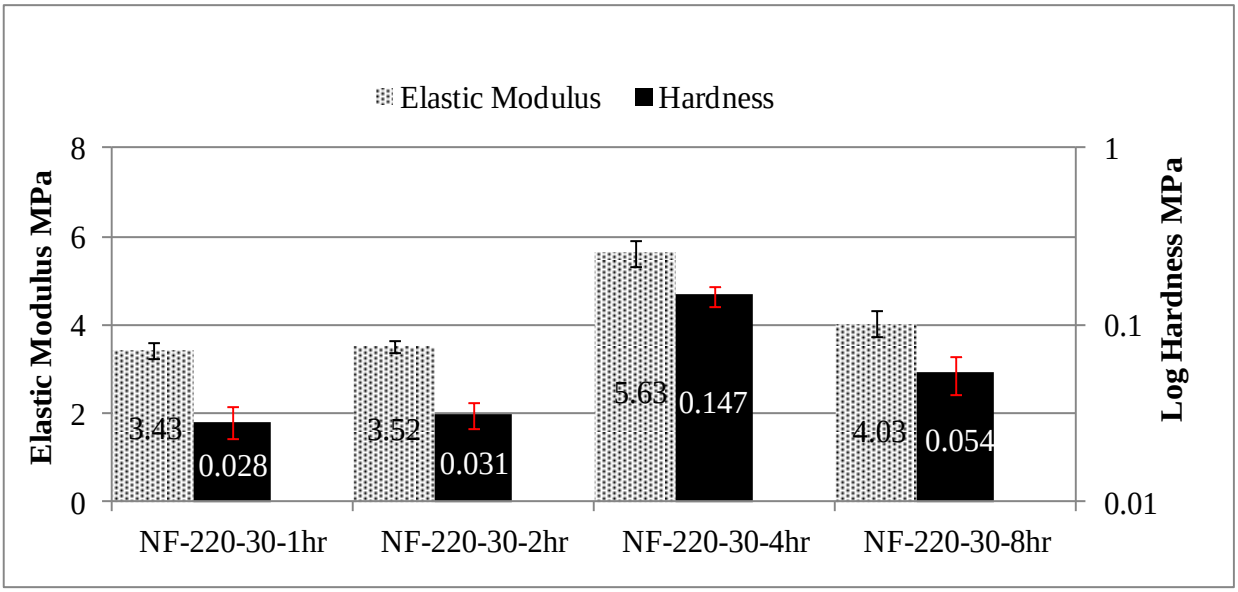

Figure 5.13. Hardness and elastic modulus for the samples interacted at 220°C and 30Hz.

Figure 5.14 illustrates the force vs. indentation depth profiles for the samples interacted at 220°C with 50Hz after 1, 2, 4, and 8 hours of interaction time. A more prevalent behavior of increase of indentation depth after 8hrs of interaction time can be observed, indicating the decreased resistance of the CRMA to indentation load.

Figure 5.15 illustrates the hardness and elastic modulus values for the samples interacted at 220°C and 50Hz after 1, 2, 4, and 8hrs of interaction time. At 8hrs of interaction time the elastic modulus values showed a steep reduction (3.8MPa). The same behavior was observed for the hardness values.

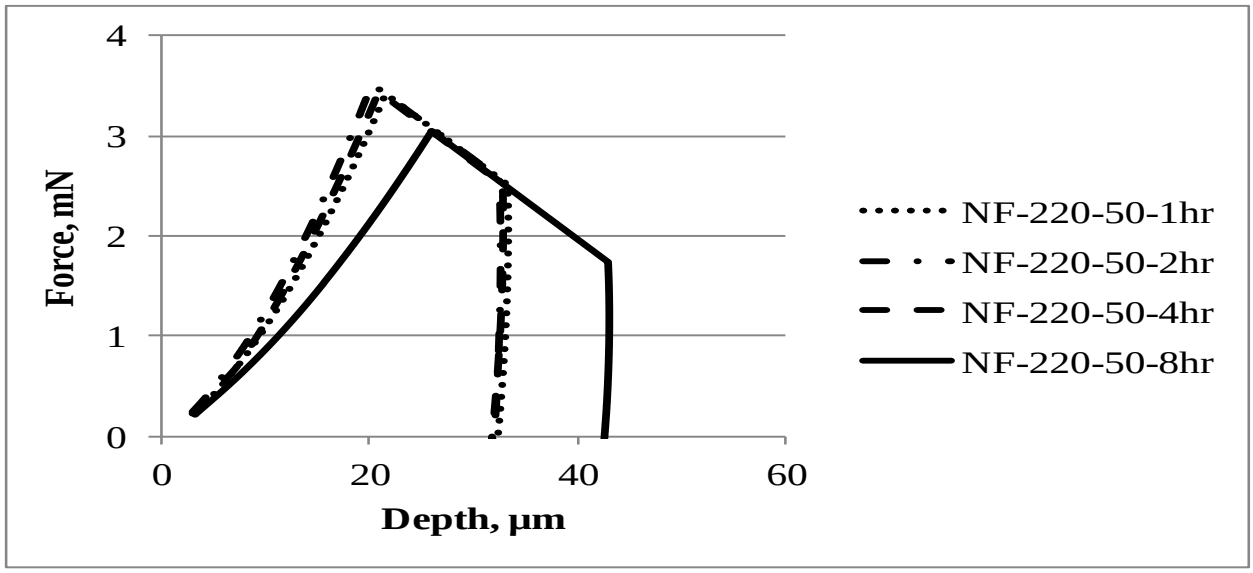

Figure 5.14. Force vs indentation depth profile for the samples interacted at 220°C and 50Hz.

This is explained in terms of the increased deploymerization and devulcanization of CRM released components into the CRMA liquid phase, as explained earlier [116, 122, 124].

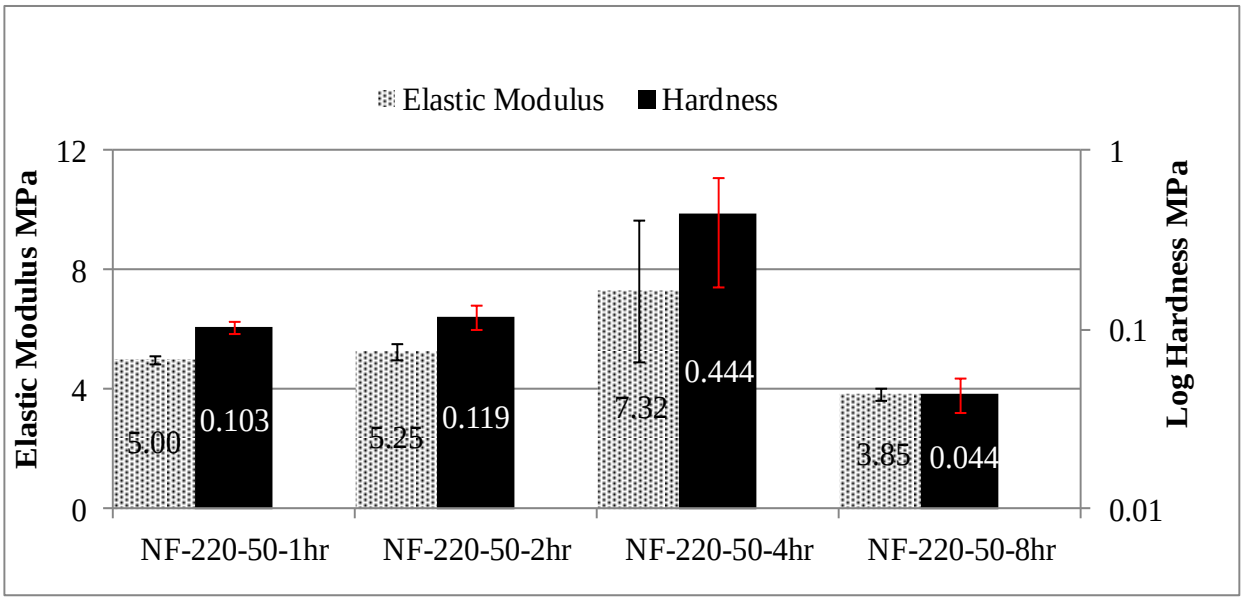

Figure 5.15. Hardness and elastic modulus for the samples interacted at 220°C and 50Hz.

Relation between the CRM Activities and the Michromechanical Properties of Asphalt

In this section, the relation between the micromechanical performance of asphalt thin layers and the release and dissolution of CRM components is investigated. This is carried out to establish a connection between the CRM dissolved amounts and released components and the development of 3D network structures in asphalt and their relations to the micromechanical behavior of asphalt thin layer.

Figure 5.16 (a) and (b) illustrates the change in compositional analysis of extracted CRM from the asphalts HU-64 and HU-52 interacted at a temperature of 190°C and mixing speed of 50Hz after 15min of interaction time, respectively.

As shown in Figure 5.16, the as received CRM compositions are 7% oily components, 28% natural rubber, 21% synthetic rubber, and 44% filler components. Figure 5.16(a) shows that after 15min of interaction time the CRM dissolution in the HU-64 asphalt was 18%, with oily

components reaching 2% and the natural rubber of about 23%. On the other hand, the synthetic rubber decreased to 17% and the filler components was 40%.

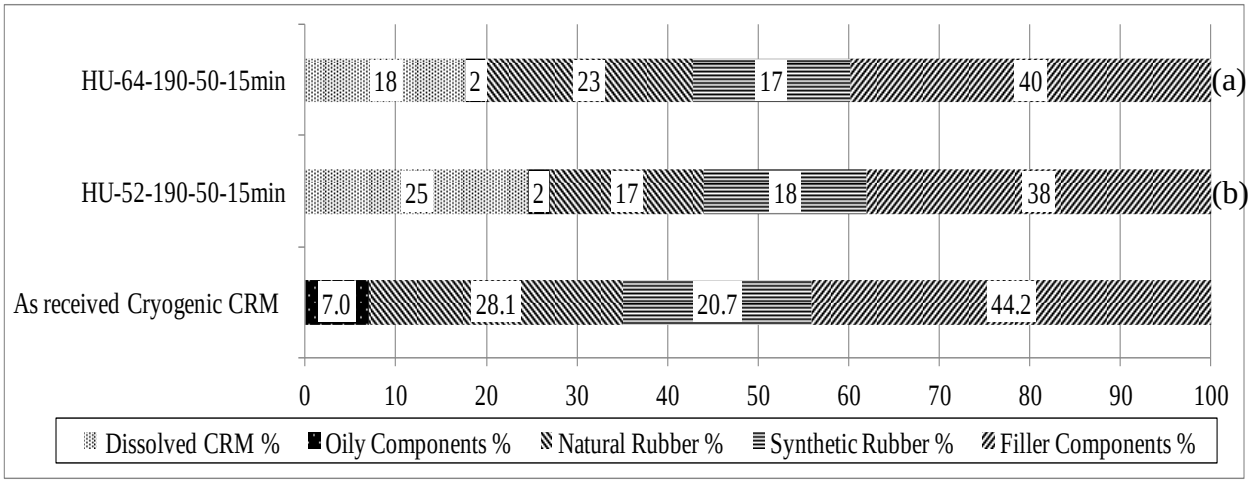

Figure 5.16. Components concentration in extracted CRM samples (a) Hu-64 and (b) Hu-52 in comparison with original CRM after 15min interaction time.

Figure 5.16(b) shows higher values for the CRM dissolution and components release in the HU-52 samples, where the CRM dissolution was 25%, with oily components reaching 2% and the natural rubber of about 17%. On the other hand, the synthetic rubber decreased to 18% and the filler components was 38%. Since different PG grade asphalts have different aromatic components that may affect the interaction process. With the utilization of both types of asphalts, we are investigating performance based applicability for the high and low temperature climate conditions areas. Relating that to the behavior of HU-52 modified asphalt, it can be seen that such behavior can be attributed to the higher saturates and aromatics found in the lower grade asphalt (HU-52) as compared to the HU-64 that would swell the CRM more and thus leads to increased dissolution and components release [22].

Figure 5.17 illustrates the force vs. indentation depth profiles for the asphalt samples HU-52 and HU-64 interacted at 190°C with 50Hz after 15min of interaction time.

As can be seen from Figure 5.17, for both asphalt types investigated, the max load values shows a continuous decrease during the dwell time, similar observations were recorded in the literature for the indentation of asphalt [89].This was explained in terms of the decrease in contact area due to delayed (viscous) flow of asphalt binders at the indentation location [89]. Another reason is the minute scale load carrying capacity of the asphalt binders and binder softening which results in being virtually impossible to keep the maximum applied load constant [89]. After 15min of interaction time, the final indentation depth was almost 23μm for the HU-64, while it was four folds more for the HU-52.

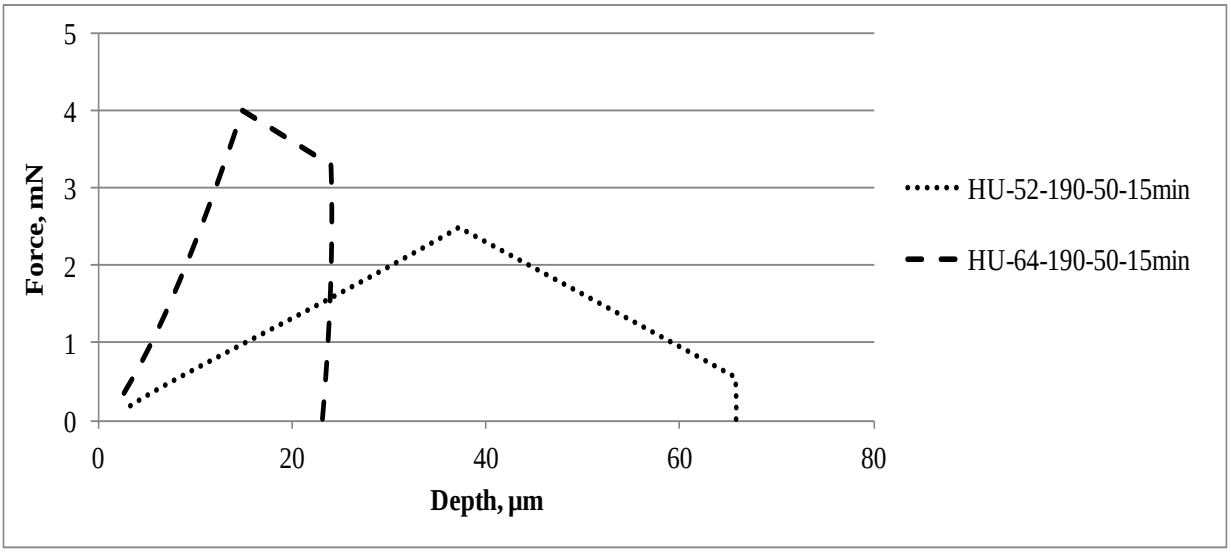

Figure 5.17. Force vs indentation depth profile for the samples interacted after 15min.

Figure 5.18 (a) and (b-) shows the change in compositional analysis of extracted CRM from the HU-64 and HU-52 asphalt samples interacted at a temperature of 190°C and mixing speed of 50Hz after 60min of interaction time, respectively. -

As shown in Figure 5.18(a), utilization of interaction time of 60min resulted in a 22% partial dissolution in CRM with the major components released expressed in terms of oily components and natural rubber. The oily components reached 2%, the natural rubber reached 20%,

the synthetic rubber reached 16%, and the filler components reached 40%, from original values of 7, 28, 21, and 44%, respectively. On the other hand, for the HU-52 asphalt illustrated in Figure 5.18(b), the CRM dissolution was 30%, with oily components still at 2% and the natural rubber decreasing to 14%, the synthetic rubber at 18% and thefiller components was 36%.

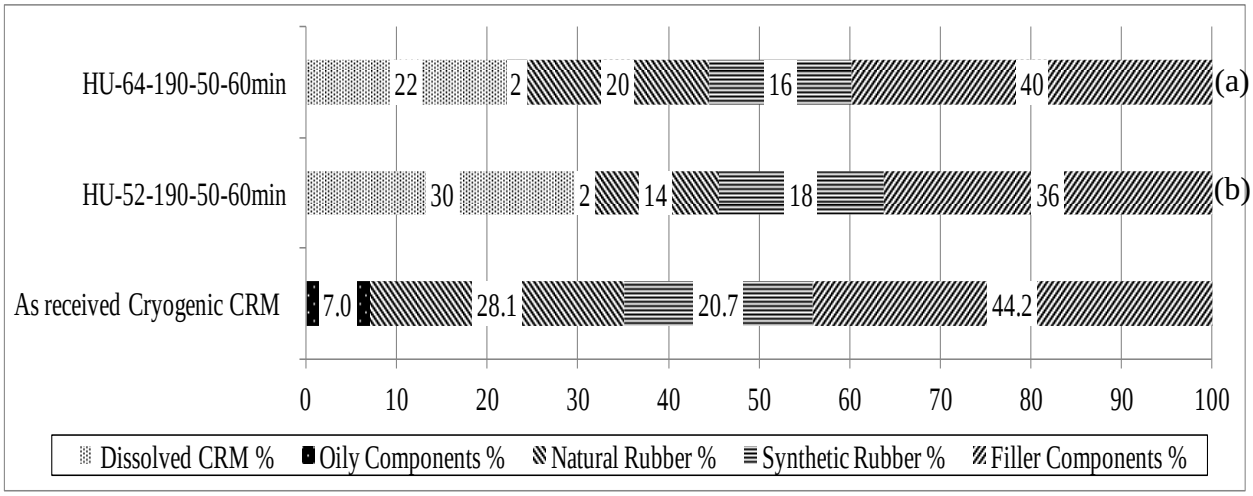

Figure 5.18. Components concentration in extracted CRM samples (a) Hu-64 and (b) Hu-52 in comparison with original CRM after 60min interaction time.

Figure 5.19 illustrates the force vs. indentation depth profiles for the HU-52 and HU-64 samples interacted at 190°C with 50Hz after 60min of interaction time.

As shown in Figure 5.19, after 60min of interaction time, the final indentation depth for the HU-64 samples decreased to almost 19μm from 23 μm (for the samples interacted with same conditions after 15min of interaction time illustrated in Figure 5.17). On the other hand, the indentation depth value was more than the double for HU-52 samples. Relating that to the CRM dissolution and components release illustrated in Figures 5.16 and 5.18, it can be inferred that the increase in CRM dissolution and components release lead to having CRMA with higher resistance to indentation force as expressed in the decreased indentation depth for the samples with higher CRM dissolution and components release.

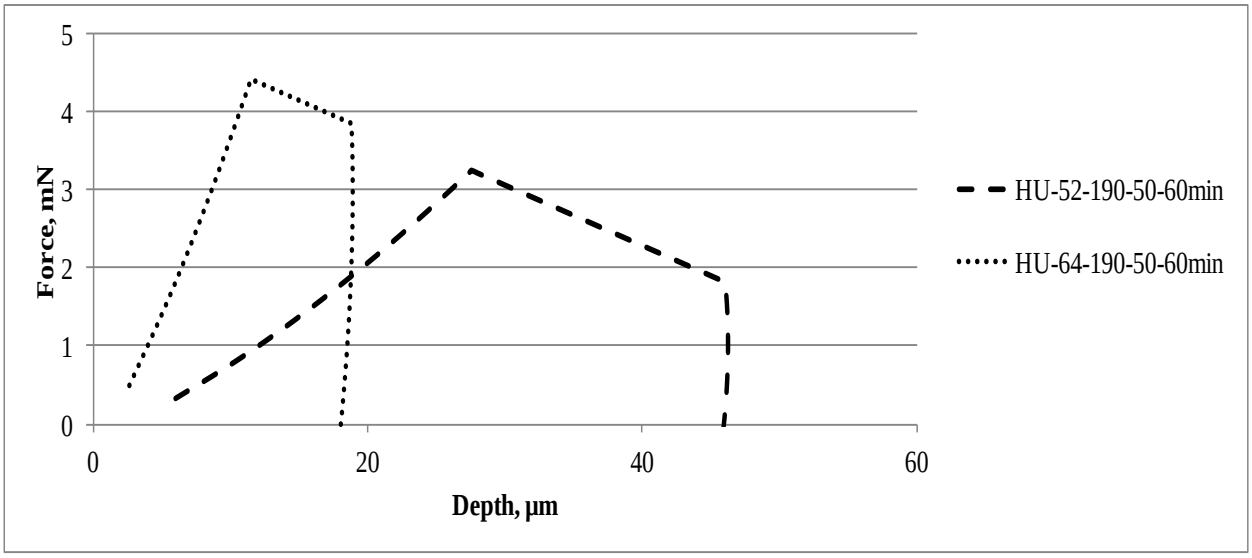

Figure 5.19. Force vs indentation depth profile for the samples interacted after 60min.

Figure 5.20 (a) and (b) illustrates the change in compositional analysis of extracted CRM for the Hu-64 and HU-52 asphalt samples interacted at a temperature of 190°C and mixing speed of 50Hz after 120min of interaction time, respectively. As shown in Figure 5.20(a), the HU-64 samples had a CRM partial dissolution of 55% with oily components at 2% value, the natural rubber reaching 10%, the synthetic rubber decreasing to 11%, and the filler components reaching 23%, from original values of 7, 28, 21, and 44%, respectively.

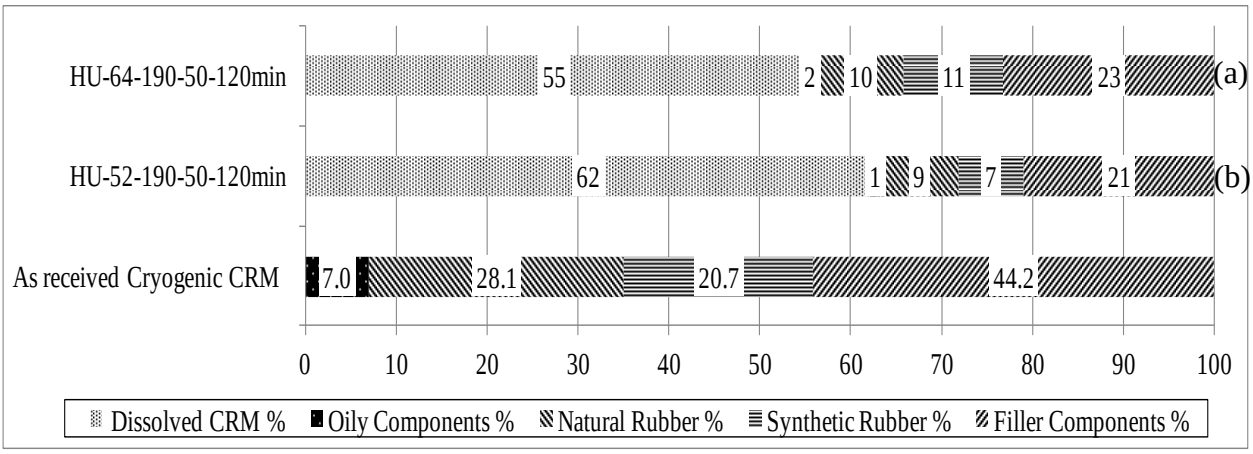

Figure 5.20. Components concentration in extracted CRM samples (a) Hu-64 and (b) Hu-52 in comparison with original CRM after 120min interaction time.

Figure 5.20(b) shows a 62% partial dissolution in CRM extracted from HU-52 asphalts with oily components reaching 1%, the natural rubber became 9%, the synthetic rubber reached 7%, and the filler components reached 21%. Figure 5.20 shows a major increase in the dissolution as well as components release of CRM as compared to Figures 5.18 and 5.16. For both asphalt types investigated, the dissolution of CRM after 120min of interaction time was more than double that of the samples interacted at 60min and almost triple that of the samples interacted at 15min.

Figure 5.21 shows the force vs. indentation depth profiles for the HU-52 and HU-64 asphalt samples interacted at 190°C with 50Hz after 120min of interaction time.

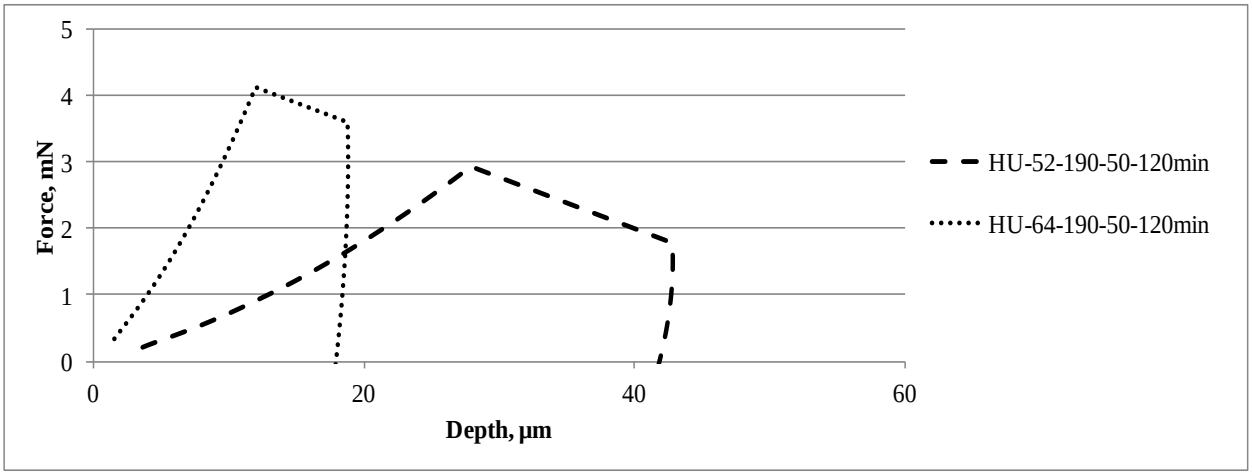

Figure 5.21. Force vs indentation depth profile for the samples interacted after 120min.

As illustrated in Figure 5.21 for the HU-64 asphalt, after 120min of interaction time, the final indentation depth decreased to 18µm. While for the HU-52 asphalt the indentation depth was 41µm. Relating that to the CRM dissolution and components release illustrated in Figures 5.18 and 5.20, it can be seen that although there exists a major increase in CRM dissolution and components release for both asphalts' CRM extracted samples interacted at 120min as compared to those interacted at either 60 and 15min, this was not manifested in the form of significant increase in the resistance to indentation force for the samples interacted at 120min over the other

two samples. This can be explained in terms of the insufficiency of the CRM dissolved amounts and released components that were not enough to alter the internal network structure of the CRMA, as will be shown later.

Figure 5.22 (a) and (b) shows the change in compositional analysis of extracted CRM for the HU-64 and HU-52 samples interacted at a temperature of 190°C and mixing speed of 50Hz after 240min of interaction time, respectively.

As shown in Figure 5.22(a), for the HU-64 asphalt extracted CRM, the partial dissolution in CRM increased to 69%. The oily components decreased to 1% value, the natural rubber reached 6%, the synthetic rubber decreased to 8%, and the filler components were 16%. Figure 5.22(a) illustrates a 14% increase in the dissolution of CRM for samples interacted at 240min as compared to the CRM dissolution for samples interacted at 120min (illustrated in Figure 5.20). For the extracted CRM from HU-52 illustrated in Figure 5.22(b), the CRM partial dissolution was 78% with oily components at 1% value, the natural rubber reaching 7%, the synthetic rubber decreasing to 7%, and the filler components reaching 21%.

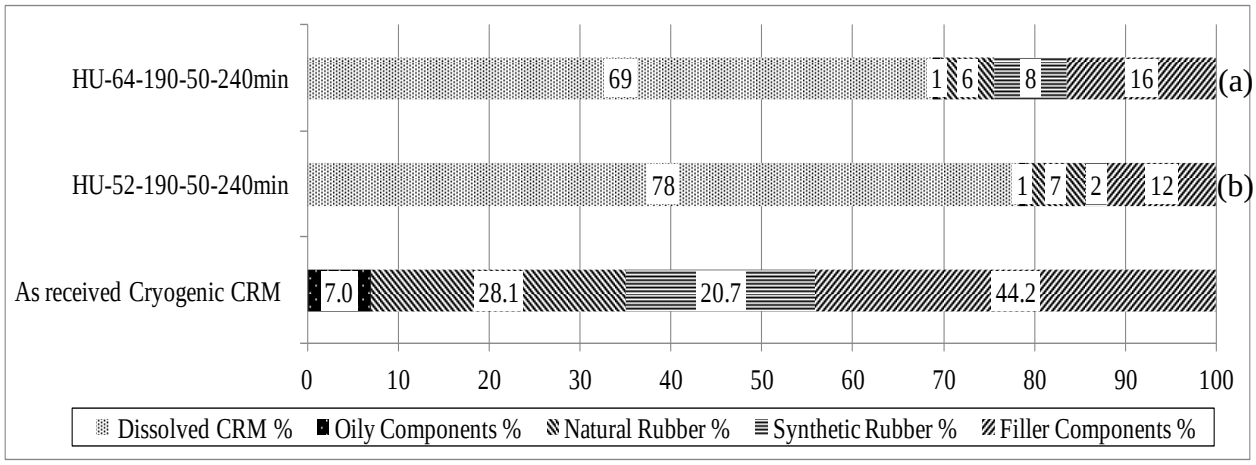

Figure 5.22. Components concentration in extracted CRM samples (a) Hu-64 and (b) Hu-52 in comparison with original CRM after 240min interaction time.

Figure 5.23 shows the force vs. indentation depth profiles for the HU-52 and HU-64 asphalt samples interacted at 190°C with 50Hz after 240min of interaction time.

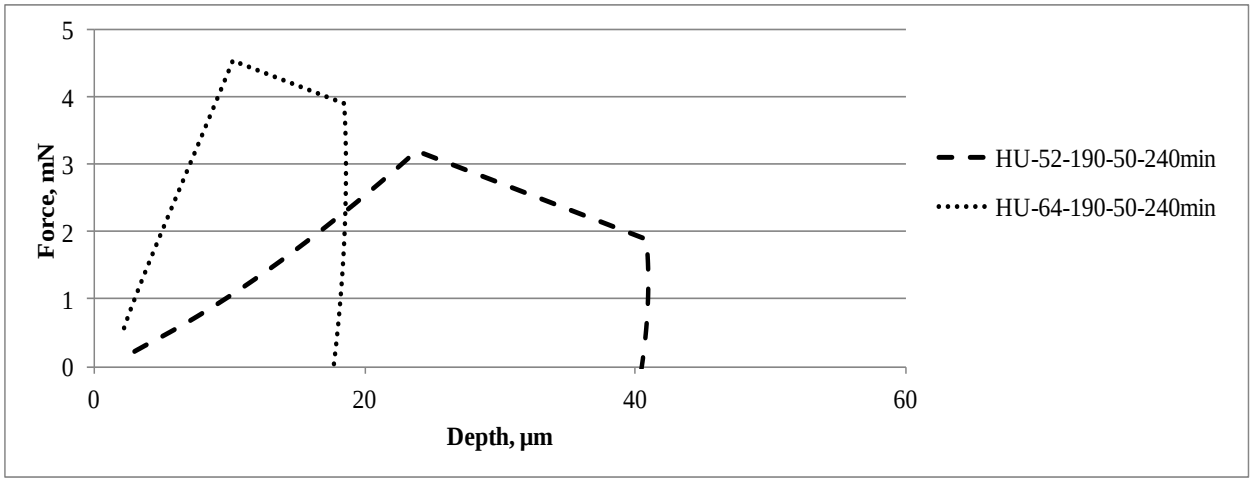

Figure 5.23. Force vs indentation depth profile for the samples interacted after 240min.

For both asphalt types investigated, minimal decrease in the indentation depth can be seen for the samples interacted at 240min of interaction time as compared to those interacted at 120min. Relating that to the CRM dissolution and components release illustrated in Figures 5.20 and 5.22, it can be seen that although there is significant increase in CRM dissolution and components release for the samples interacted at 240min as compared to those interacted at either 120, this was not manifested in the form of a major increase in the resistance to indentation force for the samples interacted at 240min over the other sample interacted at 120min. As explained earlier, this is due to insufficiency of the CRM dissolved amounts and released components that were not enough to alter the internal network structure of the CRMA.

Figure 5.24 (a) and (b) illustrates the change in compositional analysis of extracted CRM form HU-64 and Hu-52 with the increase of interaction time for the samples interacted at temperature of 190°C and mixing speed of 50Hz after 480min of interaction time, respectively.

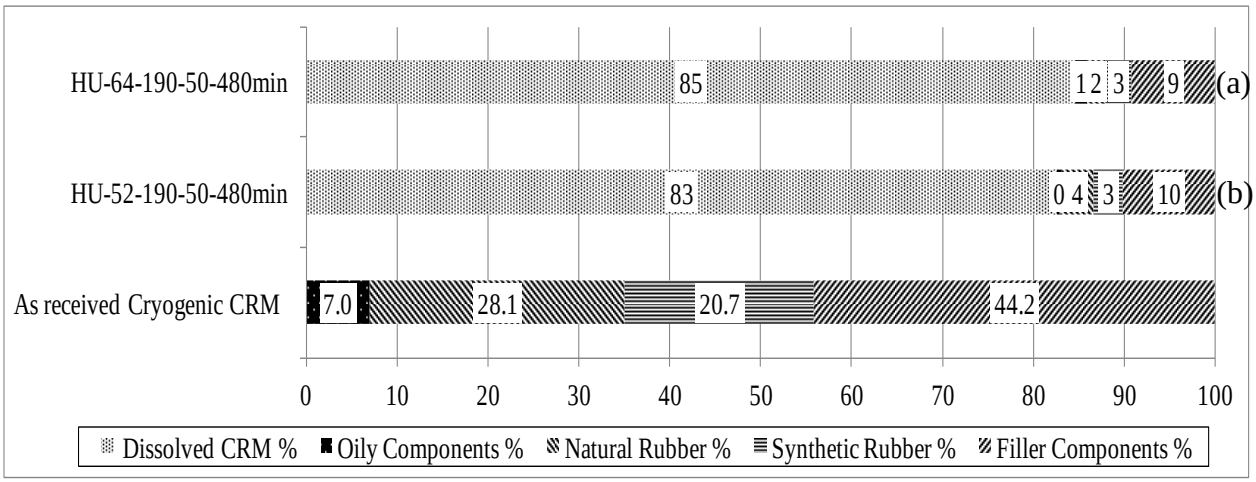

Figure 5.24. Components concentration in extracted CRM samples (a) Hu-64 and (b) Hu-52 in comparison with original CRM after 480min interaction time.

As shown in Figure 5.24(a), for the HU-64 extracted CRM, 85% partial dissolution in CRM with major release of all CRM components can be seen, where the oily components reached 1%, the natural rubber reached 2%, the synthetic rubber reached 3%, and the filler components reached 9%, from original values of 7, 28, 21, and 44%, respectively. The same trend can be seen for the extracted CRM from HU-52 asphalt, illustrated in Figure 5.24(b). The partial dissolution in CRM increased to 83%. The oily components decreased to almost 0% value, the natural rubber reached 4%, the synthetic rubber decreased to 3%, and the filler components were 10%.

Figure 5.25 shows a different trend for the indentation depth as compared to the previously illustrated samples for both asphalt types (HU-52 and HU-64) interacted at 190°C with 50Hz at 15, 60, 120, and 240min of interaction time. A major decrease in the indentation depth occurs at 480min of interaction time, where the indentation depth reached almost half the value as compared to 60min of interaction time. This behavior is attributed to the increased devulcanization of CRM with minimal occurrence of depolymerization effects that resulted in the formation of 3D

entangled network structures in the liquid phase of CRMA that lead to such major decrease in the indentation depth [121, 124, 125].

Figure 5.26(a) and (b) shows the hardness and elastic modulus values for the HU-64 and HU-52 samples interacted at 190°C and 50Hz after 15, 60, 120, 240 and 480min of interaction time, respectively.

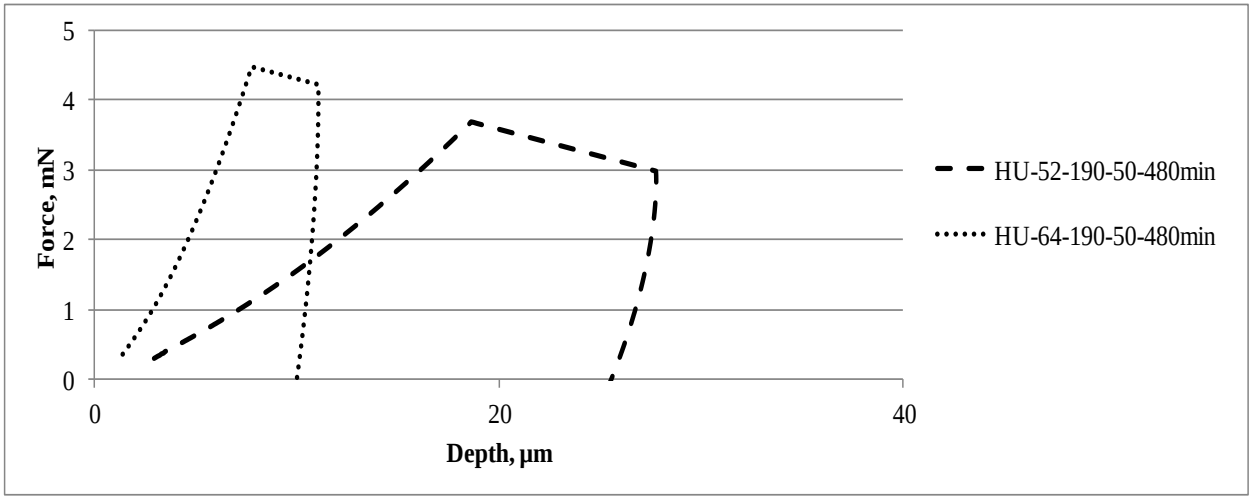

Figure 5.25. Force vs indentation depth profile for the samples interacted after 480min.

As shown in Figure 5.26(a), a continuous increase in the hardness for both asphalt types investigated can be seen with the increase of interaction time. For the HU-64 asphalt, the hardness values were 0.35, 0.58, 0.61, 0.77 and 3.02MPa, after 15, 60, 120, 240 and 480min of interaction time. While for the HU-52 asphalt, the hardness values were 0.12, 0.26, 0.23, 0.38 and 0.89MPa, after 15, 60, 120, 240 and 480min of interaction time.

On the other hand for the elastic modulus values, illustrated in Figure 5.26(b), for HU-64 asphalt samples were 7.8, 9.5, 10.1, 10.6 and 20.9MPa, after 15, 60, 120, 240 and 480min, respectively. The elastic modulus values for the HU-52 samples were 7.8, 9.5, 9.4, 11.6 and 15.7MPa, after 15, 60, 120, 240 and 480min, respectively. Looking at the elastic modulus values for both asphalt types investigated after 480min of interaction time it can be seen that the values

showed major enhancement and was almost double the values of the samples at 15min interaction time. On the other hand, the hardness had a major increase of more than 8 times when the interaction time was increased from 15min to 480min for both asphalts. As explained earlier, such distinctive increase in hardness and elastic modulus values after 480min of interaction time is explained in terms of the development of 3D entangled network structure in the CRMA liquid phase which is associated with such combination of moderate interaction temperature (190°C) and high interaction speed (50Hz) [95, 121, 124, 125].

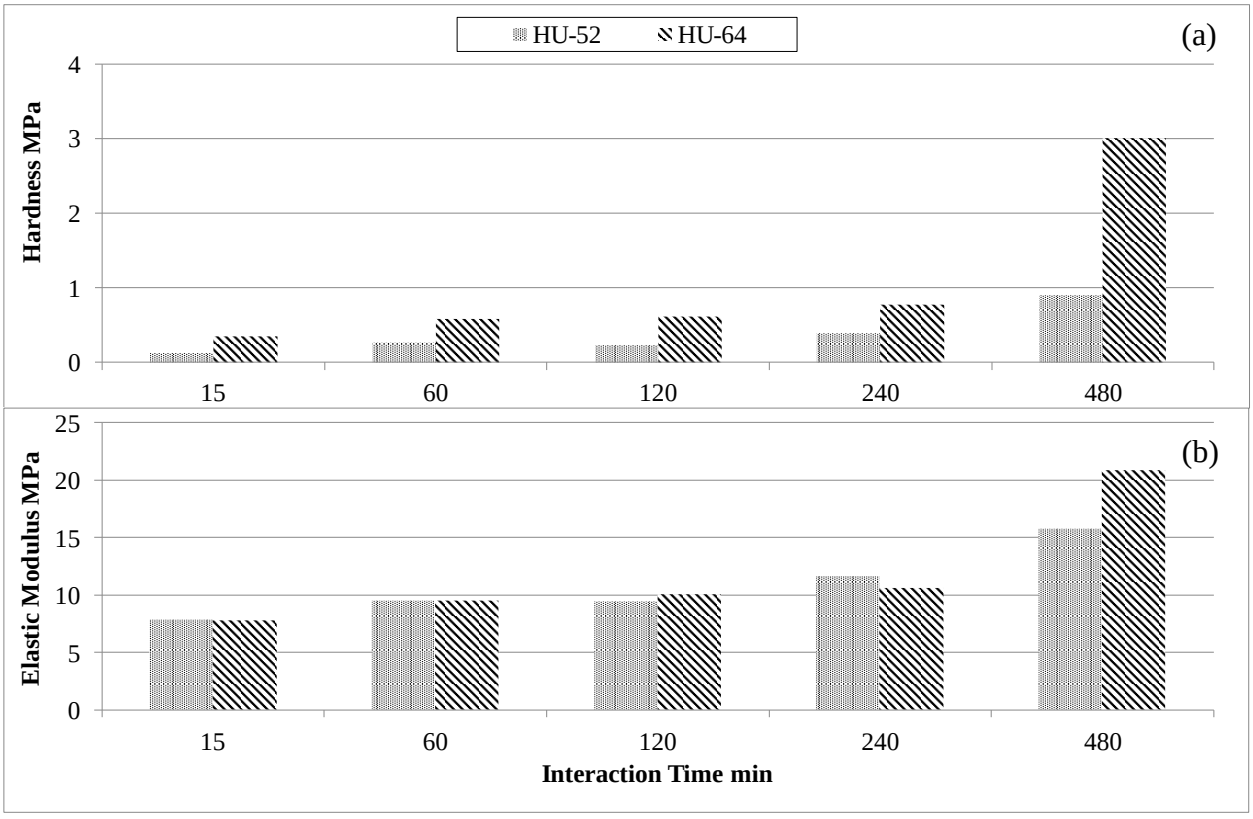

Figure 5.26. Comparison of (a) hardness and (b) elastic modulus for the samples interacted at 190°C and 50Hz for the different interaction times.

In this chapter it is clear that the network development in asphalt has significant effect on the enhancement of the asphalt in service properties on the macro and micro scale. In the coming

chapter we investigate the effect of the asphalt and CRM complements on the formation of the network. This gives us an insight about the role of each of the CRM and asphalt components in the formation of the network in asphalt.

CHAPTER SIX. EFFECT OF ASPHALT COMPONENTS ON THE DEVELOPEMENT OF THE NETWORK STRUCTURESAND SURFACE MORPHOLOGY OF ASPHALTS AND RUBBER MODIFIED ASPHALTS

Introduction

In this chapter it is aimed to investigate in depth the role of each of the asphalt fractions (components) on the formation of the network structures in asphalt. In addition, the effect of the asphalt and CRM components role in the network structures formation and their relation to the surface morphology of the modified asphalt is also investigated. The investigation of asphalt and CRM components effects on network structures formation is carried out by utilizing fractionation, thermal, and chemical tests on the different asphalt fractions. In addition, the comparison between the asphalt different fractions components and the CRM as received components is also carried out in the thermal and chemical investigation tests carried out in this chapter to delineate which asphalt fractions are behaving similar to that of the CRM components during the network structures formation.

Column Chromatography Analysis

In this section, the investigation of the effect of change of different asphalt fractions (asphaltenes, saturates, naphthene aromatics, and polar aromatics) amounts on network structures formation is carried out. This gives an idea about the specific role of each of the asphalt fractions on the formation of network structures in asphalt.

Figure 6.1(a, b, c and D) illustrates the effect of asphalt type on the different fractions of asphalts. As can be seen from Figure 6.1(a) for the neat asphalts, HU-52 has the lowest asphaltene content followed by HU-64 and then NF-58. The saturates are highest for HU-52 and almost equal for HU-64 and NF-58

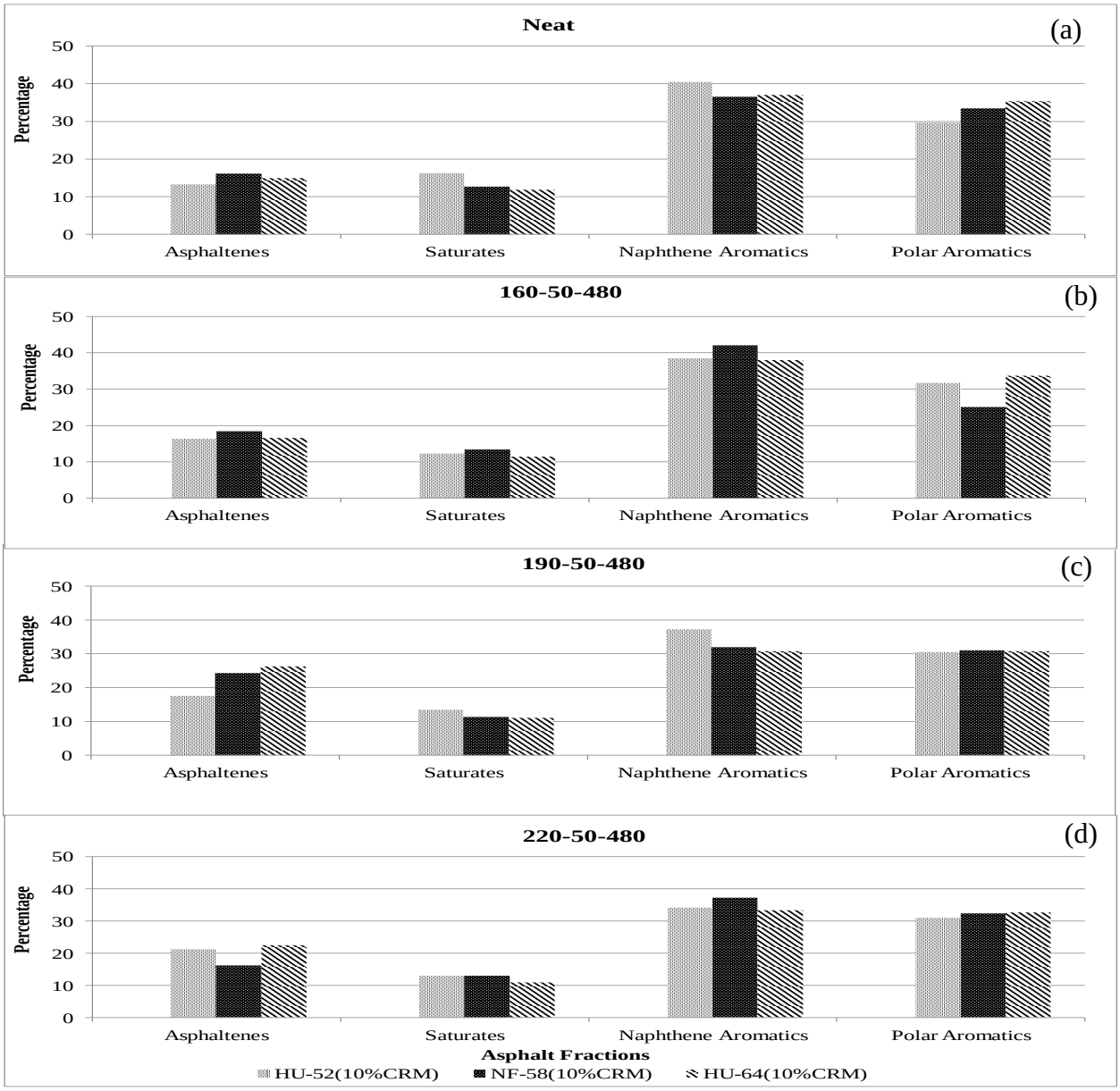

Figure 6.1. Effect of asphalt type on the different asphalt fractions (a) Neat, (b) interacted at 160°C-50Hz-480min, (c) interacted at 190°C-50Hz-480min, (d) interacted at 220°C-50Hz-480min.

The Naphthene are most for HU-64, followed by NF-58 and lastly HU-52. As illustrated in Figure 6.1(b), after 480min of interaction at 160°C and 50Hz, while utilizing 10%CRM, the asphaltenes increased for all asphalts but with almost similar ratios as that of the neat samples. The HU-52 saturates decreased, while slight increase occurred for the NF-58 ones. The HU-64 had almost same saturates value. The naphthene aromatics had a slight decrease for HU-52 and

slight increase for HU-64, while it had a decrease for NF-58. The Polar aromatics of HU-52 increased, while it decreased for NF-58, while it remained almost the same for HU-64. As illustrated in Figure 6.1(c), after 480min of interaction at 190°C and 50Hz, while utilizing 10%CRM, the asphaltenes increased for all asphalts with HU-64 of maximum increase, followed by NF-58 and lastly Hu-52. The saturates slightly increased for HU-52, while it decreased for HU-52 and NF-58. The naphthene aromatics were almost similar for HU-52 and had a decrease for HU-64 and NF-58. The Polar aromatics of HU-52 and HU-64decreased, while it increased for NF-58.

Figure 6.1(d) illustrates the change in asphalts fractions after 480min of interaction at 220°C and 50Hz, while utilizing 10%CRM. As seen from the Figure, the asphaltenes increased for HU-52 and HU-64, while it was almost the same for NF-58. The saturates slightly decreased for HU-52 and HU-64, while it remained constant for NF-58. The naphthene aromatics decreased for HU-52 and HU-64, while it had a slight increase for NF-58. The Polar aromatics of HU-52 showed a slight increase, while those for HU-64 and NF-58 decreased.

Effect of CRM Type

Figure 6.2 illustrates the effect of CRM type on the different asphalt fractions. As can be seen from the Figure, the asphaltene fraction increased for all the CRM types investigated, however the major increase was with the utilization of CRM type followed by WTG and lastly TR.
For saturates, decrease in the values was recorded. The most decrease was calculated for the asphalts modified with CRM followed by WTG and lastly TR. The same observation of fractions decrease can be seen for the naphthene aromatics fraction values. The asphalts modified with CRM had very minor decrease in the naphthene aromatics, whereas the WTG and TR had major decrease in such fraction. The polar aromatics fractions of asphalts modified with CRM showed

almost similar values. On the other hand, the asphalts modified with WTG or TR had almost similar increase in the polar aromatics values.

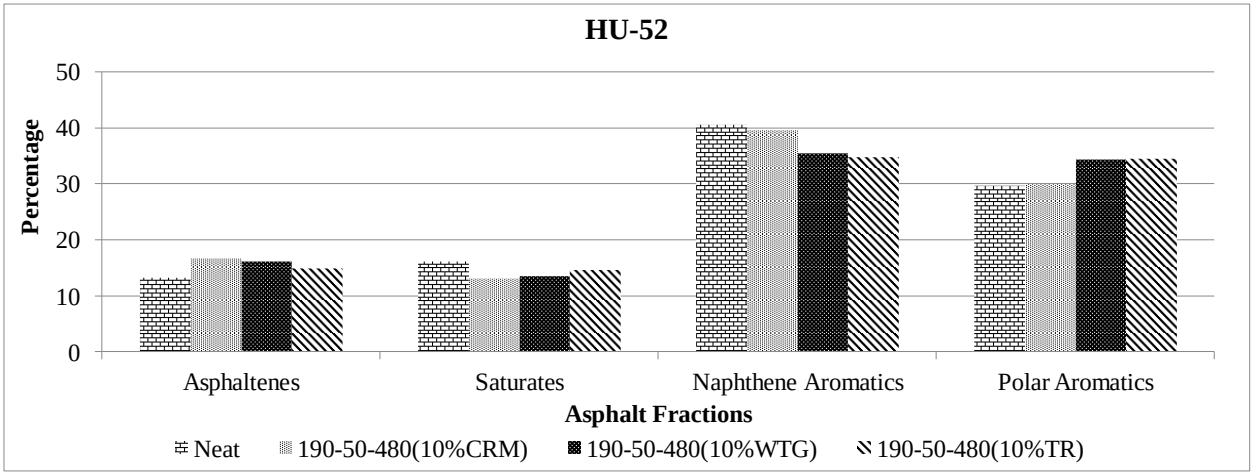

Figure 6.2. Effect of CRM type on the different asphalt fractions.

Effect of Temperature

The effect of interaction temperature on the different asphalt fractions investigated is illustrated in Figure 6.3 (a, b, and c) for asphalts; HU-52, NF-58, and HU-64, respectively.

As can be seen from Figure 6.3(a), for the HU-52 asphalt, the asphaltenes fractions show a gradual increase with the increase of interaction temperature. On the other hand, saturates fractions decreased for all interaction temperatures investigated with almost similar values. The naphthene aromatics fractions showed a gradual decrease with the increase of interaction temperature. The polar aromatics showed minor increase for all interaction temperatures investigated, with the samples interacted at 160°C and 50Hz of highest value of increase.

The trend of the asphalt fractions change with interaction temperature for the NF-58 asphalt is illustrated in Figure 6.3(b). As can be seen from the figure, a different behavior can be seen in comparison to that of the HU-52 asphalt. Asphaltenes fractions had major increase for the samples interacted at 190°C and 50Hz, followed with those interacted at 220°C and 50Hz, and

lastly the samples interacted at 160°C and 50Hz. The behavior of saturates showed different trend, where the samples interacted at 190C and 50Hz showed minimal decrease in that fraction. On the other hand, the samples interacted at 160°C and 220°C with 50Hz had almost constant saturates fractions. Naphthene aromatics fractions increased for samples interacted at 160°C and 220°C with 50Hz, while it decreased for the samples interacted at 190°C and 50Hz. The polar aromatics fractions showed most decrease for the samples interacted at 160°C and 50Hz, while minimal decrease was recorded for the samples interacted at the other two interaction temperatures.

The behavior of the asphalt fractions change with interaction temperature for the HU-64 asphalt is illustrated in Figure 6.3(c). A similar trend for the asphaltene fractions as that of the NF-58 can be seen for the HU-64 fractions, where major increase for the samples interacted at 190°C and 50Hz is measured, followed with those interacted at 220°C and 50Hz, and lastly the samples interacted at 160°C and 50Hz. Saturates fraction almost remained constant for all the temperatures investigated. Naphthene aromatics fractions for samples interacted at 160°C and 50Hz almost remained constant, while it decreased for samples interacted at 190°C and 220°C with 50Hz. The samples interacted at 190°C and 50Hz had the most decrease in amount. The polar aromatics fractions showed most decrease for the samples interacted at 190°C and 50Hz, while minimal decrease was recorded for the samples interacted at the other two interaction temperatures

Effect of Mixing Speed

The effect of mixing speed on the different asphalt fractions investigated is illustrated in Figure 6.4 (a, b, and c) for asphalts; HU-52, NF-58, and HU-64, respectively.

As can be seen from Figure 6.4(a), for the HU-52 asphalt, the asphaltenes fractions show almost equal increase with the utilization of 190°C with 10Hz and 50Hz of interaction speed. On the other hand, saturates fractions shows almost equal decrease for both interaction speeds investigated with almost similar values. The naphthene aromatics fractions showed a gradual decrease with the increase of mixing speed. The polar aromatics showed minimal increase for all interaction speed investigated, with the samples interacted at 190°C with 50Hz of highest value of increase.

The trend of the asphalt fractions change with interaction speed for the NF-58 asphalt is illustrated in Figure 6.4(b). As can be seen from the figure, a different behavior can be seen in comparison to that of the HU-52 asphalt. Asphaltenes fractions had gradual increase for the samples interacted at 190°C with 10Hz, followed with those interacted at 190°C with 50Hz. The behavior of saturates showed different trend, where the samples interacted at 190°C with 50Hz showed minimal decrease in that fraction. On the other hand, the samples interacted at 190°C with 10Hz had almost constant saturates fractions.

The naphthene aromatics fractions showed a gradual decrease with the increase of mixing speed. The polar aromatics showed minimal increase for the samples interacted at 190°C with 10Hz speed, while the samples interacted at 190°C with 50Hz showed decrease in the values of polar aromatics fractions.

The behavior of the asphalt fractions change with interaction speed for the HU-64 asphalt is illustrated in Figure 6.4(c). A major increase in asphaltene fractions can be seen for the samples interacted at 190°C with 50Hz, whereas a minimal increase can be seen for the samples interacted at 190°C with 10Hz.

Saturates fraction almost remained constant for 190°C with 50Hz interaction speed, while it slightly decreased at 190°C with 10Hz interaction speed. Naphthene aromatics fractions for samples interacted at 190°C with 10Hz almost remained constant, while it decreased for samples interacted at 190°C with 50Hz. The polar aromatics fractions showed most decrease for the samples interacted at 190°C and 50Hz, while minimal increase was recorded for the samples interacted at 190°C and 10Hz.

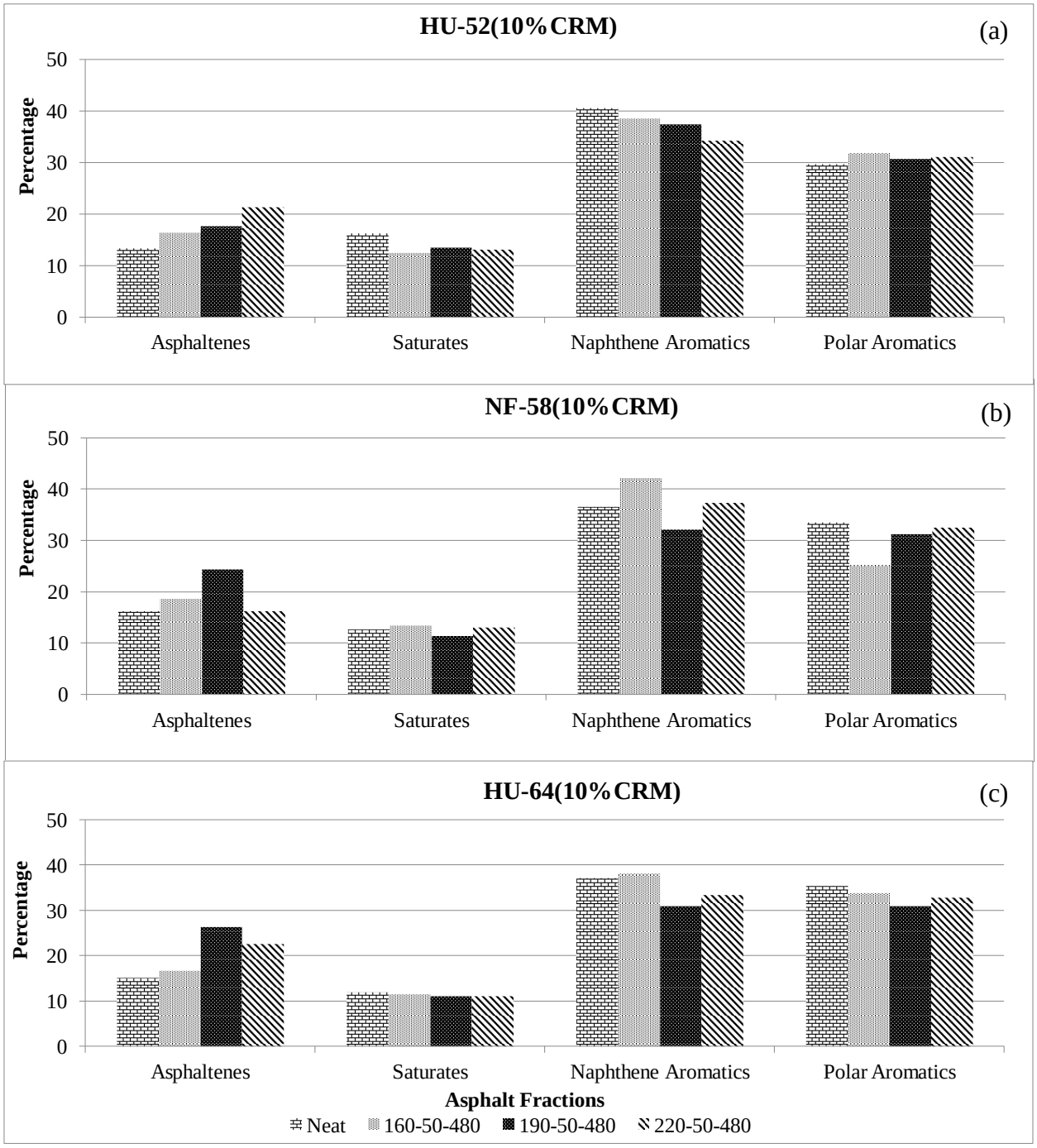

Figure 6.3. Effect of interaction temperature on the different asphalt fractions (a) HU-52, (b) NF-58, and (c) HU-64.

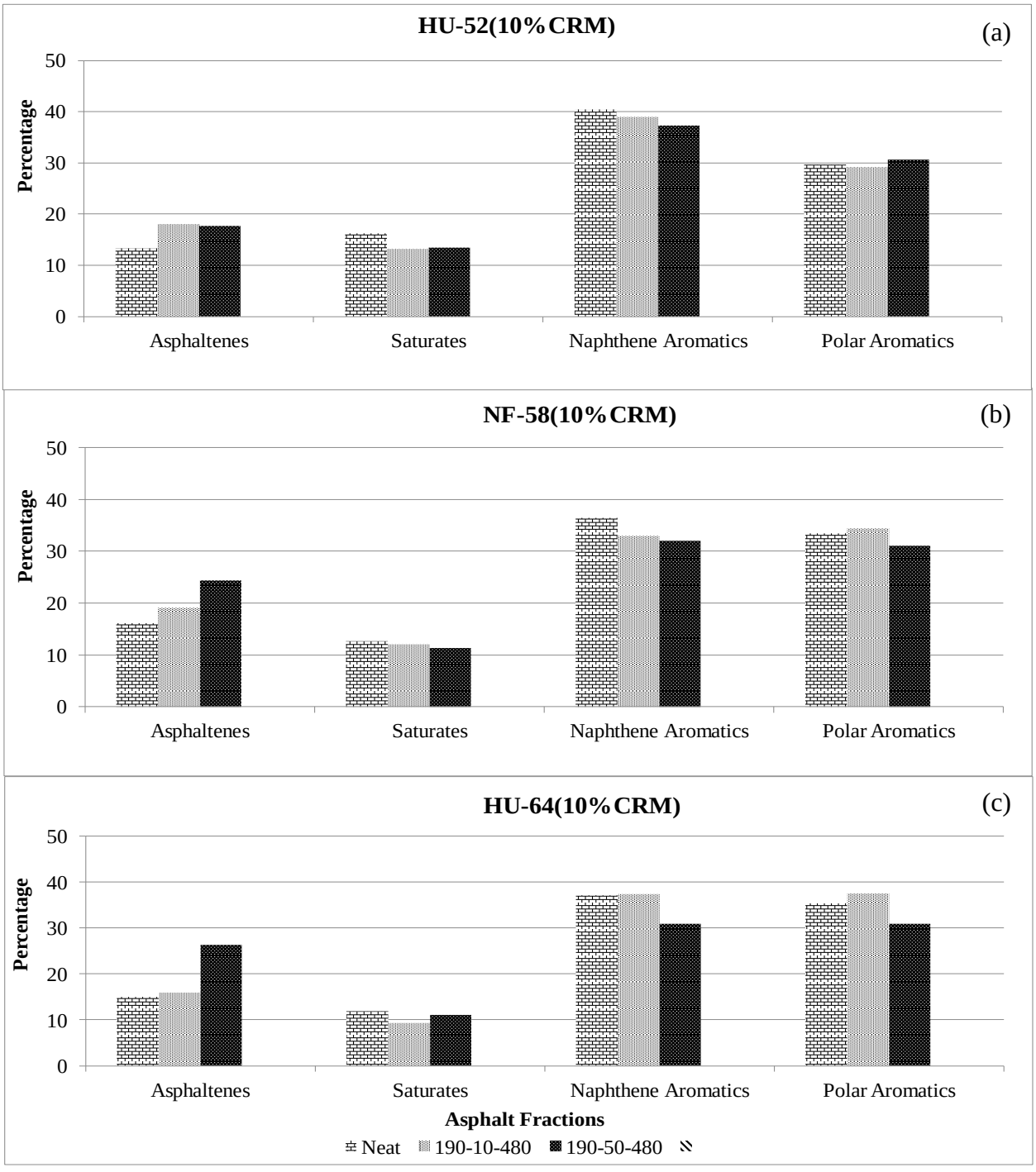

Figure 6.4. Effect of mixing speed on the different asphalt fractions (a) HU-52, (b) NF-58, and (c) HU-64.

Stepwise TGA Analysis

In this section the utilization of stepwise isothermal TGA is carried out on the asphalt fractions. This is carried out to investigate the thermal behavior change of the asphalt fractions as compared to that of the original CRM TGA behavior. This is carried out to determine which fractions behaved as those of CRM components and how that affected the formation of network structures in asphalt.

Various researchers have investigated the behavior of asphalt utilizing TGA, in a particular study by Xu and Huang, they utilized combined TGA+FTIR to investigate the combustion mechanism of asphalt binder [126]. From this study, we were able to identify the combustion products for asphalt for the different TGA temperature ranges. Those products can be identified as follows; from temperature ranges (300-405°C), the asphalt combustion products are; CO_2, CO, H_2O, CH_4, formaldehydes, formic acid, aromatic compounds, hydrocarbons, heptane, etc. On the other hand, from temperature ranges (405-490°C), the asphalt combustion products are; CO_2, CO, H_2O, CH_4, alcohols, phenols, formaldehydes, formic acid, methanol, hydrocarbons, heptane, etc. Lastly, from temperature ranges (490-570°C), the asphalt combustion products are; CO_2, CO, H_2O, alcohols, phenols, formaldehydes, formic acid, hydrocarbons, heptane, etc. [126].As can be seen from the products from each temperature range, some similar products are combusted. Thus in the analysis of the TGA, the specific products combusted per each temperature won't be addressed separately, but rather the comparison involving the change in the steps positions and percentage per each asphalt TGA thermograph to that of the neat asphalt and as received CRM. This is carried out to identify how the CRM affected the thermal behavior of asphalt, and whether CRM components migrated to the asphalt or not. As explained earlier in the experimental design section, the CRM poses known specific temperature ranges identifying the

components present in it. Those can be summarized as follows; The first region (25–300°C) is related to the oily components in the CRM, the second region (300°C to 350°C) is corresponded to natural rubber portion of the CRM and the third region (350 to 500°C) is corresponded to synthetic rubber portion of the CRM and finally the residue above 500°C is corresponded to filler components, like carbon black, in the CRM [54, 59-61].

Figure 6.5 (a and b) illustrates the stepwise TGA analysis results for the fractions; asphaltenes and saturates, of CRMA sample interacted at 190°C and 10Hz after 8hr of interaction time as compared to HU-52 neat and CRM components, respectively.

As can be seen from Figure 6.5(a), almost 90% of the asphaltene components for the investigated sample fill within the synthetic rubber steps range. This indicates that at such combination of medium interaction temperature (190°C) and with the utilization of low interaction speed (10Hz), most of the asphaltene fractions components were altered through the interaction with CRM to have a combustion behavior similar to that of synthetic rubber components of CRM, however this doesn't necessarily indicate that most of the asphaltene components are synthetic rubber, owing to the limited percentage of CRM (10%) utilized in the interaction with asphalt, indicating that it is rather a shift in the behavior of the asphaltene combustion rather than migration of the synthetic rubber from CRM to the asphaltene. This would be further elaborated in the FTIR analysis section discussed hereafter.

As can be seen from Figure 6.5(b), almost 18% of the saturates components for the investigated sample fill within the synthetic rubber steps range. This indicates that at such combination of medium interaction temperature (190°C) and with the utilization of low interaction speed (10Hz), almost 1/5 of fractions components were altered through the interaction with CRM to have a combustion behavior similar to that of synthetic rubber components of CRM.

However, as explained earlier, this doesn't necessarily indicate that 18% of the saturates components are synthetic rubber, owing to the limited percentage of CRM (10%) utilized in the interaction with asphalt, indicating that it is rather a shift in the behavior of the saturates combustion rather than migration of the synthetic rubber from CRM to the saturates. The presence/absence of peaks of synthetic rubber in the saturates FTIR analysis section discussed hereafter would provide evidence of whether the synthetic rubber components did actually migrate to the saturates, or it is merely a shift in the combustion behavior of saturates.

Figure 6.6 (a and b) illustrates the stepwise TGA analysis results for the fractions; naphthen aromatics and polar aromatics, of CRMA sample interacted at 190°C and 10Hz after 8hr of interaction time as compared to HU-52 neat and CRM components, respectively.

As can be seen from Figure 6.6(a), almost 30% of the naphthene aromatics components for the investigated sample fill within the synthetic rubber steps range.

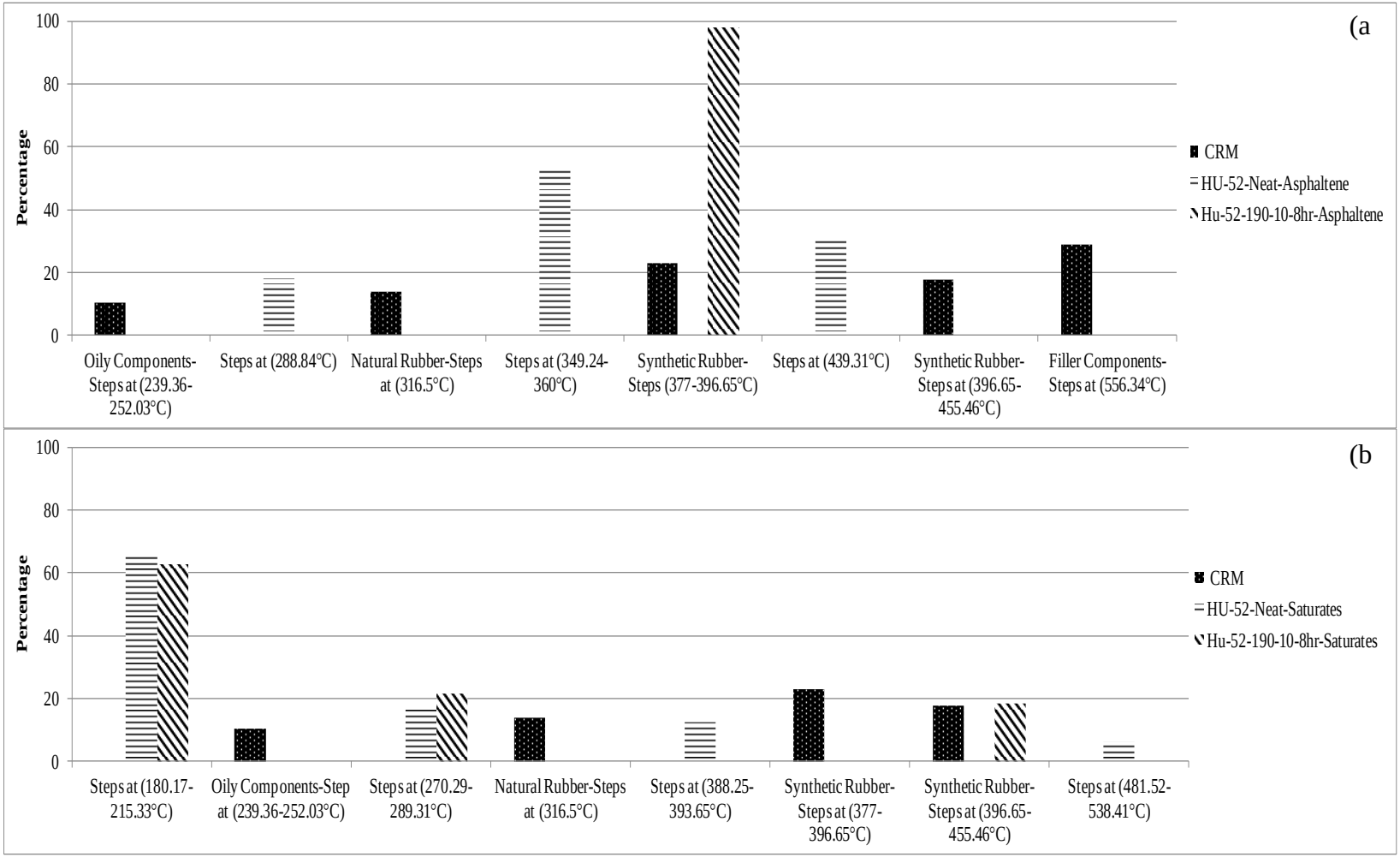

Figure 6.5. Stepwise TGA analysis results for the fractions; (a)asphaltenes and (b)saturates, of the CRMA sample interacted at 190°C and 10Hz after 8hr of interaction time as compared to HU-52 neat and CRM components.

This indicates that at such combination of medium interaction temperature (190°C) and with the utilization of low interaction speed (10Hz), 1/3 of the naphthene aromatics fractions components were altered through the interaction with CRM to have a combustion behavior similar to that of synthetic rubber components of CRM, however as explained earlier, this doesn't necessarily indicate that most of the naphthene aromatics components are synthetic rubber, owing to the limited percentage of CRM (10%) utilized in the interaction with asphalt, indicating that it is rather a shift in the behavior of the naphthene aromatics combustion rather than migration of the synthetic rubber from CRM to the naphthene aromatics. This would be further investigated in the FTIR analysis section discussed hereafter.

As can be seen from Figure 6.6(b), almost 70% of the polar aromatics components for the investigated sample fill within the synthetic rubber steps range. This indicates that at such combination of medium interaction temperature (190°C) and with the utilization of low interaction speed (10Hz), almost 3/4 of fractions components were altered through the interaction with CRM to have a combustion behavior similar to that of synthetic rubber components of CRM, however as explained earlier, this doesn't necessarily indicate that 70% of the polar aromatics components are synthetic rubber, owing to the limited percentage of CRM (10%) utilized in the interaction with asphalt, indicating that it is rather a shift in the behavior of the polar combustion rather than migration of the synthetic rubber from CRM to the polar aromatics. The presence/absence of peaks of synthetic rubber in the polar aromatics FTIR analysis section discussed hereafter would provide evidence of whether the synthetic rubber components did actually migrate to the polar aromatics, or it is merely a shift in the combustion behavior of polar aromatics.

Figure 6.7 (a and b) illustrates the stepwise TGA analysis results for the fractions; asphaltenes and saturates, of CRMA sample interacted at 190°C and 50Hz after 8hr of interaction time as compared to HU-52 neat and CRM components, respectively.

As can be seen from Figure 6.7(a), almost 80% of the asphaltene components for the investigated sample fill within the synthetic rubber steps range. This indicates that at such combination of medium interaction temperature (190°C) and with the utilization of high interaction speed (50Hz), most of the asphaltene fractions components were altered through the interaction with CRM to have a combustion behavior similar to that of synthetic rubber components of CRM, however this doesn't necessarily indicate that most of the asphaltene components are synthetic rubber, owing to the limited percentage of CRM (10%) utilized in the interaction with asphalt, indicating that it is rather a shift in the behavior of the asphaltene combustion rather than migration of the synthetic rubber from CRM to the asphaltene. This would be further elaborated in the FTIR analysis section discussed hereafter.

As can be seen from Figure 6.7(b), almost 19% of the saturates components for the investigated sample fill within the synthetic rubber steps range. In addition, 22% of the components fill within the oily components range. This indicates that at such combination of medium interaction temperature (190°C) and with the utilization of high interaction speed (50Hz), almost 1/5 of fractions components were altered through the interaction with CRM to have a combustion behavior similar to that of synthetic rubber components and oily components of CRM.

However, as explained earlier, this doesn't necessarily indicate that 19% of the saturates components are synthetic rubber or that 20% are oily components, owing to the limited percentage of CRM (10%) utilized in the interaction with asphalt, indicating that it is rather a shift in the

behavior of the saturates combustion rather than migration of the synthetic rubber or oily components from CRM to the saturates.

The presence/absence of peaks of synthetic rubber in the saturates FTIR analysis section discussed hereafter would provide evidence of whether the synthetic rubber components did actually migrate to the saturates, or it is merely a shift in the combustion behavior of saturates.

Figure 6.8 (a and b) illustrates the stepwise TGA analysis results for the fractions; naphthene aromatics and polar aromatics, of CRMA sample interacted at 190°C and 50Hz after 8hr of interaction time as compared to HU-52 neat and CRM components, respectively.

As can be seen from Figure 6.8(a), almost 35% of the polar aromatics components for the investigated sample fill within the synthetic rubber steps range. This indicates that at such combination of medium interaction temperature (190°C) and with the utilization of high interaction speed (50Hz), almost one third of the naphthene aromatics fractions components were altered through the interaction with CRM to have a combustion behavior similar to that of synthetic rubber components of CRM, however as explained earlier, this doesn't necessarily indicate that most of the naphthene aromatics components are synthetic rubber owing to the limited percentage of CRM (10%) utilized in the interaction with asphalt.

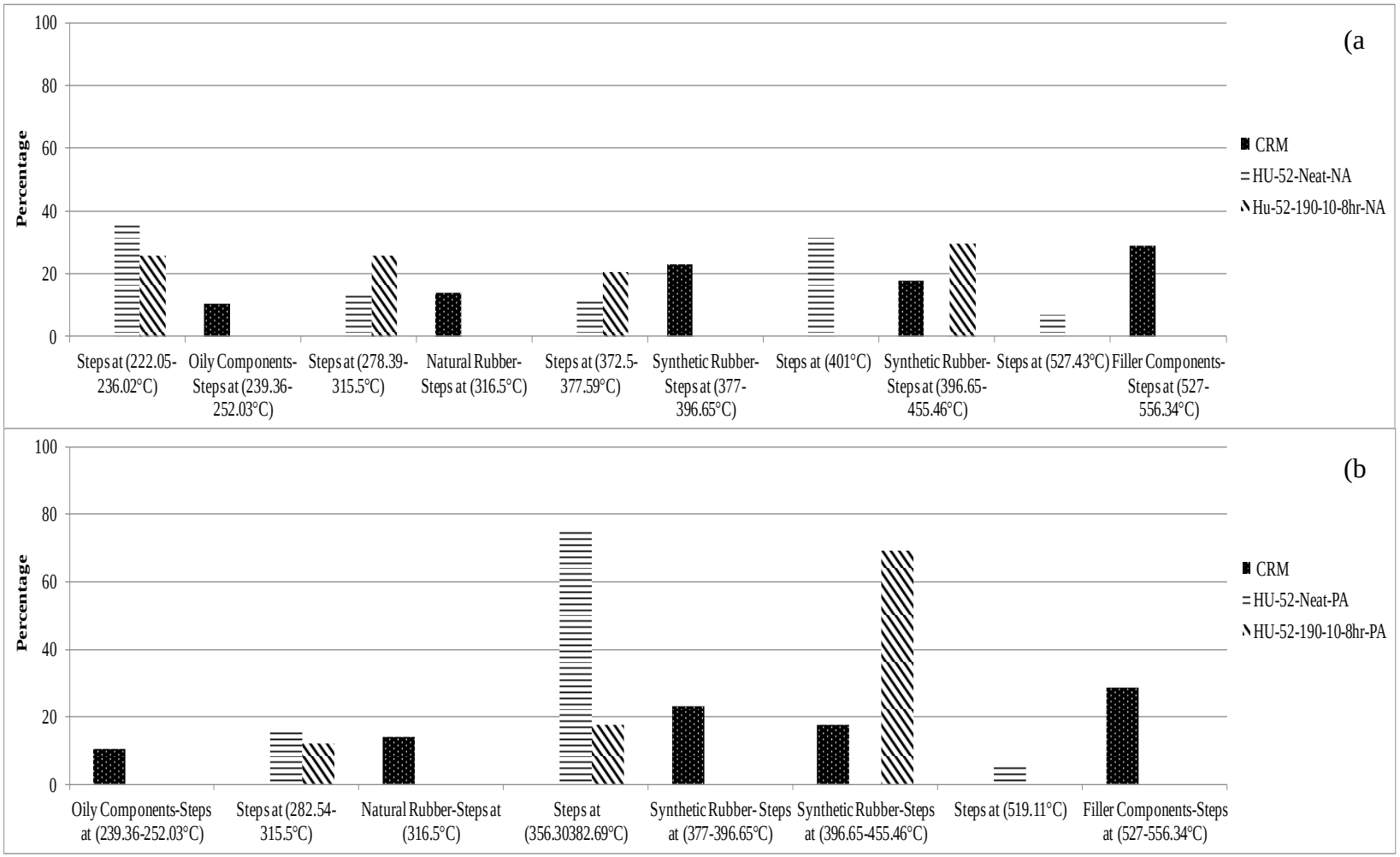

Figure 6.6. Stepwise TGA analysis results for the fractions; (a)naphthene aromatics and (b)polar aromatics, of the CRMA sample interacted at 190°C and 10Hz after 8hr of interaction time as compared to HU-52 neat and CRM components.

This indicates that it is rather a shift in the behavior of the naphthene aromatics combustion rather than migration of the synthetic rubber from CRM to the naphthene aromatics.This would be further investigated in the FTIR analysis section discussed hereafter.

As can be seen from Figure 6.8(b), almost 80% of the polar aromatics components for the investigated sample fill within the synthetic rubber steps range. This indicates that at such combination of medium interaction temperature (190°C) and with the utilization of high interaction speed (50Hz), almost 4/5 of fractions components were altered through the interaction with CRM to have a combustion behavior similar to that of synthetic rubber components of CRM, however as explained earlier, this doesn't necessarily indicate that 80% of the polar aromatics components are synthetic rubber, owing to the limited percentage of CRM (10%) utilized in the interaction with asphalt, indicating that it is rather a shift in the behavior of the polar combustion rather than migration of the synthetic rubber from CRM to the polar aromatics. The presence/absence of peaks of synthetic rubber in the polar aromatics FTIR analysis section discussed hereafter would provide evidence of whether the synthetic rubber components did actually migrate to the polar aromatics, or it is merely a shift in the combustion behavior of polar aromatics.

Figure 6.9 (a and b) illustrates the stepwise TGA analysis results for the fractions; asphaltenes and saturates, of CRMA sample interacted at 220°C and 50Hz after 8hr of interaction time as compared to HU-52 neat and CRM components, respectively.

As can be seen from Figure 6.9(a), no components for the investigated sample fill within the synthetic rubber steps range. This indicates that at such combination of high interaction temperature (220°C) and with the utilization of high interaction speed (50Hz), most of the asphaltene fractions components lost the CRM modification effect as a result of the increased depolymerization and devulcanization effects [20, 24]. This lead to have the asphaltene of almost similar com-

bustion behavior to that of neat asphalt asphaltene, with the presence of traces of filler components from the CRM that were able to withstand the combination of high interaction speed and temperature. This would be further elaborated in the FTIR analysis section discussed hereafter.

As can be seen from Figure 6.9(b), the same trend of lack of components for the investigated sample to fill within the synthetic rubber steps range was evident. This indicates that at such combination of high interaction temperature (220°C) and with the utilization of high interaction speed (50Hz), most of the saturates fractions components lost the CRM modification effect as a result of the increased depolymerization and devulcanization effects [20, 24]. This lead to have the saturates of almost similar combustion behavior to that of neat asphalt saturates, with the presence of some filler components from the CRM that were able to withstand the combination of high interaction speed and temperature.

Figure 6.10 (a and b) illustrates the stepwise TGA analysis results for the fractions; naphthene aromatics and polar aromatics, of CRMA sample interacted at 220°C and 50Hz after 8hr of interaction time as compared to HU-52 neat and CRM components, respectively.

As can be seen from Figure 6.10(a), almost 10% of the naphthene aromatics components for the investigated sample fill within the synthetic rubber steps range. This indicates that at such combination of high interaction temperature (220°C) and with the utilization of high interaction speed (50Hz), 10% of the naphthene aromatics fractions components were altered through the interaction with CRM to have a combustion behavior similar to that of synthetic rubber components of CRM, however as explained earlier, this doesn't necessarily indicate that most of the naphthene aromatics components are synthetic rubber owing to the limited percentage of CRM (10%) utilized in the interaction with asphalt.

As can be seen from Figure 6.10(b), almost 80% of the polar aromatics components for the investigated sample fill within the synthetic rubber steps range. This indicates that at such combination of high interaction temperature (220°C) and with the utilization of high interaction speed (50Hz), almost 4/5 of fractions components were altered through the interaction with CRM to have a combustion behavior similar to that of synthetic rubber components of CRM, however as explained earlier, this doesn't necessarily indicate that 80% of the polar aromatics components are synthetic rubber, owing to the limited percentage of CRM (10%) utilized in the interaction with asphalt, indicating that it is rather a shift in the behavior of the polar combustion rather than migration of the synthetic rubber from CRM to the polar aromatics. The presence/absence of peaks of synthetic rubber in the polar aromatics FTIR analysis section discussed hereafter would provide evidence of whether the synthetic rubber components did actually migrate to the polar aromatics, or it is merely a shift in the combustion behavior of polar aromatics.

Figure 6.11 (a and b) illustrates the stepwise TGA analysis results for the fractions; asphaltenes and saturates, of CRMA sample interacted at 190°C and 50Hz after 8hr of interaction time as compared to HU-64 neat and CRM components, respectively.

As can be seen from Figure 6.11(a), almost 85% of the asphaltene components for the investigated sample fill within the synthetic rubber steps range. This indicates that at such combination of medium interaction temperature (190°C) and with the utilization of high interaction speed (50Hz), most of the asphaltene fractions components were altered through the interaction with CRM to have a combustion behavior similar to that of synthetic rubber components of CRM, however this doesn't necessarily indicate that most of the asphaltene components are synthetic rubber, owing to the limited percentage of CRM (10%) utilized in the interaction with asphalt, indicating that it is rather a shift in the behavior of the asphaltene combustion rather than

migration of the synthetic rubber from CRM to the asphaltene. This would be further elaborated in the FTIR analysis section discussed hereafter.

As can be seen from Figure 6.11(b), almost 18% of the saturates components for the investigated sample fill within the synthetic rubber steps range. In addition, 40% of the components fill within the oily components range. This indicates that at such combination of medium interaction temperature (190°C) and with the utilization of high interaction speed (50Hz), almost 1/5 of fractions components were altered through the interaction with CRM to have a combustion behavior similar to that of synthetic rubber components and oily components of CRM.

However, as explained earlier, this doesn't necessarily indicate that 18% of the saturates components are synthetic rubber or that 40% are oily components, owing to the limited percentage of CRM (10%) utilized in the interaction with asphalt, indicating that it is rather a shift in the behavior of the saturates combustion rather than migration of the synthetic rubber or oily components from CRM to the saturates. The presence/absence of peaks of synthetic rubber in the saturates FTIR analysis section discussed hereafter would provide evidence of whether the synthetic rubber components did actually migrate to the saturates, or it is merely a shift in the combustion behavior of saturates.

Figure 6.12 (a and b) illustrates the stepwise TGA analysis results for the fractions; naphthene aromatics and polar aromatics, of CRMA sample interacted at 190°C and 50Hz after 8hr of interaction time as compared to HU-64 neat and CRM components, respectively.

As can be seen from Figure 6.12(a), almost 40% of the polar aromatics components for the investigated sample fill within the synthetic rubber steps range. In addition, another 40% fill within the oily components range. This indicates that at such combination of medium interaction temperature (190°C) and with the utilization of high interaction speed (50Hz), almost 80% of the

naphthene aromatics fractions components were altered through the interaction with CRM to have a combustion behavior similar to that of synthetic rubber components and oily components of CRM, however as explained earlier, this doesn't necessarily indicate that most of the naphthene aromatics components are synthetic rubber or oily components, owing to the limited percentage of CRM (10%) utilized in the interaction with asphalt, indicating that it is rather a shift in the behavior of the naphthene aromatics combustion rather than migration of the synthetic rubber or oily components from CRM to the naphthene aromatics. This would be further investigated in the FTIR analysis section discussed hereafter.

As can be seen from Figure 6.12(b), almost 30% of the polar aromatics components for the investigated sample fill within the synthetic rubber steps range. This indicates that at such combination of medium interaction temperature (190°C) and with the utilization of high interaction speed (50Hz), almost 1/3 of fractions components were altered through the interaction with CRM to have a combustion behavior similar to that of synthetic rubber components of CRM, however as explained earlier, this doesn't necessarily indicate that 30% of the polar aromatics components are synthetic rubber, owing to the limited percentage of CRM (10%) utilized in the interaction with asphalt, indicating that it is rather a shift in the behavior of the polar combustion rather than migration of the synthetic rubber from CRM to the polar aromatics.

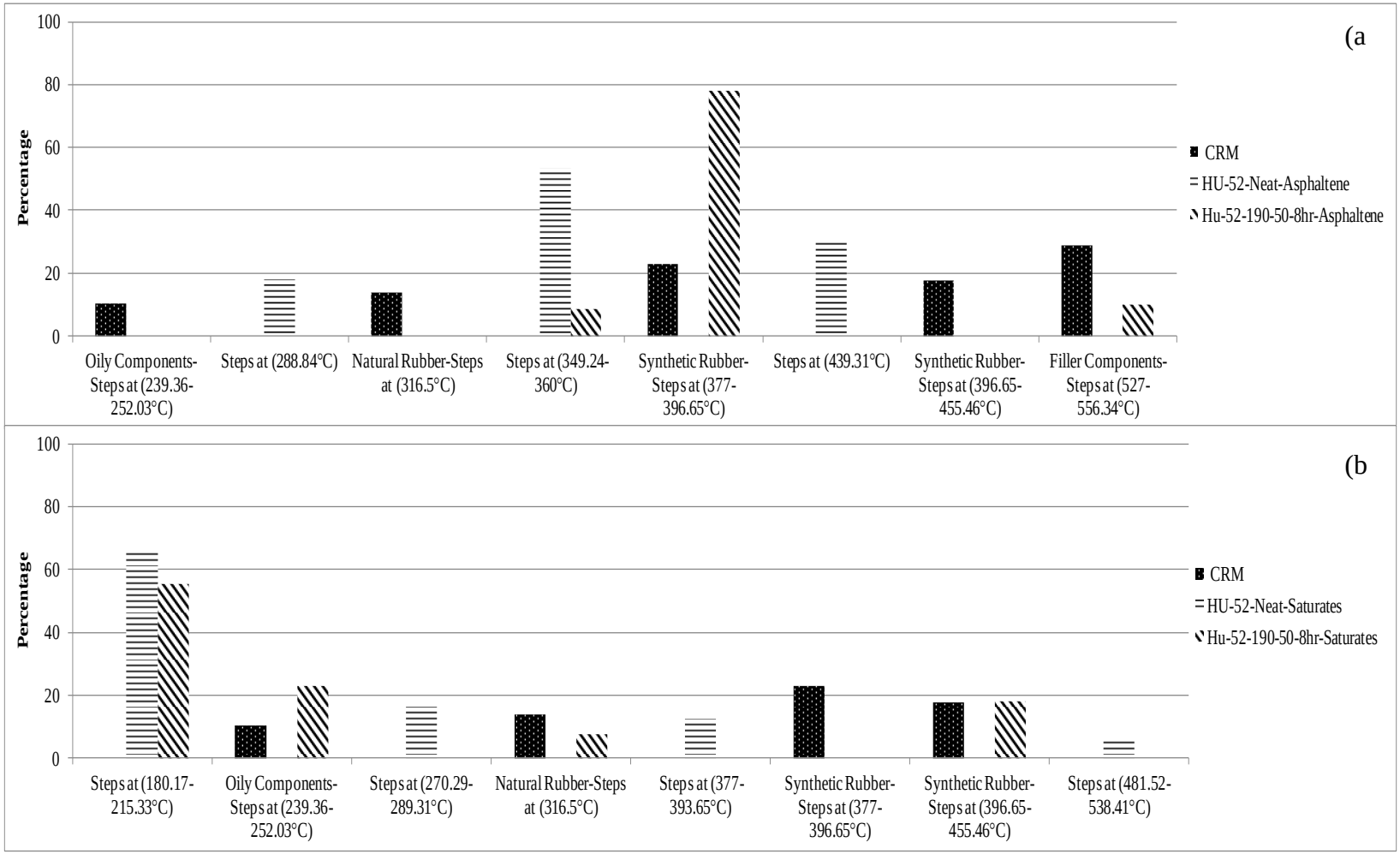

Figure 6.7. Stepwise TGA analysis results for the fractions; (a)asphaltenes and (b)saturates, of the CRMA sample interacted at 190°C and 50Hz after 8hr of interaction time as compared to HU-52 neat and CRM components.

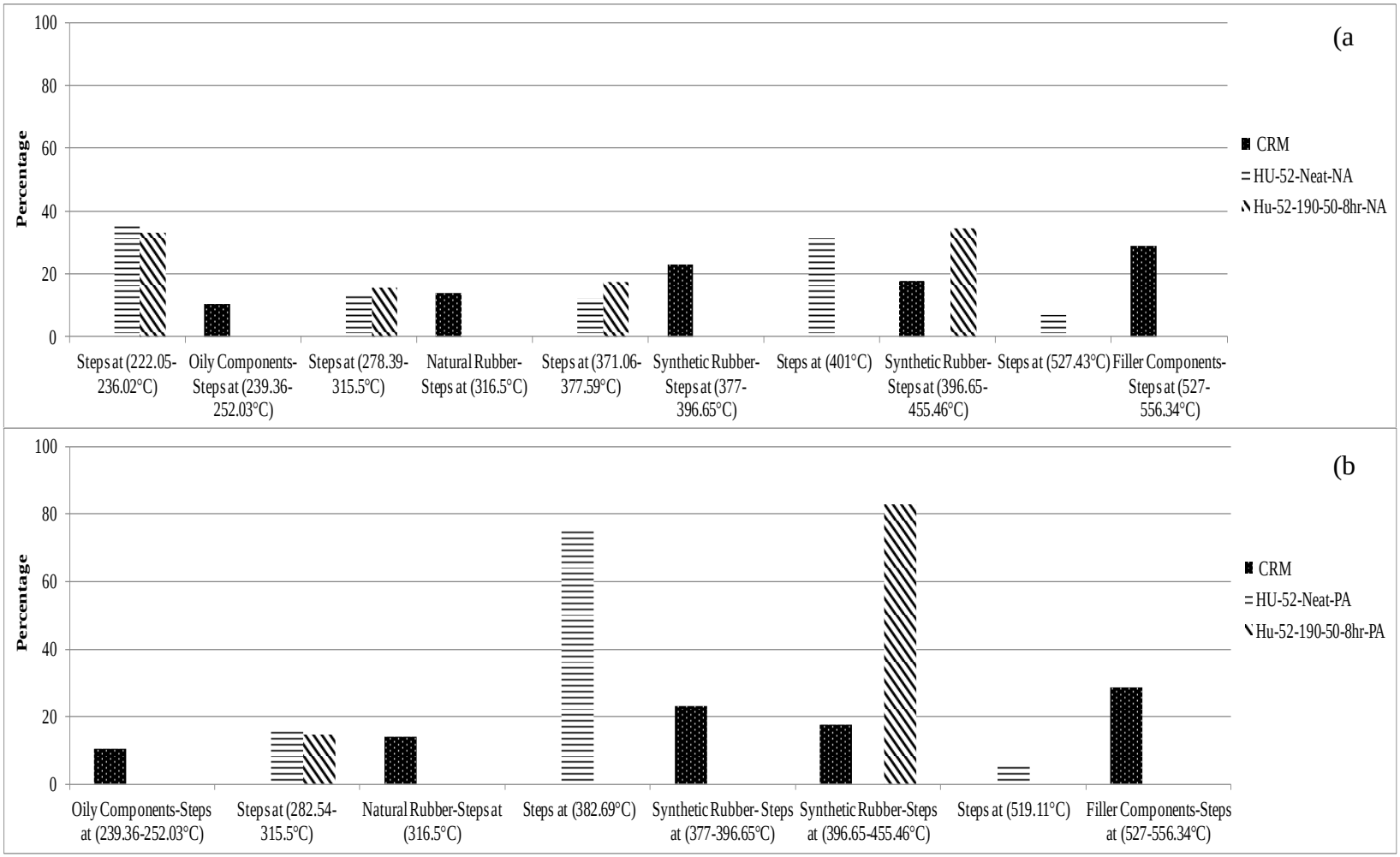

Figure 6.8. Stepwise TGA analysis results for the fractions; (a)naphthene aromatics and (b)polar aromatics, of the CRMA sample interacted at 190°C and 50Hz after 8hr of interaction time as compared to HU-52 neat and CRM components.

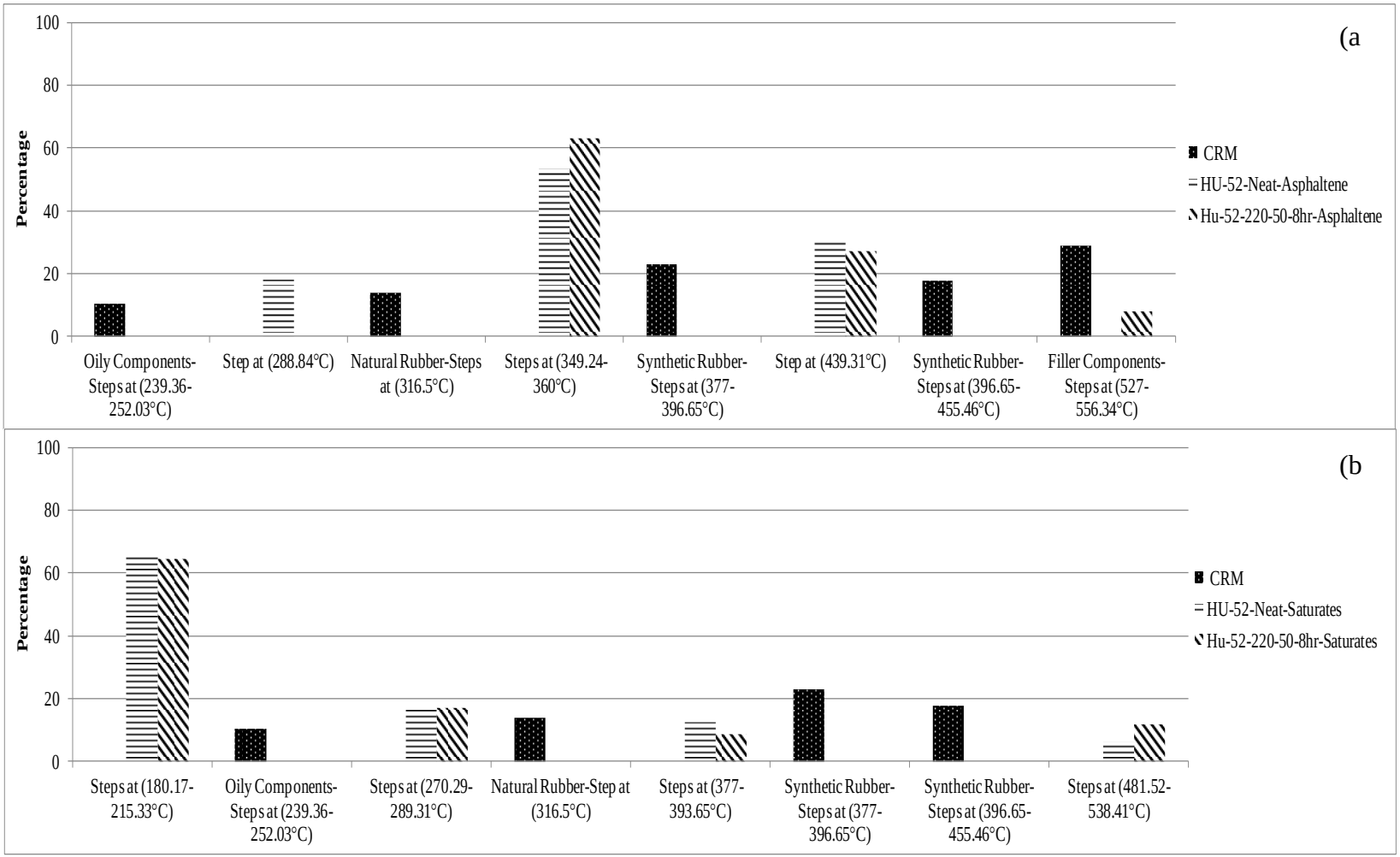

Figure 6.9. Stepwise TGA analysis results for the fractions; (a)asphaltenes and (b)saturates, of the CRMA sample interacted at 220°C and 50Hz after 8hr of interaction time as compared to HU-52 neat and CRM components.

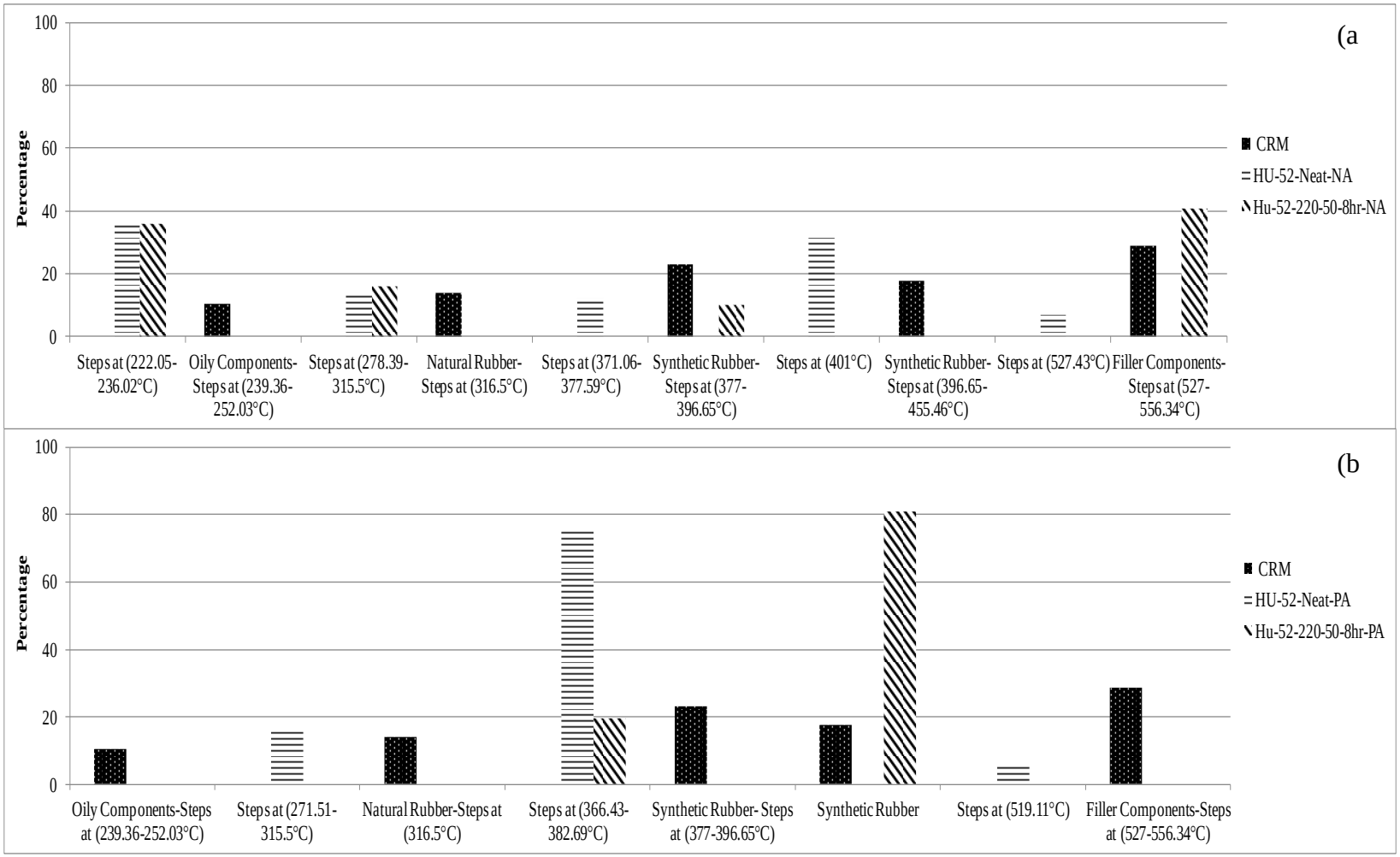

Figure 6.10. Stepwise TGA analysis results for the fractions; (a)naphthene aromatics and (b)polar aromatics, of the CRMA sample interacted at 220°C and 50Hz after 8hr of interaction time as compared to HU-52 neat and CRM components.

The presence/absence of peaks of synthetic rubber in the polar aromatics FTIR analysis section discussed hereafter would provide evidence of whether the synthetic rubber components did actually migrate to the polar aromatics, or it is merely a shift in the combustion behavior of polar aromatics.

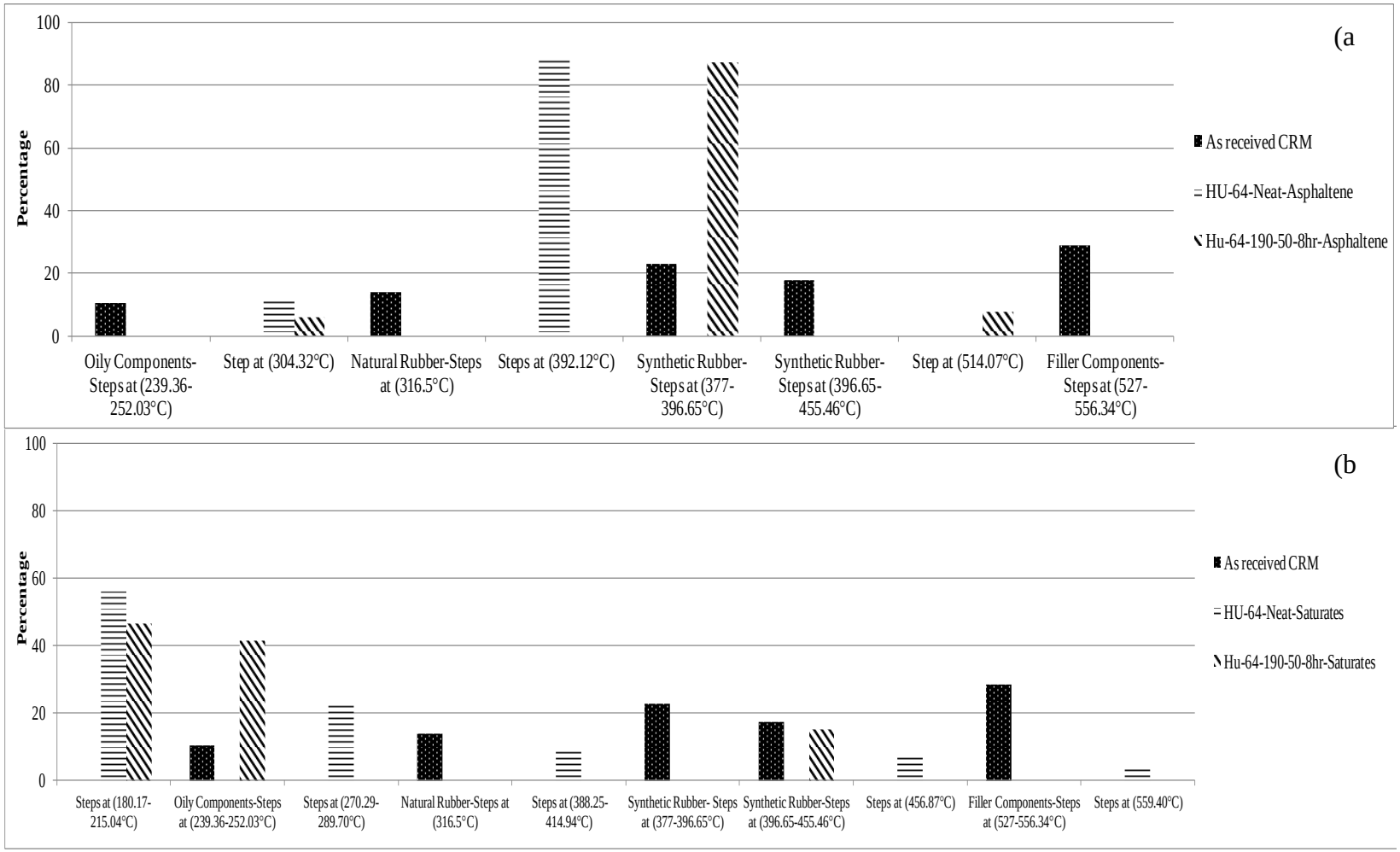

Figure 6.11. Stepwise TGA analysis results for the fractions; (a)asphaltenes and (b)saturates, of the CRMA sample interacted at 190°C and 50Hz after 8hr of interaction time as compared to HU-64neat and CRM components.

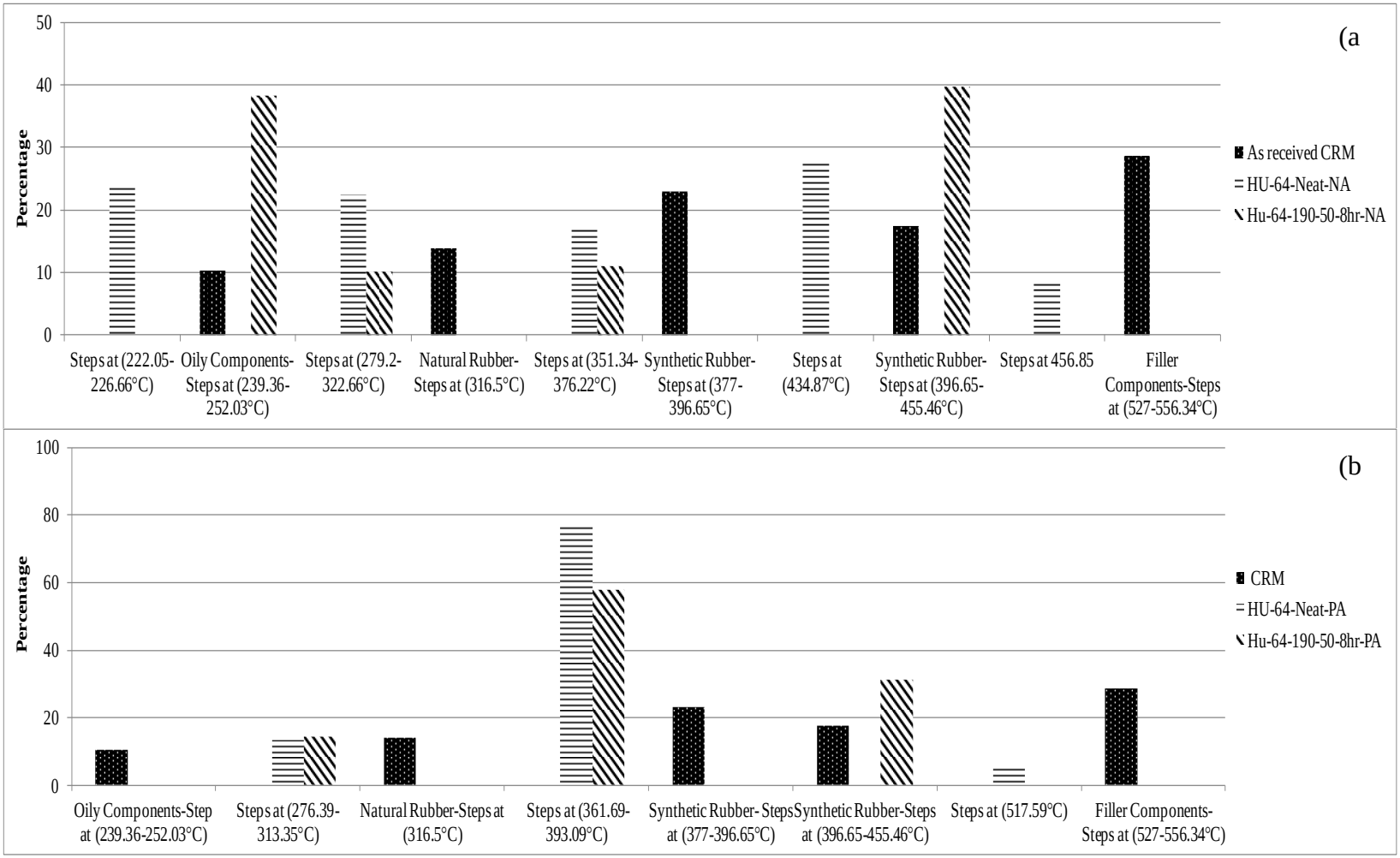

Figure 6.12. Stepwise TGA analysis results for the fractions; (a)naphthene aromatics and (b)polar aromatics, of the CRMA sample interacted at 190°C and 50Hz after 8hr of interaction time as compared to HU-64 neat and CRM components.

FTIR Analysis

In this section weutilize FTIR analysis on the asphalt neat fractions and compare to that of the fractions of asphalt after interacting with CRM. This would provide an idea of how the network structures in asphalt are formalized through altering which components of the asphalt fractions. As discussed in the literature review chapter, various researchers have attempted to identify FTIR peaks for the CRM and asphalt. Distinctive FTIR peaks for both the asphalt and CRM have been addressed in the literature review chapter with regards to various previous research works. In this section we would be addressing the change of such peaks, if present, in addition to investigating the appearance/disappearance of distinctive peaks in the FTIR spectra of the different asphalt fractions after interaction with CRM.

Figure 6.13illustrates the FTIR spectra comparison for the asphaltenes of neat and samples interacted at 190°C with 10Hz after 8hr of interaction time for the HU-52 asphalt.

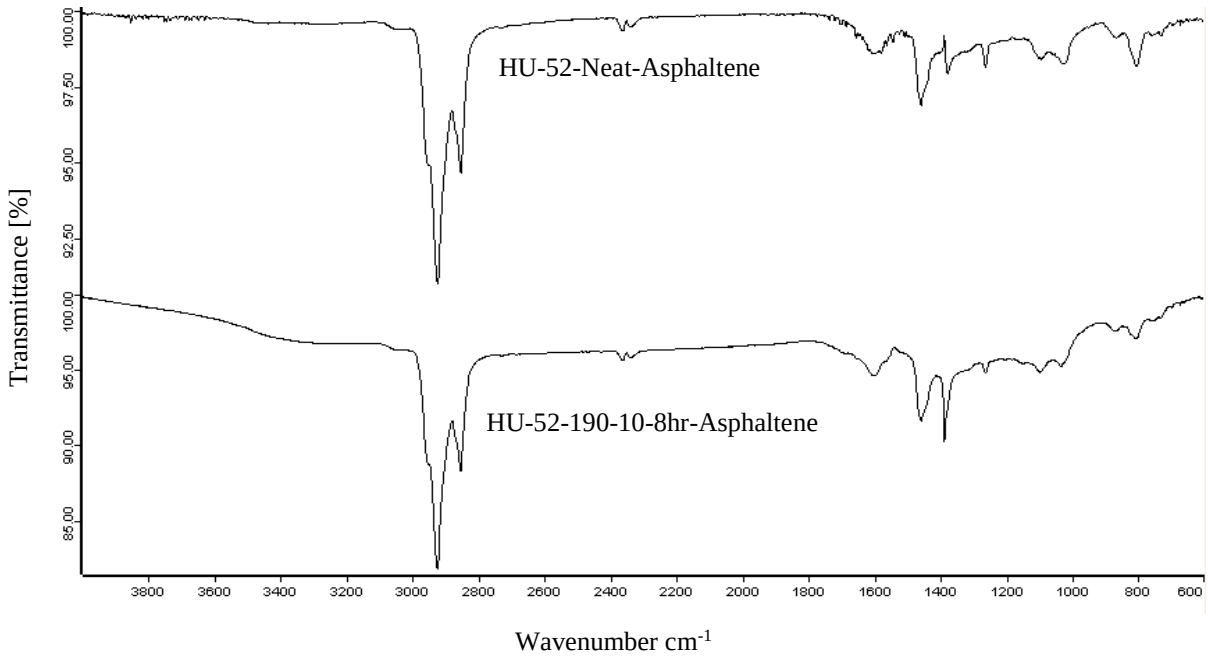

Figure 6.13. FTIR spectra comparison for CRM as compared to the asphaltenes of neat and samples interacted at 190°C with 10Hz after 8hr of interaction time.

As can be seen from the figure, a decrease in the intensity of asphaltene peaks for the samples interacted at 190°C and 10Hz after 8hr of interaction time in the wavenumber region from 600 to 1200 cm^{-1}. This might suggest that some of the benzene rings have migrated to the CRM [31].In addition, the TGA behavior of the same samples showed components with similar combustion behavior to that of synthetic rubber with almost 90%. This might indicate that some of the asphaltene fractions components have migrated to CRM, while most of the remaining components were altered to have thermal behavior similar to that of synthetic rubber.

Figure 6.14 illustrates the FTIR spectra comparison for the saturates of neat and samples interacted at 190C with 10Hz after 8hr of interaction time for the HU-52 asphalt. As can be seen from the figure, the decrease of peaks for the CRMA be seen at 801 and 1020 cm^{-1}, those peaks are accounted for the C-H vibration of benzene ring and S=O stretching, respectively [27, 31, 66, 67].

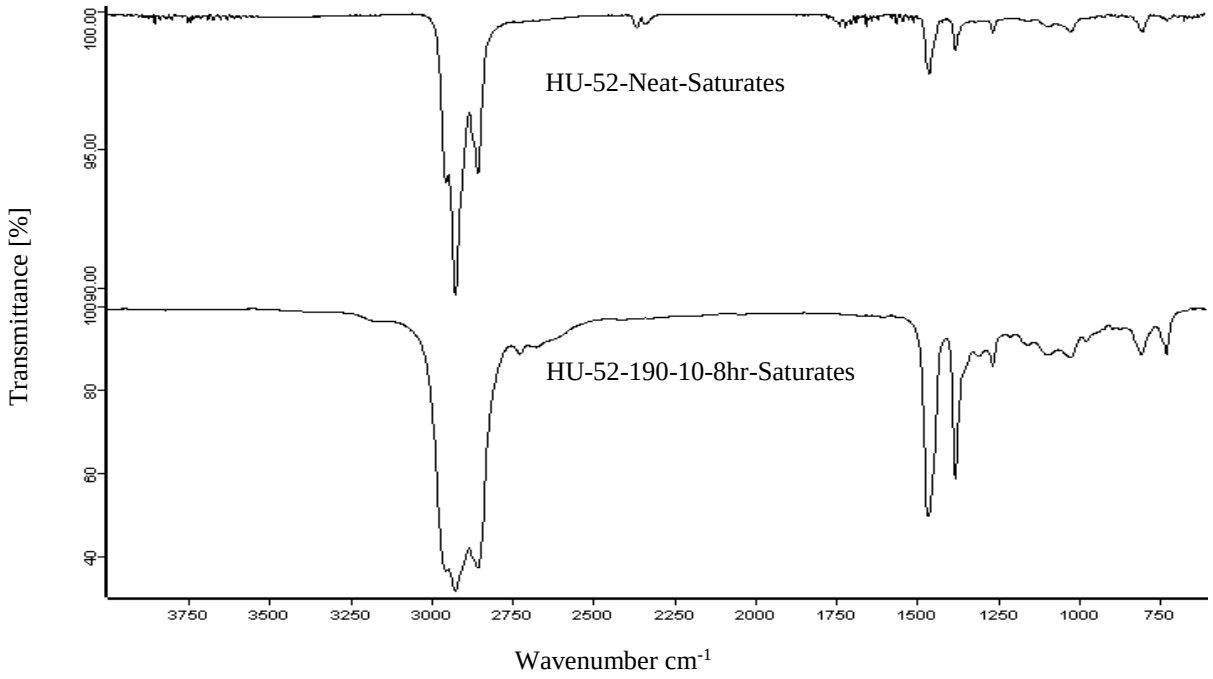

Figure 6.14. FTIR spectra comparison for CRM as compared to the saturates of neat and samples interacted at 190C with 10Hz after 8hr of interaction time.

This might indicate that for the saturates of the samples interacted at 190°C and 10Hz after 8hr of interaction time, some of the benzene rings as well as the S=O have migrated to the CRM.The TGA behavior of the same samples showed components with similar combustion behavior to that of synthetic rubber with almost 19%. This might indicate that some of the saturates fractions components have migrated to CRM, while some CRM components moved to the asphalt leading to the change of the saturates fraction to have thermal behavior of remaining components to be similar to that of synthetic rubber.

Figure 6.15 illustrates the FTIR spectra comparison for the naphthene aromatics of neat and samples interacted at 190°C with 10Hz after 8hr of interaction time for the HU-52 asphalt. As can be seen from the figure, almost similar spectra can be seen for the CRMA in comparison with neat asphalt. This indicates that the observed 30% of naphthene aromatics for the same sample that had thermal combustion behavior as that of synthetic rubber are mainly naphthene aromatics components with altered thermal behavior structure rather than being actually synthetic rubber.

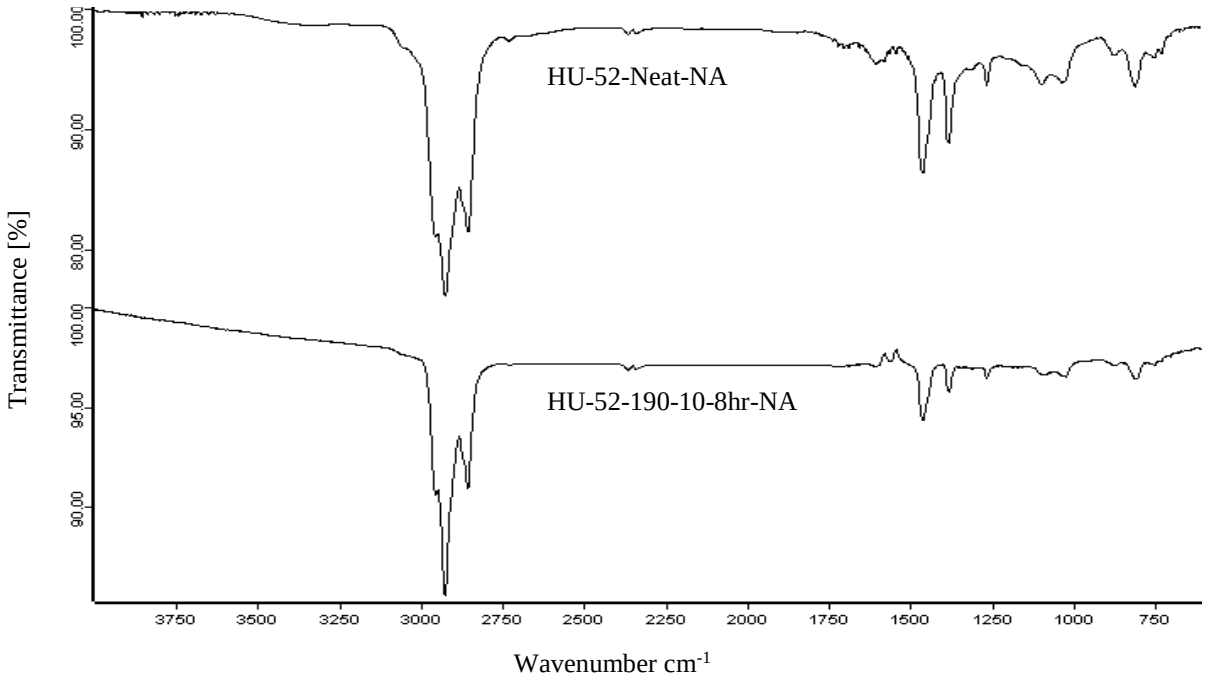

Figure 6.15. FTIR spectra comparison for CRM as compared to the naphthene aromatics of neat and samples interacted at 190C with 10Hz after 8hr of interaction time.

Figure 6.16 illustrates the FTIR spectra comparison for the polar aromatics of neat and samples interacted at 190°C with 10Hz after 8hr of interaction time for the HU-52 asphalt. As can be seen from the figure, almost similar spectra can be seen for the polar aromatics of the neat and the CRMA. However, a week peak can be seen at 969.85cm^{-1}for the CRMA sample, this peak is attributable to the bending vibration of trans 1, 4-2 alkenes in poly butadiene [75]. This indicates that some of the polymeric components from CRM have migrated to the polar aromatics of samples interacted at 190°C and 10Hz after 8hr of interaction time.

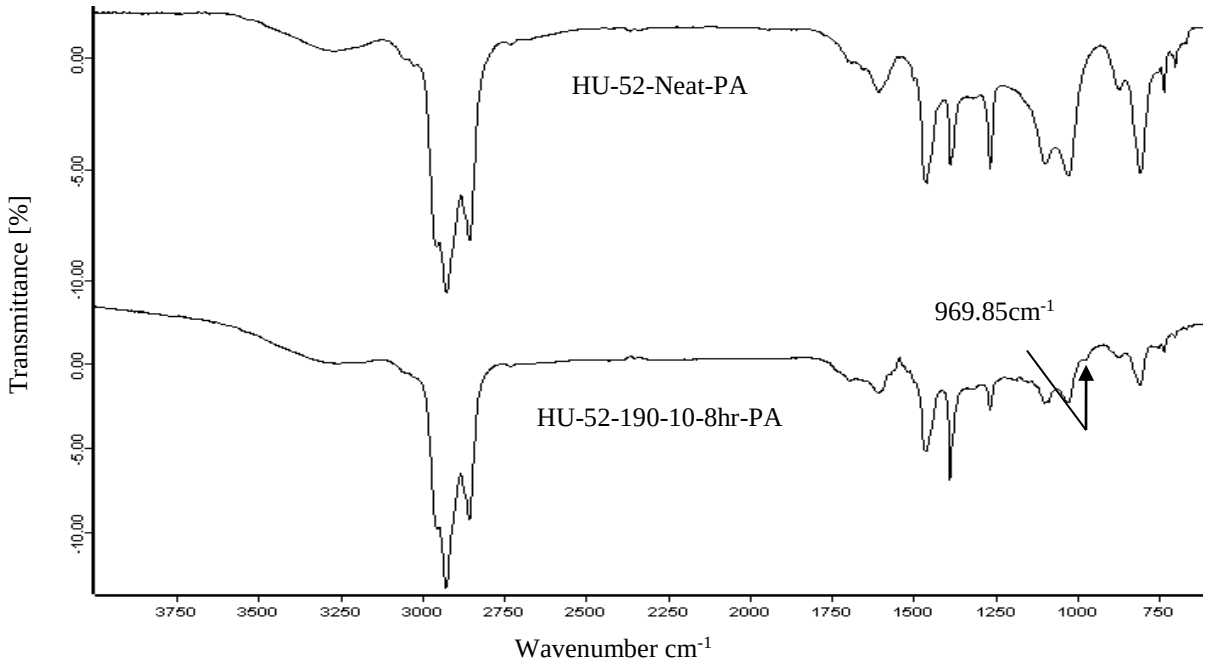

Figure 6.16. FTIR spectra comparison for CRM as compared to the polar aromatics of neat and samples interacted at 190C with 10Hz after 8hr of interaction time.

The TGA behavior of the same samples showed components with similar combustion behavior to that of synthetic rubber with almost 70%. This might indicate that some of the polar aromatics fractions components have migrated to CRM, while some CRM components moved to the asphalt leading to the change of polar aromatics to have thermal behavior of remaining components to be similar to that of synthetic rubber.

Figure 6.17 illustrates the FTIR spectra comparison for the asphaltenes of neat and samples interacted at 190°C with 50Hz after 8hr of interaction time for the HU-52 asphalt. As can be seen from the figure, almost similar spectra can be seen for the polar aromatics of the neat and the CRMA. However, a week peak can be seen at 969.85cm^{-1}for the CRMA sample, this peak is attributable to the bending vibration of trans 1, 4-2 alkenes in poly butadiene [75].

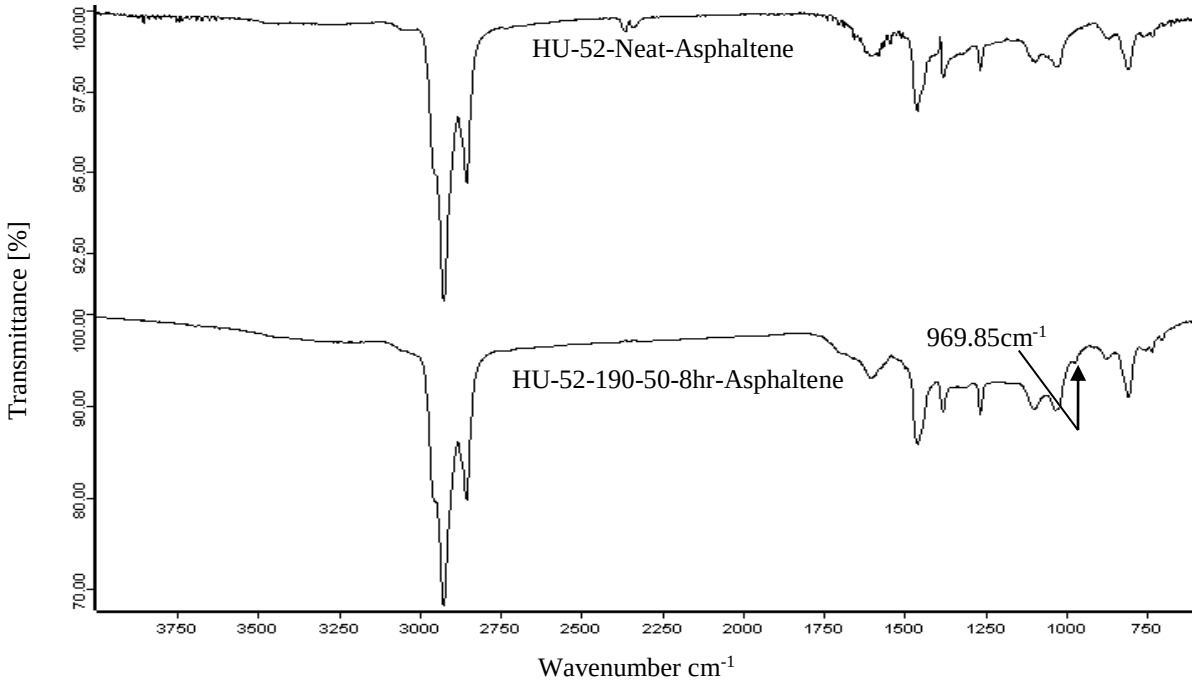

Figure 6.17. FTIR spectra comparison for CRM as compared to asphaltenes of neat and samples interacted at 190°C with 50Hz after 8hr of interaction time.

This indicates that some of the polymeric components from CRM have migrated to the asphaltenes of samples interacted at 190°C and 50Hz after 8hr of interaction time. The TGA behavior of the same samples showed components with similar combustion behavior to that of synthetic rubber with almost 80%. This might indicate that some of the asphaltenes fractions components have migrated to CRM, while some CRM components moved to the asphalt leading to the change of asphaltenes to have thermal behavior of remaining components to be similar to that of synthetic rubber.

Figure 6.18 illustrates the FTIR spectra comparison for the saturates of neat and samples interacted at 190°C with 50Hz after 8hr of interaction time for the HU-52 asphalt.

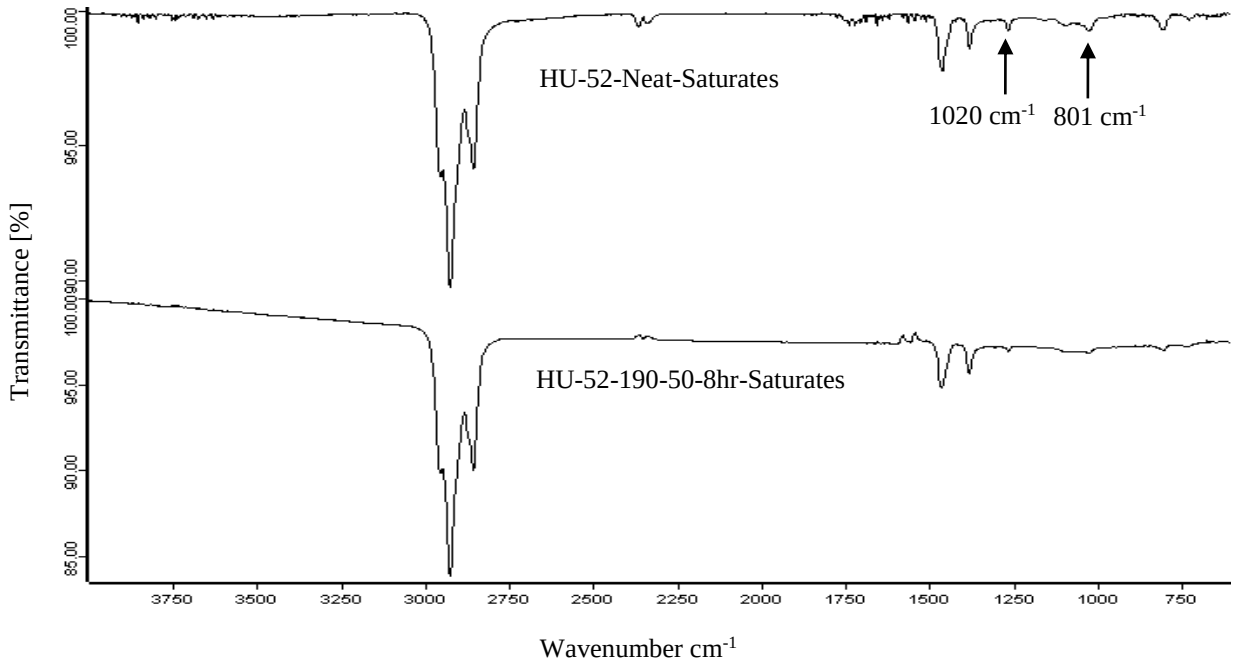

Figure 6.18. FTIR spectra comparison for CRM as compared to saturates of neat and samples interacted at 190°C with 50Hz after 8hr of interaction time.

As can be seen from the figure, the disappearance of peaks for the CRMA can be at 801 and 1020 cm^{-1}, those peaks are accounted for the C-H vibration of benzene ring and S=O stretching, respectively [27, 31, 66, 67]. This indicates that for the saturates of the samples interacted at 190°C and 10Hz after 8hr of interaction time, some of the benzene rings as well as the S=O have migrated to the CRM. The TGA behavior of the same samples showed components with similar combustion behavior to that of synthetic rubber with almost 19% and the oily components with almost 22%. This might indicate that some of the saturates fractions components have migrated to CRM, while some CRM components moved to the asphalt leading to the change of the saturates fraction to have thermal behavior of remaining components to be similar to that of synthetic rubber.

Figure 6.19 illustrates the FTIR spectra comparison for the naphthene aromatics of neat and samples interacted at 190°C with 50Hz after 8hr of interaction time for the HU-52 asphalt.

As can be seen from the figure, almost similar spectra can be seen for the CRMA in comparison with neat asphalt. This indicates that the observed 35% of naphthene aromatics for the same sample that had thermal combustion behavior as that of synthetic rubber are mainly naphthene aromatics components with altered thermal behavior structure rather than being actually synthetic rubber.

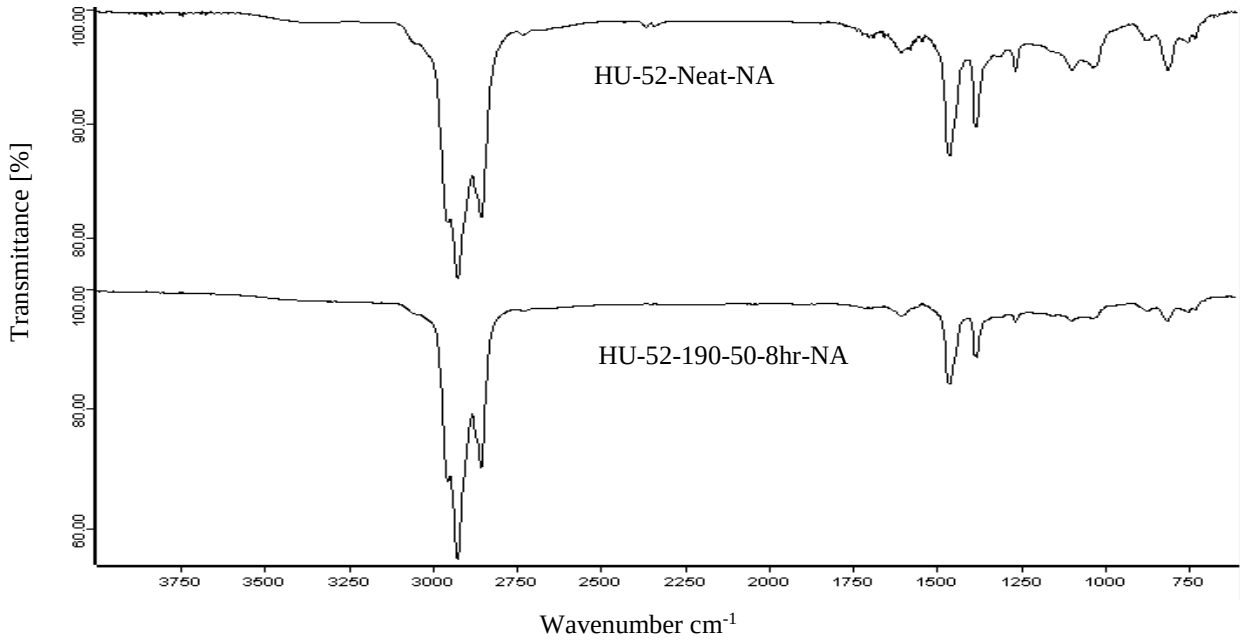

Figure 6.19. FTIR spectra comparison for CRM as compared to the naphthene aromatics of neat and samples interacted at 190°C with 50Hz after 8hr of interaction time.

Figure 6.20 illustrates the FTIR spectra comparison for the polar aromatics of neat and samples interacted at 190°C with 50Hz after 8hr of interaction time for the HU-52 asphalt.

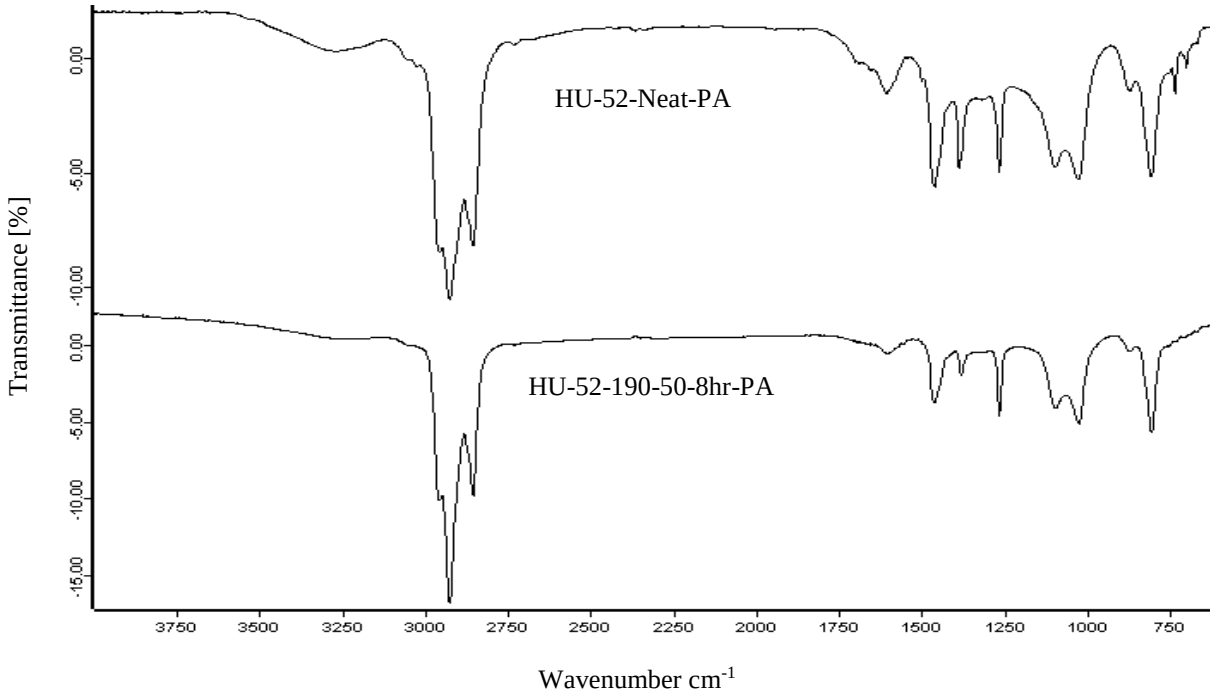

Figure 6.20. FTIR spectra comparison for CRM as compared to the polar aromatics of neat and samples interacted at 190°C with 50Hz after 8hr of interaction time.

As can be seen from the figure, almost similar spectra can be seen for the polar aromatics of the neat and the CRMA. However, weeker peaks can be seen for the CRMA sample. This indicates that some of the asphalt components have migrated to the CRM from polar aromatics for samples interacted at 190°C and 50Hz after 8hr of interaction time. The TGA behavior of the same samples showed components with similar combustion behavior to that of synthetic rubber with almost 80%. This might indicate that some of the polar aromatics fractions components have migrated to CRM, while some CRM components moved to the asphalt leading to the change of polar aromatics to have thermal behavior of remaining components to be similar to that of synthetic rubber.

Figure 6.21 illustrates the FTIR spectra comparison for CRM as compared to the asphaltenes of neat and samples interacted at 220°C with 50Hz after 8hr of interaction time for the HU-52 asphalt. As can be seen from the figure, almost similar spectra can be seen for the CRMA in comparison with neat asphalt. This indicates that at such combination of high interaction speed (50Hz) and temperature (220°C), the governing mechanisms are the devulcanization and depolymerization leading to the annihilation of the CRM modification effects [20, 24].

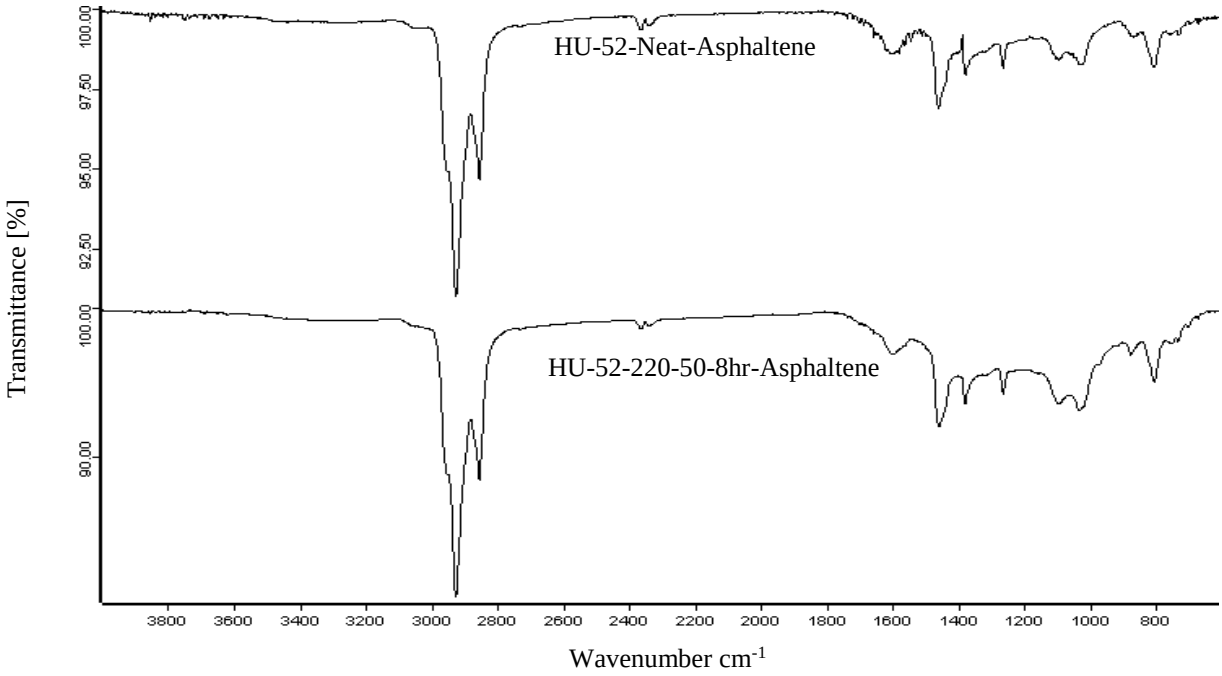

Figure 6.21. FTIR spectra comparison for CRM as compared to asphaltenes of neat and samples interacted at 190°C with 50Hz after 8hr of interaction time.

Figure 6.22 illustrates the FTIR spectra comparison for CRM as compared to the saturates of neat and samples interacted at 220°C with 50Hz after 8hr of interaction time. As can be seen from the figure, almost similar spectra can be seen for the CRMA in comparison with neat asphalt. This indicates that at such combination of high interaction speed (50Hz) and temperature (220°C), the governing mechanisms are the devulcanization and depolymerization leading to the annihilation of the CRM modification effects [20, 24].

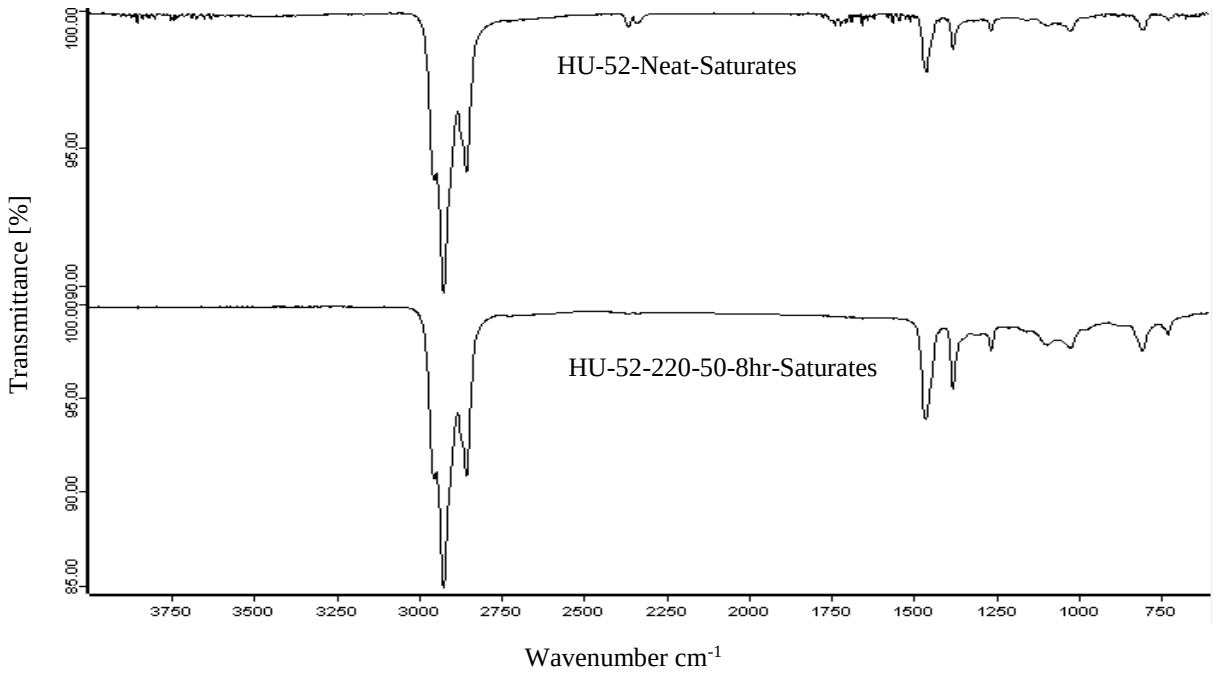

Figure 6.22. FTIR spectra comparison for CRM as compared to the saturates of neat and samples interacted at 220°C with 50Hz after 8hr of interaction time.

Figure 6.23 illustrates the FTIR spectra comparison for CRM as compared to the naphthene aromatics of neat and samples interacted at 220°C with 50Hz after 8hr of interaction time for the HU-52 asphalt. As can be seen from the figure, almost similar spectra can be seen for the CRMA in comparison with neat asphalt. This indicates that at such combination of high interaction speed (50Hz) and temperature (220°C), the governing mechanisms are the devulcanization and depolymerization leading to the annihilation of the CRM modification effects [20, 24].

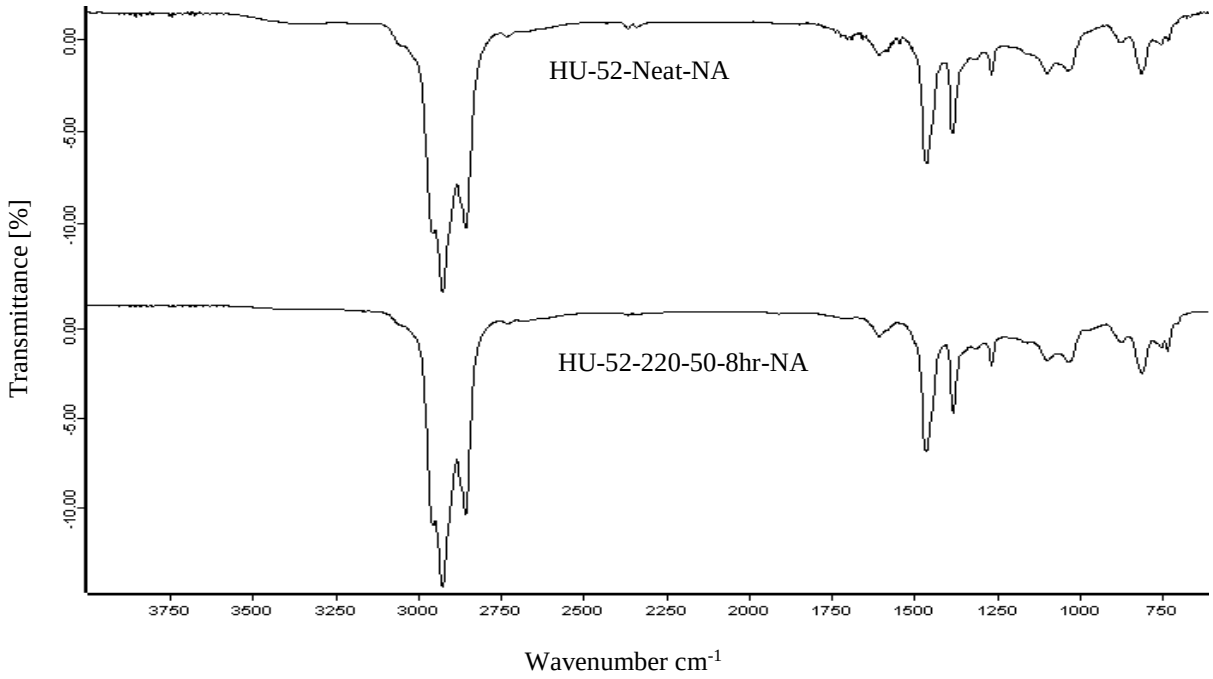

Figure 6.23. FTIR spectra comparison for CRM as compared to the naphthene aromatics of neat and samples interacted at 220°C with 50Hz after 8hr of interaction time.

Figure 6.24 illustrates the FTIR spectra comparison for CRM as compared to the polar aromatics of neat and samples interacted at 220C with 50Hz after 8hr of interaction time for the HU-52 asphalt.

As can be seen from the figure, almost similar spectra can be seen for the CRMA in comparison with neat asphalt. This indicates that the observed 80% of polar aromatics for the same sample that had thermal combustion behavior as that of synthetic rubber are mainly polar aromatics components with altered thermal behavior structure rather than being actually synthetic rubber.

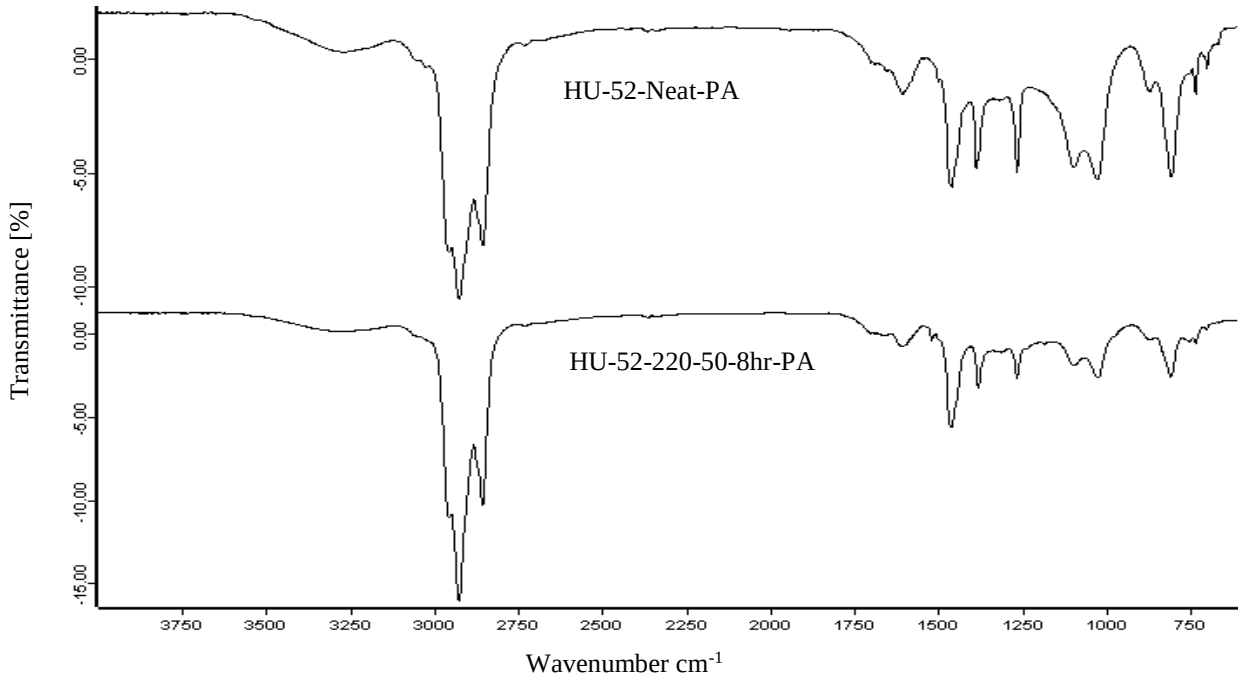

Figure 6.24. FTIR spectra comparison for CRM as compared to the polar aromatics of neat and samples interacted at 220°C with 50Hz after 8hr of interaction time.

AFM Investigation

In the current work phase detection atomic force microscopy (PDM) was utilized for the investigation of the morphology of CRMA liquid phase after interaction with CRM. Being an intermittent contact AFM method[110], PDM thus alleviates problems associated with tip pollution by soft and adhesive bitumen, which leads to the dragging of material on its surface [111]. Image is thus produced by recording the difference between the oscillation signal sent to the instrument cantilever and its actual oscillation as it is affected by tip sample interactions [112]. PDM can thus effectively map domains with various rheological properties [113, 114].

Figure 6.25 (a and b) illustrates the PDM images for the HU-52-Neat samples at 100X100µm and 20X20µm scan area, respectively. As explained in the literature, when observing the asphalt microstructure by utilizing PDM we should consider the fact that such microstructure is governed by the aggregation of fused aromatic rings into domains of various sizes and shapes [127].

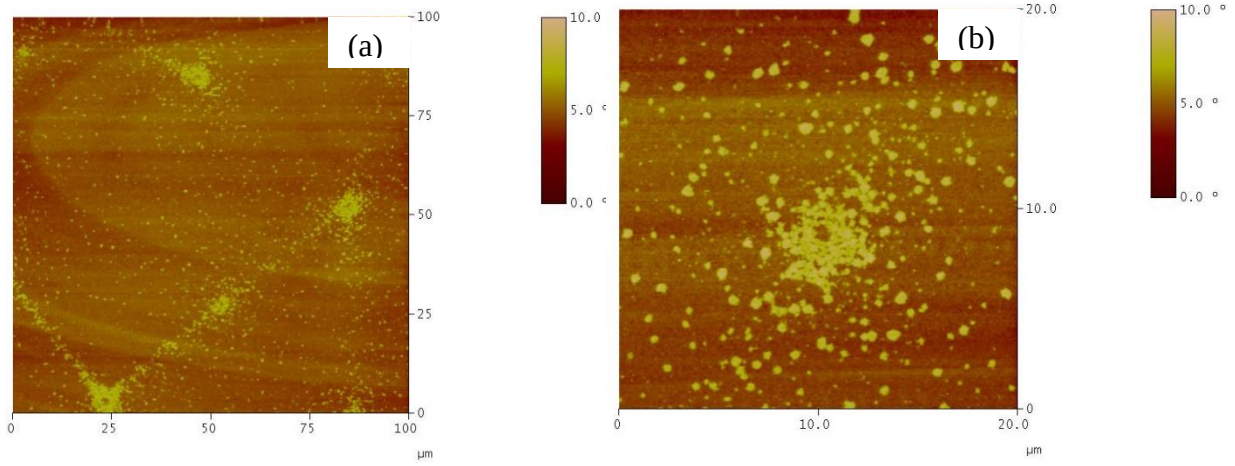

Figure 6.25. PDM images for the HU-52-Neat samples at; a) 100X100 and b) 20X20µm scan area.

In addition, other contributing factors can be the extent of functional groups in addition to other factors that are influential besides the average ring structure in determining bitumen stiffness [127]. Relating that to the morphology observed for the HU-52-Neat samples illustrated in Figure 6.25, it can be deduced that the neat asphalt is composed of two main passes, a matrix and dispersoids. However, the exact nature and type of such phases is out of the scope of this research work. In our study of the morphology of CRMA, we will investigate the change in morphology from that of the neat sample.

Figure 6.26-illustrates the PDM images for the HU-52 interacted at 190°C and 50 Hz after; (a)1, (b)2, (c)4, and (d)8hr of interaction time utilizing 100X100µm scan area.

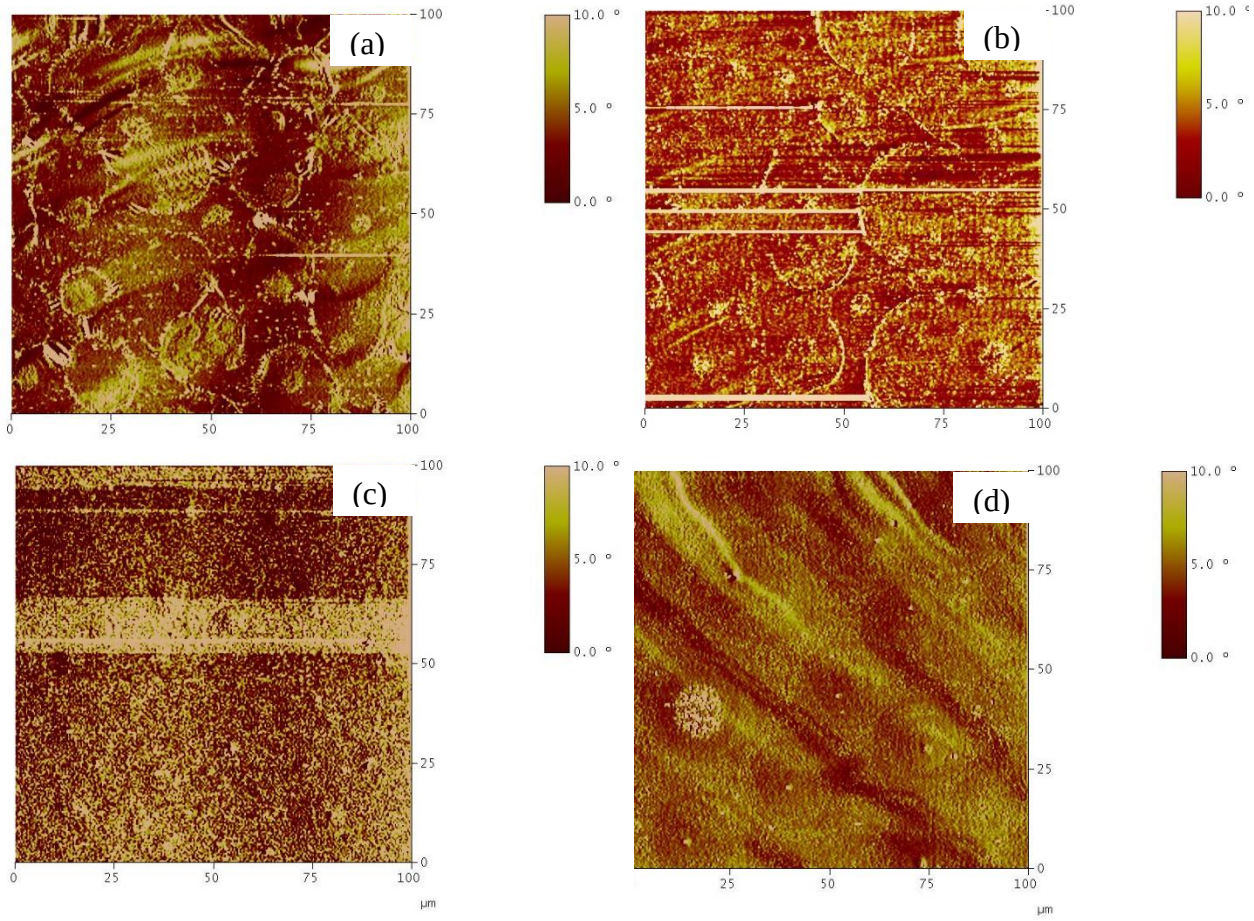

Figure 6.26. PDM images for the HU-52-interacted at 190°C and 50Hz after; a) 1 and b) 2, c) 4, and d) 8 hr interaction time utilizing a scan area of 100X100µm.

As can be seen from Figure 6.26(a), circular domains (agglomerations) with scattered dispersoids can be seen after 1 hr of interaction time. However, the trend of agglomeration can still be related to that of the neat asphalt sample.

Figure 6.26(b) elaborates that, after 2hr of interaction time, the dispersoids are disintegrating with the scattered circular domains still prevalent.

Figure 6.26(c) illustrates a well distributed finer dispersoids with very small agglomerates present after 4 hr of interaction time.

Figure 6.26(d) shows a much finer scattered phase within a second phase matrix, taking a linear (lamellar) overall distribution.

Figure 6.27 illustrates the PDM images for the HU-52 interacted at 190°C and 50 Hz after; (a)1, (b)2, (c)4, and (d)8hr of interaction time utilizing 20X20µm scan area.

As can be seen from Figure 6.27(a), the circular domains are clearly seen and it can be inferred that they encapsulate the original dispersoids phase found in the neat sample. This indicates that after 1hr of interaction time, the original asphalt components and buildup still maintain the structure of asphalt.

Figure 6.27(b) elaborate the dissolution of the dispersoids agglomerations and their substitution with finer more organized phase. This indicates that after 2hr of interaction time, the exchange of components between asphalt and CRM is taking place and starting to affect the asphalt buildup structure.

Figure 6.27(c) shows more abundant distributed dispersoids without apparent agglomeration. One important observation is that the morphology of the CRMA sample in this stage resembles that of polymer modified asphalt ones with low percentage of polymer modifier[128-130].

Figure 6.27(d) shows a much more organized phase in the matrix having a fine lamellar like structure. Such lamellar structure have been found to resemble the formation of network in asphalts [131]. This indicates that the formation of network in CRMA is a gradual process that starts with the dissolution of the asphalt original phase domains and continues through the interaction of asphalt with CRM and components exchange that results in the formation of the network structure eventually [131].

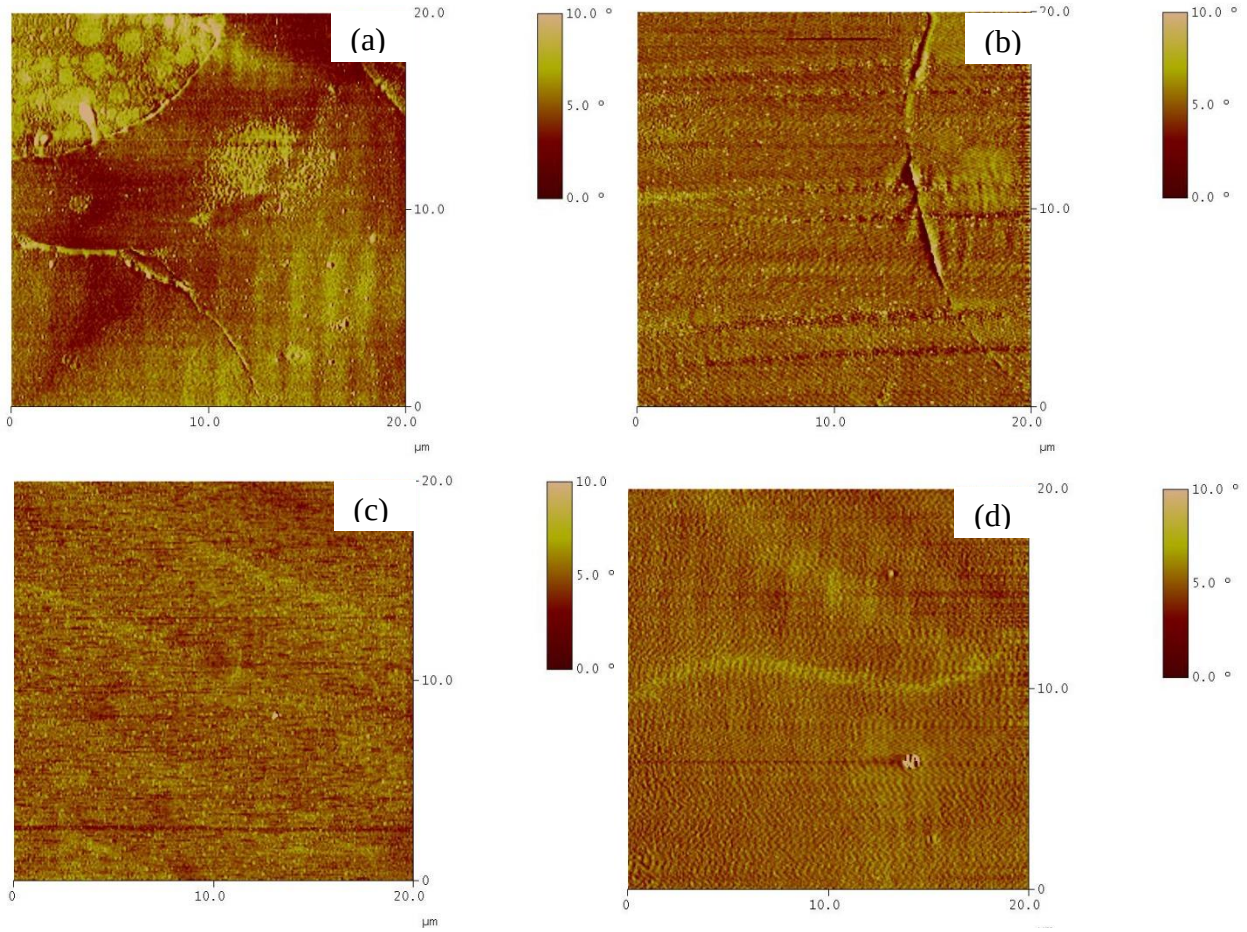

Figure 6.27. PDM images for the HU-52-interacted at 190°C and 50Hz after; a) 1 and b) 2, c) 4, and d) 8 hr interaction time utilizing a scan area of 20X20μm.

Figure 6.28 (a and b) illustrates the PDM images for the HU-64-Neat samples at 100X100 and 20Xarea20µm scan area, respectively. As can be seen from Figure 6.28 (a and b), HU-64-Neat asphalt is composed of evenly dispersed dispersoids that are of about 0.5 to 1 µm in size in a matrix on another phase. As explained earlier, the exact nature and type of such phases is out of the scope of this research work. In our study of the morphology of CRMA, we will investigate the change in morphology from that of the neat sample.

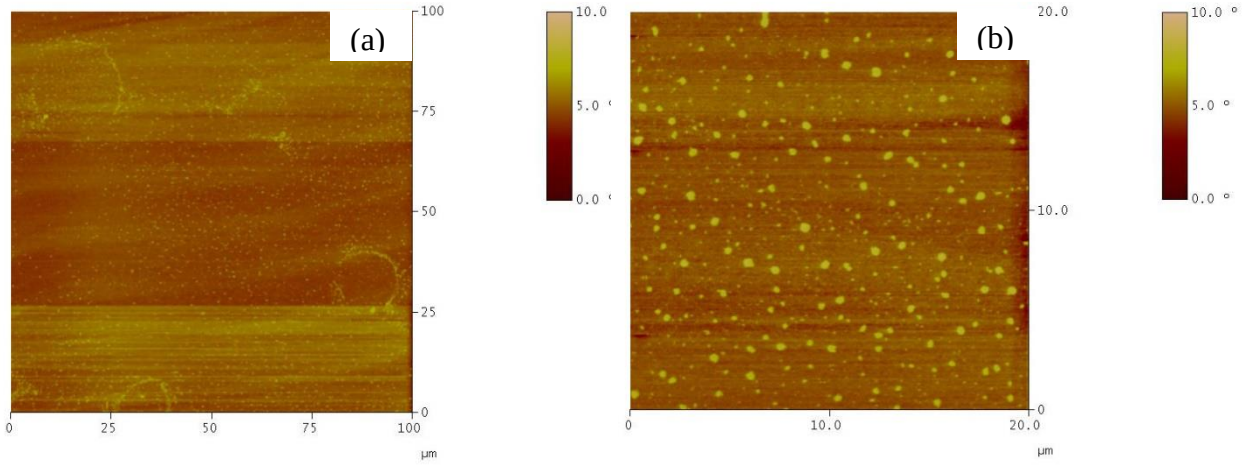

Figure 6.28. PDM images for the HU-64-Neat samples at; a) 100X100 and b) 20X20µm scan area.

Figure 6.29 illustrates the PDM images for the HU-64 interacted at 190°C and 50 Hz after; (a)1, (b)2, (c)4, and (d)8hr of interaction time utilizing 100X100µm scan area. As can be seen from Figure 6.29(a), circular clusters with surrounding scattered dispersoids can be seen after 1 hr of interaction time. However, unlike the case of HU-52, the trend of agglomeration can't be related to that of the neat asphalt sample as the HU-64 asphalts had no apparent phase agglomerations.

Figure 6.29(b) elaborates that, after 2hr of interaction time, the clusters are still present unlike what was occurring with the HU-52 asphalt at same interaction conditions.

Figure 6.29(c) illustrates a well distributed finer coarser dispersoids with same clusters present after 4 hr of interaction time.

Figure 6.29(d) shows a buildup of phase clusters around the original ones, indicating that the exchanged components from CRM took part in the formation of the network structure.

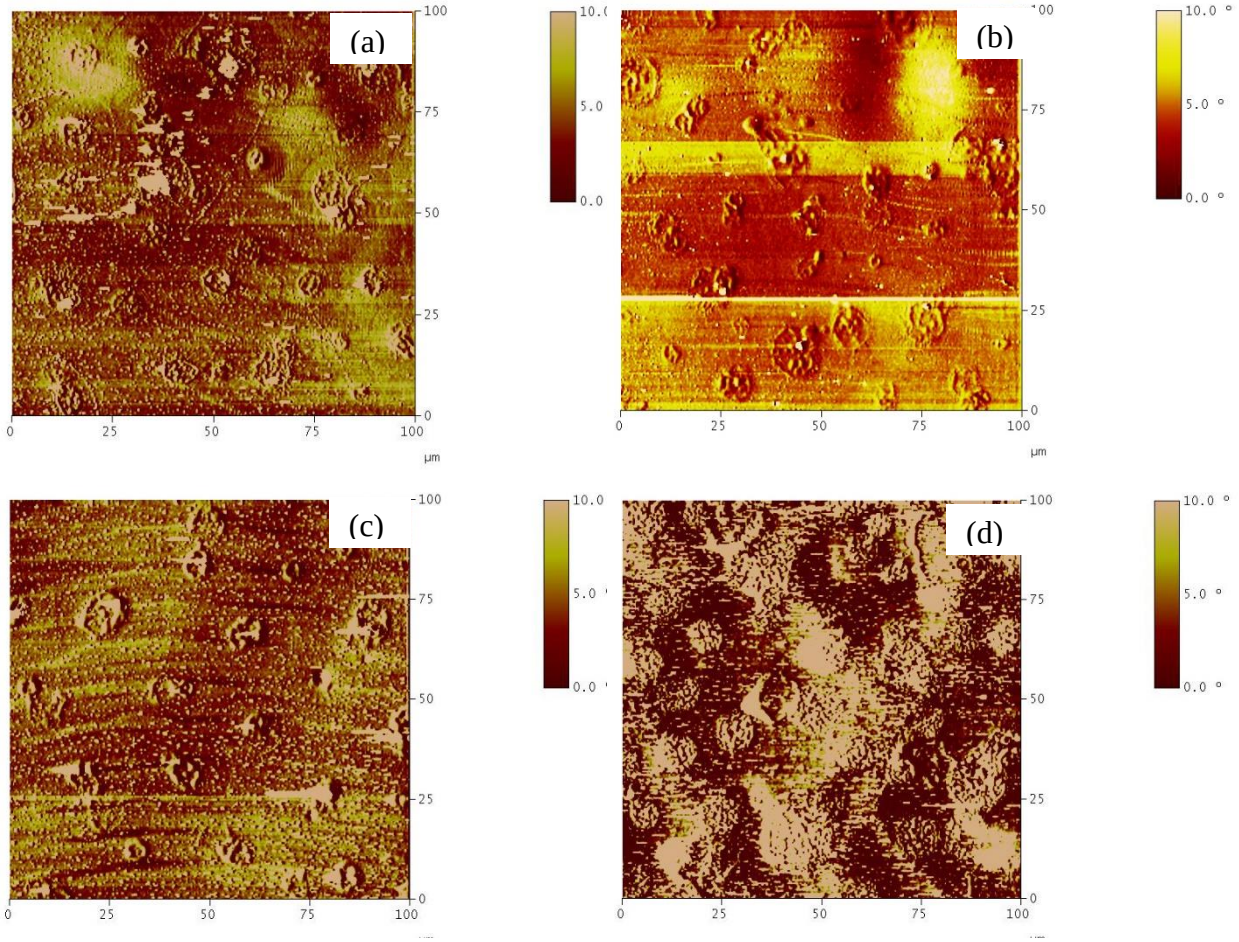

Figure 6.29. PDM images for the HU-52-interacted at 190°C and 50Hz after; a) 1 and b) 2, c) 4, and d) 8 hr interaction time utilizing a scan area of 100X100µm.

Figure 6.30 illustrates the PDM images for the HU-64 interacted at 190°C and 50 Hz after; (a)1, (b)2, (c)4, and (d)8hr of interaction time utilizing 20X20µm scan area.

As can be seen from Figure 6.30(a), well dispersed particulates are evenly distributed among the matrix. However, it should be noticed that such image is probably focusing on an area lacking the clusters illustrated in Figure 6.29(a).This indicates that although both the HU-52 and HU-64 showed evidence for the network formation, however the mechanism of the network formation is different among the different asphalt types (PG- grade).

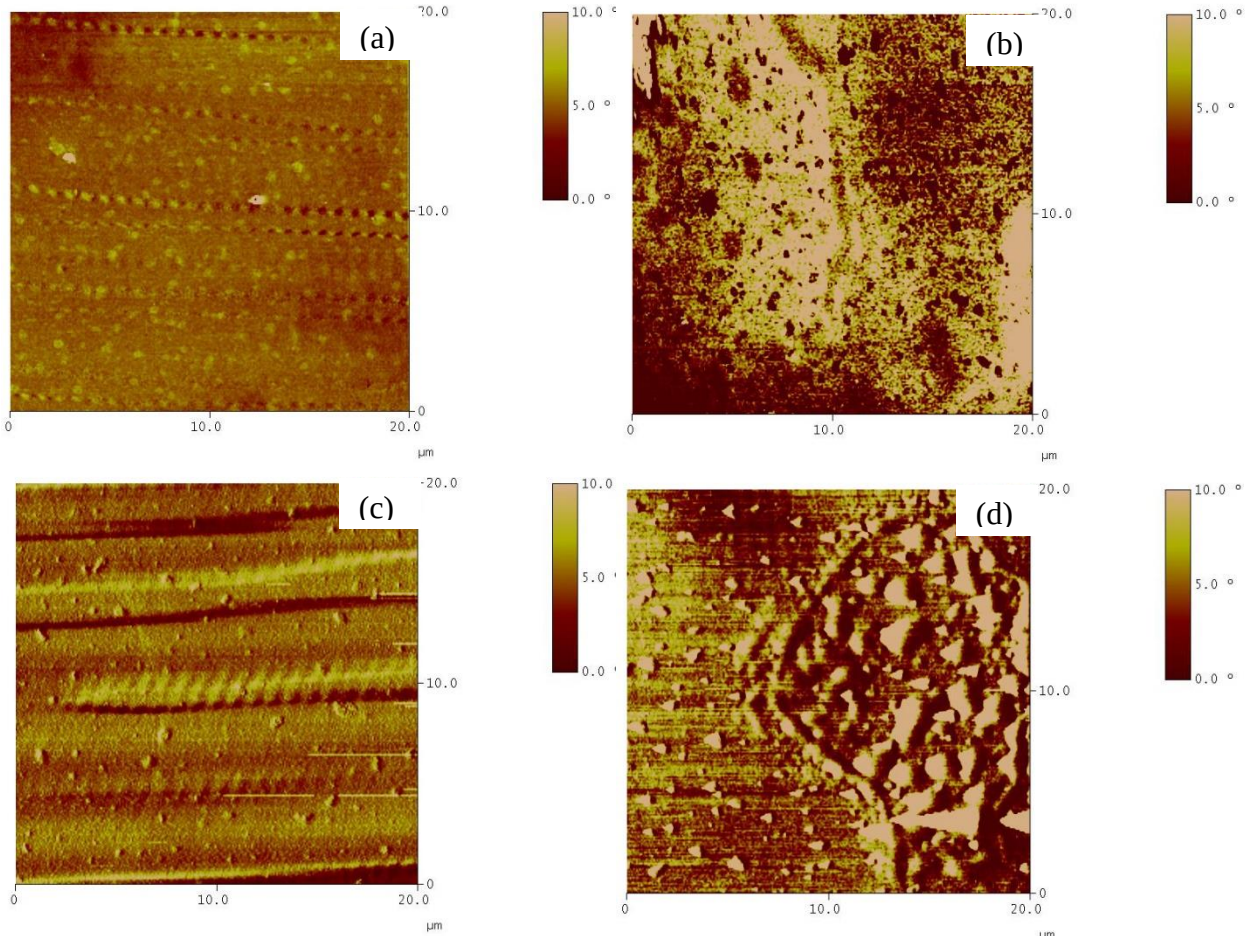

Figure 6.30. PDM images for the HU-52-interacted at 190°C and 50Hz after; a) 1 and b) 2, c) 4, and d) 8 hr interaction time utilizing a scan area of 20X20µm.

Figure 6.30(b) elaborate a major change in morphology after 2hr of interaction time, where there exists areas of phases in which dispersoids of the other phase is present. This might give evidence to phase inversion, which is a known mechanism in polymer modified asphalts.

Figure 6.30(c) shows more abundant well distributed surface emerging dispersoids without apparent agglomeration. Again, an important observation is that the morphology of the CRMA sample in this stage resembles that of polymer modified asphalt ones with moderate percentage of polymer modifier [128-130].

Figure 6.30(d) shows a unique close-up to one of the clusters observed previously in the large scan area images. As can be seen from the image, there exists two different phase with variation in dispersoids size and altitude. Presence of polymer modifier has been known to produce rough surface for polymer modified asphalt. It is suggested that although both asphalts had network structures within, however the nature and morphology of such network varies based on the asphalt source.

GPC Analysis of the Asphalt and Asphalt Fractions

In this section GPC analysis was carried out on selected whole asphalt liquid phase samples as well as fractionated liquid phase samples to investigate the effect of the development of internal network structures on the molecular attributes of whole asphalts as well as the fractions of asphalts.

Figure 6.31(a, b, and c) illustrates the GPC chromatogram comparisons for the unfractioned liquid phase neat and CRMA interacted at 190°C, 50Hz after 8hr interaction time for asphalts; HU-52, NF-58, and HU-64, respectively. As can be seen from the figure, for all the asphalt types investigated, a distinctive peak in the range between 9-11 min elution times can be seen. Those peaks had an Mw that ranges from 22,000-24,000 g/(avg mol weight). As those samples were the ones that developed the network structures in their liquid phase, it is believed that such peaks are attributed to the released polymeric components from CRM.

To better investigate the exact changes in the molecular attributes of the CRMA, investigation of the change in the weight average molecular weight (Mw) and Polydispersity index (PDI) are carried out hereafter.

Figure 6.32(a, b, and c) illustrates the change in the weight average molecular weight and polydispersity for the unfractioned liquid phase neat as compared to CRMA interacted at 190°C, 50Hz after 8hr interaction time for asphalts; HU-52, NF-58, and HU-64, respectively. As can be seen for Figure 6.32(a) for the HU-52 asphalts, the PDI for the neat asphalt was 4.4, while the Mw was 4127 g/(avg mol weight). On the other hand, the PDI for the CRMA interacted at 190°C, 50Hz after 8hr interaction time was 8.3, while the Mw was 9646 g/(avg mol weight). This indicates that the development of the network structure in the HU-52 asphalts was associated with almost doubling the PDI and Mw indicating the migration of molecules from CRM to the liquid phase of the asphalt as well as formation of associations between such molecules and those of the asphalt.

On the other hand, for Figure 6.32(b) for the NF-58 asphalts, the PDI for the neat asphalt was 3.5, while the Mw was 3632 g/(avg mol weight). The PDI for the CRMA interacted at 190°C, 50Hz after 8hr interaction time was 7.6, while the Mw was 10539 g/(avg mol weight). This indicates that the development of the network structure in the NF-58 asphalts was associated with almost doubling the PDI and tripling the Mw indicating the migration of molecules from CRM to the liquid phase of the asphalt as well as formation of associations between such molecules and those of the asphalt.

Figure 6.32(c) indicates similar trend for HU-64 asphalts where the PDI for the neat asphalt was 5.7, while the Mw was 6175 g/(avg mol weight). The PDI for the CRMA interacted at 190°C, 50Hz after 8hr interaction time was 6.4, while the Mw was 8971 g/(avg mol weight).

This indicates that the development of the network structure in the HU-64 asphalts was associated with minor increase in the PDI as well as the Mw indicating lesser migration of molecules from CRM to the liquid phase of the asphalt as well as lesser formation of associations between such molecules and those of the asphalt as compared to the softer asphalts HU-52 and NF-52.

To better address the change of the molecular attributes of asphalt as a result of interaction with CRM, the investigation of the molecular attributes of the neat asphalt and CRMA fractions is carried.

Figure 6.33(a and b) illustrates the GPC chromatogram comparisons for the asphaltenes and saturates fractions of HU-52 neat and CRMA interacted at 50Hz at different temperatures after 8hr interaction time, respectively.

As can be seen from Figure 6.33(a), the samples interacted at 160°C, 50Hz and 8hr interaction times showed almost similar GPC chromatogram as that of the neat asphaltenes. On the other hand, a shift to the lift of the chromatogram is seen for the samples interacted at 190 and 220°C with 50Hz after 8hr interaction time. The shift in the chromatogram to the left indicates increase in the molecular size distribution.

Figure 6.33(b) shows the same trend of similarity between the samples interacted at 160°C, 50Hz and 8hr interaction times and the neat ones is observed. In addition, samples interacted at 190 and 220°C with 50Hz after 8hr interaction time had a shift to the lift of the chromatogram indicating increase in the molecular size distribution.

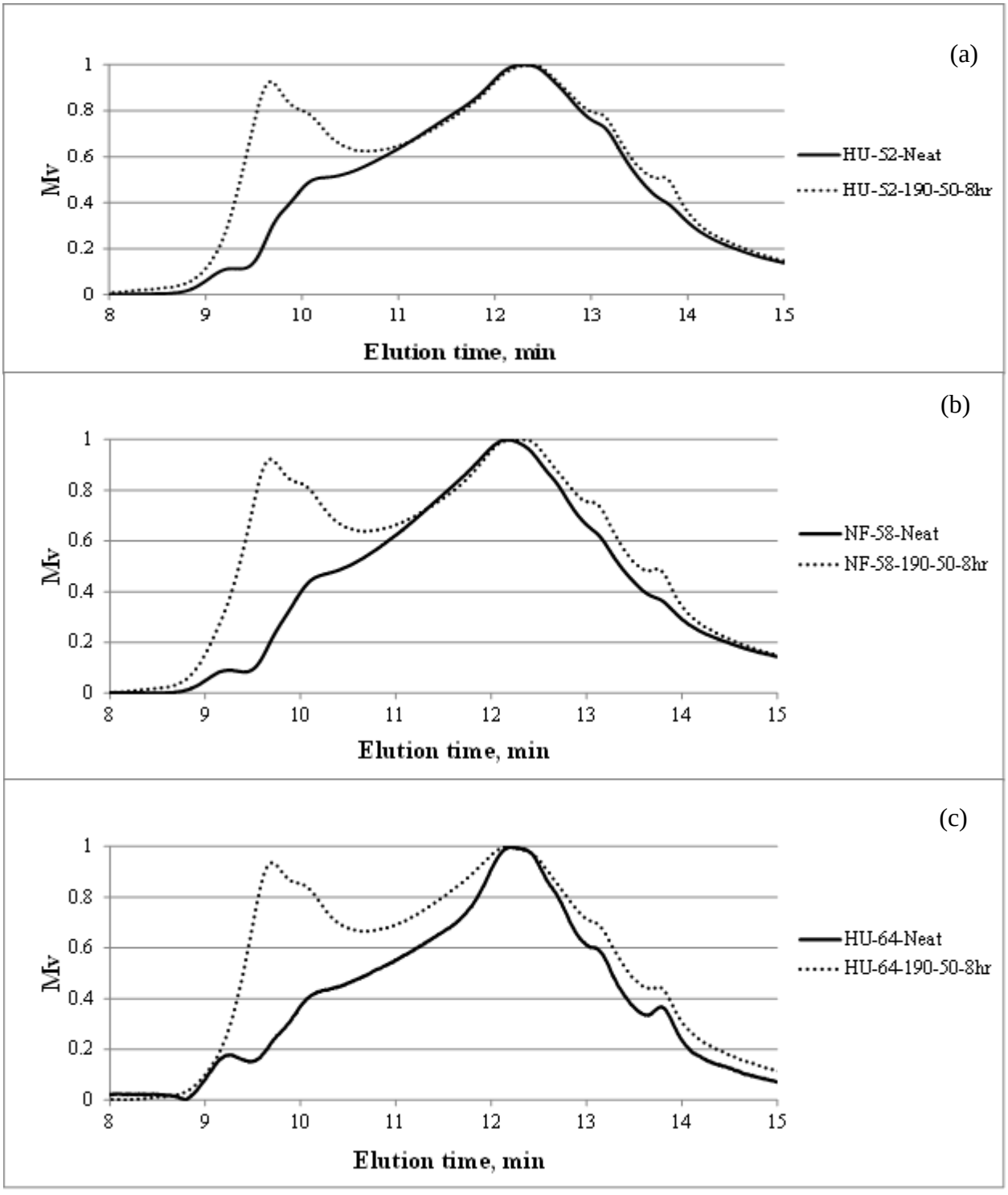

Figure 6.31. GPC chromatogram comparisons for the unfractioned liquid phase neat and CRMA interacted at 190°C, 50Hz after 8hr interaction time for asphalts; a)HU-52, b) NF-58, and c) HU-64.

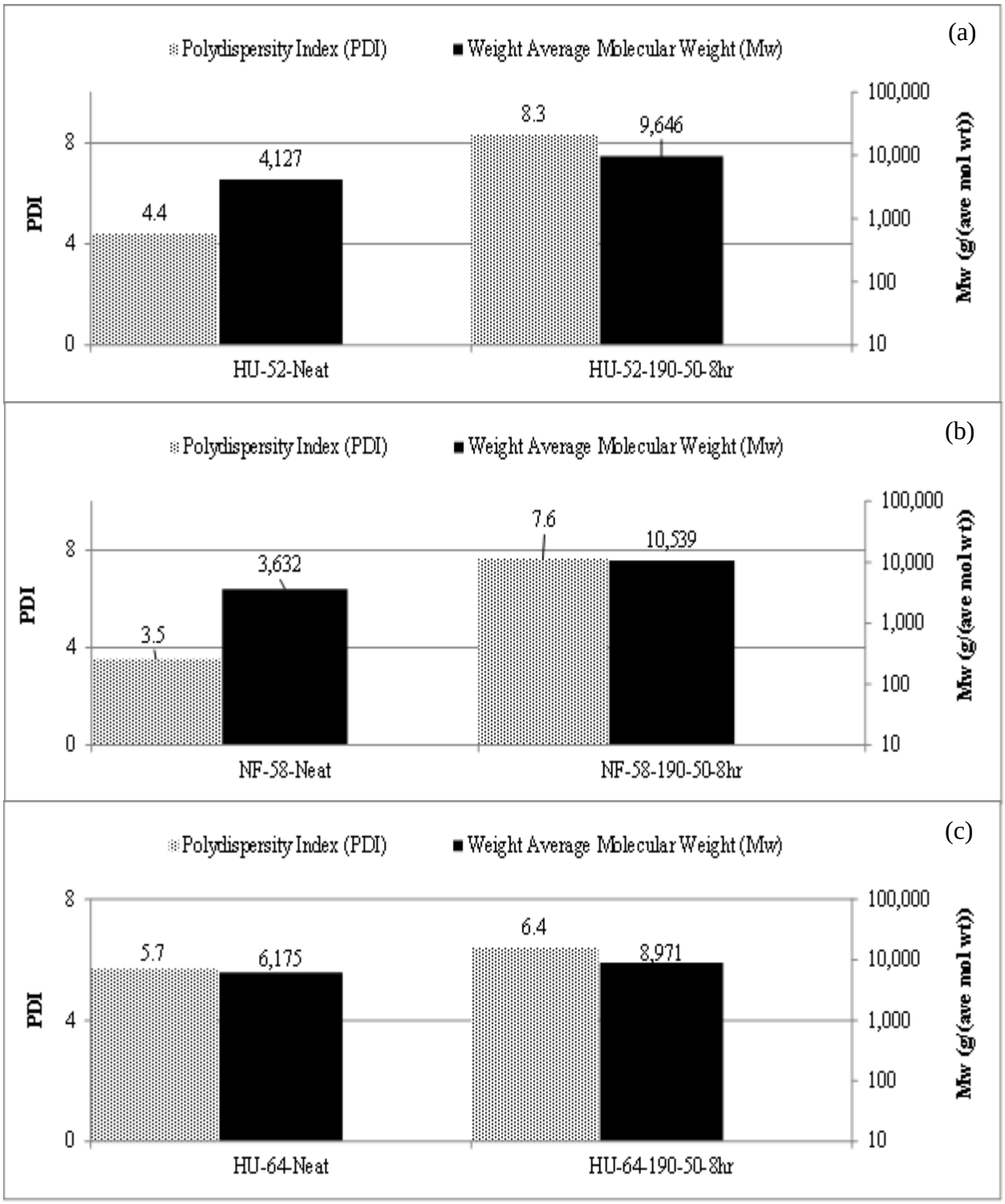

Figure 6.32. Weight average molecular weight and polydispersity comparison for the un-fractioned liquid phase neat and CRMA interacted at 190°C, 50Hz after 8hr interaction time for asphalts; a)HU-52, b) NF-58, and c) HU-64.

Figure 6. 34(a and b) illustrates the GPC chromatogram comparisons for the NA and PA fractions of HU-52 neat and CRMA interacted at 50Hz at different temperatures after 8hr interaction time, respectively.

As can be seen from Figure 6.34(a), almost similar chromatogram can be seen for the interacted samples as compared to the neat ones. This indicates minor change in the molecular size distribution for the NA fractions.

Figure 6.34(b) shows a different trend, where the PA fractions of the samples interacted at either 190 or 220°C with 50Hz after 8hr interaction time showed a shift to the left of the chromatogram indicating an increase in the molecular size distribution. On the other hand, the GPC chromatogram of the samples interacted at 160°C and 50Hz after 8hr interaction time showed similarity to the neat asphalt ones indicating minor change in the molecular size distribution.

To better investigate the exact changes in the molecular attributes of the CRMA, investigation of the change in the weight average molecular weight (Mw) and Polydispersity index (PDI) are carried out hereafter.

Figure 6.35(a, b, c, and d) illustrates the weight average molecular weight (Mw) and polydispersity(PDI) comparison for the asphaltenes, saturates, NA, and PA of HU-52 neat and CRMA interacted at 50Hz at different temperatures after 8hr interaction time, respectively.

As can be seen for Figure 6.35(a) for the asphaltenes fraction, the PDI for the neat asphalt was 4.2, while the Mw was 11973 g/(avg mol weight). On the other hand, the PDI for the CRMA interacted at 160°C, 50Hz after 8hr interaction time was 4.3, while the Mw was 12979 g/(avg mol weight). This indicates that for such samples the change in the molecular attributes of the asphaltenes fractions were minor. On the other hand, the PDI for the CRMA interacted at 190°C,

50Hz after 8hr interaction time was 6.6, while the Mw was 18313 g/(avg mol weight). This indicates that the development of the network structure in the samples interacted at 190°C and 50Hz after 8hr interaction time was associated with an increase of about 50% of the PDI and Mw indicating the migration of molecules from CRM to the asphaltenes of such samples as well as formation of associations between such molecules and those of the asphaltenes.

On the other hand, the PDI for the CRMA interacted at 220°C, 50Hz after 8hr interaction time was 6.8, while the Mw was 16930 g/(avg mol weight). This indicates that for such samples although there exists a change in the molecular attributes of the asphaltenes fractions, however this was not reflected on the physical properties for such samples which suffered deteriorated micro and macro mechanical properties.

As can be seen for Figure 6.35(b) for the saturates fraction, the PDI for the neat asphalt was 4.6, while the Mw was 2982 g/(avg mol weight). On the other hand, the PDI for the CRMA interacted at 160°C, 50Hz after 8hr interaction time was 8.7, while the Mw was 5667 g/(avg mol weight). This indicates that for such samples although the change in the molecular attributes of the saturates fractions were almost doubled, yet this was not reflected on the physical properties of such samples who had minor improvement on the micro and macro mechanical properties. On the other hand, the PDI for the CRMA interacted at 190°C, 50Hz after 8hr interaction time was 9, while the Mw was 6039 g/(avg mol weight). This indicates that the development of the network structure in the samples interacted at 190°C and 50Hz after 8hr interaction time was associated with an increase of about 100% of the PDI and Mw indicating the migration of molecules from CRM to the saturates of such samples as well as formation of associations between such molecules and those of the saturates.

On the other hand, the PDI for the CRMA interacted at 220°C, 50Hz after 8hr interaction time was 3.9, while the Mw was 2198 g/(avg mol weight). This indicates that for such samples there exists a minor decrease in the molecular attributes of the saturates fractions. This was not reflected on the physical properties for such samples which suffered deteriorated micro and macro mechanical properties.

As can be seen for Figure 6.35(c) for the NA fraction, the PDI for the neat asphalt was 7.7, while the Mw was 6142 g/(avg mol weight). On the other hand, the PDI for the CRMA interacted at 160°C, 50Hz after 8hr interaction time was 6.8, while the Mw was 5050 g/(avg mol weight). This indicates that for such samples the change in the molecular attributes of the NA fractions was minor. This was reflected on the physical properties of such samples who had minor improvement on the micro and macro mechanical properties. On the other hand, the PDI for the CRMA interacted at 190°C, 50Hz after 8hr interaction time was 6.5, while the Mw was 5042 g/(avg mol weight). This indicates that the development of the network structure in the samples interacted at 190°C and 50Hz after 8hr interaction time was not associated with an increase of the PDI and Mw of the NA fractions indicating there was no migration of molecules from CRM to the NA of such samples.

On the other hand, the PDI for the CRMA interacted at 220°C, 50Hz after 8hr interaction time was 7.7, while the Mw was 5376 g/(avg mol weight). This indicates that for such samples there exists a minor decrease in the molecular attributes of the NA fractions. This was not reflected on the physical properties for such samples which suffered deteriorated micro and macro mechanical properties.

As can be seen for Figure 6.35(d) for the PA fractions, the PDI for the neat asphalt was 3.3, while the Mw was 4654 g/(avg mol weight). On the other hand, the PDI for the CRMA in-

teracted at 160°C, 50Hz after 8hr interaction time was 4.1, while the Mw was 5888 g/(avg mol weight). This indicates that for such samples the change in the molecular attributes of the PA fractions were minor. On the other hand, the PDI for the CRMA interacted at 190°C, 50Hz after 8hr interaction time was 4.1, while the Mw was 6392 g/(avg mol weight). This indicates that the development of the network structure in the samples interacted at 190°C and 50Hz after 8hr interaction time was associated with an increase of about 30% of the PDI and Mw indicating the migration of molecules from CRM to the PA of such samples as well as formation of associations between such molecules and those of the PA.

On the other hand, the PDI for the CRMA interacted at 220°C, 50Hz after 8hr interaction time was 8.4, while the Mw was 5453 g/(avg mol weight). This indicates that for such samples although there exists a change in the molecular attributes of the PA fractions, however this was not reflected on the physical properties for such samples which suffered deteriorated micro and macro mechanical properties.

Figure 6.36(a and b) illustrates the GPC chromatogram comparisons for the asphaltenes and saturates fractions of NF-58 neat and CRMA interacted at 190°C and 50Hz after 8hr interaction time, respectively. As can be seen from Figure 6.36(a), a shift to the lift of the chromatogram is seen for the CRMA asphaltenes samples. The shift in the chromatogram to the left indicates increase in the molecular size distribution.

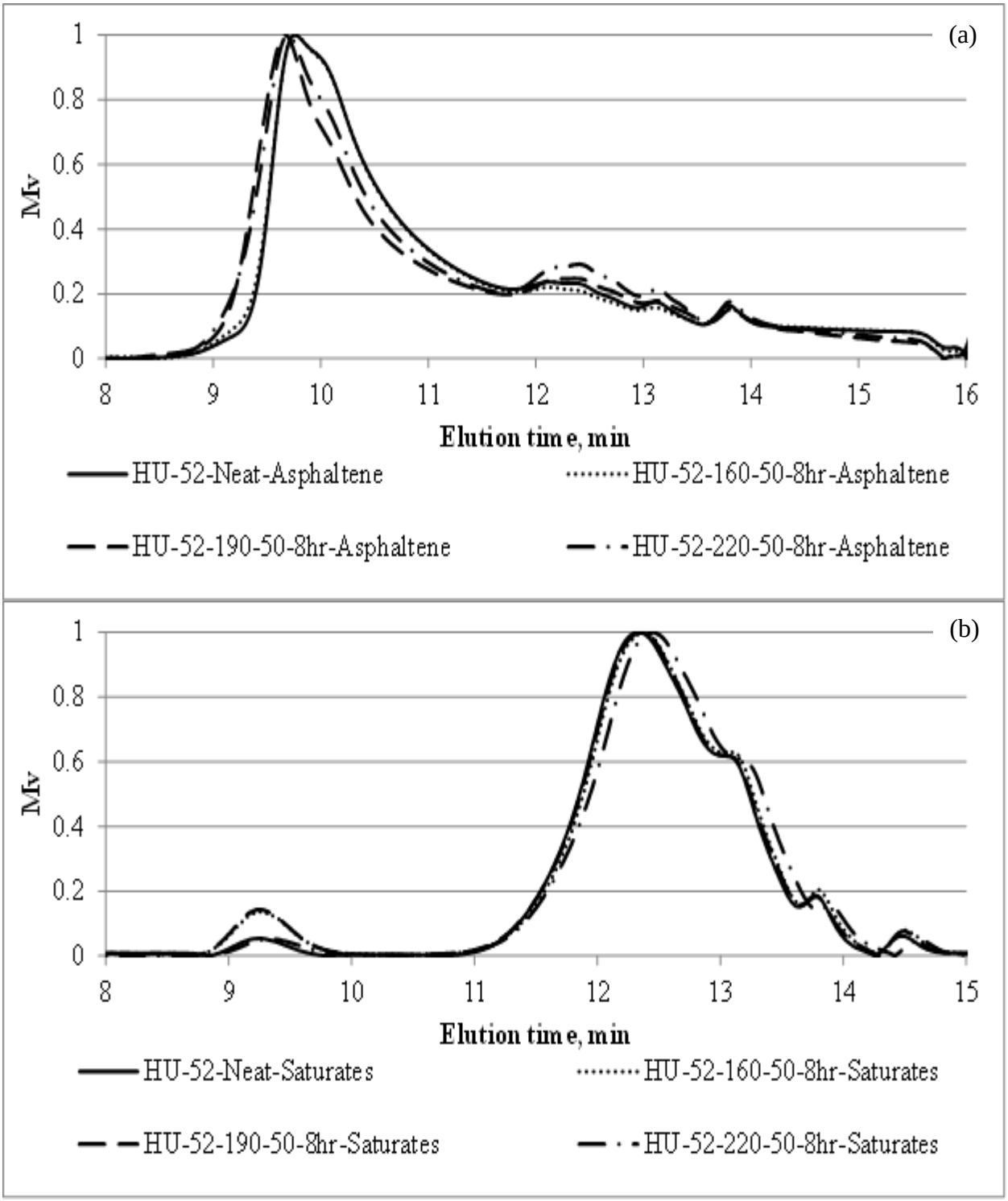

Figure 6.33. GPC chromatogram comparisons for the fractions of HU-52 neat and CRMA interacted at 50Hz at different temperatures after 8hr interaction time; a) Asphaltenes, b) Saturates.

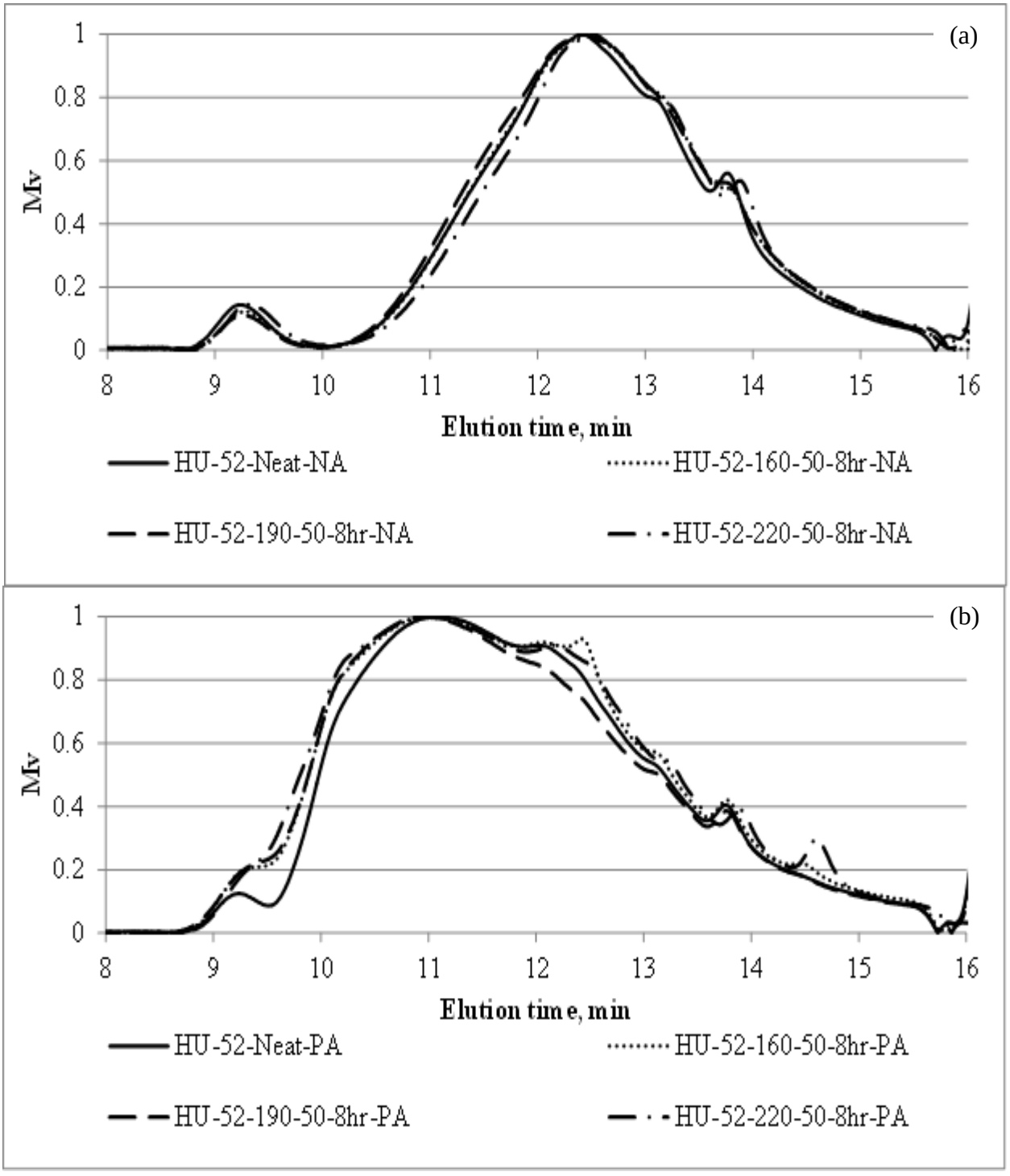

Figure 6.34. GPC chromatogram comparisons for the fractions of HU-52 neat and CRMA interacted at 50Hz at different temperatures after 8hr interaction time; a) NA, b) PA.

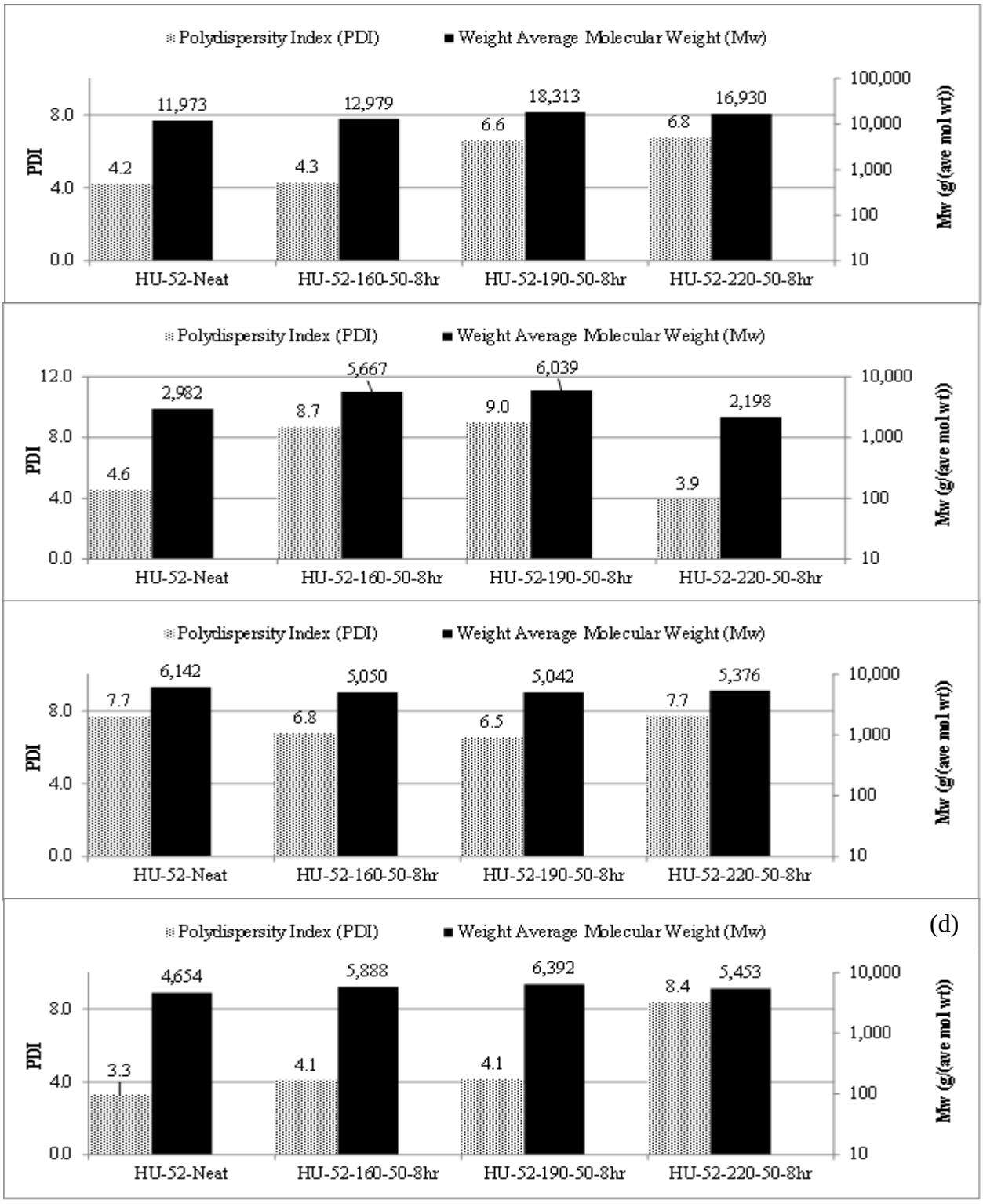

Figure 6.35. Weight average molecular weight and polydispersity comparison for the HU-52 neat and CRMA interacted at 50Hz at different temperatures after 8hr interaction time; a)Asphaltenes, b) Saturates, c) NA, and d) PA.

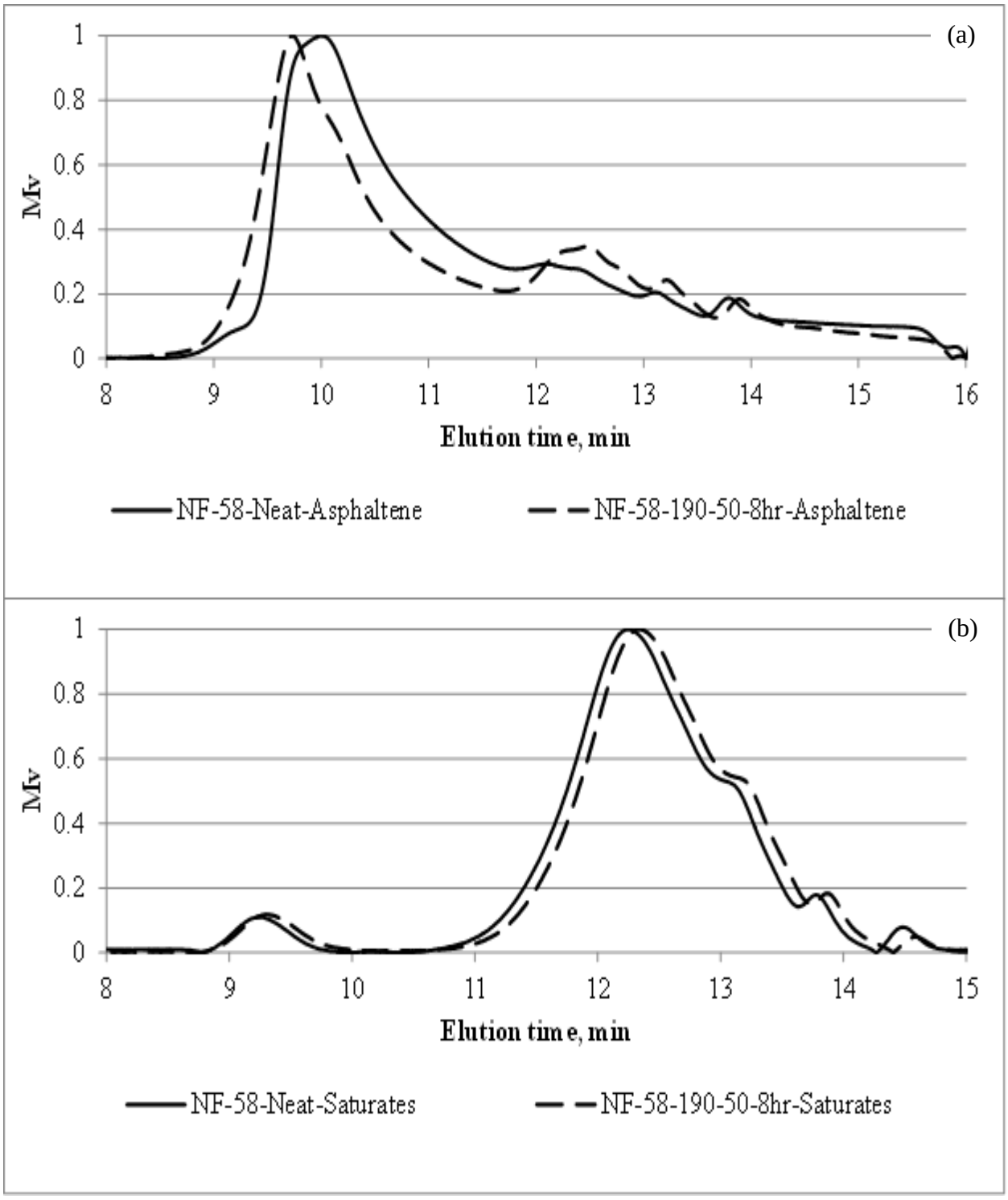

Figure 6.36. GPC chromatogram comparisons for the fractions of NF-58 neat and CRMA interacted at 50Hz at different temperatures after 8hr interaction time; a) Asphaltenes, b) Saturates.

As can be seen from Figure 6.36(b), almost similar chromatogram can be seen for the interacted samples as compared to the neat ones. This indicates minor change in the molecular size distribution for the saturates fractions.

Figure 6. 37(a and b) illustrates the GPC chromatogram comparisons for the NA and PA fractions of NF-58 neat and CRMA interacted at 50Hz and 190°C after 8hr interaction time, respectively.

As can be seen from Figure 6.37(a), almost similar chromatogram can be seen for the interacted samples as compared to the neat ones. This indicates minor change in the molecular size distribution for the NA fractions.

Figure 6.37(b) shows a different trend, where the PA fractions of the samples interacted at 190°C with 50Hz after 8hr interaction time showed a shift to the left of the chromatogram indicating an increase in the molecular size distribution.

To better investigate the exact changes in the molecular attributes of the CRMA, investigation of the change in the weight average molecular weight (Mw) and Polydispersity index (PDI) are carried out hereafter.

Figure 6.38(a, b, c, and d) illustrates the weight average molecular weight (Mw) and polydispersity(PDI) comparison for the asphaltenes, saturates, NA, and PA of NF-58 neat and CRMA interacted at 50Hz and 190°C after 8hr interaction time, respectively.

As can be seen for Figure 6.38(a) for the asphaltenes fraction, the PDI for the neat asphalt was 4.1, while the Mw was 10518 g/(avg mol weight). On the other hand, the PDI for the CRMA interacted at 190°C, 50Hz after 8hr interaction time was 7.6, while the Mw was 15888 g/(avg mol weight). This indicates that the development of the network structure in the samples interacted at 190°C and 50Hz after 8hr interaction time was associated with an increase of about 60%

of the PDI and Mw indicating the migration of molecules from CRM to the asphaltenes of such samples as well as formation of associations between such molecules and those of the asphaltenes.

As can be seen for Figure 6.38(b) for the saturates fraction, the PDI for the neat asphalt was 6.5, while the Mw was 4693 g/(avg mol weight). On the other hand, the PDI for the CRMA interacted at 190°C, 50Hz after 8hr interaction time was 6.9, while the Mw was 4438 g/(avg mol weight). This indicates that the development of the network structure in the samples interacted at 190°C and 50Hz after 8hr interaction time was not associated with any increase of the PDI and Mw indicating that there was no the migration of molecules from CRM to the saturates of such samples.

As can be seen for Figure 6.38(c) for the NA fraction, the PDI for the neat asphalt was 13.8, while the Mw was 11742 g/(avg mol weight). On the other hand, the PDI for the CRMA interacted at 190°C, 50Hz after 8hr interaction time was 16.3, while the Mw was 13009 g/(avg mol weight). This indicates that the development of the network structure in the samples interacted at 190°C and 50Hz after 8hr interaction time was associated with an increase of the PDI and Mw of the NA fractions indicating there was minor migration of molecules from CRM to the NA of such samples.

As can be seen for Figure 6.38(d) for the PA fractions, the PDI for the neat asphalt was 4.8, while the Mw was 6121 g/(avg mol weight). On the other hand, the PDI for the CRMA interacted at 190°C, 50Hz after 8hr interaction time was 4.2, while the Mw was 5686 g/(avg mol weight).

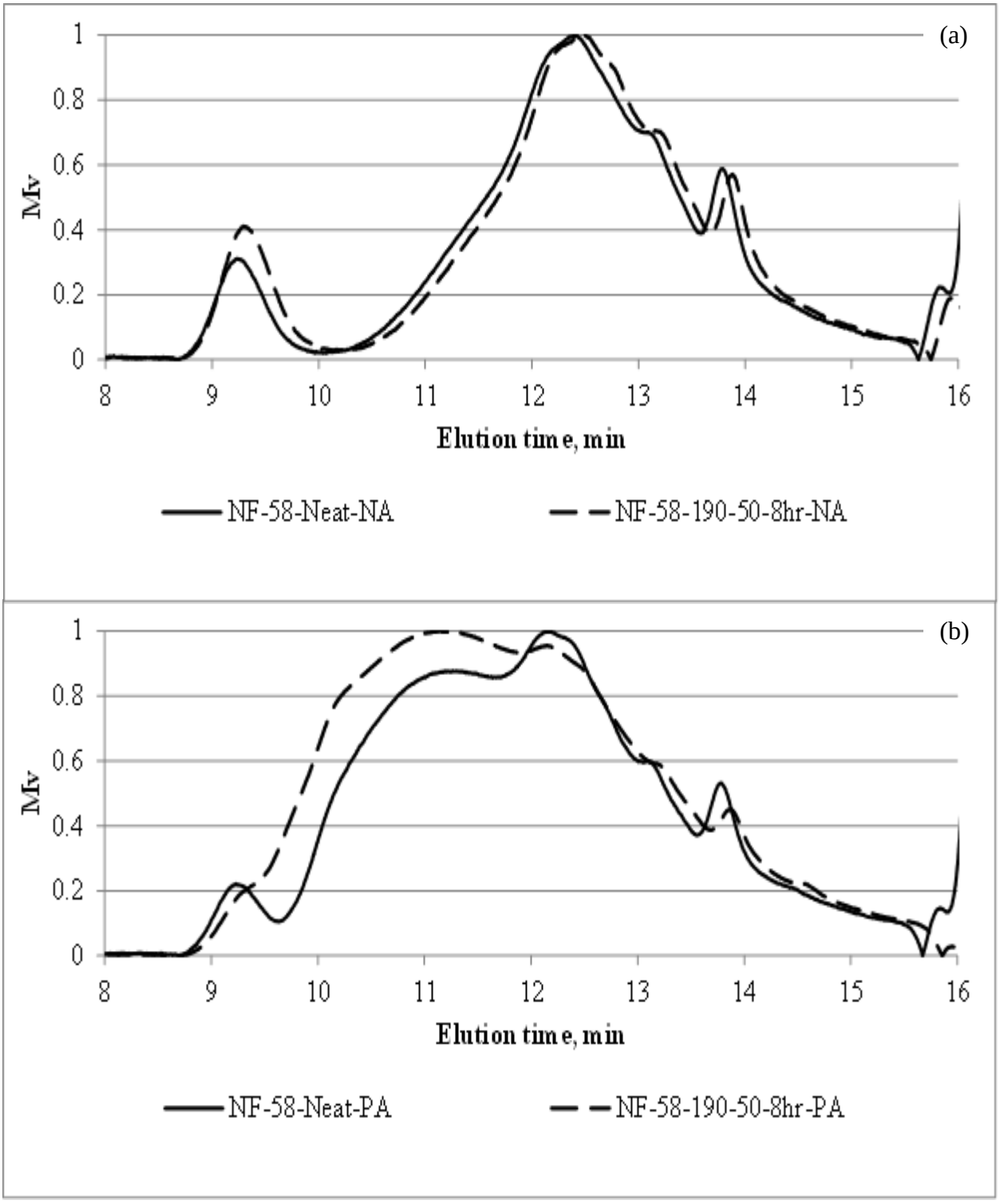

Figure 6.37. GPC chromatogram comparisons for the fractions of NF-58 neat and CRMA interacted at 50Hz at different temperatures after 8hr interaction time; a) NA, b) PA.

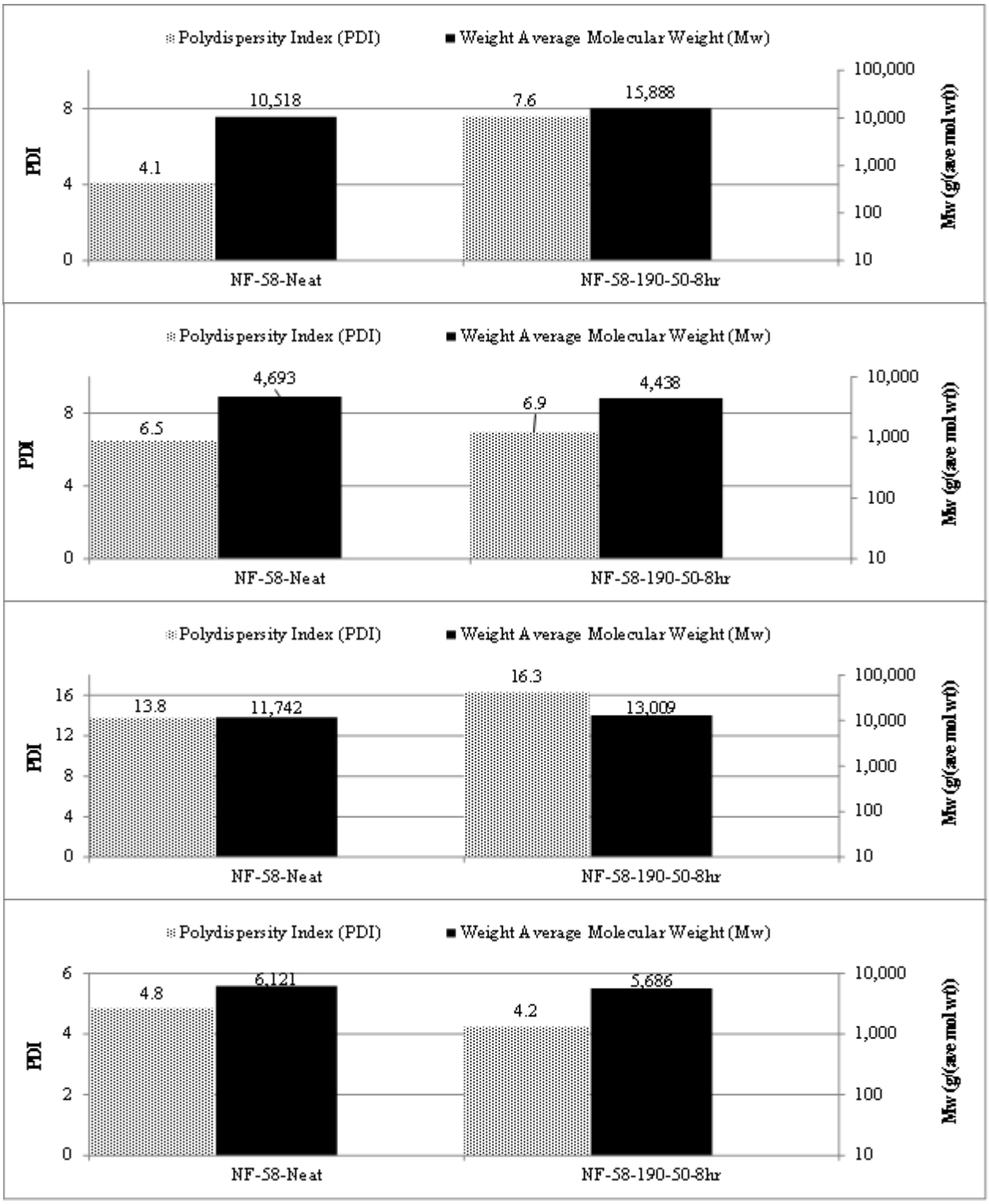

Figure 6.38. Weight average molecular weight and polydispersity comparison for the NF-58 neat and CRMA interacted at 50Hz at different temperatures after 8hr interaction time; a)Asphaltenes, b) Saturates, c) NA, and d) PA.

This indicates that the development of the network structure in the samples interacted at 190°C and 50Hz after 8hr interaction time was not associated with an increase of the PDI and Mw indicating the migration of molecules from CRM to the PA of such samples.

Figure 6.39(a and b) illustrates the GPC chromatogram comparisons for the asphaltenes and saturates fractions of HU-64 neat and CRMA interacted at 190°C and 50Hz after 8hr interaction time, respectively. As can be seen from Figure 6.39(a), a shift to the lift of the chromatogram is seen for the CRMA asphaltenes samples. The shift in the chromatogram to the left indicates increase in the molecular size distribution.

As can be seen from Figure 6.39(b), a decrease in the chromatogram can be seen for the interacted samples as compared to the neat ones. This indicates minor change in the molecular size distribution for the saturates fractions.

Figure 6. 40(a and b) illustrates the GPC chromatogram comparisons for the NA and PA fractions of HU-64 neat and CRMA interacted at 50Hz and 190°C after 8hr interaction time, respectively.

As can be seen from Figure 6.40(a), a minor decrease in the chromatogram can be seen for the interacted samples as compared to the neat ones. This indicates minor change in the molecular size distribution for the NA fractions.

Figure 6.40(b) shows a different trend, where the PA fractions of the samples interacted at 190°C with 50Hz after 8hr interaction time showed a shift to the left of the chromatogram indicating an increase in the molecular size distribution.

To better investigate the exact changes in the molecular attributes of the CRMA, investigation of the change in the weight average molecular weight (Mw) and Polydispersity index (PDI) are carried out hereafter.

Figure 6.41(a, b, c, and d) illustrates the weight average molecular weight (Mw) and polydispersity(PDI) comparison for the asphaltenes, saturates, NA, and PA of HU-64 neat and CRMA interacted at 50Hz and 190°C after 8hr interaction time, respectively.

As can be seen for Figure 6.41(a) for the asphaltenes fraction, the PDI for the neat asphalt was 5.9, while the Mw was 15434 g/(avg mol weight). On the other hand, the PDI for the CRMA interacted at 190°C, 50Hz after 8hr interaction time was 5.8, while the Mw was 13092 g/(avg mol weight). This indicates that the development of the network structure in the samples interacted at 190°C and 50Hz after 8hr interaction time was not associated with an increase of the PDI and Mw but rather a decrease indicating that there might be migration of molecules from the asphaltenes to the CRM of such samples.

As can be seen for Figure 6.41(b) for the saturates fraction, the PDI for the neat asphalt was 11.7, while the Mw was 8717 g/(avg mol weight). On the other hand, the PDI for the CRMA interacted at 190°C, 50Hz after 8hr interaction time was 7.5, while the Mw was 4753 g/(avg mol weight). This indicates that the development of the network structure in the samples interacted at 190°C and 50Hz after 8hr interaction time was not associated with any increase of the PDI and Mw but rather a decrease indicating that there might have occurred a migration of molecules from saturates to the CRM of such samples.

As can be seen for Figure 6.41(c) for the NA fraction, the PDI for the neat asphalt was 20.8, while the Mw was 18833 g/(avg mol weight). On the other hand, the PDI for the CRMA interacted at 190°C, 50Hz after 8hr interaction time was 4.8, while the Mw was 3406 g/(avg mol weight). This indicates that the development of the network structure in the samples interacted at 190°C and 50Hz after 8hr interaction time was associated with a major decreaseof the PDI and

Mw of the NA fractions indicating there was major migration of molecules from NA to the CRM of such samples.

As can be seen for Figure 6.41(d) for the PA fractions, the PDI for the neat asphalt was 4.2, while the Mw was 5456 g/(avg mol weight). On the other hand, the PDI for the CRMA interacted at 190°C, 50Hz after 8hr interaction time was 8.8, while the Mw was 5686 g/(avg mol weight).

This indicates that the development of the network structure in the samples interacted at 190°C and 50Hz after 8hr interaction time was not associated with an increase of the PDI and Mw indicating the migration of molecules from CRM to the PA of such samples.

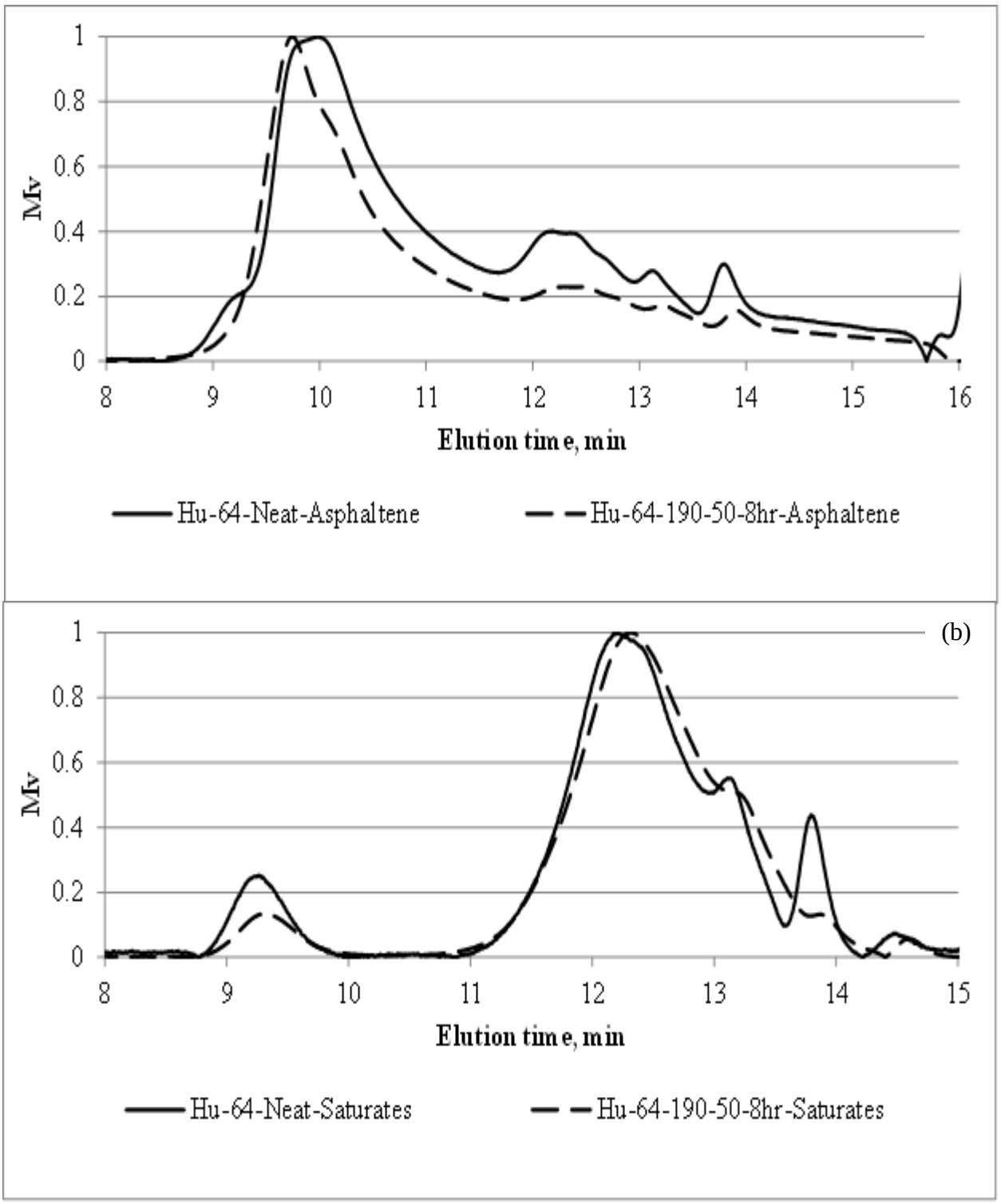

Figure 6.39. GPC chromatogram comparisons for the fractions of HU-64 neat and CRMA interacted at 50Hz at different temperatures after 8hr interaction time; a) Asphaltenes, b) Saturates.

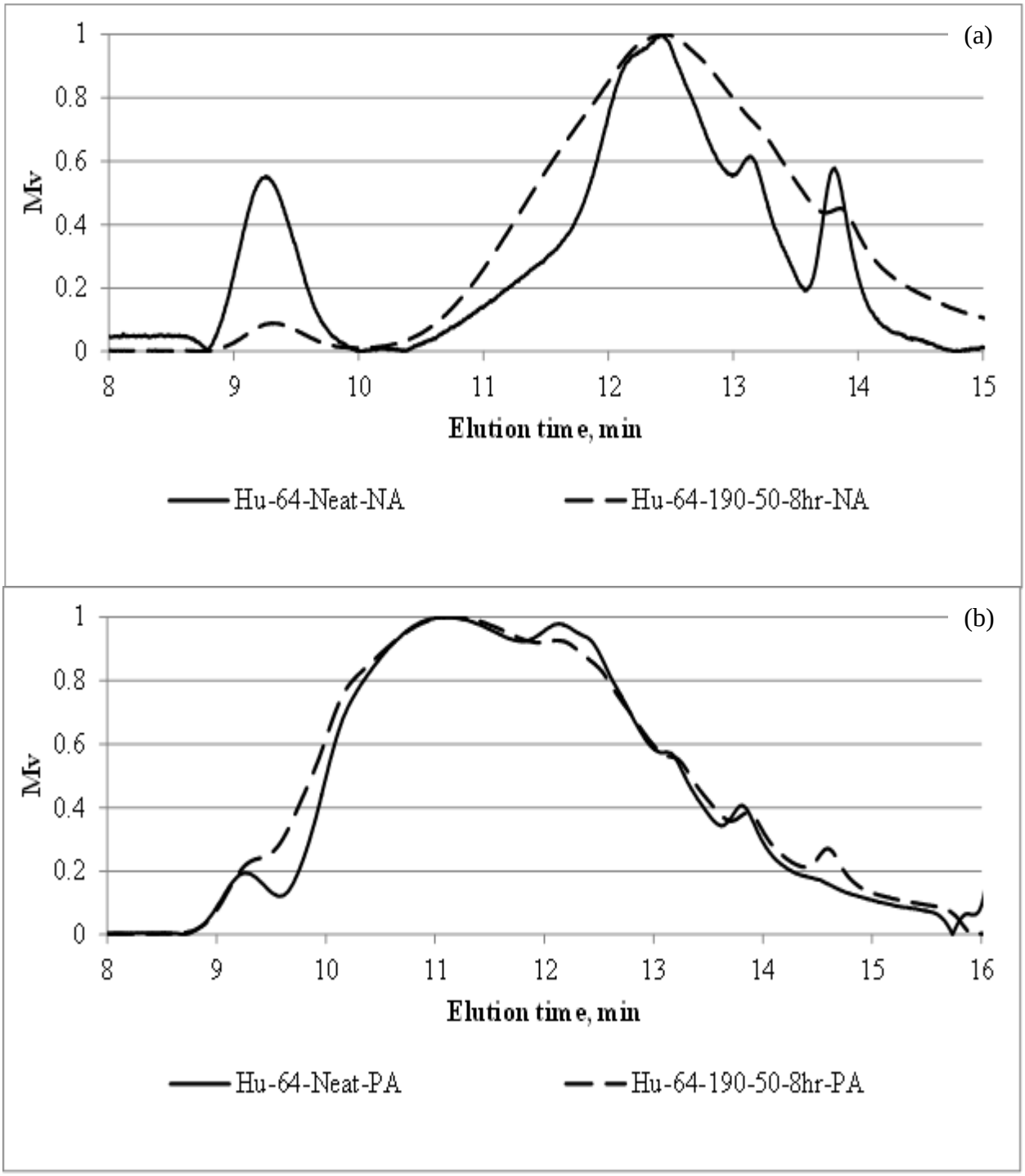

Figure 6.40. GPC chromatogram comparisons for the fractions of HU-64 neat and CRMA interacted at 50Hz at different temperatures after 8hr interaction time; a) NA, b) PA.

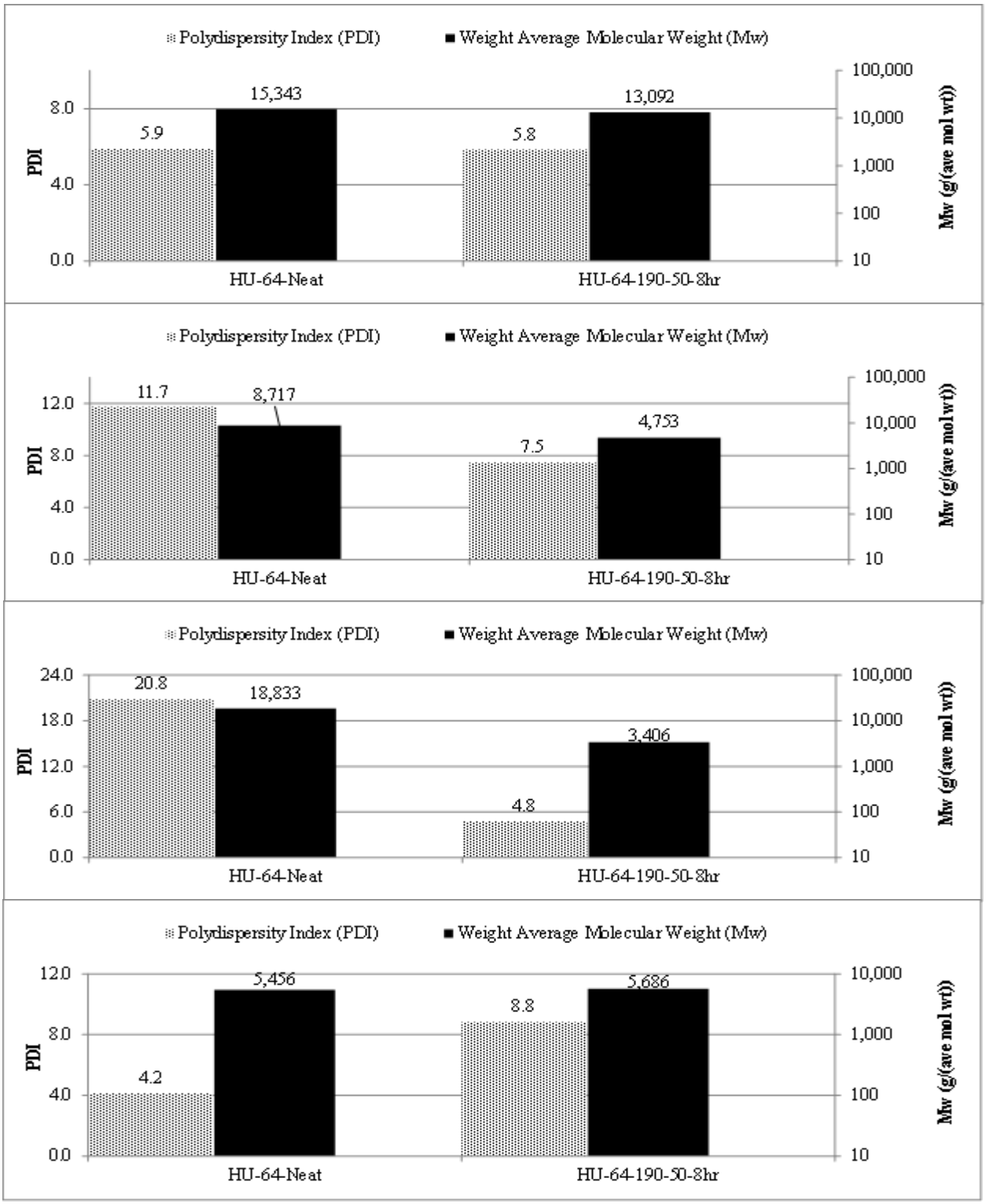

Figure 6.41. Weight average molecular weight and polydispersity comparison for the HU-64 neat and CRMA interacted at 50Hz at different temperatures after 8hr interaction time; a)Asphaltenes, b) Saturates, c) NA, and d) PA.

Microstructure Changes in Asphalt Binder after Interaction with CRM

In this section, a link between the information found in the literature and the findings of the research carried out are established. To better delineate the nature of the change in the microstructure of the asphalt binder as a result of interaction with CRM, the change in the asphalt's macro, micro, chemical, thermal, morphological and molecular attributes as a result of interaction with CRM and the formation of the network structures in asphalt will be highlighted. In addition, the dissolution and release of CRM particles as a results on interaction with asphalt and how it affects the asphalt's network structure will be elaborated.

To start with, one should first highlight the changes that occur asphalt's macro mechanical properties as a result of formation of the network structure. The whole matrix CRMA dynamic mechanical analysis results showed that there exist an occurrence of a distinct plateau region that appears on the phase angle graph. The appearance of the plateau region in the polymer modified asphalt samples indicates the creation of 3D entangled internal network structure in asphalt [119, 120]. The plateau region was much expressed for the samples interacted at 190°C and 50Hz, however it was also evident for the rest of samples interacted at the other interaction conditions. The occurrence of this plateau, however, in CRMA doesn't necessarily mean that there exists a network structure in the CRMA whole matrix, as this can be as a result of the presence of the CRM particle by themselves or any other factors resulting from the interaction between CRM and the asphalt binder. On the other hand, the interrupted shear flow tests carried out on the liquid phase of CRMA showed the occurrence of shear stress overshoot for the samples interacted at 190°C and 50Hz after 8hrs interaction time. As reported in the literature, such behavior for the shear stresses indicates the existence of 3D internal network structure [50, 122]. Based on the results obtained from this work and after comparison with the literature, as entangled polymeric

systems are known to show the same behavior of stress overshoots and recovery of peak magnitudes of stress overshoots with time, it can be deduced that there exists a 3D network structure within the liquid phase of the CRMA at the previously highlighted interaction conditions [50].

Based on the GPC analysis results on the liquid phase of CRMA, GPC chromatograms illustrates major LMS% increase for the samples that were proven to develop the network in their liquid phase. The largest shift of the chromatograms' profile towards the left can be related to 50Hz interaction speed as compared to the 10Hz and 30Hz chromatograms at the utilized interaction times. A consistent increase in the LMS fractions for the CRMA that starts from almost 3.5% at 15min interaction time and maximizes to 10.5% at 8 hrs of interaction time. For both the 10Hz and 30Hz interaction speeds, the increase in LMS% can be attributed to the rubber absorbance of low molecular weight aromatics leading to increased proportion of asphaltenes in liquid phase of asphalt. However, the extent of increase of the LMS in the case of the high speed of the 50Hz cannot be explained in terms of CRM absorbance of low molecular weight fractions of asphalt only because of the occurrence of other mechanisms at such a high speed, namely depolymerization and devulcanization of CRM [23, 122]. It is expected that for the high interaction speed samples, CRM particles are partially devulcanized and depolymerized in the asphalt resulting in the release of CRM components into the liquid phase of asphalt. It is suggested that the increase in the LMS for this specific interaction condition is due to the association of such released components with the liquid phase of asphalt resulting in the formation of the detected 3D network structure.

The FTIR investigation of the CRMA liquid phase showed that peaks for the out-of-plane C-H bends of the aromatic ring can be clearly seen at 698 and 756 cm^{-1} for the Polystyrene for the samples that developed the network in their liquid phase In addition, peaks at 966 cm^{-1} for

the trans component in Polybutadiene are present also. This indicates that at combination of high interaction speed (50Hz) and moderate interaction temperature (190°C), two mechanisms are involved in CRM interaction with asphalt; the first is the rubber absorbance of low molecular weight maltenes, whereas the most intense mechanism is occurrence of devalcunization leading to the partial dissolution of CRM in the liquid phase of asphalt. Unlike the samples that didn't develop the network structure in their liquid phase interacted at at other interaction conditions where the CRM components release is minimal and the main CRM interaction with asphalt is the CRM absorbance of low molecular weight maltenes [22].

The investigation of the release of CRM components into the asphalt liquid phase also provided an idea about the CRM components that takes part in the network formation for the samples that developed the network in their liquid phase. For the samples interacted at temperature of 190°C and mixing speed of 50Hz that developed the network structure in their liquid phase, a different behavior for the dissolution as well as the discharge of CRM components can be seen at such combination of moderate interaction temperature (190°C) and high mixing speed (50Hz), where 82.3% partial dissolution in CRM was calculated. For such interaction conditions, major CRM components release was calculated, where the oily components became 0.5%, the natural rubber reached 4.9%, the synthetic rubber decreased to 2.5%, and the filler components reached 9.8%, from original values of 7, 28.1, 20.7, and 44.2%, respectively. Relating the aforementioned extracted CRM compositional analysis to the superior rheological values for both G* and δ of the same samples and the shear stress overshoot behavior, indicates that at such combination of high mixing speed (50Hz) and moderate interaction temperature (190°C), the release of CRM is not only limited to the oily components and the natural rubber but rather involves all CRM components including the remaining synthetic rubber as well as the filler components.

Such release of CRM components helps initiating and sustaining the formation of 3D network structure that significantly enhances the CRMA rheological properties (G* and δ). This can be explained in terms of occurrence of devulcanization effects that lead to the release of rubber components into the liquid phase of asphalt. However, at such combination of interaction conditions (190°C and 50Hz), depolymerization effects are not major, thus the released rubber components are not readily destroyed (by depolymerization) and thus can undergo other processes involving the association within the CRMA liquid phase resulting in the produced 3D network structure, as discussed earlier for the FTIR testing.

The micromechanical properties of the CRMA that developed the network structure in their liquid phase showed a different trend for the indentation depth than the samples interacted at either 160°C (with 30 or 50Hz) or 190°C with 30Hz that didn't develop the network structure in their liquid phase. The indentation depth shows minimal decrease up to 2hrs of interaction time, however, a major decrease in the indentation depth occurs after 4 and 8hrs to decrease to almost half the value at interaction time of 8hrs as compared to 1hr of interaction time. This behavior is attributed to the increased devulcanization of CRM with minimal occurrence of depolymerization effects that resulted in the formation of 3D entangled network structures in the liquid phase of CRMA that lead to such major stiffening in the CRMA thus resulting in decreased indentation depth [50, 124]. On the other hand, the elastic modulus values showed a gradual increase from 1hr(4.3MPa) to 2hrs(4.7MPa) of interaction time. However, starting from 4hrs the elastic modulus values showed major enhancement (8.5MPa) and was almost double the values of the samples at 2hrs (4.7MPa). After 8hrs of interaction time, the elastic modulus was 10.6MPa. On the other hand, the hardness had a major increase of almost 5 times when the interaction time was increased from 2hrs(0.09MPa) to 4hrs(0.47MPa). The hardness values continue

to increase at 8hrs to be 0.7MPa. As explained earlier, such distinctive increase in hardness and elastic modulus values after 4 and 8hrs of interaction time is explained in terms of the development of 3D entangled network structure in the CRMA liquid phase which is associated with such combination of moderate interaction temperature (190°C) and high interaction speed (50Hz) [50, 124].

The stepwise TGA tests carried out on the asphalt fractions of the liquid phase of the CRMA provided an insight about the status of the released CRM components that migrated from CRM to asphalt. The Step wise TGA on the asphaltene of the liquid phase for the samples that developed the network structures showed that almost 80% of the asphaltene components for the investigated sample fill within the synthetic rubber steps range. This indicated that at such combination of medium interaction temperature (190°C) and with the utilization of high interaction speed (50Hz), most of the asphaltene fractions components were altered through the interaction with CRM to have a combustion behavior similar to that of synthetic rubber components of CRM, however this doesn't necessarily indicate that most of the asphaltene components are synthetic rubber, owing to the limited percentage of CRM (10%) utilized in the interaction with asphalt, indicating that it is rather a shift in the behavior of the asphaltene combustion rather than migration of the synthetic rubber from CRM to the asphaltene. For the saturates, almost 19% of the components for the investigated sample fill within the synthetic rubber steps range. In addition, 22% of the components fill within the oily components range. This indicates that at such combination of medium interaction temperature (190°C) and with the utilization of high interaction speed (50Hz), almost 1/5 of fractions components were altered through the interaction with CRM to have a combustion behavior similar to that of synthetic rubber components and oily components of CRM. However, this doesn't necessarily indicate that 19% of the saturates com-

ponents are synthetic rubber or that 20% are oily components, owing to the limited percentage of CRM (10%) utilized in the interaction with asphalt, indicating that it is rather a shift in the behavior of the saturates combustion rather than migration of the synthetic rubber or oily components from CRM to the saturates. For the Polar aromatics of the investigated sample, almost 35% of them fill within the synthetic rubber steps range. This indicates that at such combination of medium interaction temperature (190°C) and with the utilization of high interaction speed (50Hz), almost one third of the naphthene aromatics fractions components were altered through the interaction with CRM to have a combustion behavior similar to that of synthetic rubber components of CRM.

The FTIR investigation of the asphalt fractions was used as a complimentary method to investigate the status of the released components of CRM into the fractions of the liquid of CRMA. The FTIR spectra comparison for the asphaltenes of neat and samples interacted at 190°C with 50Hz after 8hr of interaction time for the HU-52 asphalt. Almost similar spectra can be seen for the asphaltenes of the neat and the CRMA. However, a week peak can be seen at 969.85cm-1 for the CRMA sample, this peak is attributable to the bending vibration of trans 1, 4-2 alkenes in poly butadiene [75].

The AFM images for the HU-52 samples that developed the network in their liquid phase showed abundant distributed dispersoids without apparent agglomeration. In addition, the morphology of the CRMA sample after 4hrs interaction time resembled that of polymer modified asphalt ones with low percentage of polymer modifier[128-130]. However after 8hrs interaction time, a much more organized phase in the matrix having a fine lamellar like structure. Such lamellar structure have been found to resemble the formation of network in asphalts [131]. This indicated that the formation of network in CRMA is a gradual process that starts with the disso-

lution of the asphalt original phase domains and continues through the interaction of asphalt with CRM and components exchange that results in the formation of the network structure eventually [131]. The networks morphology for the HU-64 asphalts showed a buildup of phase clusters around the original ones, indicating that the exchanged components from CRM took part in the formation of the network structure. In addition, a unique close-up to one of the clusters observed showed that there exists two different phase with variation in dispersoids size and altitude. Presence of polymer modifier has been known to produce rough surface for polymer modified asphalt. It is suggested that although both asphalts had network structures within, however the nature and morphology of such network varies based on the asphalt source.

On the other hand, the separation index results for the whole matrix samples interacted at 190°C and 50Hz were 41, 22, 5, and 2% for the samples interacted at 1, 2, 4, and 8hrs interaction time. The values of the separation index of the liquid phase were almost 1% for all interaction times. This indicated that the formation of the 3D network structure at such combination of interaction temperature (190°C) and speed (50Hz) with the increase of interaction time resulted in altering the CRMA known physical instability behavior and produced a physical stable CRMA starting from 4hrs of interaction time. Relating this to the extracted CRM from CRMA for the same samples illustrated in the CRM thermogravimetric analysis and to the FTIR analysis testing, it can be deduced that at 8hrs of interaction time, the CRM dissolved and released components are sufficient to initiate and sustain 3D network structure that has not only enhanced the CRMA rheological properties but also alleviated the CRM known problem of storage instability through reaching a separation index of only 2% as a result of the well-defined 3D network structure at such interaction time that has involved most of the CRM released components to further alleviate the physical storage instability problem.

However, the low temperature behavior of the samples that developed the networks in their liquid phase was different from the known behavior of CRMA that normally shows enhancement in such properties. After 15min of interaction time, the samples exhibited reduced stiffening as a result of CRM swelling and the increase of its effective size at such low interaction time, where the CRM acted as cushion absorbing the developed thermal stresses accumulated in the CRMA as a result of thermal contraction. However, upon increasing the interaction time to 1, 2, 4 and 8hrs stiffening of the CRMA was prevalent as a result of the increase of the CRM dissolution and component release. It should be noticed that despite the increase in stiffening of the CRMA with the progression of the interaction time, however all the samples were in compliance with PG requirement of having S of value smaller than 300MPa. On the other hand, for the m-value behavior for the same samples, slight decrease was recorded in comparison with the as received sample, up to 2hrs of interaction time, indicating that the rate of stress relaxation exhibited by the CRMA suffered slight deterioration. Upon increasing the interaction time to 4hrs, the m-value was exactly 0.3, satisfying the PG requirement. However, at 8hrs of interaction time, the m-value as less than 0.3.

The utilization of UMO with CRM for the modification of asphalt and their effect on the developed network structure was investigated. It was found that the addition of 3% UMO to the asphalt resulted in deterioration in both the G* and δ. On the other hand, upon the utilization of 10% CRM only, enhancement in both the G* and δ was observed. The combined use of 10% CRM and 3% UMO had a plateau effect for both the G* and δ values, but with values tending to slightly deteriorate at the end of interaction time (120 minutes). On the other hand, the addition of UMO only to asphalt resulted in the disturbance of the asphalt's continuous three-dimensional associations leading to the observed deterioration in both G* and δ for the sample modified with

3% UMO only. Enhancements in rutting, fatigue, and thermal cracking were also attributable to the utilization of 10% CRM and 3% UMO together for the modification of asphalt. This is due to the fact that most of the components of UMO fall in the category of saturates. Thus they tend to get absorbed by CRM and thus facilitate the interaction between CRM and asphalt by substituting of the saturates fractions form asphalt.

To summarize what was highlighted for the CRMA network formation, based on the results obtained from the TGA, FTIR, GPC, and fractionation, it is suggested that during the interaction between asphalt and CRM, the CRM first absorbs the components of saturates and polar aromatics from asphalt and continuous to swell. With the increase of interaction time, the CRM starts dissolving in asphalt and releases its polymeric components. The polymeric components then migrates to the asphaltenes and continuous to swell. The swelling actually occurs to the Polystyrene (PS) polymers of the released polymeric CRM, while the Polybutadiene (PB) polymers acts as nodes in between the swelled PS leading to the development of the swelled entangled network structures in CRMA that profoundly enhances the properties of CRMA. Figure 6.42(a, b, c, d, e, f) illustrates the progression of the network structure development with time; with respect to proposed network model development after; a) 1, b) 2, c) 4, d) 8hr interaction time and e) CRM dissolution and component release, and (f) CRMA hardness and elastic modulus. As can be seen from the proposed model, the internal network structure starts with the release of the CRM rubber components that starts to have the Polystyrene (PS) polymers swelling with the asphalt light molecular fractions while the Polybutadiene (PB) polymers do not swell. This continues leading to having the PB acting as nodes for the entangled network structures. The release of the CRM polymeric components can be seen in Figure 6.42(e). On the other hand,

the formation of the entangled network structure leads to superior enhancement in the macro and micro mechanical properties as seen from Figure 6.42(f).

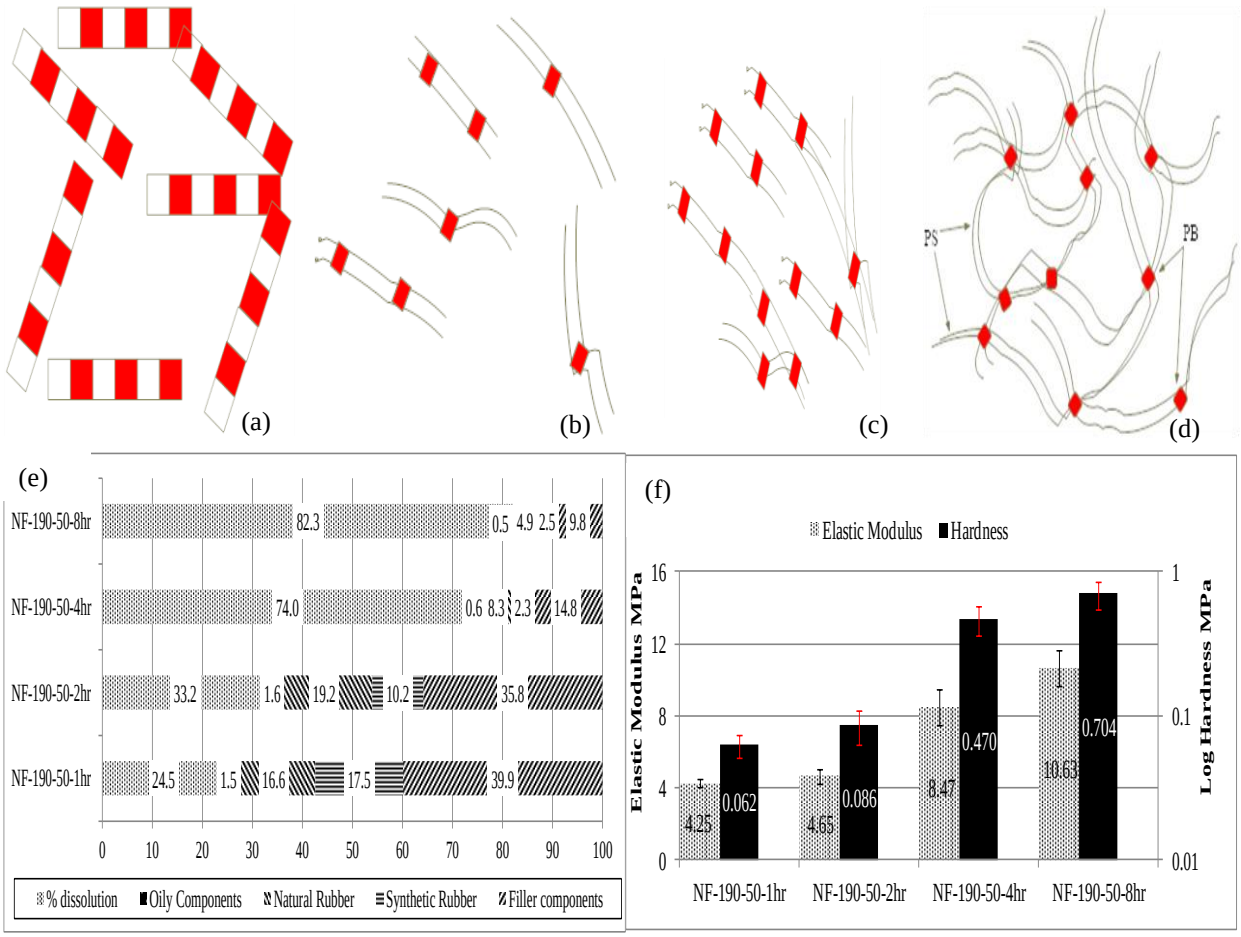

Figure 6.42. Progression of the network structure development with time; (a)1hr, b)2hr, c)4hr, and d)8hr, (II) CRM dissolution and component release, and (III) CRMA hardness and elastic modulus.

CHAPTER SEVEN. EFFECT OF THE DEVELOPED NETWORK STRUCTURE ON THE STORAGE STABILITY OF ASPHALTS AND RUBBER MODIFIED ASPHALTS

Introduction

In this chapter we investigate the effect of the developed network structure on the storage stability of asphalt binder. One of the most challenging problems associated with utilizing CRM in asphalt is the deteriorated final storage stability of the modified asphalt binder. Thus the improvement of the storage stability of the CRMA represents a major target.

Whole Matrix Samples Analysis After 8hrs of Interaction Time

In this section the storage stability of the whole matrix samples is investigated at the end of the interaction time (8hrs). This gives an idea about the in-service expected storage stability of the modified asphalt binders before mixing and compaction.

Figure 7.1(a, b, c) illustrates preliminary analysis for the storage stability results for the CRMA whole matrix samples. Figure 7.1(a, b, c) shows the values of the separation index for the whole matrix samples interacted at different interaction speeds (10Hz, 30Hz and 50Hz) at interaction temperatures of (a)160°C, (b)190°C, and (c)220°C after 8hrs of interaction time, respectively. As can be seen from Figure 7.1(a), at interaction temperature of 160°C, increasing the interaction speed from 10Hz up to 30 and 50Hz resulted in minor improvement in the storage stability, where the value of the separation index was 61% for the samples interacted with 160°C and 10Hz after 8hrs of interaction time, whereas, the separation index was 57% for the samples interacted with 160°C and 30Hz. The best value for the separation index at 160°C interaction temperature was for the samples interacted at mixing speed of 50Hz (51%). The deteriorated values of the separation index at such low interaction temperature (160°C) even with the utilization of high mixing speed (50Hz) can be explained in terms of the aforementioned extracted

CRM dissolution and compositional analysis where at such low interaction temperature and even with the utilization of higher mixing speed, the dissolved CRM amounts and components are minor, in addition to the fact that the CRM undergoes swelling processes by absorbing light aromatics from the asphalt liquid phase leading to the increase in CRM effective size [22]. The increase of CRM effective size lead to such deteriorated storage stability at such interaction conditions.

Figure 7.1(b) illustrates the values of the separation index for the whole matrix samples interacted at interaction speeds (10Hz, 30Hz and 50Hz) and interaction temperature of 190°C. As can be seen from Figure 7.1(b), a gradual enhancement in the separation index values can be seen by the increase of the interaction speed from 10Hz up to 30Hz, where the separation index decreases from 43 to 30%, respectively. However, a major enhancement in the separation index can be seen for the samples interacted at 190°C and 50Hz after 8hrs of interaction time, where the separation index decreased to only 2%. The deteriorated storage stability of CRMA at interaction temperature (190°C) with the lower interaction speeds (10 and 30Hz) can be explained in terms of the extracted CRM dissolved amounts and components explained earlier in the CRM thermogravimetric analysis section, although the release of CRM is increased at such interaction temperature (190°C) in comparison to the previously explained behavior of the samples interacted at 160°C, however, the utilization of low (10Hz) and moderate (30Hz) interaction speed was not sufficient to initiate and sustain the formation of 3D network structure that was able to significantly improve the storage stability for the samples interacted at the same interaction temperature (190C), but with higher interaction speed 50Hz.

Figure 7.1(c) illustrates the values of the separation index for the samples interacted at interaction speeds (10Hz, 30Hz and 50Hz) and interaction temperature of 220°C. A continuous

enhancement in the value of the separation index can be seen with the increase in the interaction speed. This can be explained in terms of the severe CRM dissolution at such high interaction temperature that resulted in the annihilation of the CRM particle effect by extensive depolymerization and devulcanization.

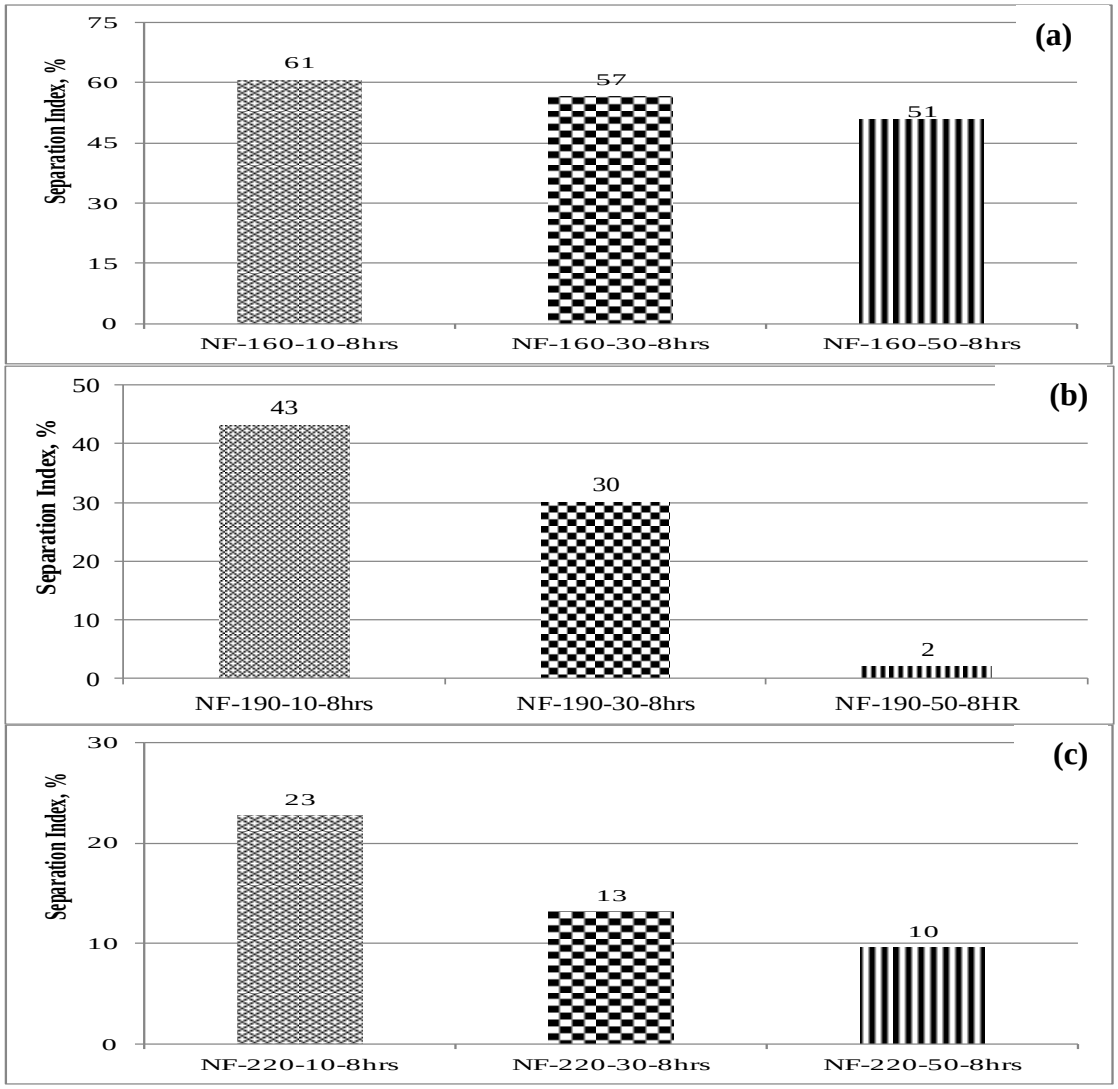

Figure 7.1. Development of separation index of CRMA interacted under different interaction speed at temperatures (a)160°C, (b)190°C, and (c)220°C.

It should be noted that although the storage stability is improving, yet this was on the expense of the rheological parameters values that suffered deterioration with the increase of inter-

action speed, as can be seen from the rheological analysis section for those samples. It should also be noted that for the samples interacted at 220°C and 50Hz, although the CRM dissolved amounts and components were more than those for the samples interacted at 190°C and 50Hz (samples showing 3D network structure), however the separation index was significantly lower for the samples that developed 3D network structure. This indicates that the improvement in the storage stability for the samples that developed 3D network structure was not merely because of the annihilation of the CRM particle effect (the case for the samples interacted at 220°C and 50hz), but rather as a result of the development of the 3D network structure.

We decided to investigate the storage stability of the liquid phase and compare it to the whole matrix storage stability. We chose to investigate the storage stability of the liquid phase and whole matrix for samples interacted at higher interaction speeds (30Hz and 50Hz) for the three temperatures investigated (160°C, 190°C, and 220°C), because at such interaction speeds the decrease in CRM particle size is more manifested.

Liquid Phase and Whole Matrix Comparison Analysis of Selected Samples

In this section a comparison is carried out between the whole matrix and liquid phase storage stability behavior. This provides an important insight about the effect of the network structure on the storage stability behavior and whether it is just merely dissolution of the CRM particles that improves the storage stability or rather the presence of the network structures themselves.

Figure 7.2 illustrates the development of separation index of whole matrix and liquid phase of CRMA interacted at temperature 160°C and interaction speed (a)30Hz, and (b)50Hz, after 1, 2, 4, and 8hrs of interaction time.

As shown in Figure 7.2(a), the separation index for the whole matrix samples interacted at 160°C and 30Hz was 65% after 1hr of interaction time and decreased to 64, 62, and 57% after 2, 4, and 8hrs of interaction time, respectively. However, the separation index for the liquid phase of the same samples was of much lower values, 2%, for all the interaction times investigated. This indicates that the samples interacted at 160°C and 30 Hz suffered only from physical instability with no apparent phase separation.

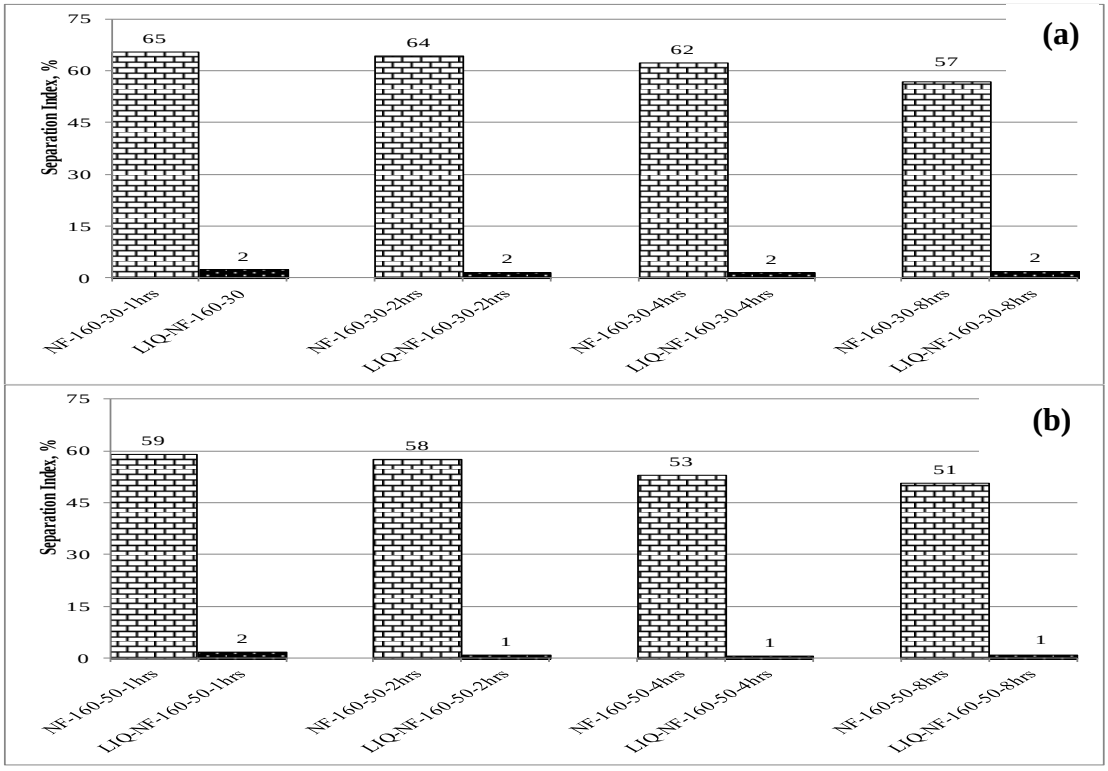

Figure 7.2. Development of separation index of whole matrix and liquid phase of CRMA interacted at temperature 160°C and interaction speed (a)30Hz, and (b)50Hz, for the different interaction times.

We can draw the same conclusion for the samples interacted at 160°C and 50Hz illustrated in Figure 7.2(b). The separation index of the whole matrix was 59, 58, 53, and 51% for the samples interacted at 1, 2, 4, and 8hrs, respectively. The separation index for the liquid phase was 2% after 1hr of interaction time and decreased to 1% for the samples interacted at 2, 4, and

8hrs. The increase of interaction speed (from 30 to 50Hz) at the same temperature (160°C) lead to minor improvement of the separation index of both the whole matrix samples as well as the liquid phase ones.

Figure 7.3 illustrates the development of separation index of whole matrix and liquid phase of CRMA interacted at temperature 190°C and interaction speed (a)30Hz, and (b)50Hz, after 1, 2, 4, and 8hrs of interaction time.

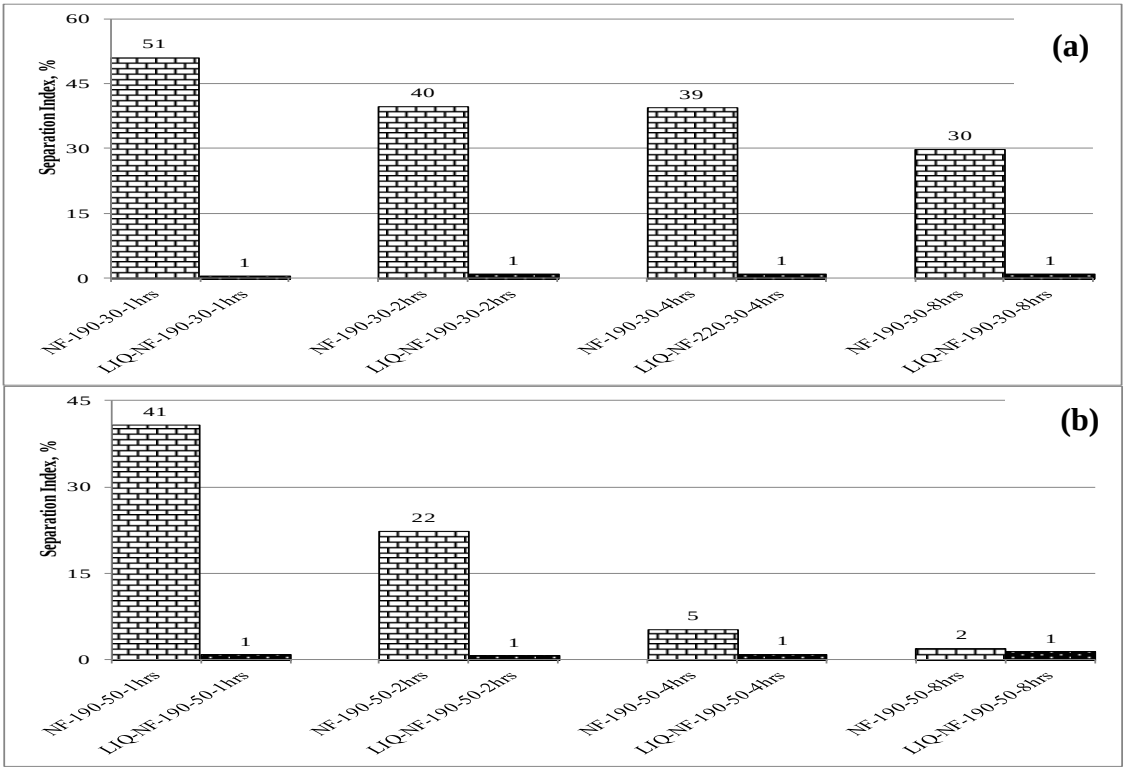

Figure 7.3. Development of separation index of whole matrix and liquid phase of CRMA interacted at temperature 190°C and interaction speed (a)30Hz, and (b)50Hz, for the different interaction times.

Figure 7.3(a), shows a continuous decrease in the separation index of the whole matrix with the increase of interaction times for the samples interacted at 190°C and 30Hz. The separation index of the whole matrix was 51, 40, 39, 30% after 1, 2, 4, and 8hrs of interaction time, respectively. The separation index for the liquid phase was 1% for all interaction times investigat-

ed. The values of the whole matrix separation index indicate the existence of physical storage instability problem at such interaction conditions. On the other hand, the values of the liquid phase separation index show no phase separation problems. Figure 7.3(b) shows a different trend for the separation index results for the whole matrix samples interacted at 190°C and 50Hz. The whole matrix separation index values were 41, 22, 5, and 2% for the samples interacted at 1, 2, 4, and 8hrs interaction time. The values of the separation index of the liquid phase were almost 1% for all interaction times. The formation of the 3D network structure at such combination of interaction temperature (190°C) and speed (50Hz) with the increase of interaction time resulted in altering the CRMA known physical instability behavior and produced a physical stable CRMA starting from 4hrs of interaction time. Relating this to the extracted CRM from CRMA for the same samples illustrated in the CRM thermogravimetric analysis and to the FTIR analysis sections, it can be deduced that at 8hrs of interaction time, the CRM dissolved and released components are sufficient to initiate and sustain 3D network structure that has not only enhanced the CRMA rheological properties but also alleviated the CRM known problem of storage instability through reaching a separation index of only 2% as a result of the well-defined 3D network structure at such interaction time that has involved most of the CRM released components to further alleviate the physical storage instability problem.

Figure 7.4 illustrates the development of separation index of whole matrix and liquid phase of CRMA interacted at temperature 220°C and interaction speed (a)30Hz, and (b)50Hz, after 1, 2, 4, and 8hrs of interaction time.

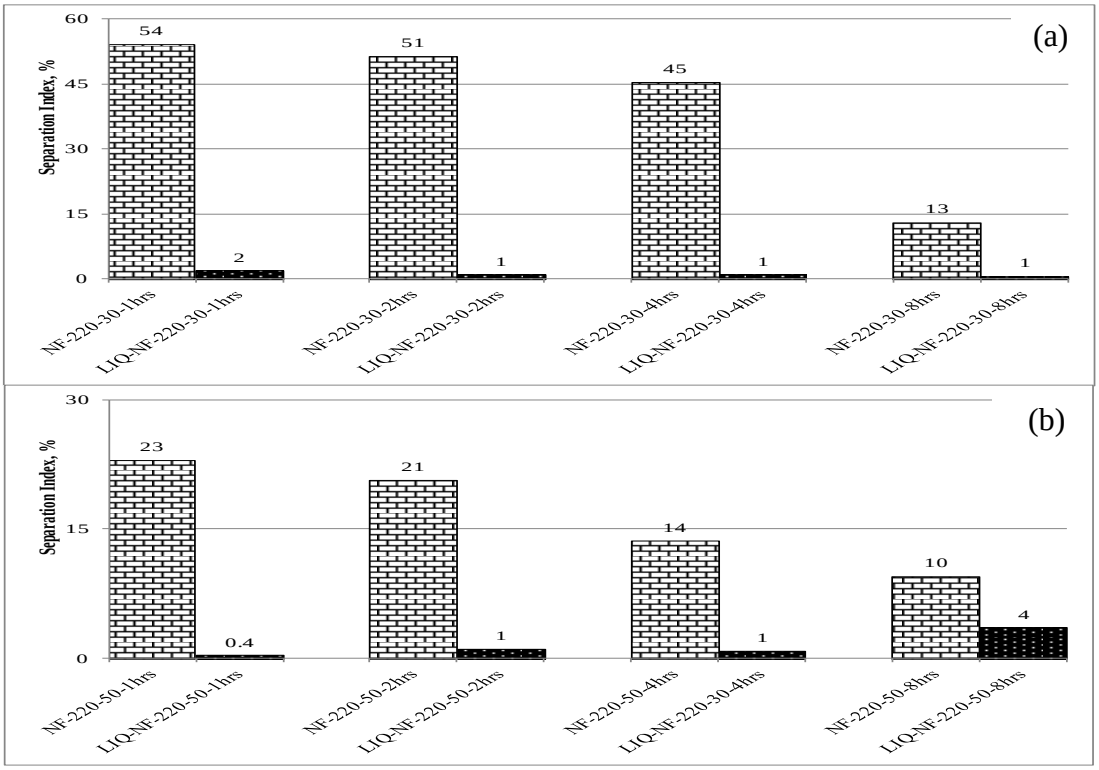

Figure 7.4. Development of separation index of whole matrix and liquid phase of CRMA interacted at temperature 220°C and interaction speed (a)30Hz, and (b)50Hz, for the different interaction times.

Figure 7.4(a) shows a decrease in the whole matrix separation index starting from 54 to 50, 45, and finally 13% for the interaction times; 1, 2, 4, and 8hrs, respectively. The value of the liquid phase separation index was 1% after 8hrs of interaction time. Unexpectedly, the separation index values for the whole matrix samples interacted at 190°C and 30Hz were better than those interacted at 220°C and 30Hz at 1, 2, and 4hrs of interaction time. This indicates that the increased interaction temperature leads to deteriorated physical storage stability. On the other hand, upon increasing the interaction time to 8hrs, the decrease in CRM particle size, as a result of increased depolymerization and devulcanization, leads to improved physical storage stability. Figure 7.4(b) shows increase in the liquid phase separation index indicating phase instability. This happens as a result of the severe devulcanization and depolymerization of CRM that leads

to release of most of the polymeric components as well as filler components. The effect of polymeric components is annihilated as a results of the combination of increased interaction temperature and speed, however, the filler components are not affected by the interaction conditions and because they have higher density than asphalt they tend to produce this phase instability problem [132].

In this section we investigated the effect of temperature, CRM percentage and CRM type on the storage stability of CRMA for HU-52 asphalt.

Figure 7.5 illustrates the development of separation index of whole matrix for the HU-52 CRMA; (a) Effect of temperature, (b) Effect of CRM%, and (c) Effect of CRM type.As can be seen from Figure 7.5(a), after 8hr of interaction time, the separation index of the samples interacted at 160°C and 50Hz was 49%. This indicates deteriorated storage stability for such samples. This is mainly because of the swelling of the CRM particles with the light aromatics at such combination of low interaction temperature (160°C), and even with the utilization of a high mixing speed (50Hz), leading to the decrease of the inter-particle distance between CRM particles [22]. On the other hand, the separation index for the samples interacted at 190°C and 50Hz showed a distinctive enhancement. The value for the separation index at such interaction conditions was only 1%. This is mainly due to the formation of 3D network structure at such combination of interaction temperature (190°C) and speed (50Hz) after 8hr of interaction time that resulted in altering the CRMA known physical instability behavior and produced a physical stable CRMA.

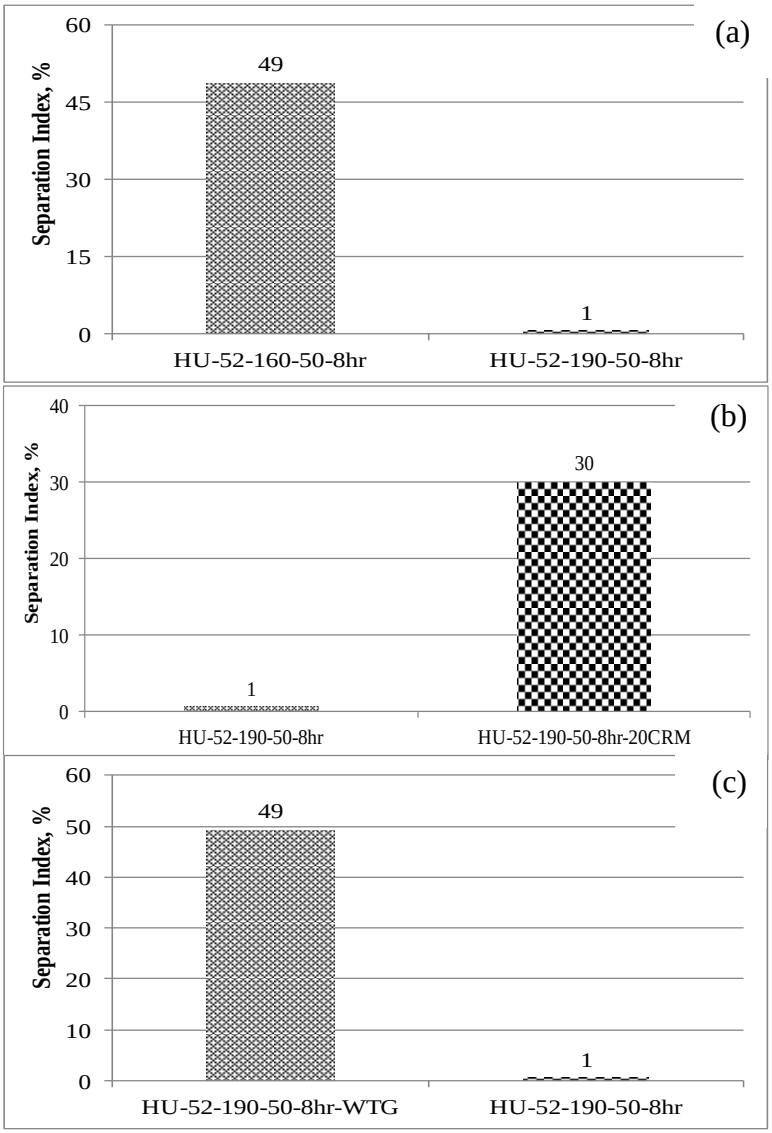

Figure 7.5. Development of separation index of whole matrix for HU-52 CRMA; (a) Effect of temperature, (b)Effect of CRM%, and (c) Effet of CRM type.

Relating this to the extracted CRM from CRMA for the same samples illustrated in the CRM thermogravimetric analysis and to the FTIR analysis sections, it can be deduced that at 8hrs of interaction time, the CRM dissolved and released components are sufficient to initiate and sustain 3D network structure that has not only enhanced the CRMA rheological properties but also alleviated the CRM known problem of storage instability through reaching a separation

index of only 1% as a result of the well-defined 3D network structure at such interaction time that has involved most of the CRM released components to further alleviate the physical storage instability problem.

As can be seen from Figure 7.5(b), after 8hr of interaction time, the separation index of the samples having a 20% CRM interacted at 190°C and 50Hz was 30%. This indicates deteriorated storage stability for such samples. This is mainly because of the increased percentage of CRM and their swelling with the light aromatics which overshadowed the effect of the medium interaction temperature (190°C), and even with the utilization of a high mixing speed (50Hz), as a result of the decrease of the inter-particle distance between CRM particles [22]. On the other hand, as explained earlier for the samples with 10%CRM interacted at 190C and 50Hz, the separation index was only 1% as a result of the developed 3D entangled network structure.

Figure 7.5(c) illustrates the separation index for samples utilizing 10%WTG as compared to those utilizing 10%CRM after 8hr of interaction time. The separation index of the samples having a 10%WTG interacted at 190°C and 50Hz was 49%. This indicates deteriorated storage stability for such samples. This is can be explained in terms of the source of the waste rubber utilized, where for WTG the source of waste rubber is passenger cars, while for CRM it is a mixed source of waste rubber. This indicates that the waste rubber from passenger cars is not compatible with the utilized asphalt in this research work. This lead to the swelling of WTG waste rubber with the light aromatics which overshadowed the effect of the medium interaction temperature (190°C), and even with the utilization of a high mixing speed (50Hz), as a result of the decrease of the inter-particle distance between CRM particles [22]. On the other hand, as explained earlier for the samples with 10%CRM interacted at 190C and 50Hz, the separation index was only 1% as a result of the developed 3D entangled network structure.

CHAPTER EIGHT. EFFECT OF DEVELOPED NETWORK STRUCTURE ON THE LOW TEMPERATURE PROPERTIES OF ASPHALTS AND RUBBER MODIFIED ASPHALTS

Introduction

In this chapter the investigation of the low temperature properties of modified asphalt binders is carried out. This is carried out in terms of the performance-based aspects other than the materials based ones. The low temperature properties of asphalt is a very important aspect of asphalt in-service behavior. A modified asphalt with deteriorated low temperature properties would be prone low temperature thermal cracking that would severely deteriorated its in-service performance.

Low Temperature Properties Results

Figure 8.1 (I and II) illustrates for the NF-58 asphalt the progression of the low temperature parameters, (I)S and (II)m-value after 8hrs of interaction time, for the different interaction speeds (10Hz, 30Hz and 50Hz) at interaction temperatures of a)160°C, b)190°C, and c)220°C, respectively.

As can be seen from Figure 8.1(I-a) for the developed stiffness values, after 8hrs of interaction time, the CRMA samples interacted at 160°C and 10, 30, and 50Hz were less prone to stiffening than the as received binder. This can be explained in terms of the CRM swelling and increase of its effective size with minor CRM dissolution and release at such low interaction temperature (160°C) leading to have the CRM acting as cushion absorbing the developed thermal stresses accumulated in the CRMA as a result of thermal contraction. On the other hand, for the m-value behavior for the same samples, illustrated in Figure 8.1(II-a), slight decrease was recorded in comparison with the as received sample indicating that the rate of stress relaxation

exhibited by the CRMA suffered slight deterioration. However, for both the S and m-value, the recorded values for the CRMA at such interaction parameters satisfied the PG requirements of S being less than 300MPa and m-value higher than 0.3.

Figure 8.1(I-b) and (II-b) illustrates the low temperatures S and m-value for the samples interacted with interaction temperature 190°C and interaction speeds 10, 30, and 50Hz after 8hrs of interaction time, respectively.

As can be seen from Figure 8.1(I-b), increasing the interaction speed had the effect of stiffening the CRMA as a result of decrease of CRM particle size effect , explained earlier for the samples interacted at 160°C, that would have helped in absorbing the developed thermal stresses. However, all the CRMA samples synthesized at such interaction parameters satisfied the PG requirements of S being lower than 300MPa. On the other hand, a different behavior was attributed to the m-value for samples interacted at interaction temperature 190°C and interaction speeds 10, 30, and 50Hz, illustrated in Figure 8.1(II-b). As can be seen in Figure 8.1(II-b), the utilization of lower interaction speeds of either 10 or 30Hz resulted in a similar behavior as that recorded earlier for the samples interacted at 160°C, where value suffered slight deterioration as a result of partial dissolution of CRM particles at such combination of interaction temperature (190°C) and mixing speed (10 and 30Hz) that resulted minor deterioration in rate of stress relaxation exhibited by m-value of lower values as compared to the as received samples. A more acute decrease for the m-value was found for the samples interacted at 190C and 50Hz, where the samples' m-value didn't satisfy the minimum of 0.3.

The behavior of the low temperature parameters S and m-value for the samples interacted at 220°C and 10, 30, and 50Hz is illustrated in Figure 8.1(I-c) and (II-c), respectively.

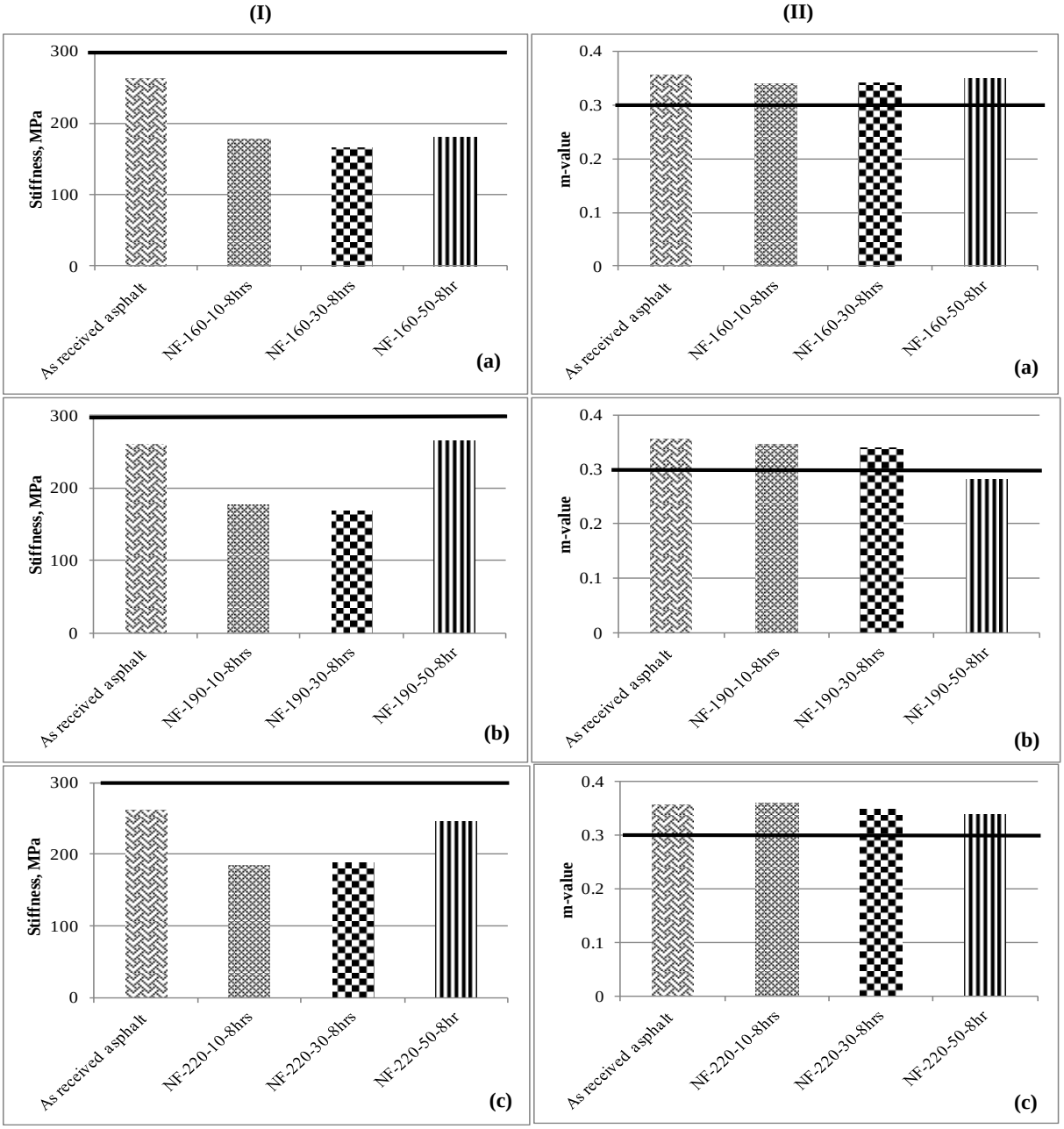

Figure 8.1. Development of low temperature parameters of CRMA interacted under different interaction speed: (I)S and (II)m-value at temperatures (a)160°C, (b)190°C, and (c)220°C.

As can be seen in Figure 8.1(I-c), increasing the interaction speed resulted in increased stiffening for the CRMA, with the samples interacted at 50Hz of almost equivalent S value as that of the as received sample. As explained earlier for such combination of high interaction

speed (50Hz) and interaction temperature (220°C), despite the high amounts of dissolved and released CRM components as illustrated in the CRM thermogravimetric analysis section, the effect of CRM is almost annihilated by the severe depolymerization and devulcanization resulting in deteriorating the low temperature properties. However, it should be noticed that despite the apparent stiffening in the CRMA at such combination of interaction conditions, all the investigated samples satisfied the PG requirement of S being lower than 300MPa. Figure 8.1(II-c) illustrates the m-value behavior for the same samples, it can be seen that a slight decrease was recorded in comparison with the as received sample m-value. However, for all investigated samples, the recorded m-value for the CRMA at such interaction parameters satisfied the PG requirements of m-value being higher than 0.3.

To address in detail the low temperature behavior of the samples that developed 3D entangled network structure, Figure 8.2(a,b) illustrates the change of the S and m-value with increase of interaction time for the samples interacted at 190°C and 50Hz, respectively.

As can be seen from Figure 8.2(a), after 15min of interaction time, the samples exhibited reduced stiffening as a result of CRM swelling and the increase of its effective size at such low interaction time, where the CRM acted as cushion absorbing the developed thermal stresses accumulated in the CRMA as a result of thermal contraction. However, upon increasing the interaction time to 1, 2, 4 and 8hrs stiffening of the CRMA was prevalent as a result of the increase of the CRM dissolution and component release.

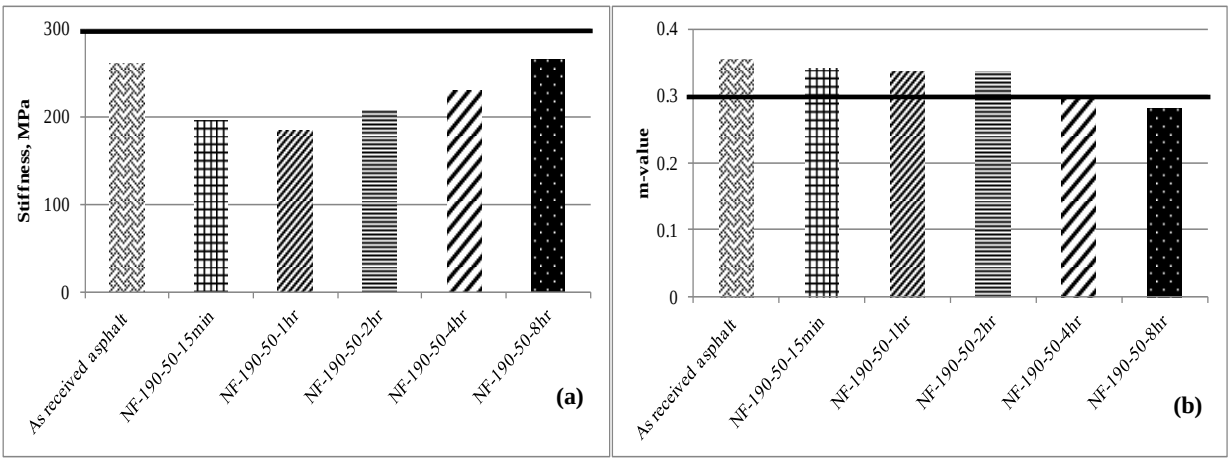

Figure 8.2. Development of low temperature parameters of CRMA interacted under 50Hz interaction speed and temperature 190°C: (a)S and (b)m-value.

It should be noticed that despite the increase in stiffening of the CRMA with the progression of the interaction time, however all the samples were in compliance with PG requirement of having S of value smaller than 300MPa. On the other hand, for the m-value behavior for the same samples, illustrated in Figure 8.2(b), slight decrease was recorded in comparison with the as received sample, up to 2hrs of interaction time, indicating that the rate of stress relaxation exhibited by the CRMA suffered slight deterioration. Upon increasing the interaction time to 4hrs, the m-value was exactly 0.3, satisfying the PG requirement. However, at 8hrs of interaction time, the m-value as less than 0.3 for the reasons explained earlier.

CHAPTER NINE. EFFECT OF REJUVENATING AGENTS ON THE NETWORK STRUCTURE OF ASPHALTS AND RUBBER MODIFIED ASPHALTS

Introduction

In this chapter the effect of rejuvenating agents, specifically used motor oil, on the development of the network structures in asphalt and CRMA is investigated. The utilization of waste or used motor oils (UMO) in asphalt industry is an important path for the cradle to cradle approach of sustainable development methodology. Instead of landfilling UMO it is utilized in asphalt and an added value would be to have enhancement in the in-service properties of the modified asphalt as a result of addition of UMO.

Effect of Used Motor Oil on the Network Structure Developed in CRMA

In this section the effect of UMO on the development of network structures in the whole matrix as well as the liquid phase of CRMA is carried out, only HU-64 asphalt is being investigated in this chapter.

Effect of UMO and CRM on the Internal Structure of Asphalt Whole Matrix

Figure 9.1 shows the temperature sweep viscoelastic properties for rheological properties (a) G* and (b) δ for the samples interacted at 160°C, 30Hz after 120 minutes with 3% UMO, 10% CRM, or both modifiers after 120 minutes of interaction time, respectively.

It can be seen from the Figure 9.1(a) that the behavior of the samples with CRM is almost similar with or without UMO addition, where the effect of CRM modification over the UMO alone modified samples is mainly manifested at higher testing temperatures, this is in agreement with other studies [4], which show that the CRM modification of asphalt mainly affects its high temperature properties and by decreasing the testing temperature, the changes in physical properties reduces to a marginal level.

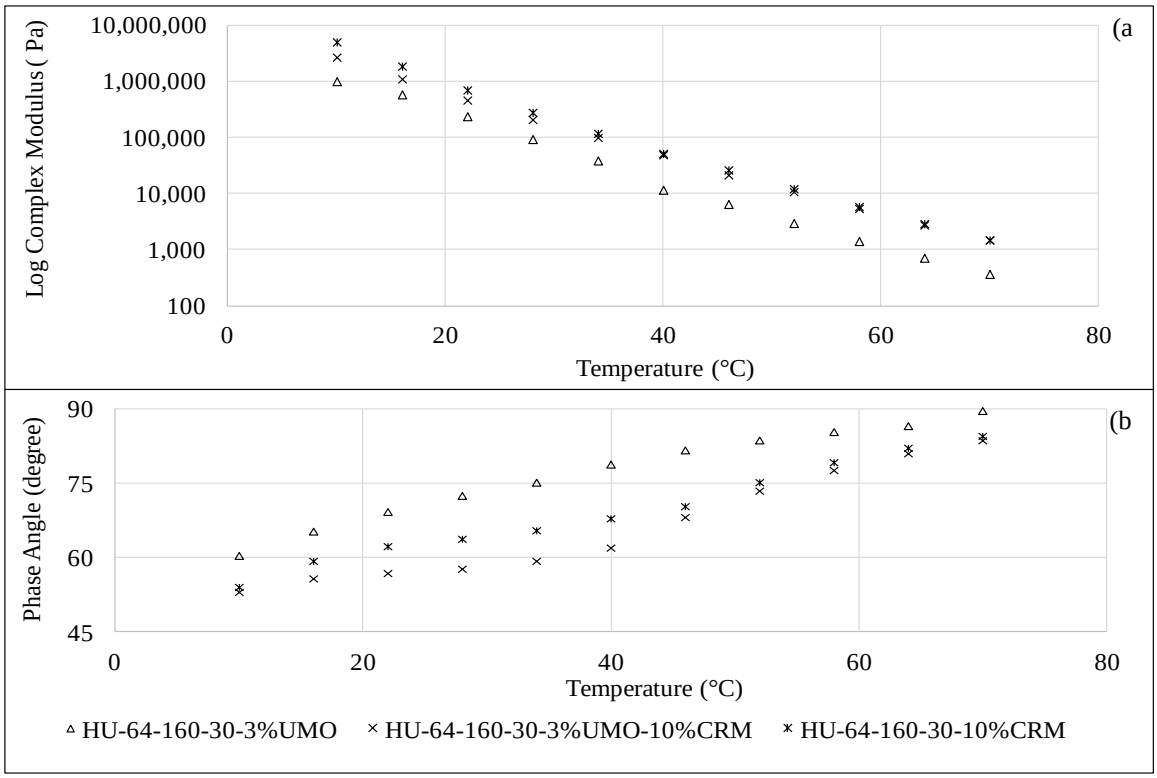

Figure 9.1. Temperature sweep viscoelastic properties for rheological properties (a) G* and (b) δ, for the samples interacted at 160°C, 30Hz after 120 minutes with 3% UMO and/or 10% CRM.

On the other hand, a distinctive behavior for the δ can be seen for the samples modified with CRM or CRM+UMO illustrated in Figure 9.1(b). Results in Figure 9.1(b) show that by addition of CRM or CRM+UMO to asphalt, a distinct plateau region appears on the phase angle graph. The appearance of the plateau region indicates of the creation of 3D entangled internal network structure in asphalt [119, 120]. It can be seen that the sample with 3%UMO and 10%CRM shows a more distinct plateau region compared to the sample with 10%CRM interacted at the same interaction conditions. This indicates that the combination of 10%CRM and 3%UMO released components in asphalt at the utilized interaction conditions (i.e. 160°C, 30Hz after 120 minutes) that were capable of forming 3D internal network structure in the asphalt ma-

trix. The molecular size distribution changes of the asphalt fractions and UMO as a result of the formation of such 3D internal network structure are investigated and discussed in sections bellow. On the other hand, addition of UMO only to the asphalt gave no such plateau behavior, indicating that the presence of UMO modifier alone can't initiate the formation of such 3D internal network structure.

Figure 9.2 shows the temperature sweep viscoelastic properties of for rheological properties (G*) and (δ) for the samples interacted at 160°C, 30Hz after 120 minutes with 9% UMO, 20% CRM, or both modifiers after 120 minutes of interaction time, respectively.

The same behavior illustrated in Figure 9.1(a) can be seen in Figure 9.2(a), where the effect of CRM modification for samples with CRM in the presence or absence of UMO over the samples modified with UMO alone is mainly manifested at higher testing temperatures, especially for the samples with 20%CRM+9%UMO.

Results in Figure 9.2(b) show that the increase in CRM or CRM+UMO percentage leads to more intensified plateau region behavior. Unlike the samples modified with 10%CRM and 3%UMO (illustrated in Figure 9.1(b)), the plateau behavior is more manifested for the samples with 20% CRM over those modified with 20%CRM and 9%UMO. This indicates the at the utilized interactions conditions (i.e. 160°C, 30Hz after 120 minutes) and with the utilization of 9%UMO even in the presence of 20%CRM, the 3D internal network structure is disrupted.

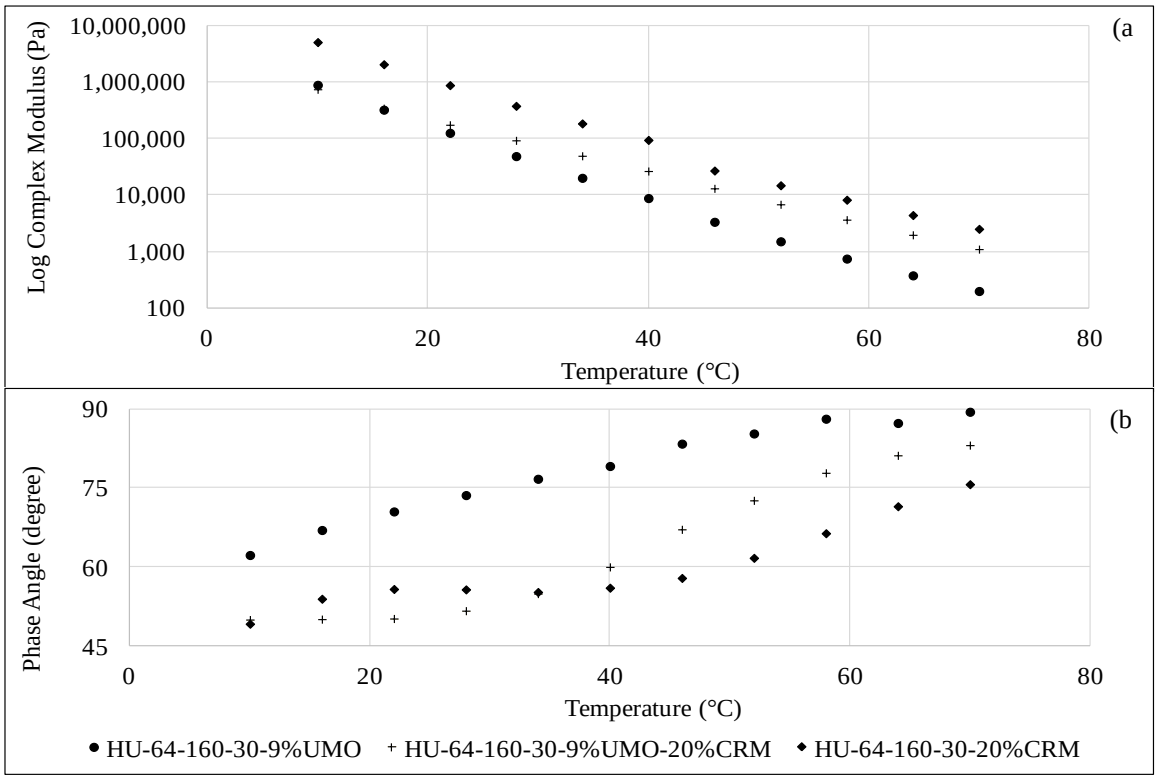

Figure 9.2. Temperature sweep viscoelastic properties for rheological properties (a) G* and (b) δ, for the samples interacted at 160°C, 30Hz after 120 minutes with 9% UMO and/or 20% CRM.

As the case for asphalts modified with 3%UMO (illustrated in Figure 9.1), addition of 9%UMO only to the asphalt resulted in the absence of plateau behavior, indicating that the presence of UMO modifier alone can't initiate the formation of such 3D internal network structure.

Figure 9.3 shows the temperature sweep viscoelastic properties for rheological properties (a) G* and (b) δ for the samples interacted at 190°C and 30Hz with 3% UMO, 10% CRM, or both modifiers after 120 minutes of interaction time, respectively.

Results in Figure 9.3(a) show similarity with the results of the samples interacted at 160°C and 30Hz illustrated in Figure 9.1(a).

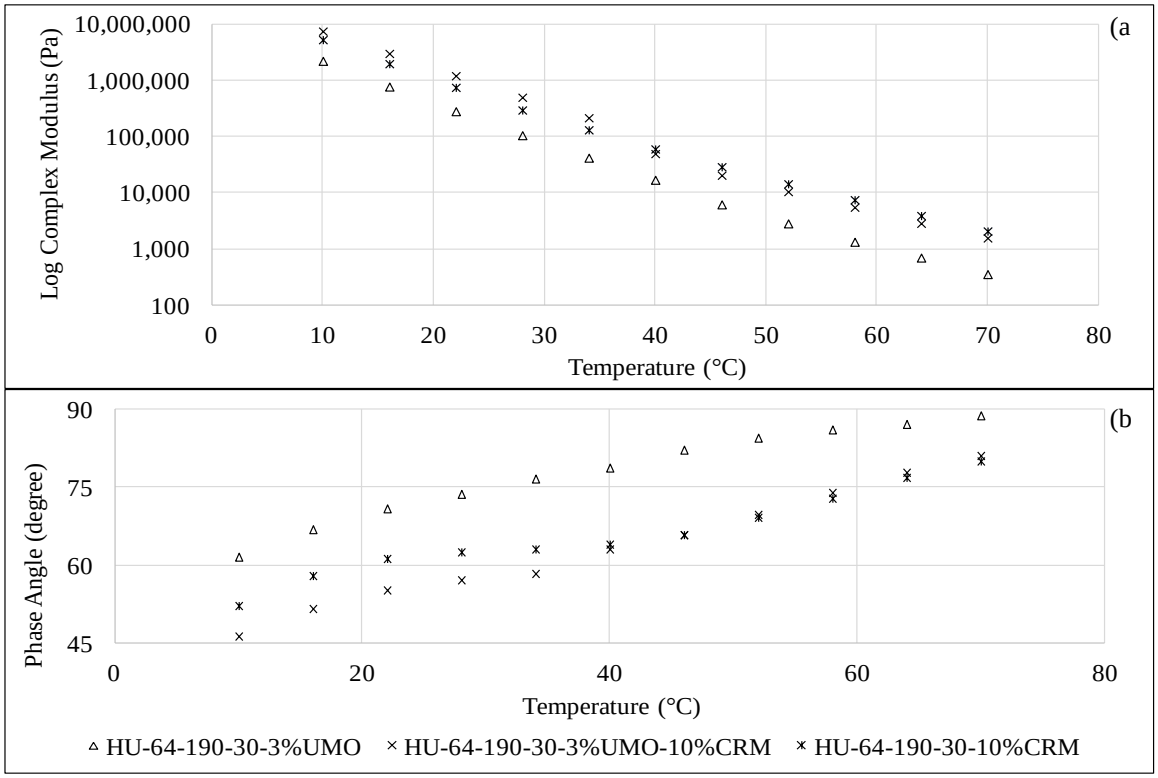

Figure 9.3. Temperature sweep viscoelastic properties for rheological properties (a) G* and (b) δ, for the samples interacted at 190°C, 30Hz after 120 minutes with 3% UMO and/or 10% CRM.

On the other hand, results in Figure 9.3(b) show lower values for the δ at lower testing temperature, indicating better ealsticity. In addition, the plateau behavior for the samples interacted with 10%CRM and 3%UMO at 190°C and 30Hz showed a stronger trend over those interacted at 160°C and 30Hz (illustrated in Figure 9.1 (b)) for the same interaction time (120 minutes). This indicates that the released components of the CRM in asphalt, in the presence of UMO, at interaction conditions of 190°C and 30Hz are more capable of forming 3D internal network structure in the asphalt matrix.

Figure 9.4 shows the temperature sweep viscoelastic properties for rheological properties (a) G* and (b) δ for the samples interacted at 190°C, 30Hz with 9% UMO, 20% CRM, or both modifiers after 120 minutes of interaction time, respectively.

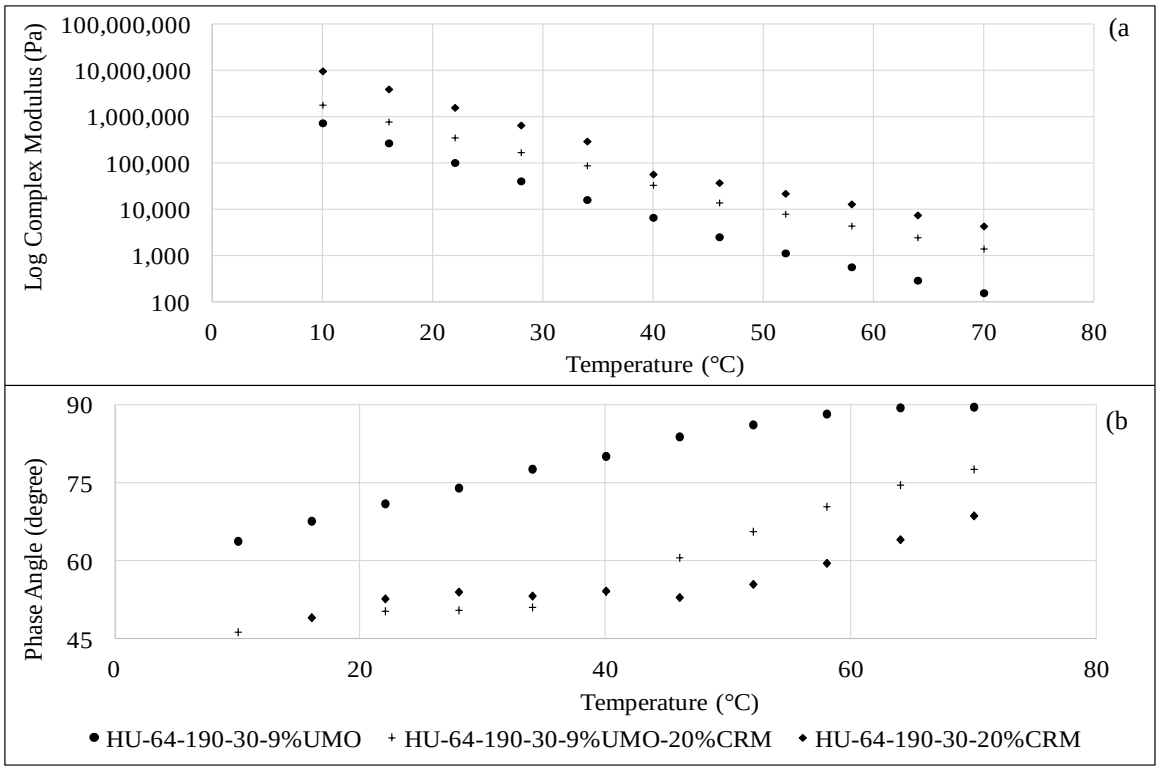

Figure 9.4. Temperature sweep viscoelastic properties for rheological properties (a) G* and (b) δ, for the samples interacted at 190°C, 30Hz after 120 minutes with 9% UMO and/or 20% CRM.

Figure 9.4 (a), indicates that the G* values of the samples having 9%UMO are of lower values, in contrast with the samples with 20%CRM or 20%CRM+9%UMO.

As can be seen from Figure 9.4 (b), the behavior of the samples with 20% CRM and 9 % UMO interacted at 190°C and 30Hz shows a stronger plateau trend over those with the same modifiers that are interacted at 160°C and 30Hz (illustrated in Figure 9.2(b) for the same interaction time of 120 minutes. This indicates that in the presence of both UMO and CRM the utilization of interaction conditions of 190°C and 30Hz as compared to 160°C and 30Hz results in better modifying the internal structure of the asphalt as expressed in stronger plateau behavior indicating better formation for the 3D internal network structure.

Effect of UMO and CRM on the Internal Structure of Asphalt Liquid Phase

Figure 9.5 illustrates the rheological properties; (a) Complex modulus (G*) and (b) phase angle (δ) for the samples interacted at 160°C with 3%UMo, 10%CRM or both modifiers. As shown in the Figure, the addition of 3% UMO to the asphalt resulted in deterioration in both the G* and δ. On the other hand, upon the utilization of 10% CRM only, enhancement in both the G* and δ was observed. The combined use of 10% CRM and 3% UMO had a plateau effect for both the G* and δ values, but with values tending to slightly deteriorate at the end of interaction time (120 minutes). On the other hand, the addition of UMO only to asphalt resulted in the disturbance of the asphalt's continuous three-dimensional associations leading to the observed deterioration in both G* and δ for the sample modified with 3% UMO only.

Figure 9.6 (a and b) illustrates the rheological properties (G*) and (δ) for the samples interacted at 160°C with 9% UMO, 20% CRM, or both modifiers, respectively. A marked difference can be seen in the enhancement of both rheological parameters (G* and δ) for the sample with 20% CRM; this is due to the swelling of CRM before removal of the CRM particles from the liquid phase [133]. In addition, for the sample with 20% CRM and 9% UMO, deterioration can be observed after 30 minutes of interaction time in both rheological parameters and continues until the end of the interaction time (120 minutes).

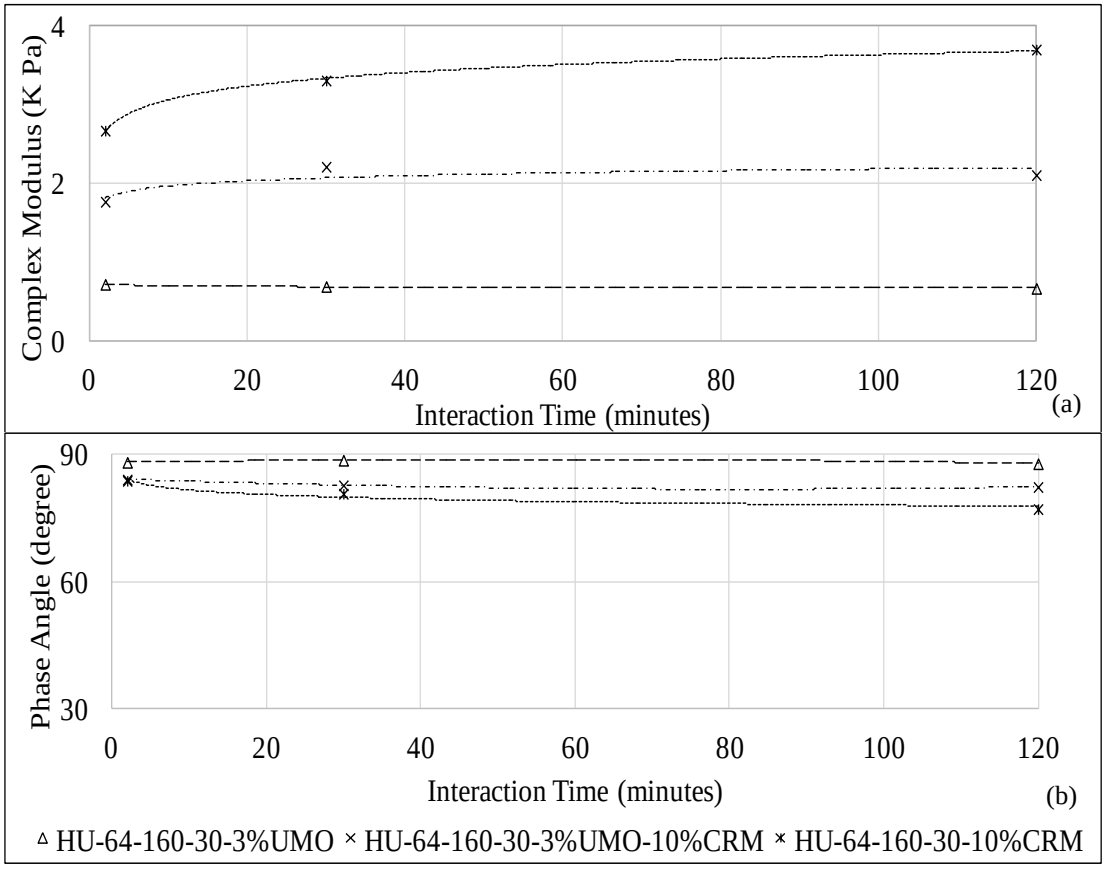

Figure 9.5. Rheological properties of the samples interacted with 3% UMO, 10% CRM, or both at 160C and 30Hz: (a) G* and (b) δ

This can result from the increased amount of UMO (9%) that significantly disturbed the asphalt's continuous three-dimensional associations, even in the presence of 20% CRM. This behavior of severe deterioration in both G* and δ was largely manifested in the sample with 9% UMO only.

Figure 9.7 illustrates the rheological properties; (a) Complex modulus (G*) and (b) phase angle (δ) for the samples interacted at 190°C with 3% UMO, 10% CRM, or both modifiers.

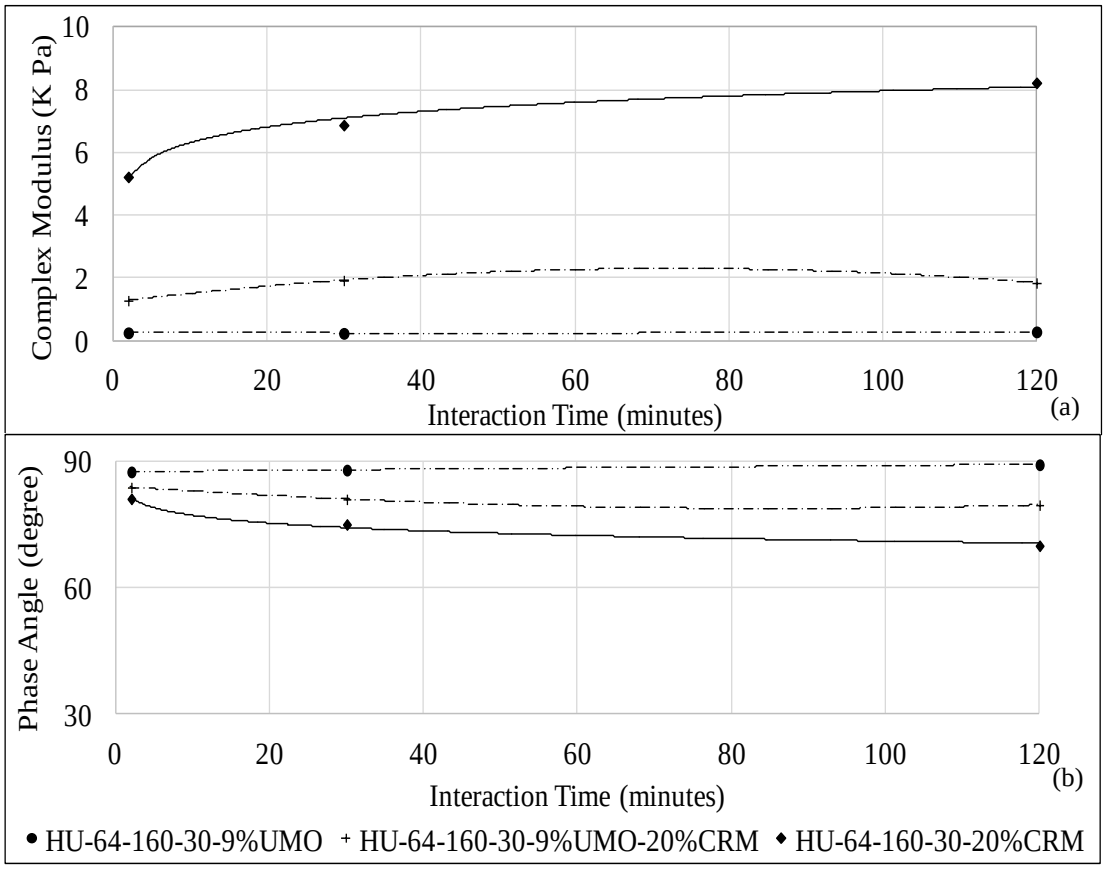

Figure 9.6. Rheological properties of the samples interacted with 9% UMO, 20% CRM or both at 160°C and 30Hz: (a) G* and (b) δ

A distinctive behavior can be seen for the samples with 10% CRM and 3 % UMO. There is continuous enhancement in both the G* and δ alongside the interaction time. Similar enhancements, with higher extent, can be seen for the sample with 10% CRM only. At such combination of moderate interaction temperature (190°C) and mixing speed (30 Hz) the interaction of CRMA. This is due to the occurrence of devulcanization processes of CRM that lead to the release of CRM components into the liquid phase of asphalt. This results in enhancements in the network structure of the CRMA whether UMO is present or not. On the other hand, the use of 3% UMO only resulted in deterioration in both the G* and δ as a result of the disturbance of the network structure of asphalt, as explained earlier.

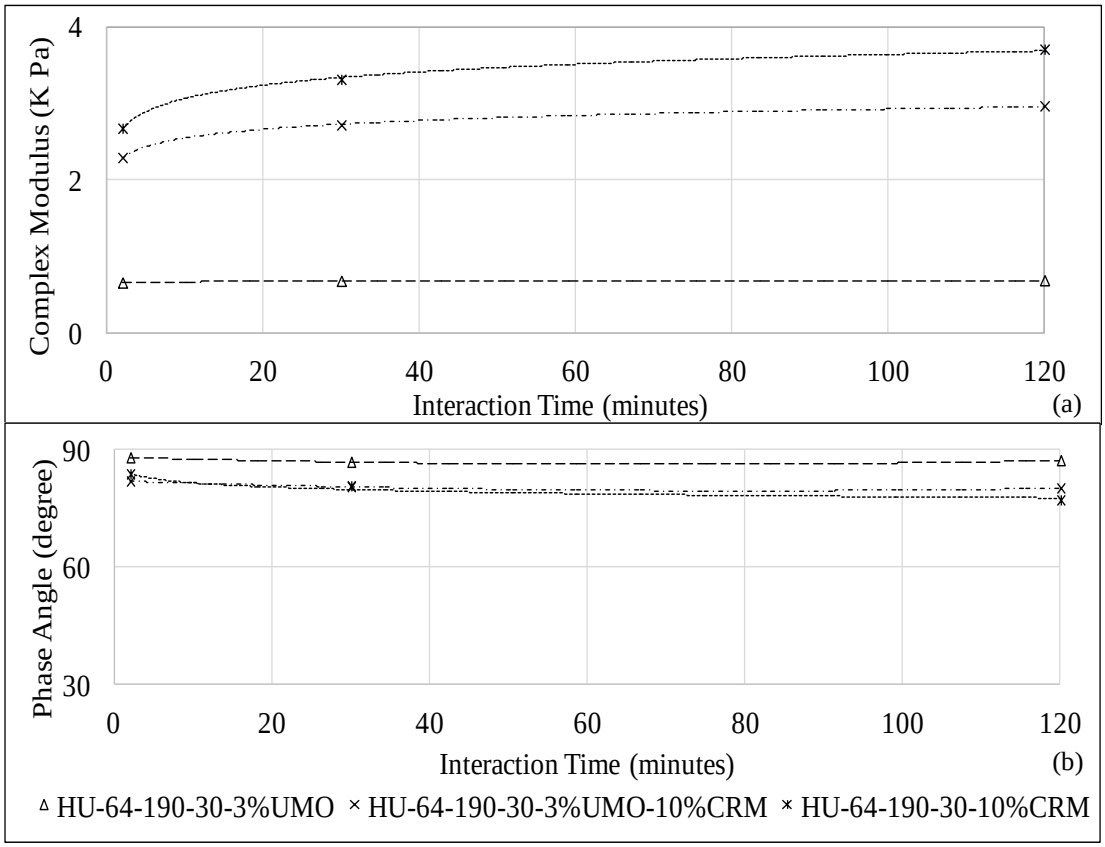

Figure 9.7. Rheological properties of the samples interacted with 3% UMO, 10% CRM or both at 190°C and 30Hz: (a) G* and (b) δ

Figure 9.8 (a and b) illustrates the rheological properties (G*) and (δ) for the samples interacted at 190°C with 9% UMO, 20% CRM, or both modifiers, respectively.

As shown previously for the sample interacted at 160°C, a marked difference can be seen in the enhancement of both rheological parameters (G* and δ) for the sample with 20% CRM; this is due to the swelling of CRM particles before their removal from the liquid phase as well as the occurrence of devulcanization at such interaction temperature (190°C) [122]. In addition, for the sample with 20% CRM and 9% UMO, unlike the behavior for the samples at 160°C, enhancements can be observed after 30minutes of interaction time in both rheological parameters and continue through the end of the interaction time (120 minutes). On the other hand, severe deterioration in both G* and δ was largely manifested in the sample with 9% UMO only.

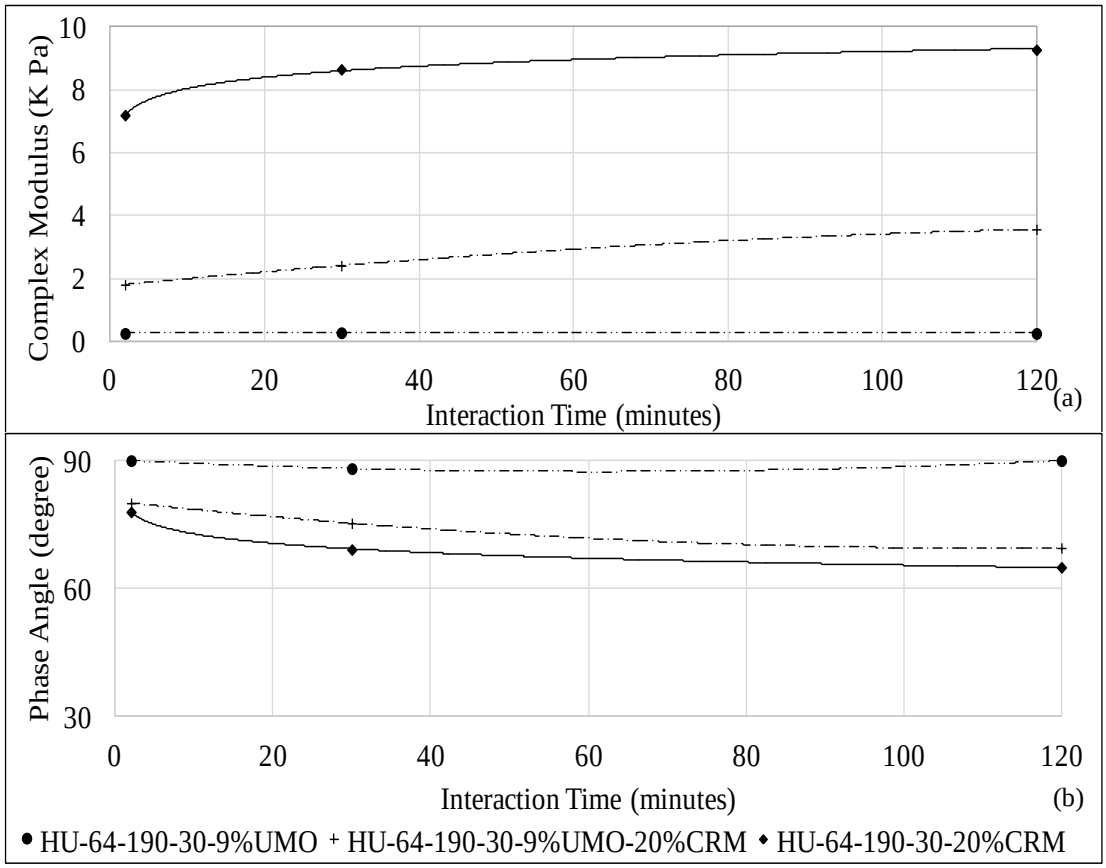

Figure 9.8. Rheological properties of the samples interacted with 9% UMO, 20% CRM or both at 190°C and 30Hz: (a) G* and (b) δ

Figure 9.9 illustrates the temperature sweep viscoelastic properties of the liquid phase for rheological properties (G*) and (δ) for the samples interacted at 160°C with 3% UMO, 10% CRM, or both modifiers after 120 minutes of interaction time, respectively.

In Figure 9.9, results show agreement with other studies which have shown that the CRM modification of asphalt mainly affects its high temperature properties and by decreasing the testing temperature the changes in physical properties reduce to a marginal level [4]. Results in Figure 9.9(b) show that the behavior of the δ lacks the presence of a plateau behavior, indicating lack of network structure in the liquid phase of modified asphalts [119, 134].

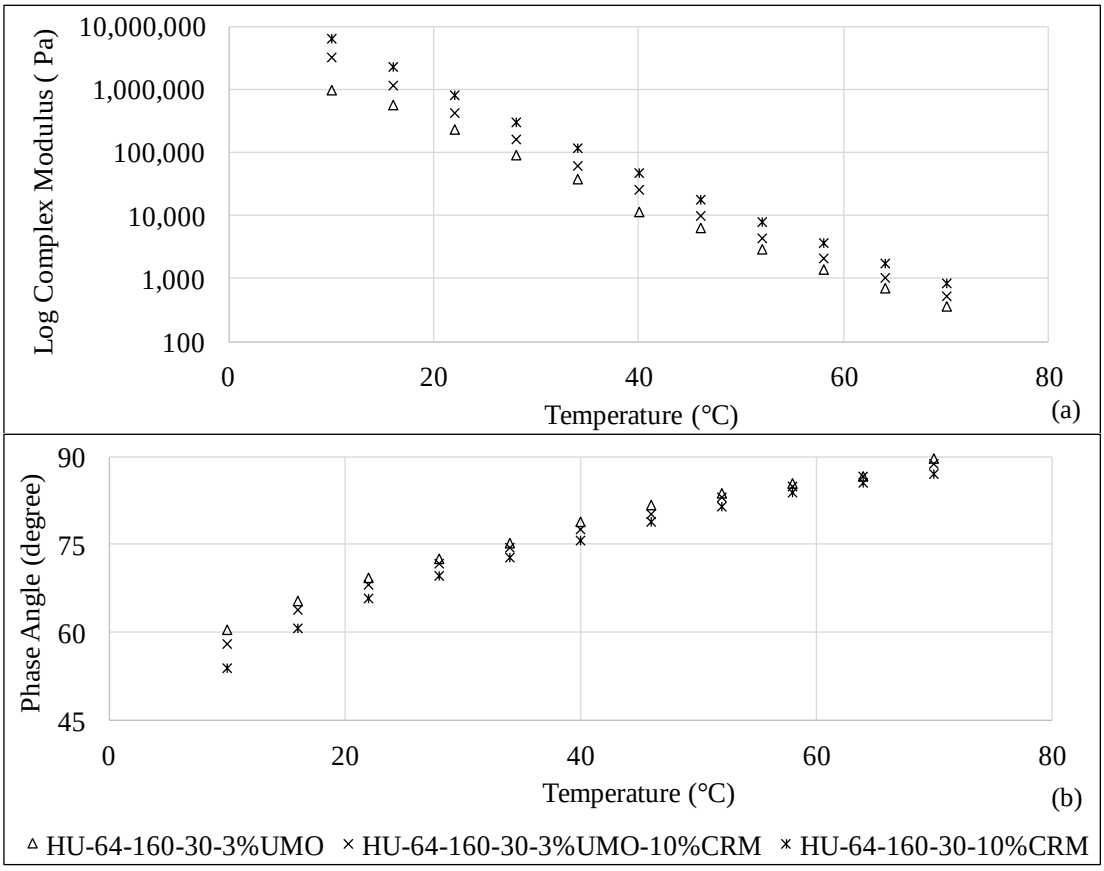

Figure 9.9. Temperature Sweep Viscoelastic Properties of Liquid Phase samples interacted with 3% UMO, 10% CRM or both at 160°C and 30Hz: (a) G* and (b) δ

Figure 9.10 shows the temperature sweep viscoelastic properties of liquid phase for rheological properties (G*) and (δ) for the samples interacted at 160°C with 9% UMO, 20% CRM, or both modifiers after 120 minutes of interaction time, respectively. It can be seen from the Figure that the behavior of the samples with UMO is almost similar with or without CRM addition. This

indicates that the addition of the UMO significantly annihilated the network associations within the modified asphalt liquid phase.

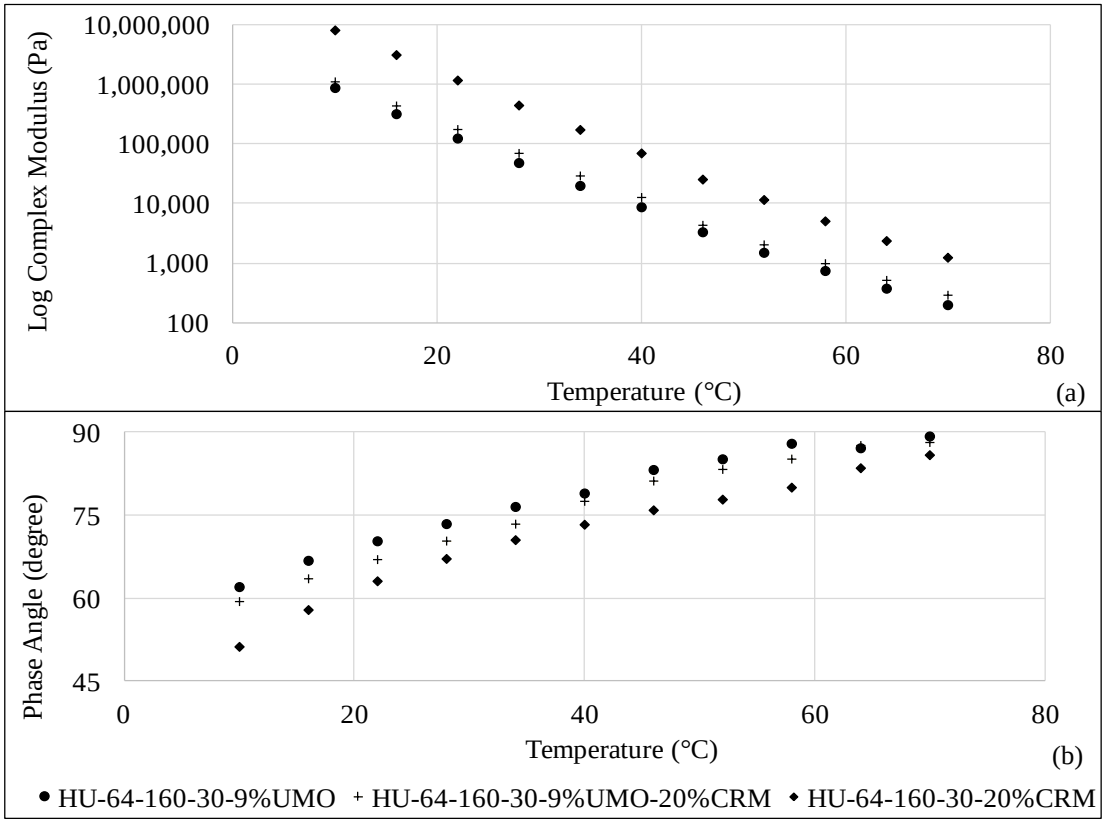

Figure 9.10. Temperature Sweep Viscoelastic Properties of Liquid Phase samples interacted with 9% UMO, 20% CRM or both at 160°C and 30Hz: (a) G* and (b) δ

Figure 9.11 shows the temperature sweep viscoelastic properties of the liquid phase for rheological properties (G*) and (δ) for the samples interacted at 190°C with 3% UMO, 10% CRM, or both modifiers after 120 minutes of interaction time, respectively. Results in Figure 9.11(b) show a distinctive behavior. Where, similarity can be observed between the behavior of both samples with 10% CRM only or 10% CRM and 3% UMO between 20°C and after 50°C. This indicates that the released components of the CRM in asphalt, in the presence of UMO, at certain interaction temperature (190°C and 30Hz) are capable of forming internal network in the asphalt matrix. The effect of such network was previously manifested by the enhancement in

both G* and δ values of such sample as compared to the sample with 10% CRM only (illustrated in Figure 9.7(a, b)).

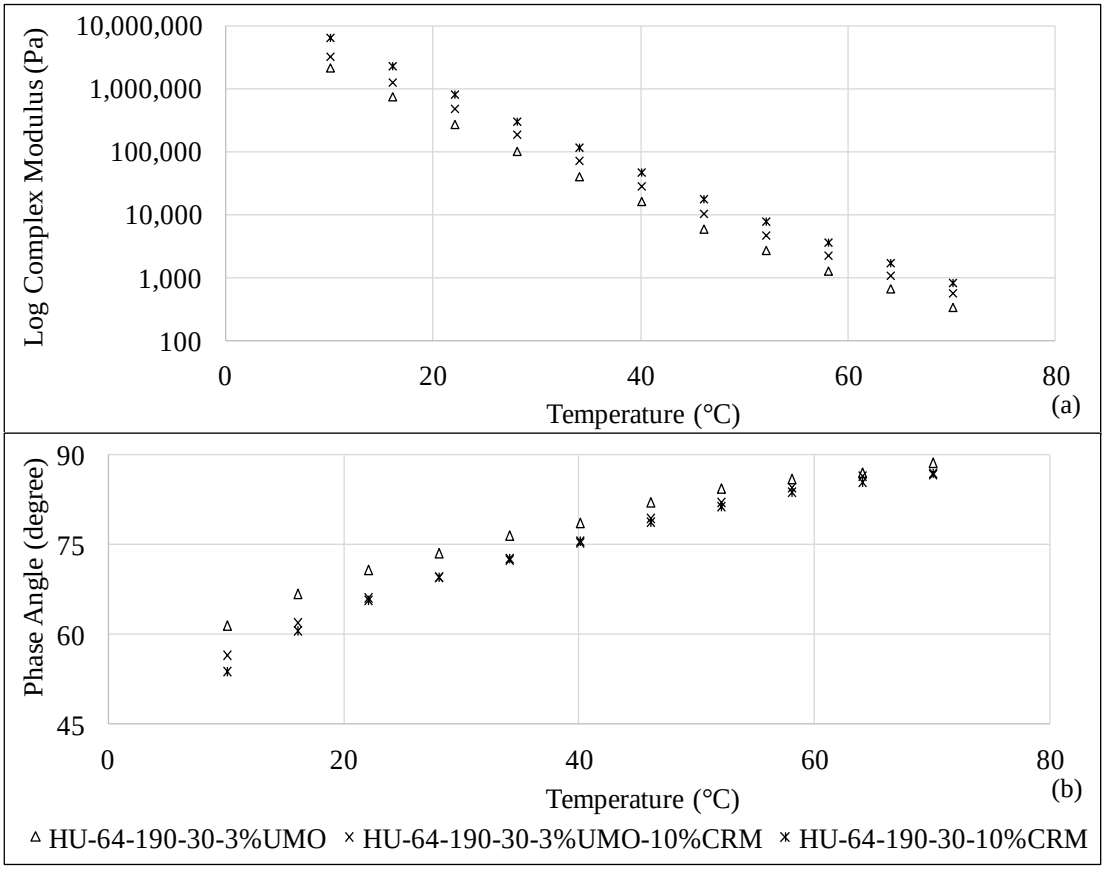

Figure 9.11. Temperature Sweep Viscoelastic Properties of Liquid Phase samples interacted with 3% UMO , 10% CRM or both at 190°C and 30Hz: (a) G* and (b) δ

Figure 9.12 shows the temperature sweep viscoelastic properties of liquid phase for rheological properties (G*) and (δ) for the samples interacted at 190°C with 9% UMO, 20% CRM, or both modifiers after 120 minutes of interaction time, respectively.

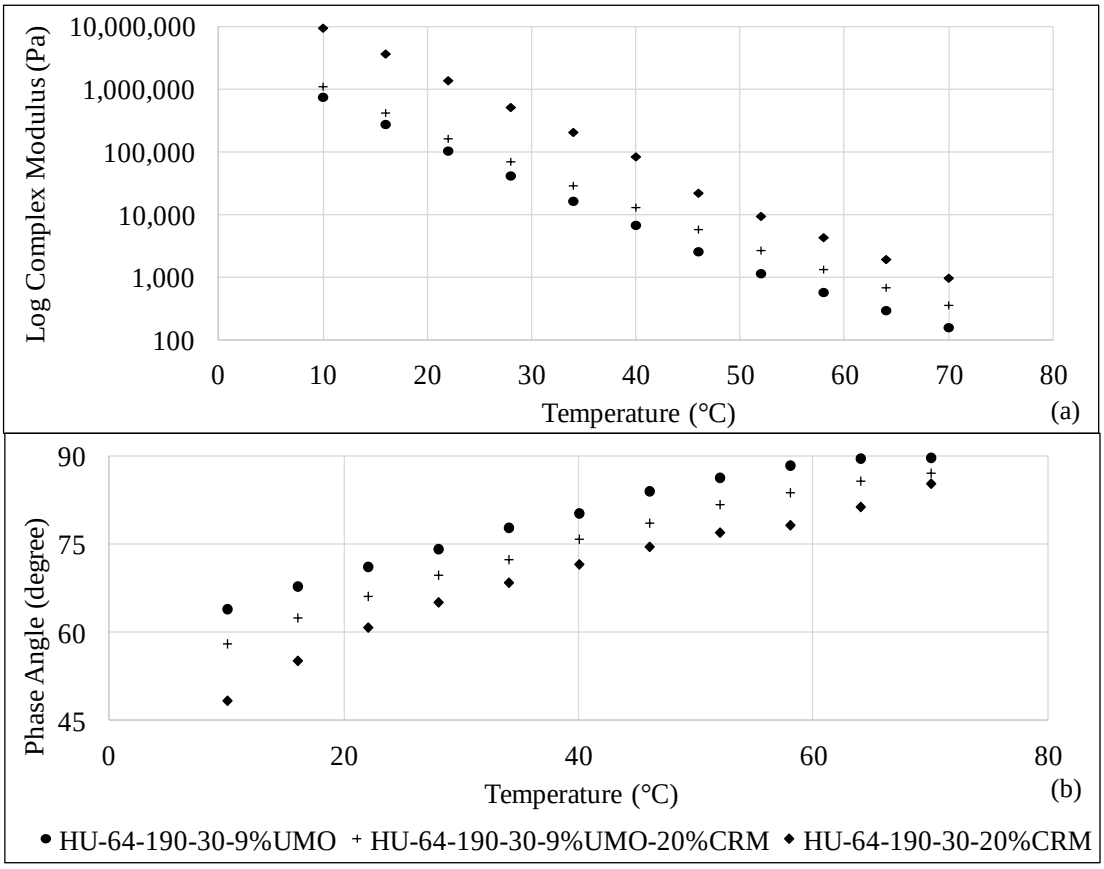

Figure 9.12. Temperature Sweep Viscoelastic Properties of Liquid Phase samples interacted with 9% UMO, 20% CRM or both at 190°C and 30Hz: (a) G* and (b) δ

Figure 9.12 (a), indicates that the G* values of the samples having UMO, either with or without CRM, are of similar values, in contrast with the samples with CRM only. As can be seen from Figure 9.12 (b), the behavior of the samples with 20% CRM and 9% UMO shows an intermediate trend between those that have 20% CRM only and those that contain 9% UMO only.

Effect of UMO and CRM on the Micromechanical Properties of Asphalt Liquid Phase

In this section the effect of UMO on the micromechanical properties of CRMA is carried out. This provides an important insight with regards to simulating the behavior of thin asphalt film as that laid on aggregate surface during mixing and compaction of HMA.

Figure 9.13 illustrates (a) the force vs. indentation depth profiles and (b) comparison of hardness and elastic modulus for the samples interacted at 160°C with 3% UMO, 10% CRM, or both modifiers, after 120 minutes of interaction time.

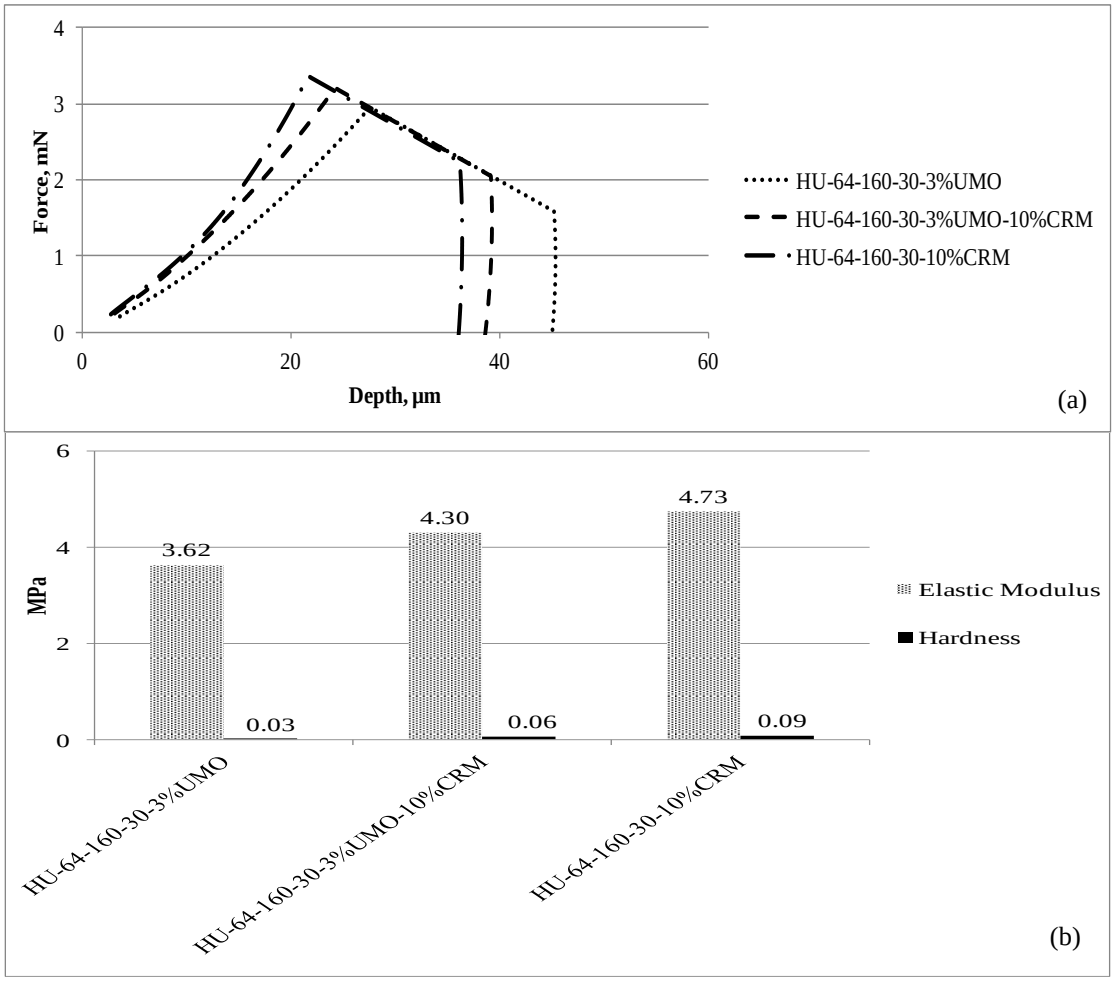

Figure 9.13. Micromechanical behavior of samples interacted at 160°C and 30Hz with 3% UMO, 10% CRM or both at 120 minutes interaction time: a) Force vs indentation depth profile, (b) Comparison of hardness and elastic modulus

As can be seen from Figure 9.13 (a), the max load values show a continuous decrease during the dwell time, similar observations were recorded in the literature for the indentation of asphalt [89]. This was explained in terms of the decrease in contact area due to delayed (viscous) flow of asphalt binders at the indentation location [89]. Another reason is the minute scale load

carrying capacity of the asphalt binders and binder softening which results in it being virtually impossible to keep the maximum applied load constant [89]. For the sample with only 3% UMO, the indentation depth was about 45 µm. For the sample with 10% CRM and 3% UMO the indentation depth was about 38 µm. However, upon utilizing 10% CRM only, further reduction in the indentation depth was recorded.

Figure 9.13 (b) shows the hardness and elastic modulus values for the same samples. As shown in Figure 9.13 (b), a continuous increase in both the hardness and elastic modulus can be seen with the utilization of CRM with oil in asphalt and with CRMA only. The elastic modulus of samples was 3.62, 4.3, and 4.73Mpa, for the asphalt samples modified with 3% UMO, 3% UMO with 10% CRM, and 10% CRM, respectively. On the other hand, the hardness of the samples was 0.03, 0.06, and 0.09 MPa. This indicates that at such a combination of interaction temperature (160°C) and interaction speed (30Hz) the increase in the elastic modulus values occurs gradually with addition of CRM, whereas for the hardness, a major increase occurs when CRM is added to asphalt with UMO (almost double the values). This could be as a result of the higher absorption of the low molecular weight aromatics of asphalt by the CRM that lead to stiffer binder [22].

Figure 9.14 illustrates (a) the force vs. indentation depth profiles and (b) comparison of hardness and elastic modulus for the samples interacted at 160°C with 9% UMO, 20% CRM, or both modifiers after 120 minutes of interaction time.

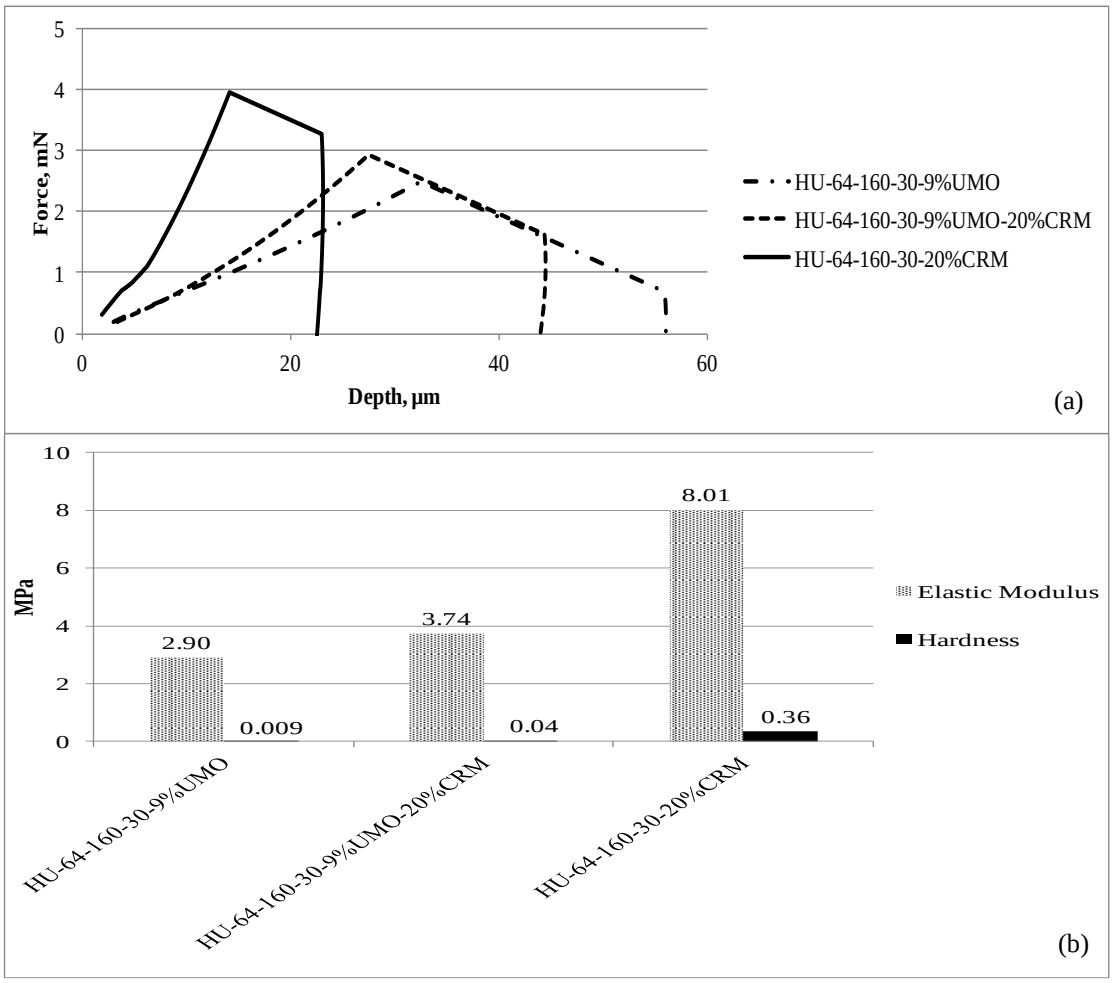

Figure 9.14. Micromechanical behavior of samples interacted at 160°C and 30Hz with 9% UMO, 20% CRM or both at 120 minutes interaction time: a) Force vs indentation depth profile, (b) Comparison of hardness and elastic modulus.

Figure 9.14 (a) shows a different trend than the samples interacted at 160°C with 30Hz with 3% UMO and 10% CRM. For the samples with 9% UMO only, the indentation depth is about 55 µm. However, upon addition of 20% CRM, a steep decrease in the indentation depth ranging around 45 µm is observed. On the other hand, for the samples with 20% CRM, the indentation depth was almost 23 µm. As illustrated in Figure 9.14 (b), an increase in both the hardness and elastic modulus values is evident after the addition of CRM. The elastic modulus was 2.9 MPa for the sample with 9% UMO and increased to 3.74, and 8.01MPa, for the samples

modified by 9% UMO with 20% CRM, and 20% CRM, respectively. The same trend was seen for the hardness values that were 0.009, 0.04, and 0.36 MPa, for the aforementioned samples.

Figure 9.15 illustrates (a) the force vs. indentation depth profiles and (b) comparison of hardness and elastic modulus for the samples interacted at 190°C with 3% UMO, 10% CRM, or both modifiers after 120 minutes of interaction time.

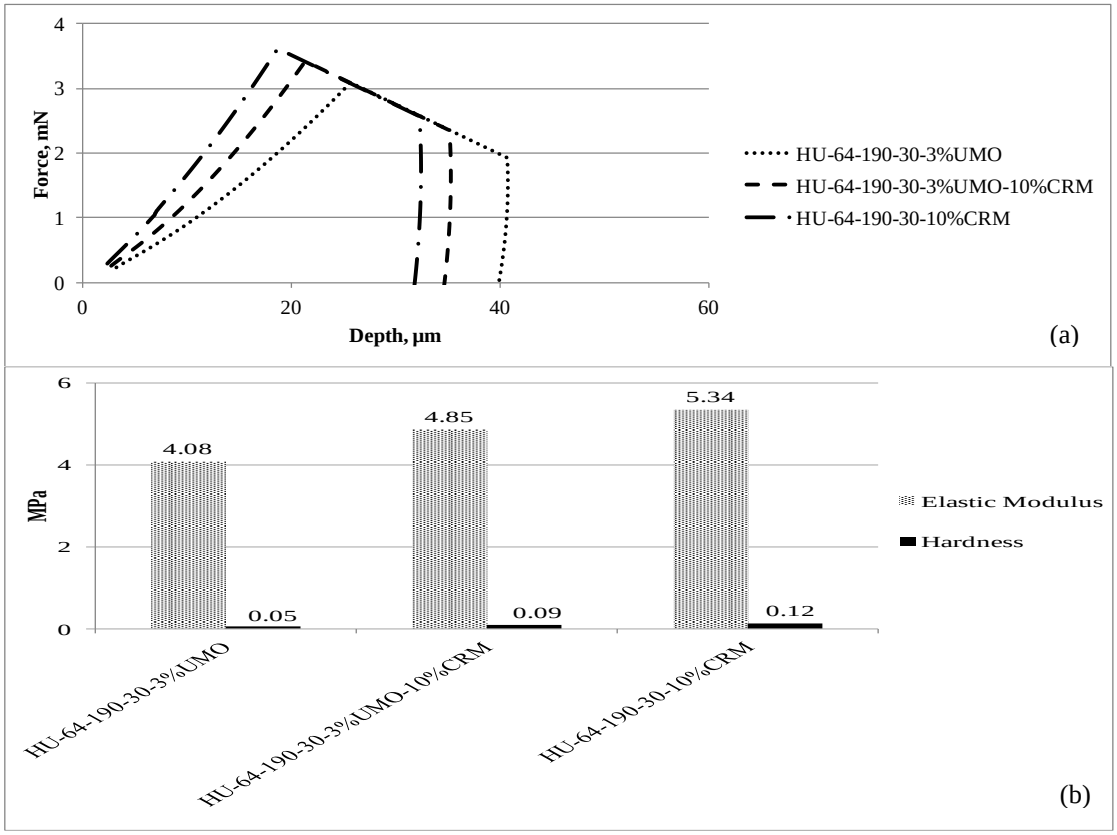

Figure 9.15. Micromechanical behavior of samples interacted at 190°C and 30Hz with 3% UMO, 10% CRM or both at 120 minutes interaction time: a) Force vs indentation depth profile, (b) Comparison of hardness and elastic modulus.

Figure 9.15 (a) shows a similar trend to the samples interacted at 160°C with 30 Hz with 3% UMO and 10% CRM. For the samples with 3% UMO only, the indentation depth is about 40 µm. However, upon addition of 10% CRM, we observe a minor decrease in the indentation depth to be about 35 µm. On the other hand, for the samples with 10% CRM, the indentation depth was

almost 30 µm. As illustrated in Figure 9.15 (b), an increase in both the hardness and elastic modulus values is evident after the addition of CRM. The elastic modulus was 4.08 MPa for the sample with 3% UMO and increased to 4.85, and 5.34 MPa, for the samples modified by 3% UMO with 10% CRM, and 10% CRM, respectively. The same trend was seen for the hardness values that were 0.05, 0.09, and 0.12 MPa, for the aforementioned samples. It should be noticed that, upon increasing the interaction temperature from 160°C to 190°C, and with the utilization of 10% CRM with 3% UMO, the values of the hardness and elastic modulus show enhancement for the same sample conditions. This is direct result of the development in the asphalts internal structure that was proven in the temperature sweep section.

Figure 9.16 illustrates (a) the force vs. indentation depth profiles and (b) comparison of hardness and elastic modulus for the samples interacted at 190°C with 9% UMO, 20% CRM, or both modifiers after 120 minutes of interaction time.

Figure 9.16 (a) shows a different trend from that seen in the samples interacted at 190°C with 30 Hz with 3% UMO and 10% CRM. For the samples with 9% UMO only, the indentation depth is about 45 µm. However, upon addition of 20% CRM, we observe almost no change in the indentation depth ranging around 45 µm. On the other hand, for the samples with 20% CRM, the indentation depth was almost 20 µm. As illustrated in Figure 9.16 (b), a decrease in both the hardness and elastic modulus values is evident after the addition of CRM for the samples with UMO. The elastic modulus was 3.71 MPa for the sample with 9% UMO and decreased to 3.6, for the samples modified by 9% UMO with 20% CRM. However, a major increase in the elastic modulus (9.18 MPa) was recorded for the samples with 20% CRM only. The same trend was seen for the hardness values that were 0.004, 0.03, and 0.48 MPa, for the aforementioned samples.

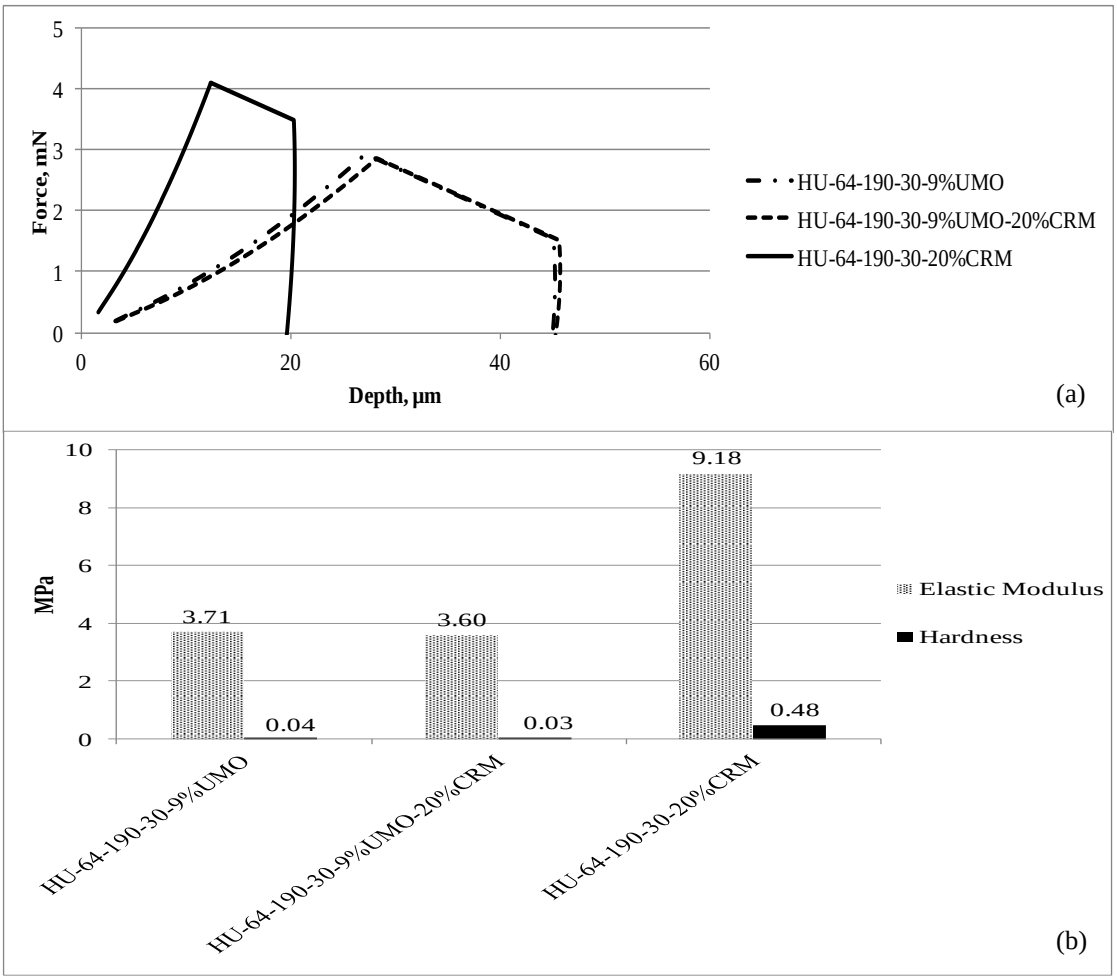

Figure 9.16. Micromechanical behavior of samples interacted at 190°C and 30Hz with 9% UMO, 20% CRM or both at 120 minutes interaction time: a) Force vs indentation depth profile, (b) Comparison of hardness and elastic modulus.

Effect of UMO and CRM on the Short Term Aging Behavior of Asphalt (Rutting Susceptibility)

Starting this section and the following two sections, we will be investigating samples interacted at 190°C and 30Hz. In this section the short term aging (simulating the aging during mixing and compaction of HMA) in investigated.

Figure 9.17 shows the behavior of the rutting parameter (G*/sin δ) for the (a) unaged and (b) Rotating Thin Film Oven (RTFO) aged residue of unmodified HU-64 samples compared to samples modified with 3%UMO only, 10%CRM only, and 3%UMO+10%CRM. In this Figure all samples were interacted up to 120 minutes.

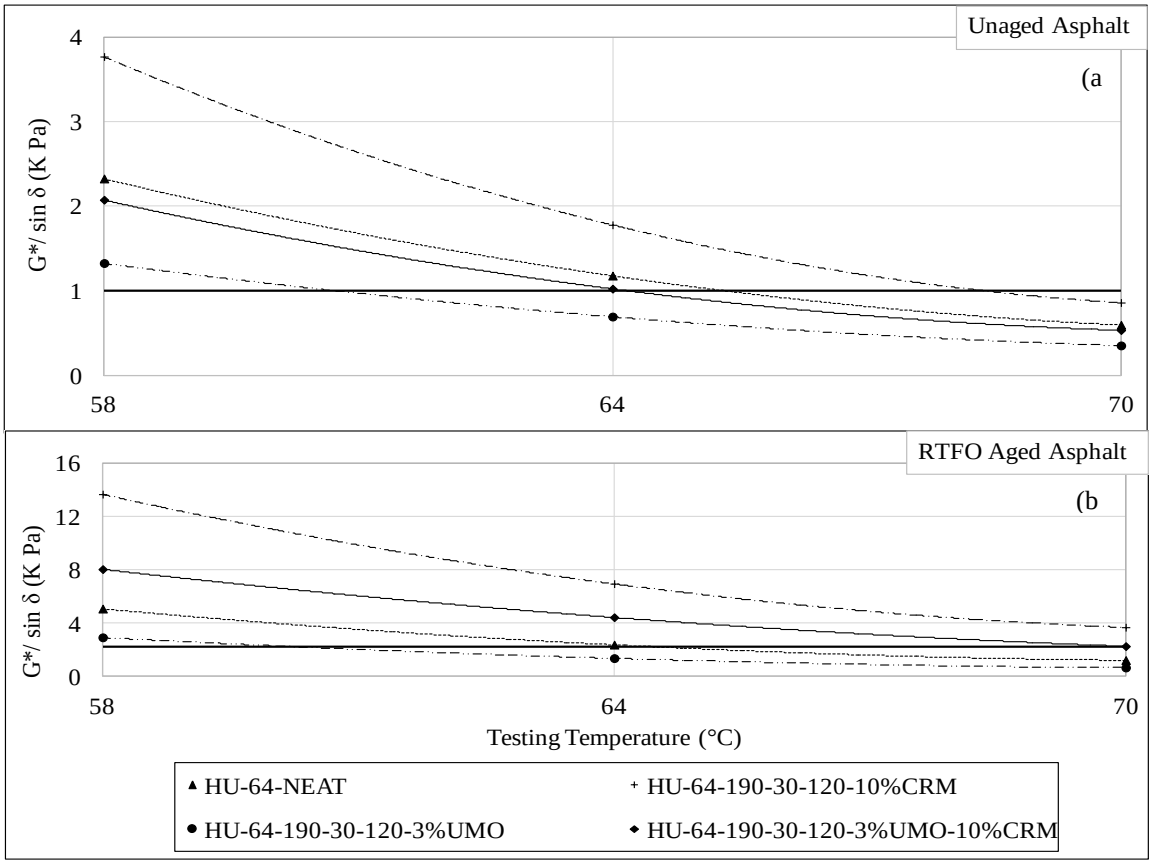

Figure 9.17. Effect of UMO and/or CRM on (a) unaged and (b) short term aging behavior of asphalt.

The PG grading system mandates that the rutting parameter (G*/ sinδ) is above 1 KPa for unaged asphalt and 2.2 KPa for RTFO aged asphalt (Horizontal black lines) at temperature of

64°C for the asphalt utilized in this research work (PG 64-22). As shown in Figure 9.17(a) for the unaged samples, the highest values for G*/sin δ were observed for the samples mixed with 10%CRM. However, both the neat and samples modified with 3%UMO and 10%CRM fulfilled the requirement. Similarly, for the RTFO aged residue samples, illustrated in Figure 9.17(b), the best enhancement in the rutting resistance behavior is attributable to the sample having CRM only. However, it can be seen from the Figure that the sample with both 10%CRM and 3%UMO was well above the 2.2 KPa PG grading requirement at 64°C testing temperature, while it was just at that values for the 70°C testing temperature. On the other hand, the sample modified with UMO only suffered deterioration of its rutting resistance parameter (G*/sin δ<2.2KPa) at 64°C.

Effect of UMO and CRM on the Long Term Aging Behavior of Asphalt (Fatigue Cracking Susceptibility)

Figure 9.18 shows the behavior of the fatigue parameter (G*. sin δ) for the Pressure Aging Vessel (PAV) residue of PG 64-22 neat asphalt sample compared to samples modified with 3%UMO only, 10%CRM only, and 3%UMO+10%CRM.

The samples were interacted at an interaction temperature of 190°C with 30Hz interaction speed. In this Figure all samples were interacted up to 120 minutes. The PG grading system mandates that the fatigue cracking parameter (G*. sinδ) is below 5000KPa (Horizontal black line). As illustrated in the Figure, the best enhancement in the long term aging resistance behavior is attributable to the sample having a combination of UMO+CRM. It is expected that the presence of UMO with CRM would lead to the absorption of the light components from the UMO into the CRM. During long term aging and under the effect of temperature, the swelled CRM particles will continue to release components into the asphalts such as antioxidants that

would resist the long term aging of asphalt. In addition, the absence of UMO would lead to the absorption of light aromatic components from the asphalt, leading to the stiffening of asphalt.

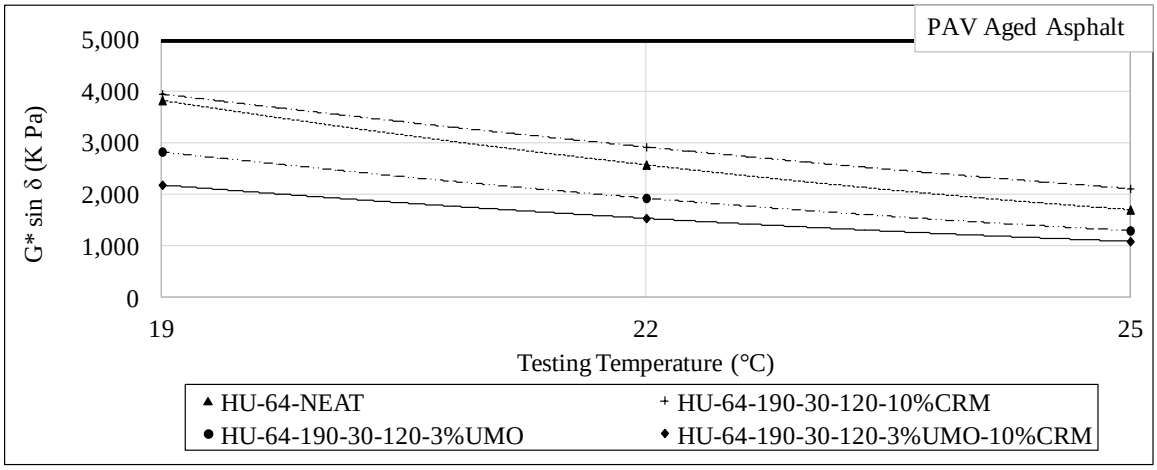

Figure 9.18. Effect of UMO and/or CRM on the long term aging behavior of asphalt.

Effect of UMO and CRM on the Low Temperature Properties of Asphalt (Thermal Cracking Susceptibility)

Figure 9.19 shows the behavior of the thermal cracking parameters (a) m-value and (b) stiffness (S) for the Pressure Aging Vessel (PAV) residue of neat HU-64 asphalt sample compared to samples modified with 3%UMO only, 10%CRM only, and 3%UMO+10%CRM.

The samples were interacted at an interaction temperature of 190°C with 30Hz interaction speed. In this Figure all samples were interacted up to 120 minutes. The PG grading system mandates that the m-value is higher than 0.3 and that S is lower than 300 MPa (Horizontal black lines). As illustrated in Figure 9.19(a), all the tested samples fulfilled the m-value requirements of PG grading system up to -34°C in service temperature. On the other hand, for the S values illustrated in Figure 9.19(b), the neat PG 64-22 asphalt showed deteriorated properties passed its low temperature grade (-22°C) while the asphalts modified with 10%CRM, 3%UMO, or 10%CRM and 3%UMO had acceptable S values up to -28°C in service temperature. As illustrat-

ed in the Figure, the utilization of both 10%CRM and 3%UMO resulted in enhancing the low temperature resistance of the asphalt by one grade (from -22°C to -28°C).

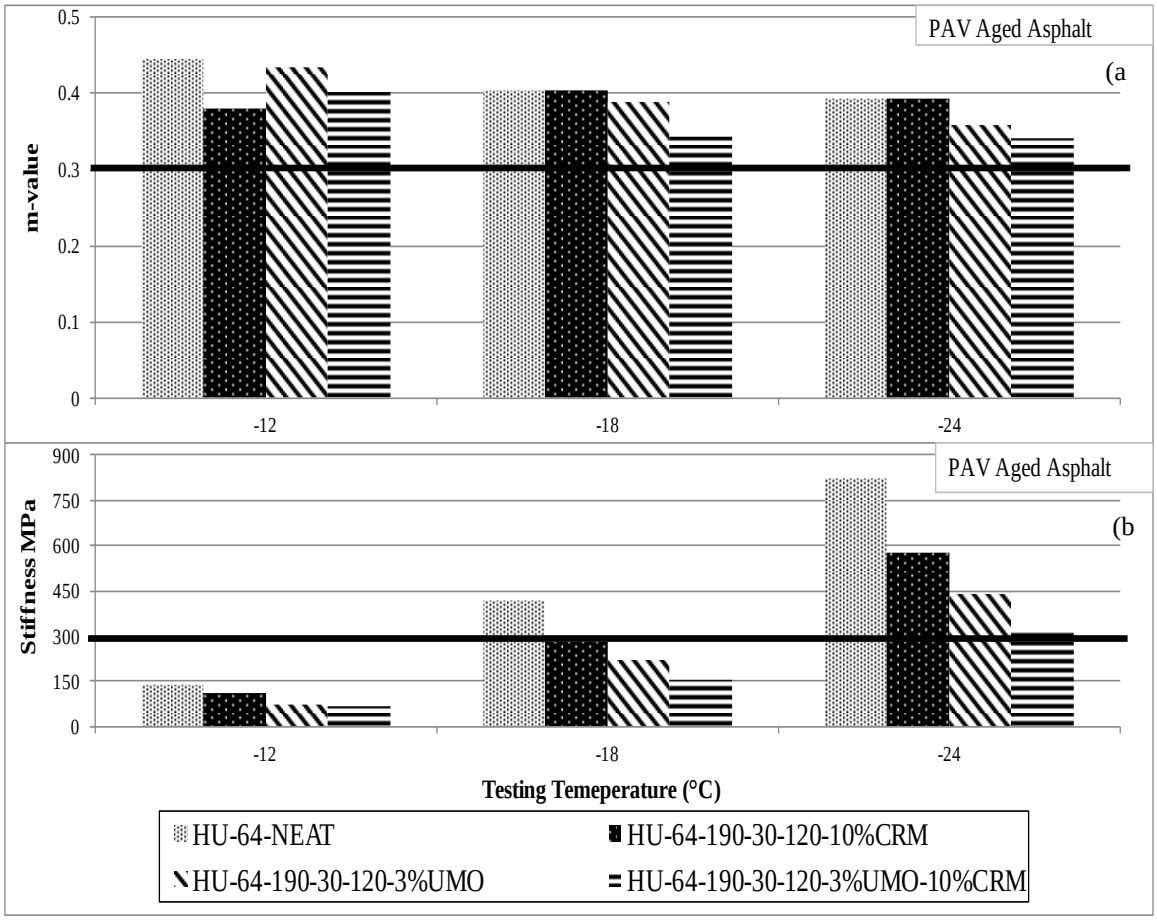

Figure 9.19. Effect of UMO and/or CRM on the low temperature parameters (a) m-value, and (b) S of asphalt.

Effect of UMO on Asphalt Fractions

In the following section we investigated the samples interacted at 160°C with 30°Hz and 190°C with 30°Hz after 2 and 30 minutes of interaction time. Percentages of modifiers were 3%UMO with 10%CRM for the samples interacted at either 160°C and 190°C with 30Hz and 9%UMO with 20%CRM for the samples interacted at 190°C with 30°Hz only.

Figure 9.20 illustrates the change in the asphalt fractions; asphaltene, saturates, naphthene aromatics and polar aromatics as a result of modification with UMO and CRM. Figure 9.20 shows that most of the components of UMO fall in the category of saturates. As illustrated in the Figure also, gradual increase in the asphaltene is associated with the addition of UMO and CRM, regardless of the interaction temperature and time. In addition, UMO and CRM lead to increase in saturates at low interaction temperature (160°C) or high UMO (9%) and CRM (20%) values at high interaction temperature (190°C). Continuous decrease in the Naphthene aromatics is associated with the addition of UMO and CRM. Polar aromatics appear to decrease with the high percentage of UMO and CRM.

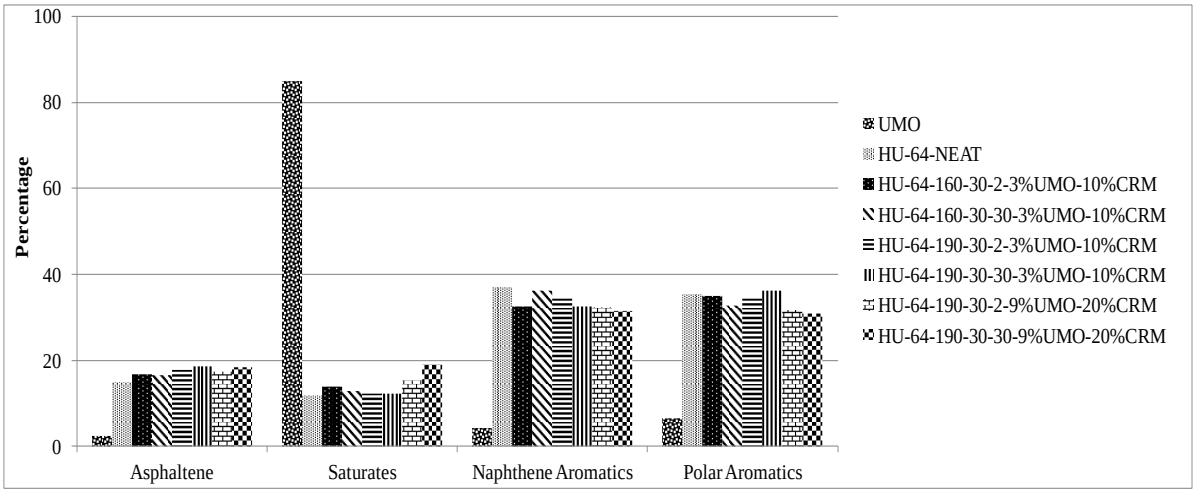

Figure 9.20. Effect of UMO and/or CRM on the four fractions of asphalt.

CHAPTER TEN. CONCLUSIONS AND RECOMMENDATIONS

Conclusions

In this research work, the existence of a 3D network structure in the liquid phase of CRMA was verified. The formation of a 3D network structure in the CRMA plays a major role in the enhancement of its rheological properties in terms of its stiffness and elasticity. Enhancements in the CRMA stiffness and elasticity provide improved rutting resistance as well as alleviated permanent deformation problems. GPC was found to be an efficient approach capable of directly relating the CRMA property enhancement (G* development) to its internal structure. The utilization of GPC and rheological testing can be employed to verify the existence of the 3D network structure in the liquid phase of CRMA. The existence of 3D network structure within the liquid phase of the CRMA has been proven to be dependent on the interaction parameters involved in the synthesis of the modified binder. The combination of moderate interaction temperature (190ºC) and high interaction speed (50Hz) was found to trigger, initiate and sustain the formation of the 3D network structure within the CRMA. A lower interaction temperature (160ºC) was not sufficient to trigger the formation of the 3D network structure even at a mixing speed of 50Hz. A higher interaction temperature of 220ºC resulted in having depolymerization and devulcanization as governing process resulting in deterioration of the modified binder rheological properties.

In the current research work, the utilization of rheological, TGA, and FTIR tests to investigate the nature of CRM components responsible for the formation of 3D entangled network structure in CRMA was carried out. It was found that; depending on the dissolved amounts and released components of CRM and the CRMA interaction synthesis conditions involved, major enhancements in the CRMA rheological properties, in terms of its stiffness (G*) and elasticity

(δ), can be achieved through the development of 3D entangled network structure in its liquid phase. The combination of moderate interaction temperature (190ºC) and high interaction speed (50Hz) was essential to control the CRM dissolution mechanism leading to the modification on the CRMA internal network structure that resulted in enhanced G* and δ. Interacting the CRMA at 160º and 50Hz resulted in CRMA with deteriorated physical properties as a result of limitation of CRM activities to swelling and minimal release. At 220ºC interaction temperature, CRM depolymerization and devulcanization process were severe resulting in deterioration of the modified binder physical properties.

In this work we introduce a correlation between the different asphalt-CRM attributes as well as synthesis conditions and the performance based behavior of thin asphalt layer over aggregate. This would provide a window for the industry to better understand how such attributes and syntheses conditions majorly affect the final product. This was achieved through the investigation of the effect of CRM activities on the hardness and elastic modulus of CRMA. It was found that the change in the CRMA's hardness and elastic modulus was dependent on the dissolution and/or release of CRM components. At the early stage of interaction time, minimal release in CRM components results in minor enhancement in the CRMA hardness and elastic modulus. With the progression of interaction time under favorable interaction conditions of moderate interaction temperature (190°C) and high mixing speed (50Hz), the released CRM components are involved in the formation of 3D entangled network structure that alter the CRMA internal network structure resulting in major enhancements in the hardness and elastic modulus. This was mainly due to the increased devulcanization of CRM with minimal occurrence of depolymerization effects that resulted in the formation of 3D entangled network structures in the liquid phase

of CRMA with the utilization of moderate interaction temperature (190°C) and high mixing speed (50Hz).

This work investigated the effect of interaction conditions of CRMA on their hardness and elastic modulus. It was found that the utilization of moderate (30Hz) to high (50Hz) interaction speeds at low interaction temperature (160°C) resulted in minimal enhancements in both the hardness and elastic modulus as a result of limitation of CRM activities to swelling by absorbance of light aromatics from asphalt. On the other hand, the utilization of moderate (190°C) interaction temperature with high interaction speed (50Hz) resulted in major property enhancements for both the hardness and elastic modulus as a result of development of 3D entangled network structure in the CRMA liquid phase. At 220°C interaction temperature, deterioration in both the hardness and elastic modulus was observed after 4 hrs of interaction time regardless of the interaction speed utilized as a result of CRM depolymerization and devulcanization processes that were severe resulting in the annihilation of the CRM modification effects.

In this work we investigated the relation between the asphalt fractions and the occurrence of 3D network structures in CRMA. This helps to provide an idea about the mechanism of formation of the internal network structures in CRMA by determining which fractions take part in the formation of the network. The presence of 3D network structures in CRMA enhances the self healing capabilities of the binder, thus leads to better in-service pavement performance. It was found that the asphalt type and fractions plays a major role in the development of the 3D network structures in CRMA. Lower PG grade asphalts with abundant saturates and naphthene aromatics produced the maximum amount of shear stress overshoot, indicating highest occurrence of 3D network structures. Cryogenic processed mixed source CR had better performance in terms of the network structure formation over the ambient processed truck or passenger cars ones. A 10%

CRM percentage had the best network structure formation over the 15% or 20%. A combination of moderate interaction temperature (190°C) and high interaction speed (50Hz) produced a well-developed 3D network structure in the CRMA.

In the current research work, the effect of the CRM dissolution and components release, under specific combination of interaction conditions, on the storage stability of the CRMA whole matrix and liquid phase was investigated. The change of the CRMA liquid phase properties plays a deterministic role in enhancing the storage stability of CRMA. The change of the CRMA liquid phase properties was expressed in the form of development of 3D network structure that occurred as a result of the release of CRM components under certain favorable conditions (interaction temperature of 190°C and interaction speed of 50Hz) that doesn't extend the depolymerization effects. The utilization of TGA verified the dissolution, release and existence of CRM components essential for the formation of the 3D network structure in CRMA that affected the CRMA properties and enhanced its storage stability.

This work investigated the effect of the addition of UMO to neat and CRMA at different interaction conditions. The changes in the macro and micromechanical properties of the modified asphalts were investigated. It was found that the utilization of UMO only as a modifier to asphalt severely deteriorates the macro and micro mechanical properties of the binder because the UMO disrupts the asphalt intermolecular associations and internal network structure, in the absence of CRM. Combining CRM with UMO as modifiers to asphalt had better results for the lower percentages of modifiers (10% CRM with 3% UMO) over the higher percentage (20% CRM with 9% UMO). A better balance between the light molecular fractions absorbed by CRM from asphalt and the compensated amounts from UMO was achieved with the utilization of 3% UMO and 10% CRM. When employing a combination of 10% CRM and 3% UMO as modifiers to the

binder, the utilization of the low interaction temperature (160°C) for the synthesis of modified asphalt was not sufficient to efficiently develop the internal network structure of the modified asphalt that leads to enhancements in both the macro and micromechanical properties of the modified asphalt. Based on the current research work, it is suggested that when UMO is to be used in asphalt modification, it should be at a rate of less than 3%, and it should be combined with at least 10% CRM. The proposed synthesis conditions are an interaction temperature of 190°C and interaction speed of 30 Hz for a period of 120 minutes.

This work investigated the effect of utilization of UMO and CRM as modifiers for asphalt. Based on the results of temperature sweep tests, addition of crumb rubber modifier (CRM) alone or with UMO results in the formation of internal network within the modified asphalt. Based on the results of short and long term aged asphalts, the utilization of combination of UMO and CRM enhanced the aging behavior of asphalt. Based on low temperature testing investigation, the utilization of the UMO and CRM enhanced the low temperature properties of asphalts. This indicates that the utilization of UMO with CRM as modifiers for asphalt would produce a more balanced asphalt matrix structure as a result of the compensation of the UMO to the fractions absorbed by CRM and also because UMO would further enhance the associations between CRM and asphalt leading to better internal network structure buildup for the modified asphalt.

Recommendations

Based on the aforementioned presented results, the future work recommendations can be summarized as follows.

It is recommended to utilize the Materials Reference Library (MRL) asphalts to investigate the development of network structures in binders as the MRL asphalts have detailed history of their properties.

Another recommendation would be to investigate in details the short and long term environmental impact of utilizing CRM and UMO on the air, soil and underground water quality.

It is also recommended to utilize CRMA in the formalization of trial mixes to investigate the interaction of CRMA with aggregates and the CRM effect the mix design performance related properties.

REFERENCES

1. Jones, D.R., *An Asphalt Primer: Understanding How the Origin and Composition of Paving-Grade Asphalt Cements Affect Their Performance*. 1992, FHWA.

2. Association, R.M., *Scrap tire markets in the United States.* 9th biennial report, 2009.

3. Adhikari, B., D. De, and S. Maiti, *Reclamation and recycling of waste rubber.* Progress in polymer science, 2000. **25**(7): p. 909-948.

4. Heitzman, M., *State of the practice: Design and construction of asphalt paving materials with crumb-rubber modifier. Final report.* 1992, Federal Highway Administration, Washington, DC (United States). Office of Engineering.

5. Mark, J.E., B. Erman, and M. Roland, *The science and technology of rubber*. 2013: Academic press.

6. Jensen, W.G. and M. Abdelrahman, *Crumb rubber in performance-graded asphalt binder*. 2006, University of Nebraska-Lincoln.

7. Anderson, D.A., et al., *Binder characterization and evaluation, volume 3: Physical characterization.* Strategic Highway Research Program, National Research Council, Report No. SHRP-A-369, 1994.

8. Bouldin, M., J. Collins, and A. Berker, *Rheology and microstructure of polymer/asphalt blends.* Rubber Chemistry and Technology, 1991. **64**(4): p. 577-600.

9. Bahia, H.U. and R. Davies, *Effect of crumb rubber modifiers (CRM) on performance related properties of asphalt binders.* Asphalt paving technology, 1994. **63**: p. 414-414.

10. Billiter, T., et al., *Physical properties of asphalt-rubber binder*. Petroleum Science and Technology, 1997. **15**(3-4): p. 205-236.

11. Navarro, F., et al., *Influence of crumb rubber concentration on the rheological behavior of a crumb rubber modified bitumen.* Energy & fuels, 2005. **19**(5): p. 1984-1990.

12. Huang, S.-C., *Rubber concentrations on rheology of aged asphalt binders.* Journal of Materials in civil Engineering, 2008. **20**(3): p. 221-229.

13. Huang, S.-C. and A.T. Pauli, *Particle size effect of crumb rubber on rheology and morphology of asphalt binders with long-term aging.* Road Materials and Pavement Design, 2008. **9**(1): p. 73-95.

14. Billiter, T., et al., *Production of asphalt-rubber binders by high-cure conditions.* Transportation Research Record: Journal of the Transportation Research Board, 1997(1586): p. 50-56.

15. Hui, J.C., G.R. Morrison, and S.A. Hesp, *Improved low-temperature fracture performance for rubber-modified asphalt binders.* Transportation research record, 1994(1436): p. 83-87.

16. Navarro, F., et al., *Influence of processing conditions on the rheological behavior of crumb tire rubber-modified bitumen.* Journal of Applied Polymer Science, 2007. **104**(3): p. 1683-1691.

17. Gopal, V.T., P.E. Sebaaly, and J. Epps. *Effect of crumb rubber particle size and content on the low temperature rheological properties of binders*. in *Transportation Research Board Annual Meeting, Washington DC, 13–17 January*. 2002.

18. Cheng, G., B. Shen, and J. Zhang, *A study on the performance and storage stability of crumb rubber-modified asphalts.* Petroleum Science and Technology, 2011. **29**(2): p. 192-200.

19. Green, E. and W.J. Tolonen, The Chemical And Physical Properties Of Asphalt Rubber Mixtures. Part I. Basic Material Behavior. 1977, Arizona Department of Transportation, Federal Highway Administration.

20. Zanzotto, L. and G. Kennepohl, *Development of rubber and asphalt binders by depolymerization and devulcanization of scrap tires in asphalt.* Transportation Research Record: Journal of the Transportation Research Board, 1996(1530): p. 51-58.

21. Abdelrahman, M., *Controlling performance of crumb rubber-modified binders through addition of polymer modifiers.* Transportation Research Record: Journal of the Transportation Research Board, 2006(1962): p. 64-70.

22. Gawel, I., R. Stepkowski, and F. Czechowski, *Molecular interactions between rubber and asphalt.* Industrial & engineering chemistry research, 2006. **45**(9): p. 3044-3049.

23. Billiter, T., et al., *Investigation of the curing variables of asphalt-rubber binder.* Petroleum science and technology, 1997. **15**(5-6): p. 445-469.

24. Abdelrahman, M. and S. Carpenter, *Mechanism of interaction of asphalt cement with crumb rubber modifier.* Transportation Research Record: Journal of the Transportation Research Board, 1999(1661): p. 106-113.

25. Abdelrahman, M., et al., *Engineering Physical Properties of Asphalt Binders through Nanoclay–Asphalt Interactions.* Journal of Materials in Civil Engineering, 2014. **26**(12): p. 04014099.

26. Chaala, A., C. Roy, and A. Ait-Kadi, *Rheological properties of bitumen modified with pyrolytic carbon black.* Fuel, 1996. **75**(13): p. 1575-1583.

27. Zhang, F., J. Yu, and J. Han, *Effects of thermal oxidative ageing on dynamic viscosity, TG/DTG, DTA and FTIR of SBS-and SBS/sulfur-modified asphalts.* Construction and Building Materials, 2011. **25**(1): p. 129-137.

28. Apeagyei, A.K., *Laboratory evaluation of antioxidants for asphalt binders.* Construction and Building Materials, 2011. **25**(1): p. 47-53.

29. Ho, R.-m., et al., *Microstructure of triblock copolymers in asphalt oligomers.* Journal of Polymer Science Part B Polymer Physics, 1997. **35**(17): p. 2857-2877.

30. Adedeji, A., et al., *Asphalt modified by SBS triblock copolymer: structures and properties.* Polymer Engineering and Science, 1996. **36**(12): p. 1707-1723.

31. Ouyang, C., et al., *Improving the aging resistance of styrene–butadiene–styrene tri-block copolymer modified asphalt by addition of antioxidants.* Polymer degradation and stability, 2006. **91**(4): p. 795-804.

32. Lamontagne, J., et al., *Comparison by Fourier transform infrared (FTIR) spectroscopy of* different ageing techniques: application to road bitumens. Fuel, 2001. 80(4): p. 483-488.

33. Branthaver, J.F., et al., Binder characterization and evaluation. Volume 2: Chemistry. 1993, SHRP report A-368.

34. Martínez-Estrada, A., et al., *Comparative study of the effect of sulfur on the morphology and rheological properties of SB-and SBS-modified asphalt.* Journal of applied polymer science, 2010. **115**(6): p. 3409-3422.

35. Zhang, B., et al., *The effect of styrene–butadiene–rubber/montmorillonite modification on the characteristics and properties of asphalt.* Construction and Building Materials, 2009. **23**(10): p. 3112-3117.

36. De Moraes, M., et al., *High temperature AFM study of CAP 30/45 pen grade bitumen.* Journal of Microscopy, 2010. **239**(1): p. 46-53.

37. Siddiqui, M.N. and M.F. Ali, *Studies on the aging behavior of the Arabian asphalts.* Fuel, 1999. **78**(9): p. 1005-1015.

38. Siddiqui, M.N., M.F. Ali, and J. Shirokoff, *Use of X-ray diffraction in assessing the aging pattern of asphalt fractions.* Fuel, 2002. **81**(1): p. 51-58.

39. Trejo, F., et al., *Characterization of asphaltenes from hydrotreated products by SEC, LDMS, MALDI, NMR, and XRD.* Energy & Fuels, 2007. **21**(4): p. 2121-2128.

40. Petersen, J., et al., *Binder Characterization and Evaluation, Volume 1*. Vol. 1. 1994: SHRP-A-367, Strategic Highways Research Program, National Research Council, Washington, DC.

41. Robertson, R.E., et al., *Chemical properties of asphalts and their relationship to pavement performance*. 1991, Strategic Highway Research Program, National Research Council.

42. Oliver, J.W., *Modification of paving asphalts by digestion with scrap rubber.* Transportation Research Record, 1981. **821**: p. 37.

43. Airey, G.D., M.M. Rahman, and A.C. Collop, *Absorption of bitumen into crumb rubber using the basket drainage method.* International Journal of Pavement Engineering, 2003. **4**(2): p. 105-119.

44. Frantzis, P., *Crumb rubber-bitumen interactions: Diffusion of bitumen into rubber.* Journal of materials in civil engineering, 2004. **16**(4): p. 387-390.

45. Takallou, H., et al., *Use of Superpave technology for design and construction of rubberized asphalt mixtures.* Transportation Research Record: Journal of the Transportation Research Board, 1997(1583): p. 71-81.

46. Sperling, L.H., *Interpenetrating polymer networks: an overview.* Interpenetrating polymer networks, 1991: p. 3-38.

47. Santangelo, P. and C. Roland, *Interrupted shear flow of unentangled polystyrene melts.* Journal of Rheology (1978-present), 2001. **45**(2): p. 583-594.

48. Tang, D., et al., *Simultaneous and gradient IPN of polyurethane/vinyl ester resin: morphology and mechanical properties.* Journal of Nanomaterials, 2009. **2009**: p. 25.

49. Chen, J.-S., M.-C. Liao, and M.-S. Shiah, *Asphalt modified by styrene-butadiene-styrene triblock copolymer: Morphology and model.* Journal of materials in civil engineering, 2002. **14**(3): p. 224-229.

50. Wekumbura, C., J. Stastna, and L. Zanzotto, *Destruction and recovery of internal structure in polymer-modified asphalts.* Journal of materials in civil engineering, 2007. **19**(3): p. 227-232.

51. Shin, E.E., et al., *Microstructure, morphology, and failure modes of polymer-modified asphalts.* Transportation Research Record: Journal of the Transportation Research Board, 1996. **1535**(1): p. 61-73.

52. Isacsson, U. and H. Zeng, *Relationships between bitumen chemistry and low temperature behaviour of asphalt.* Construction and Building Materials, 1997. **11**(2): p. 83-91.

53. Backenstow, D. and P. Flueler. *Thermal analysis for characterization*. in *Proceedings of the 9th Conference on Roofing Technology*. 1987.

54. Chen, F. and J. Qian, *Studies of the thermal degradation of waste rubber.* Waste Management, 2003. **23**(6): p. 463-467.

55. Lee, Y.S., et al., *Quantitative analysis of unknown compositions in ternary polymer blends: A model study on NR/SBR/BR system.* Journal of analytical and applied pyrolysis, 2007. **78**(1): p. 85-94.

56. Quek, A. and R. Balasubramanian, *An algorithm for the kinetics of tire pyrolysis under different heating rates.* Journal of hazardous materials, 2009. **166**(1): p. 126-132.

57. Seidelt, S., M. Müller-Hagedorn, and H. Bockhorn, *Description of tire pyrolysis by thermal degradation behaviour of main components.* Journal of Analytical and Applied Pyrolysis, 2006. **75**(1): p. 11-18.

58. Senneca, O., P. Salatino, and R. Chirone, *A fast heating-rate thermogravimetric study of the pyrolysis of scrap tyres.* Fuel, 1999. **78**(13): p. 1575-1581.

59. Williams, P.T. and S. Besler, *Pyrolysis-thermogravimetric analysis of tyres and tyre components.* Fuel, 1995. **74**(9): p. 1277-1283.

60. Prime, R.B., et al., *Thermogravimetric analysis (TGA).* Thermal Analysis of Polymers: Fundamentals and Applications, 2009: p. 241-317.

61. Parkes, G., P. Barnes, and E. Charsley, *New concepts in sample controlled thermal analysis: resolution in the time and temperature domains.* Analytical chemistry, 1999. **71**(13): p. 2482-2487.

62. SØrensen, O., *Thermogravimetric and dilatometric studies using stepwise isothermal analysis and related techniques.* Journal of Thermal Analysis and Calorimetry, 1992. **38**(1-2): p. 213-228.

63. Dong, X.-G., et al., *Thermogravimetric analysis of petroleum asphaltenes along with estimation of average chemical structure by nuclear magnetic resonance spectroscopy.* Thermochimica acta, 2005. **427**(1): p. 149-153.

64. Lucena, M.d.C.C., S.d.A. Soares, and J.B. Soares, *Characterization and thermal behavior of polymer-modified asphalt.* Materials Research, 2004. **7**(4): p. 529-534.

65. Baumgardner, G.L., et al., *Quantitative analysis of functional polymer in recycled tyre rubber used in modified asphalt binders.* Road Materials and Pavement Design, 2014. **15**(sup1): p. 263-278.

66. Masson, J.F., L. Pelletier, and P. Collins, *Rapid FTIR method for quantification of styrene-butadiene type copolymers in bitumen.* Journal of Applied Polymer Science, 2001. **79**(6): p. 1034-1041.

67. Abbas, A.R., U.A. Mannan, and S. Dessouky, *Effect of recycled asphalt shingles on physical and chemical properties of virgin asphalt binders.* Construction and Building Materials, 2013. **45**: p. 162-172.

68. Fang, C., et al., *Preparation and characterization of an asphalt-modifying agent with waste packaging polyethylene and organic montmorillonite.* Polymer Testing, 2013. **32**(5): p. 953-960.

69. Yao, H., et al., *Rheological properties and chemical analysis of nanoclay and carbon microfiber modified asphalt with Fourier transform infrared spectroscopy.* Construction and Building Materials, 2013. **38**: p. 327-337.

70. Socrates, G., *Infrared and Raman characteristic group frequencies: tables and charts*. 2004: John Wiley & Sons.

71. Zhigang, Y., Z. Yuzhen, and K. Xianming, *Modification of bitumen with desulfurized crumb rubber in the present of reactive additives.* Journal of Wuhan University of Technology-Mater. Sci. Ed., 2005. **20**(1): p. 95-97.

72. Daly, W.H., I.I. Negulescu, and I. Glover, *A Comparative Analysis Of Modified Binders: Original Asphalts And Materials Extracted From Existing Pavements.* Federal Highway Administration Report No. FHWA/LA, 2010. **10**: p. 462.

73. Ali, M.F. and M.N. Siddiqui, *Changes in asphalt chemistry and durability during oxidation and polymer modification.* Petroleum science and technology, 2001. **19**(9-10): p. 1229-1249.

74. Silverstein, R.M., et al., *Spectrometric identification of organic compounds*. 2014: John Wiley & Sons.

75. Zhang, F. and C. Hu, *The research for structural characteristics and modification mechanism of crumb rubber compound modified asphalts.* Construction and Building Materials, 2015. **76**: p. 330-342.

76. Ibrahim, I., et al., *Impact of incorporated gamma irradiated crumb rubber on the short-term aging resistance and rheological properties of asphalt binder.* Construction and Building Materials, 2015. **81**: p. 42-46.

77. Romero-Sánchez, M.D., et al., *Addition of ozone in the UV radiation treatment of a synthetic styrene-butadiene-styrene (SBS) rubber.* International journal of adhesion and adhesives, 2005. **25**(4): p. 358-370.

78. Cepeda-Jiménez, C.M., et al., *Influence of the styrene content of thermoplastic styrene–butadiene rubbers in the effectiveness of the treatment with sulfuric acid.* International journal of adhesion and adhesives, 2001. **21**(2): p. 161-172.

79. Hassan, M.M., et al., *Thermo-mechanical properties of devulcanized rubber/high crystalline polypropylene blends modified by ionizing radiation.* Journal of Industrial and Engineering Chemistry, 2013. **19**(4): p. 1241-1250.

80. Izhik, A. and N. Uriev, *Surface properties and specific features of structurization of disperse carbon black with different degrees of oxidation.* Colloid Journal, 2002. **64**(5): p. 562-566.

81. D. Pavia, G.L., G. Kriz, *Introduction to Spectroscopy: A Guide for Students of Organic Chemistry*. 3rd ed. Vol. 13. 2000, Washington Harcourt Brace College.

82. Churchill, E.V., S.N. Amirkhanian, and J.L. Burati Jr, *HP-GPC characterization of asphalt aging and selected properties.* Journal of materials in civil engineering, 1995. **7**(1): p. 41-49.

83. Siddiqui, M.N. and M.F. Ali, *Investigation of chemical transformations by NMR and GPC during the laboratory aging of Arabian asphalt.* Fuel, 1999. **78**(12): p. 1407-1416.

84. Putman, B.J. and S.N. Amirkhanian, *Characterization of the interaction effect of crumb rubber modified binders using HP-GPC.* Journal of Materials in Civil Engineering, 2010. **22**(2): p. 153-159.

85. Davison, R.R., et al., *Size exclusion chromatography of asphalts.* Handbook Of Size Exclusion Chromatography And Related Techniques: Revised And Expanded, 2003. **91**: p. 191.

86. Yapp, M.T., A.Z. Durrani, and F.N. Finn, *HP-GPC and asphalt characterization literature review*. 1991, SHRP report-A/UIR-91-503.

87. Lee, S.-J., et al., *Relation of mechanical properties of recycled aged CRM mixtures with binder molecular size distribution.* Construction and Building Materials, 2009. **23**(2): p. 997-1004.

88. Lee, S.-J., et al., *Aging analysis of rubberized asphalt binders and mixes using gel permeation chromatography.* Construction and Building Materials, 2011. **25**(3): p. 1485-1490.

89. Tarefder, R.A., A.M. Zaman, and W. Uddin, *Determining hardness and elastic modulus of asphalt by nanoindentation.* International Journal of Geomechanics, 2010. **10**(3): p. 106-116.

90. Tarefder, R.A. and H. Faisal, *Effects of dwell time and loading rate on the nanoindentation behavior of asphaltic materials.* Journal of Nanomechanics and Micromechanics, 2012. **3**(2): p. 17-23.

91. Oyen, M.L. and C.-C. Ko, *Examination of local variations in viscous, elastic, and plastic indentation responses in healing bone.* Journal of Materials Science: Materials in Medicine, 2007. **18**(4): p. 623-628.

92. Oliver, W.C. and G.M. Pharr, *An improved technique for determining hardness and elastic modulus using load and displacement sensing indentation experiments.* Journal of materials research, 1992. **7**(06): p. 1564-1583.

93. Stilwell, N. and D. Tabor, *Elastic recovery of conical indentations.* Proceedings of the Physical Society, 1961. **78**(2): p. 169.

94. Doerner, M.F. and W.D. Nix, *A method for interpreting the data from depth-sensing indentation instruments.* Journal of Materials Research, 1986. **1**(04): p. 601-609.

95. Wekumbura, C., J. Stastna, and L. Zanzotto, *Destruction and recovery of internal structure in polymer-modified asphalts.* Journal of materials in civil engineering, 2007. **19**: p. 227.

96. Jennings, P., et al., *High pressure liquid chromatography as a method of measuring asphalt composition*. 1980, FHWA-MT-79-30 Final Rpt.

97. Jennings, P. and J. Prinbanic, *The Expanded Montana Asphalt Quality Study Using High Pressure Liquid Chromatography. Final Report*. 1985.

98. Kim, K.W., J.L. Burati Jr, and J.-S. Park, *Methodology for defining LMS portion in asphalt chromatogram.* Journal of materials in civil engineering, 1995. **7**(1): p. 31-40.

99. Noureldin, A.S. and L.E. Wood, *Variations in molecular size distribution of virgin and recycled asphalt binders associated with aging.* Transportation Research Record, 1989(1228).

100. Wahhab, H.A.-A., et al., *Prediction of asphalt rheological properties using HP-GPC.* Journal of materials in civil engineering, 1999. **11**(1): p. 6-14.

101. Kim, K.W. and J.L. Burati Jr, *Use of GPC chromatograms to characterize aged asphalt cements.* Journal of Materials in Civil Engineering, 1993. **5**(1): p. 41-52.

102. Kim, K.W., et al., *Estimation of RAP's binder viscosity using GPC without binder recovery.* Journal of materials in civil engineering, 2006. **18**(4): p. 561-567.

103. 김광우, 도영수, and 써지, *Evaluation of aging characteristics of selected PMA using HP-GPC.* 한국도로학회논문집, 2004. **6**(2): p. 15-24.

104. Huang, S.-C., R. Glaser, and F. Turner, *Impact of water on asphalt aging: Chemical aging kinetic study.* Transportation Research Record: Journal of the Transportation Research Board, 2012(2293): p. 63-72.

105. Glaser, R., et al., *Low-temperature oxidation kinetics of asphalt binders.* Transportation Research Record: Journal of the Transportation Research Board, 2013(2370): p. 63-68.

106. Powell, R., et al., *Advances in Pavement Design through Full-scale Accelerated Pavement Testing.*

107. Prime, R.B., et al., *Thermogravimetric analysis (TGA).* Thermal Analysis of Polymers, Fundamentals and Applications, 2009: p. 241-317.

108. Hatakeyama, T. and L. Zhenhai, eds. *Handbook of thermal analysis*. 2000, John Wiley & Sons, Inc.

109. Ghavibazoo, A. and M. Abdelrahman, *Composition analysis of crumb rubber during interaction with asphalt and effect on properties of binder.* International Journal of Pavement Engineering, 2013. **14**(5): p. 517-530.

110. Zhong, Q., et al., *Fractured polymer/silica fiber surface studied by tapping mode atomic force microscopy.* Surface Science Letters, 1993. **290**(1): p. L688-L692.

111. Loeber, L., et al., *New direct observations of asphalts and asphalt binders by scanning electron microscopy and atomic force microscopy.* Journal of Microscopy, 1996. **182**(1): p. 32-39.

112. Stark, M. and R. Guckenberger, *Fast low-cost phase detection setup for tapping-mode atomic force microscopy.* Review of scientific instruments, 1999. **70**(9): p. 3614-3619.

113. Anczykowski, B., D. Krüger, and H. Fuchs, *Cantilever dynamics in quasinoncontact force microscopy: Spectroscopic aspects.* Physical Review B, 1996. **53**(23): p. 15485.

114. Winkler, R., et al., *Imaging material properties by resonant tapping-force microscopy: A model investigation.* Physical Review B, 1996. **54**(12): p. 8908.

115. Abdelrahman, M., *Controlling performance of crumb rubber-modified binders through addition of polymer modifiers.* Transportation Research Record: Journal of the Transportation Research Board, 2006. **1962**(1): p. 64-70.

116. Abdelrahman, M.A. and S.H. Carpenter, *Mechanism of interaction of asphalt cement with crumb rubber modifier.* Transportation Research Record: Journal of the Transportation Research Board, 1999. **1661**(1): p. 106-113.

117. Attia, M. and M. Abdelrahman, *Enhancing the performance of crumb rubber-modified binders through varying the interaction conditions.* International Journal of Pavement Engineering, 2009. **10**(6): p. 423-434.

118. Saylak, D., J. Noel, and R. Boggess. *The Duomorph-An in-situ viscoelastic characterization transducer*. in *Verein Deutscher Ingenieure, Internationale Konferenz ueber experimentelle Spannungsanalyse, 6th*. 1978.

119. Lu, X. and U. Isacsson, *Modification of road bitumens with thermoplastic polymers.* Polymer testing, 2000. **20**(1): p. 77-86.

120. Airey, G.D., *Rheological properties of styrene butadiene styrene polymer modified road bitumens☆.* Fuel, 2003. **82**(14): p. 1709-1719.

121. Ragab, M., and Abdelrahman, M., , *Effect of Interaction Conditions on the Internal Network Structure of Crumb Rubber Modified Asphalts.* Transportation research record, 2014.

122. Zanzotto, L. and G.J. Kennepohl, *Development of rubber and asphalt binders by depolymerization and devulcanization of scrap tires in asphalt.* Transportation Research Record: Journal of the Transportation Research Board, 1996. **1530**(1): p. 51-58.

123. Vonk, W. and A. Bull. *Phase phenomena and concentration effects in blends of bitumen and cariflex TR*. in *Proceedings of the 7th international roofing congress, Munich, Germany*. 1989.

124. Ragab, M., M. Abdelrahman, and A. Ghavibazoo, *Performance Enhancement of Crumb Rubber-Modified Asphalts Through Control of the Developed Internal Network Structure.* Transportation Research Record: Journal of the Transportation Research Board, 2013. **2371**(1): p. 96-104.

125. Ragab, M., Abdelrahman, Magdy , Ghavibazoo, Amir *New Approach for Selecting Crumb-Rubber-Modified Asphalts for Rutting and Permanent Deformation Resistance.* Advances in Civil Engineering Materials, 2013. **2**(1).

126. Xu, T. and X. Huang, *Study on combustion mechanism of asphalt binder by using TG–FTIR technique.* Fuel, 2010. **89**(9): p. 2185-2190.

127. MASSON, J.F., V. Leblond, and J. Margeson, *Bitumen morphologies by phase-detection atomic force microscopy.* Journal of Microscopy, 2006. **221**(1): p. 17-29.

128. Sengoz, B. and G. Isikyakar, *Evaluation of the properties and microstructure of SBS and EVA polymer modified bitumen.* Construction and Building Materials, 2008. **22**(9): p. 1897-1905.

129. Wu, S.-p., et al., *Influence of aging on the evolution of structure, morphology and rheology of base and SBS modified bitumen.* Construction and Building Materials, 2009. **23**(2): p. 1005-1010.

130. Król, J., P. Radziszewski, and K.J. Kowalski, *Influence of Microstructural Behavior on Multiple Stress Creep Recovery (MSCR) in Modified Bitumen.* Procedia Engineering, 2015. **111**: p. 478-484.

131. Pauli, A., et al., *Morphology of asphalts, asphalt fractions and model wax-doped asphalts studied by atomic force microscopy.* International Journal of Pavement Engineering, 2011. **12**(4): p. 291-309.

132. Ghavibazoo, A., M. Abdelrahman, and M. Ragab, *Effect of Crumb Rubber Modifier Dissolution on Storage Stability of Crumb Rubber-Modified Asphalt.* Transportation Research Record: Journal of the Transportation Research Board, 2013. **2370**(1): p. 109-115.

133. Putman, B.J. and S.N. Amirkhanian. *Crumb rubber modification of binders: interaction and particle effects*. in *Asphalt rubber 2006 conference, Palm Springs, USA*. 2006.

134. Airey, G.D., *Rheological properties of styrene butadiene styrene polymer modified road bitumens.* Fuel, 2003. **82**(14): p. 1709-1719.